Max von Pettenkofer Institut, Virologie der Universität München
Vorstand: Prof. Dr. med. Oliver T. Keppler

Dissertation
zum Erwerb des Doctor of Philosophy (Ph.D.) an der
Medizinischen Fakultät der
Ludwig-Maximilians-Universität zu München

The potential role of SAMHD1 in the chemotherapy of glioblastoma multiforme

vorgelegt von
Stephanie Schneider

aus
Traunstein, Deutschland

Jahr
2022

Mit Genehmigung der Medizinischen Fakultät der Ludwig-Maximilians-Universität zu München

First supervisor:	Prof. Dr. med. Oliver T. Keppler
Second supervisor:	PD Dr. rer. nat. Barbara Adler
Co-supervisor:	Dr. Ernesto Mejías Pérez

Dean: Prof. Dr. med. Thomas Gudermann

Datum der Verteidigung:

12.10.2022

Für meine Schwester Lena-Maria

Man sieht nur mit dem Herzen gut,
das Wesentliche ist für die Augen unsichtbar.

Antoine de Saint-Exupéry in "Der kleine Prinz"

Contents

Abstract

Glioblastoma multiforme (GBM) constitutes the most common primary malignant tumor in the brain with a dismal prognosis. Whereas life expectancy after first-diagnosis with GBM and under current state-of-the-art treatment regimens averages at 14.6 months, current research and clinical trials have failed to introduce more effective treatment options. In acute myeloid leukemia (AML), SAM and HD domain-containing protein 1 (SAMHD1) has been shown to limit the therapeutic efficacy of specific nucleoside analogues including cytarabine (ara-C) through cleavage of their biologically active, triphosphorylated form. The potential role of SAMHD1 for the resistance of GBM for nucleoside analogue-based chemotherapeutics has not been studied.

In this thesis, we aimed at addressing the following questions: (i) Is SAMHD1 expressed in GBM? (ii) Does methylation of the *Samhd1* promoter contribute to its expression in this tumor? (iii) Does the absence of SAMHD1 or loss of its dNTPase activity sensitize GBM cells to ara-C by increasing cells' ara-C triphosphate (ara-CTP) levels? (v) Do SAMHD1 mutations and polymorphisms found in GBM affect the cytotoxic efficacy of ara-C?

To this end, a broad panel of GBM cell lines were profiled for expression of SAMHD1 protein and mRNA using different immunoblotting and immunohistochemical approaches as well as quantitative PCR, respectively. A bisulfite sequencing assay was established to determine the DNA methylation status of cells' *Samhd1* promoter. In order to investigate the role of SAMHD1 for ara-C cytotoxicity in GBM, we interfered with SAMHD1 expression and function by treatment with Vpx-containing virus-like particles, which induce proteosomal SAMHD1 degradation, CRISPR/Cas9-mediated knockout (KO) of *Samhd1* and treatment with a small molecule inhibitor of SAMHD1, respectively, followed by ara-C treatment and luminescence-based evaluation of cells' viability. Also, SAMHD1 wildtype and a panel of functional and tumor-associated mutants were reintroduced into *Samhd1* KO cells using lentiviral vector transduction. The resulting, SAMHD1-overexpressing cells were assessed for mRNA and protein expression as well as ara-C sensitivity. Finally, liquid chromatography–tandem mass spectrometry was used to determine intracellular ara-CTP and dNTP levels.

Here, we demonstrate that SAMHD1 is broadly expressed in GBM cell lines, patient-derived xenografts (PDXs) and GBM patient tissue. We uncover that the *Samhd1* pro-

moter is unmethylated in SAMHD1-positive GBM cell lines, which demonstrates promoter methylation as a regulatory factor for its expression. Importantly, we show that depletion or inhibition of SAMHD1 sensitizes GBM cells to ara-C treatment and that the increase in ara-C cytotoxicity is linked to its dNTPase function and correlates with ara-CTP levels. We show that reconstitution of *Samhd1* KO GBM cells with SAMHD1 mutants linked to the enzyme's functionality or associated with cancer is a powerful tool to study SAMHD1. GBM-associated SAMHD1 mutations L244F, A565T and L620H sensitize GBM cells to ara-C treatment compared to parental cells and SAMHD1 wildtype reconstitution, respectively. For these specific mutants, virus-like particle-mediated SAMHD1 degradation and small molecule-based inhibition of SAMHD1 activity do not further sensitize to ara-C, indicating their potential clinical accessibility to an expanded, nucleoside analogue-based therapy. Together, this thesis identifies SAMHD1 as a regulator of chemoresistance in GBM and suggests its targeted depletion or drug-based inhibition as a potential strategy to expand the spectrum of chemotherapeutic options, including ara-C, for this highly malignant brain tumor.

List of Figures

List of Tables

List of Abbreviations

AGS	Aicardi–Goutières syndrome
AK1	Adenylate kinase isoenzyme 1
ALL	Acute lymphoblastic leukemia
AML	Acute myeloid leukemia
AMOL	Acute monocytic leukemia
Ara-C	1'-β-d-Arabinofuranosylcytosine, cytosine arabinoside, cytarabine
Ara-CDP	Ara-C diphosphate
Ara-CMP	Ara-C monophosphate
Ara-CTP	Ara-C triphosphate
ARD1	Acetyltransferase arrest defective protein 1
B-ALL	B-cell acute lymphoblastic leukemia
BBB	Blood-brain barrier
BCA	Bicinchoninic acid
BSA	Bovine serum albumin
CBTRUS	Central brain tumor registry of the United States of America
CCNU	Chlorethyl-cyclohexyl-nitroso-urea, lomustine
CD	Cluster of differentiation
CDA	Cytidine deaminase
ch	Chicken
CHIKV	Chikungunya virus
CLL	Chronic lymphocytic leukemia
CNS	Central nervous system
COSMIC	Catalogue of Somatic Mutations in Cancer
CR	Complete remission
CRISPR	Clustered regularly interspaced short palindromic repeats
CSC	Cancer stem cell
CTCL	Cutaneous T-cell lymphoma
CTRL	Control
ctDNA	Circulating tumor DNA
dCK	Deoxycytidine kinase
DCTD	Deoxycytidylate deaminase
DDB1	DNA damage-binding protein 1
DMEM	Dulbecco's modified eagle medium

DMSO	Dimethylsulfoxide
dN	2'-deoxynucleoside
DNMT	DNA methyltransferases
dNTP	Deoxynucleoside triphosphate
DNA	Deoxyribonucleic acid
dpt	Days post treatment
ds	Double-stranded
DSB	Double-strand break
DTT	1,4-Dithiothreitol
EBV	Epstein-Barr virus
EC	Endothelial cell
EDTA	Ethylenediaminetetraacetic acid disodiumsalt-dihydrate
EMA	European Medicines Agency
EGFR	Epidermal growth factor receptor
EIAV	Equine infectious anemia virus
ENT-1	Equilibrative nucleoside transporter
ERT	Endogenous reverse transcription
FACS	Fluorescence-activated cell sorting
FCS	Fetal bovine serum
FDA	Food and Drug Administration
FIV	Feline immunodeficiency virus
fwd	Forward
GBM	Glioblastoma multiforme
G-CIMP	Glioma GpG island methylator phenotype
GDC	Genomic data commons
gRNA	guideRNA
GTR	Gross total resection
HBV	Hepatitis B virus
HCMV	Human cytomegalovirus
HD	High-dose
HFF	Human foreskin fibroblast
HGG	High-grade glioma
HIV	Human immunodeficiency virus
HPV16	Human papillomavirus 16
HRP	Horseradish peroxidase
HSC	Hematopoietic stem cell
HSV-1	Herpes simplex virus 1
HTLV	Human T-lymphotropic virus
IBM	Iscove's liquid medium
IDH	Isocitrate dehydrogenase
IFN	Interferon
IHC	Immunohistochemistry
IMDM	Iscove's modified dulbecco's medium

ISG	Interferon-stimulated gene
KI	Knock-In
KO	Knockout
KPS	Karnofsky performance score
LB	Lysogeny broth
LD	Low-dose
LDS	Lithium dodecyl sulfate
LGG	Low-grade glioma
LINE-1	Long interspersed nuclear element 1
LPS	Lipopolysaccharide
LVV	Lentiviral vector
m	Mouse
MDDC	Monocyte-derived dendritic cell
MDM	Monocyte-derived macrophage
MDS	Myelodysplastic syndrome
MFI	Mean fluorescent intensity
MGMT	O^6-methylguanine-DNA methyltransferase
miRNA	microRNA
MLV	Murine leukemia virus
MPMV	Mason Pfizer monkey virus
MRI	Magnetic resonance imaging
NCI	National Cancer Institute
NEC	Not elsewhere classified
NF-κB	Nuclear factor κB
NGS	Next generation sequencing
NHL	Non-Hodgkin lymphoma
NIH	National Institute of Health
NK	Natural killer
NLS	Nuclear localisation signal
NOS	Not otherwise specified
NPC	Nuclear pore complex
NSC	Neural stem cell
NT5C2	5'-Nucleotidase II
NTC	non-target control
OPC	Oligodendrocyte precursor cell
OS	Overall survival
PAM	Protospacer adjacent motif
PBS	Phosphate-buffered saline
PCR	Polymerase chain reaction
PDX	Patient-derived xenograft
PEI	Polyethylenimine
PET	Positron emission tomography

PFA	Paraformadehyde
PFS	Progression-free survival
PFV	Prototype foamy virus
PMA	Phorbol 12-myristate-13-acetate
PTM	Post-translational modification
qPCR	Quantitative polymerase chain reaction
rb	Rabbit
rev	Reverse
RNA	Ribonucleic acid
RNR	Ribonucleotide reductase
RPMI	Roswell park memorial institute medium
RSV	Rous sarcoma virus
RT	Reverse transcriptase
SAMHD1	Sterile alpha motif and histidine-aspartate domain containing protein 1
s.d.	Standard deviation
SDS	Sodium dodecyl sulfate
SG-PERT	SYBR Green I-based product-enhanced reverse transcription
SKP2	S-Phase kinase associated protein 2
siRNA	Small interfering RNA
SIV	Simian immunodeficiency virus
SNP	Single-nucleotide polymorphism
ss	Single-stranded
TAE	Tris-acetate-EDTA
T-ALL	T-cell acute lymphoblastic leukemia
TB	Terrific broth
TBS	Tris buffered saline
TME	Tumor microenvironment
TMZ	Temozolomide
T-PLL	T cell prolymphocytic leukemia
TRC	Transcription-replication conflict
TRIM21	Tripartite motif containing 21
TTF	Tumor treating field
VLP	Virus-like particle
Vpr	Viral protein R
Vpx	Viral protein X
VSV-G	Vesicular stomatitis virus glycoprotein
WGS	Whole genome sequencing
WHO	World Health Organisation
WT	Wildtype
ZIKV	Zika virus

Chapter 1

Introduction

1.1 dNTP homeostasis

Deoxynucleoside triphosphates (dNTPs) are the molecular precursors of the DNA and RNA. They consist of a nucleobase (adenine, guanine, cytosine or thymine) bound to a deoxyribose sugar at carbon 1, which again binds a triphosphate group at its carbon 5, illustrated in figure 1.1 [1]. The four different dNTPs are therefore dATP, dCTP, dGTP, and dTTP, together referred to as dNTPs [2].
In order to survive, cells need to be able to react fast to different stimuli, including signals of stress, growth and cell division. As dNTPs are essential for the DNA replication as well as DNA damage repair and involved in signaling pathways, accurate regulation of the biosynthesis and degradation of dNTPs is crucial in cell physiology and disease prevention [3]. Imbalances in the intracellular dNTP pool may lead to DNA mutagenesis, elevated cell proliferation or tumor cell growth in the case of abnormally increased dNTP levels as well as impaired DNA damage repair, cell cycle arrest or apoptosis in cells that show lower dNTP levels [2]. The maintenance of dNTP homeostasis is therefore not only crucial for appropriate and sufficient DNA synthesis and repair, but also for genome stability.
Interestingly, the dNTPs are physiologically not represented in equal amounts as dTTPs show a higher abundance compared to the other dNTPs followed by dATP, dGTP and dCTP (table 1.1) [4].

1.2 SAMHD1

1.2.1 Structural and functional domains of SAMHD1

Sterile alpha motif and histidine-aspartate domain containing protein 1 (SAMHD1) was first identified as the human homologue of the mouse interferon (IFN)-γ induced protein expressed in human dendritic cells and its gene is located on chromosome 20 in humans (chromosome 2 in mice) [5]. The enzyme's molecular weight is 72.2 kDa and it triphospho-

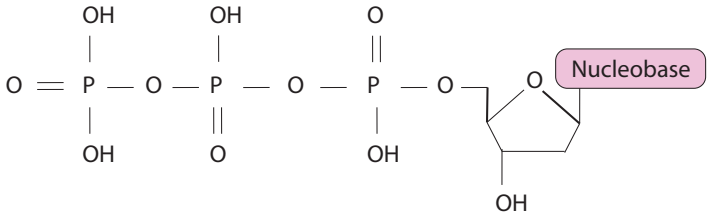

Figure 1.1: Chemical structure of deoxynucleoside triphosphate (dNTP). dNTPs consist of the nucleobase adenine, guanine, cytosine or thymine bound to deoxyribose at carbon 1 and a triphosphate group bound at carbon 5 [1].

hydrolizes dNTPs, meaning it cleaves dNTPs (i.e. dGTP, dATP, dCTP and dTTP) into their respective 2'- deoxynucleosides (dNs) and triphosphate groups (figure 1.2A) [6].
The crystal structure of SAMHD1 was resolved in 2013 [7, 8] (figure 1.2B) and consists of two domains, a sterile alpha motif (SAM) domain and a histidine-aspartate (HD) domain. A detailed domain organization is shown in figure 1.2C. The SAM domain corresponds to residues 40–109 and its biological function is still poorly understood. In 2018, Buzovetsky *et al.* indicated a role of the SAM domain in activation and regulation of mouse SAMHD1 (mSAMHD1) function [9]. In their experiments, the SAM domain was required for tetramerization of mSAMHD1, the HD domain of mSAMHD1 alone showed decreased dNTPase activity and emphasized the role of the SAM-HD domain interactions for oligomerization and activity, but could not be recapitulated with human SAMHD1 [9]. The HD domain (residues 110–626) contains the catalytic core for dNTPase function [10, 11]. Residue D311 has been shown to be essential for functional dNTPase activity [6]. Together with the residues H167, H206 and D207, this residue is able to bind metal ions [6].
In addition, several residues at the end of the C-terminus are involved in regulatory processes of the enzyme. Two cyclin-binding motifs ^{451}RXL^{453} and ^{620}LF^{621} bind a cyclin A2/cyclin-dependent kinase (CDK) complex that is able to phosphorylate SAMHD1 at residue T592 [12, 13]. The phosphorylation status at this residue determines the dNTPase activity of the enzyme (section 1.2.4). Other direct protein interactions with SAMHD1 have been confirmed with CtIP, S-Phase kinase associated protein 2 (SKP2), PP2A-B55α, cyclin L2, tripartite motif containing 21 (TRIM21) and nuclear import proteins [11]. In addition, SAMHD1 co-localizes with 53BP1, a marker for DNA double-strand breaks (DSBs) - an observation that was later confirmed by Daddacha *et al.* [14].

1.2.2 dNTPase activity of SAMHD1

When SAMHD1 is inactive, the protein exists in a monomer-dimer balance and tetramerizes upon binding to GTP/dGTP in order to constitute the catalytically active form. The SAMHD1 tetramer includes 8 allosteric sites (with one "A1" and one "A2" allosteric site

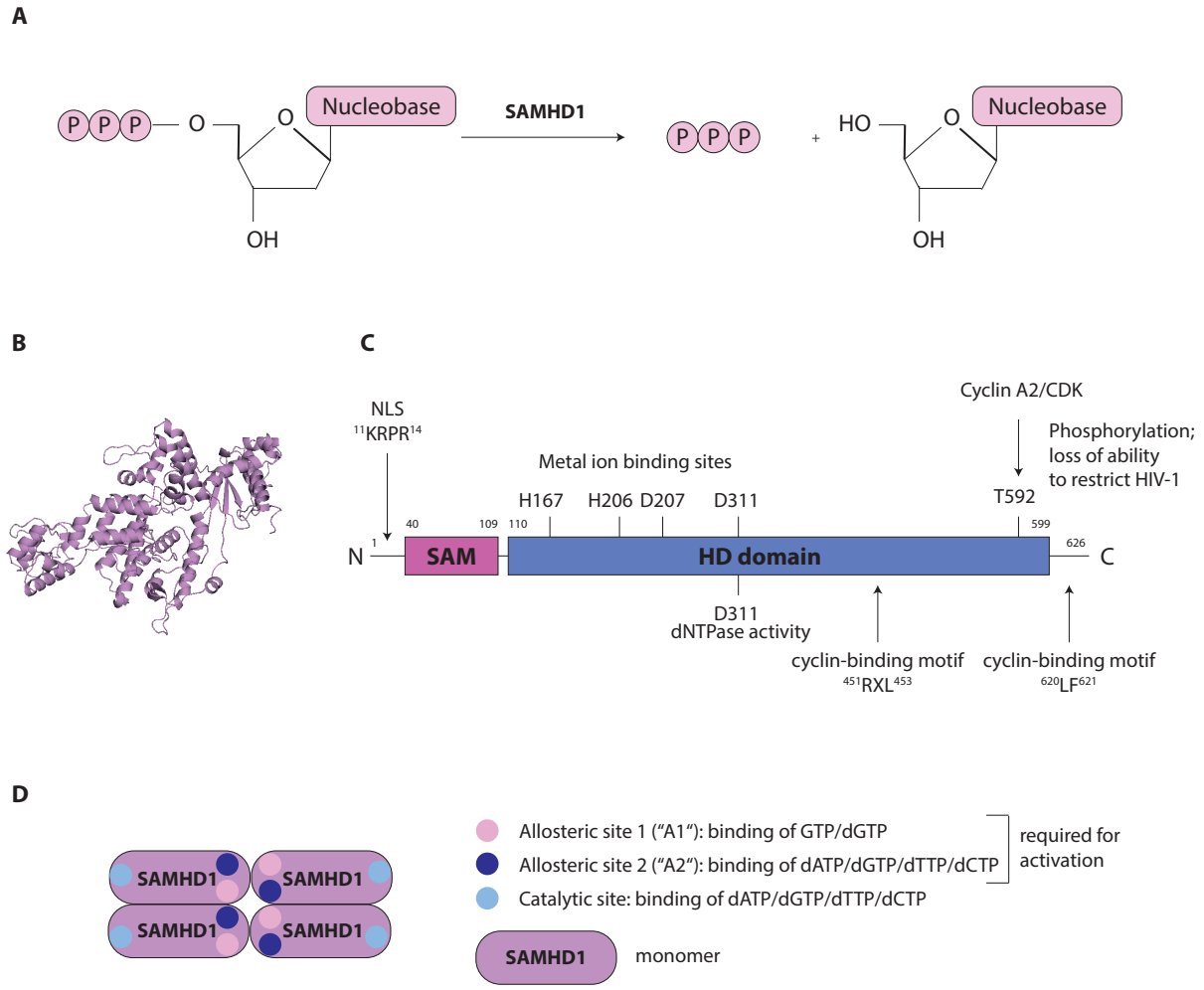

Figure 1.2: Deoxynucleoside triphosphate (dNTP) hydrolase activity, domain organization and active tetramer architecture of SAMHD1. (A) Schematic representation of the dNTPase activity of SAMHD1 triphosphohydrolizing dNTPs into 2'-deoxynucleosides (dNs) and triphosphate groups [6]. (B) Crystal structure of SAMHD1 monomer created *in silico* with PyMOL [7, 8]. (C) Schematic representation of the domain organization of SAMHD1 consisting of two domains, the sterile alpha motif (SAM) domain and the histidine-aspartate (HD) domain. Important residues and regions are indicated in the graph [6, 10, 15]. (D) Schematic representation of the enzymatically active SAMHD1 tetramer. Each of the four monomers consists of two allosteric sites ("A1" and "A2") as well as one catalytic site. Binding of nucleosides to the allosteric sites is essential for tetramer formation and stabilization, and is required for activation of SAMHD1 [11, 16].

per monomer) in which eight molecules are able to bind, contributing to the stability of the active enzyme (figure 1.2D) [16]. For tetramerization, GTP/dGTP act as cofactors binding to "A1" allosteric sites in order to build inactive dimers. Then, dATP, dGTP, dTTP or dCTP are able to bind the "A2" allosteric sites, triggering the tetramerization of SAMHD1. Interestingly, dNTPs show different binding affinities to the "A2" allosteric site (table 1.1). Then, metal ions bind to the residues H167, H206, D207 and D311 in order to support accurate dNTP substrate orientation and binding to the catalytic sites [6]. Next, SAMHD1 hydrolyzes a dNTP into 2'-dN and a triphosphate following the substrate preferences displayed in table 1.1. After successful initial activation of SAMHD1, it does no longer depend on the activator GTP for ongoing hydrolyzation and can remain as an active tetramer even after dNTP concentrations go below activating concentrations of approximately 10 μM. This may explain the prolonged low dNTP concentrations in the nm-range in non-cycling cells, resting CD4 T cells and macrophages [17].

Table 1.1: dNTP abundance and SAMHD1 preferences for binding and hydrolysis [4, 11]

Substrate functions	**Order of dNTPs**
Abundance in cycling cells	dTTP > dATP > dGTP > dCTP
Binding in "A2" allosteric site	dATP > dGTP > dTTP > dCTP
Hydrolysis rate of SAMHD1 (all dNTPs present)	dGTP > dCTP > dTTP > dATP
Hydrolysis rate of SAMHD1 (only 1 dNTP present)	dATP > dTTP > dCTP > dGTP

1.2.3 Expression and regulation of the *Samhd1* gene

1.2.3.1 SAMHD1 expression, localization and regulation

Based on *in vivo* expression profiling, *Samhd1* is expressed in hematopoetic cells, highly in non-dividing macrophages, dendritic cells and resting CD4 T cells; and it is slightly expressed in B cells, activated CD4 T cells, monocytes and natural killer (NK) cells [18]. In addition, it was shown to be expressed in most human tissues [18].
Despite its N-terminal nuclear localization signal (NLS) ^{11}KRPR^{14} [15] and the literature stating an exclusive SAMHD1 localization in the nucleus [15, 19], more and more studies show partial SAMHD1 localization in the cytosol [20, 21] underscoring that SAMHD1 is not an exclusively nuclear protein.
With regard to expression regulation, many factors can influence SAMHD1 expression levels in a cell. Firstly, SAMHD1 expression is dependent on the cell cycle stage, which the particular cell currently undergoes [22]. Whereas SAMHD1 shows high expression levels during G_0 phase, its expression is low during DNA replication in S phase [22]. Cell cycle studies in THP-1 *Samhd1* knockout (KO) cells indicated elevated cell proliferation and altered G_1/G_0 as well as G_2/M population percentages compared to SAMHD1-proficient control cells [23]. In addition, Batalis *et al.* recently showed that the single nucleotide mutation SAMHD1 T592E inhibits the cell cycle S/G2 transition in the cell cycle [24].

Secondly, SAMHD1 expression depends on the differentiation state of the cell: THP-1 cells differentiated with PMA showed elevated SAMHD1 expression levels compared to non-PMA-differentiated, cycling cells [23, 25].
Thirdly, it has been shown that the expression of certain single-stranded non-coding RNAs called microRNAs (miRNAs) can influence the expression of SAMHD1 [26, 27]. Whereas miRNA-181b expression levels inversely correlated with SAMHD1 protein levels in cutaneous T-cell lymphoma (CTCL) [26], reduced miRNA-181a and miRNA-155 expression resulted in increased SAMHD1 protein levels in astrocytes [27].
Finally, IFNs have been described to stimulate SAMHD1 expression [28]. Treatment with type I and II IFNs were downregulating microRNAs miR-181a and miR-30a, which further correlated with elevated SAMHD1 expression in primary human monocytes [28]. Importantly, the upregulation of SAMHD1 through IFN treatment has been shown to be cell-type dependent: whereas certain cell types elevate their SAMHD1 expression levels upon type I IFN treatment, such as HEK 293T, HeLa, liver cells, monocytes, microglia and the astrocytoma cell line U-87 MG, other cell types like CD4 T cells, MDMs and MDDCs did not show any change in SAMHD1 protein expression, but dephosphorylation at residue T592 [29]. In addition, the IFN-stimulated genes (ISGs) MxA, MxB, HERC5, IRF7 and IRF3 have been shown to induce SAMHD1 expression in HIV-1 patients [30]. Interestingly, the other way around, KO of *Samhd1* elevated the expression of type I IFNs and ISGs in THP-1 cells [31], which has been shown to be facilitated through the PI3K/AKT/IRF3 signaling pathway [32].

1.2.3.2 DNA methylation in the *Samhd1* promoter

DNA methylation represents a major epigenetic mechanism for gene expression regulation. It occurs at the carbon on position 5 of cytosines in CpG dinucleotides in CpG islands, regions with a CpG dinucleotides percentage of at least 50% and a length of this region of more than 200 bases [33]. Methylated promoter sites are generally associated with silenced genes resulting in strongly reduced to undetectable gene expression. Unmethylated promoter regions, on the other hand, are associated with active genes and protein expression [33]. In 2013, Silva *et al.* reported that this regulation mechanism also takes place for the *Samhd1* gene, shown in human CD4 T cells [34]. Whereas the *Samhd1* promoter of certain CD4 T cell lines (Jurkat, Sup-T1) was methylated leading to undetectable SAMHD1 protein expression, monocytic cell lines (e.g. THP-1) and primary CD4 T cells with high SAMHD1 expression levels showed an unmethylated *Samhd1* promoter. These findings point to a direct connection between the DNA methylation status of the *Samhd1* promoter and the regulation of SAMHD1 protein expression on a transcriptional level [34].
The downregulation of SAMHD1 expression through DNA methylation of its promoter has been reported in association with disease in a subtype of CTCL [35] and in lung cancer [36]. In both cases, *Samhd1* mRNA and protein expression levels were reduced compared to healthy donors, which was correlated with increased DNA methylation levels in the *Samhd1* promoter. In addition, it was shown that for lung cancer, the drug-based DNA

methylation inhibition again increased SAMHD1 protein expression [36].

1.2.4 Post-translational modifications (PTMs) of SAMHD1

1.2.4.1 Phosphorylation of SAMHD1

The cyclin A2/CDK complex is able to add a phosphate group onto SAMHD1 at residue T592 leading to the loss of HIV-1 restriction ability. The SAMHD1 mutant T592A can no longer be phosphorylated thereby loses this level of regulation. When it comes to the regulation of the dNTPase activity, discrepancies in the literature are found. Whereas several groups state that upon phosphorylation, cellular dNTP levels stay similar and SAMHD1 maintains its dNTPase activity [37, 38], other groups report tetramer destabilization due to phosphorylated SAMHD1 (pSAMHD1) and impaired dNTPase activity [39]. Likewise, SAMHD1 can be dephosphorylated at residue T592 by the phosphatase PP2A together with the regulatory subunit B55α (PP2A-B55α) [40].
Similar to the expression of SAMHD1, also its activity differs in the different stages of the cell cycle [22]. Whereas it is unphosphorylated during most of the cell cycle stages, SAMHD1 gets phosphorylated at residue T592 during the DNA replication in S phase [22].

1.2.4.2 SUMOylation of SAMHD1

SUMOylation is the binding of about 10 kDa small ubiquitin-like modifier (SUMO) proteins to lysines (K) of proteins with a consensus motif [41]. This PTM can have effects on the binding of the SUMOylated protein to other proteins as well as its function [41].
Very recently, Martinat *et al.* showed that SAMHD1's ability to restrict HIV-1 is dependent on the modification status of the residue K595. Here, they demonstrate that SUMOylation at this residue is essential for the restriction of HIV-1 in non-cycling cells [42]. SAMHD1 is SUMOylated in both dividing and non-dividing cells and exhibits a SUMO-interacting motif (SIM) [42]. Intensive SAMHD1 mutant studies revealed also that mutation at residue K595 leads to impaired SUMOylation of SAMHD1 and loss of HIV-1 restriction ability, but unchanged dNTPase activity [42]. Also, phosphorylation at T592 and SUMOylation at K595 are most likely independent processes [42].
In addition, another study showed the E3 SUMO ligase PIAS1 as an SAMHD1 interactor that promotes SUMOylation. Also here in the context of Epstein-Barr virus (EBV), SAMHD1 viral restriction is dependent on its SUMOylated state [43].

1.2.4.3 Acetylation of SAMHD1

The acetyltransferase arrest defective protein 1 (ARD1) is able to acetylate SAMHD1 at residue K405. This modification has been linked with the enhancement of its dNTPase activity *in vitro* [44]. The mutant version SAMHD1 K405R was no longer able to be acetylated and therefore lost this capacity for activity enhancement. SAMHD1 K405R mutation in lung adenocarcinoma cell line A549 reduced the amount of released triphosphates, indicating reduced dNTPase activity and higher dNTP concentrations. As a result,

the SAMHD1 K405R mutant showed elevated G_1/G_0 and reduced G_1/S transition compared to SAMHD1 wildtype, resulting in slower proliferation rates [44]. On the other hand, SAMHD1 acetylated at residue K405 led to elevated dNTPase activity, a reduced dNTP pool, elevated G_1/S transition and elevated cell proliferation [44].

1.2.5 SAMHD1 and its antiviral activity against HIV-1

Due to its dNTPase activity, SAMHD1 is a key factor in the degradation of dNTP molecules and therefore reduces the dNTP pool in the cell. Cellular dNTP molecules are essential building blocks for the viral reverse transcriptase (RT) in order to reverse transcribe the viral positive-sense (+), single-stranded RNA into double-stranded DNA [45]. Low cellular dNTP levels due to high SAMHD1 activity therefore block viral reverse transcription and restrict HIV-1 infection in non-cycling monocyte-derived dendritic cells (MDDCs) [46], monocyte-derived macrophages (MDMs) [47] and resting CD4 T cells [20, 48]. Recently, the antiviral activity of SAMHD1 has been also linked to its ability to bind nucleic acids [49] (section 1.2.7). In HIV-2 and SIV, this mechanism can be counteracted by the viral accessory protein X (Vpx, section 1.2.6) [46, 50]. SAMHD1 mutants including a mutation in the NLS localize to the cytoplasma, but are still able to restrict HIV-2 and SIV to the same extent as the wildtype protein [15].
Besides this most prominent restriction step, SAMHD1 and its dNTPase activity is also able to restrict HIV-1 during integration [51] and endogenous reverse transcription (ERT) [52]. During integration of proviral DNA into the host genome, the viral integrase leaves a 5'-end single-stranded gap between integration site and viral DNA. These two gaps need to be filled up by internal repair mechanisms using cellular dNTP molecules. In case of high SAMHD1 activity, and therefore low dNTP availability, the 5'-end repair during integration is restricted [51].
Furthermore, endogenous reverse transcription (ERT) represents a cell-free possibility for newly budded HIV particles to start reverse transcription within the particle itself and synthesize proviral DNA in part prior to infecting a new target cell. The dNTP molecules, present in the viral particle derived from the producer cell, are enclosed during the budding process. When SAMHD1 activity is high, dNTP availability in the cell is low and dNTPs are less likely to be packaged into the particle, reducing ERT activity and therefore restricting HIV-1 infection [52].
As retroviruses typically depend on dNTP availability in the target cell in order to reverse transcribe their viral genome, SAMHD1's viral restriction is a broad phenomenon seen also in other retroviruses, including equine infectious anemia virus (EIAV), feline immunodeficiency virus (FIV), Mason Pfizer monkey virus (MPMV), murine leukemia virus (MLV) and Rous sarcoma virus (RSV) [11, 53].
Besides a large number of RNA viruses, SAMHD1 also influences infections of various DNA viruses, in particular members of the virus family *Herpesviridae* including herpes simplex virus 1 (HSV-1) [54, 55], human cytomegalovirus (HCMV) [56] and Epstein-Barr virus (EBV) [57]. Whereas in RNA viruses SAMHD1 mostly interferes with reverse transcription of the viral genome, in DNA viruses it influences viral DNA genome replication, which

also depends on intracellular dNTP concentrations [55]. Apart from viruses of the family *Herpesviridae*, SAMHD1 was also shown to restrict human papillomavirus 16 (HPV16) [58], vaccinia virus [54] as well as hepatitis B virus (HBV) infection [59, 60].
Interestingly, whereas SAMHD1 fulfills an antiviral role in the majority of viruses reported, it also has been shown that SAMHD1 can act as a proviral factor in Zika (ZIKV) and Chikungunya (CHIKV) infections [61]. An overview of SAMHD1's antiviral and proviral roles is shown in table 1.2.

Table 1.2: Antiviral and proviral roles of SAMHD1 for RNA and DNA viruses [11]

Virus	Family	Genus	Genome	Phenotype
HIV-1	*Retroviridae*	Lentivirus	(+) ssRNA (RT)	antiviral [20, 46, 47, 48]
EIAV	*Retroviridae*	Lentivirus	(+) ssRNA (RT)	antiviral [53]
FIV	*Retroviridae*	Lentivirus	(+) ssRNA (RT)	antiviral [53]
RSV	*Retroviridae*	α-retrovirus	(+) ssRNA (RT)	antiviral [53]
MPMV	*Retroviridae*	β-retrovirus	(+) ssRNA (RT)	antiviral [53]
MLV	*Retroviridae*	γ-retrovirus	(+) ssRNA (RT)	antiviral [53]
HPV16	*Papillomaviridae*	α-papillomavirus	dsDNA	antiviral [58]
Vaccinia virus	*Poxviridae*	Orthopoxvirus	dsDNA	antiviral [54]
HBV	*Picornaviridae*	Hepatovirus	partially dsDNA	antiviral [59, 60]
HSV-1	*Herpesviridae*	α-herpesvirus	dsDNA	antiviral [54, 55]
HCMV	*Herpesviridae*	β-herpesvirus	dsDNA	antiviral [56]
EBV	*Herpesviridae*	γ-herpesvirus	dsDNA	antiviral [57]
ZIKV	*Flaviviridae*	Flavivirus	(+) ssRNA	proviral [61]
CHIKV	*Togaviridae*	Alphavirus	(+) ssRNA	proviral [61]

1.2.6 SAMHD1 and the viral protein X

The genomes of HIV-2 and SIV, e.g. SIV_{sm} from sooty mangabey contain a gene that codes for the Vpx, that counteracts SAMHD1 by facilitating its degradation in the nucleus [62]. By binding to SAMHD1 at its C-terminus (for HIV-2 and SIV_{sm}), Vpx recruits SAMHD1 to DCAF1 (DDB1-CUL4-associated factor 1), a complex is formed together with DDB1 (DNA damage-binding protein 1), CUL4 (cullin 4), ROC1/RBX1 (E3 ubiquitin-protein ligase) and later E2 ubiquitin-conjugating enzyme, which leads to proteosomal degradation of SAMHD1 [46, 50, 63]. The SAMHD1 residues important for Vpx-binding are R617, V618 and K622 [64].
Some SIVs like SIV_{mnd} from mandrill and SIV_{rcm} from red capped mangabey are not able to degrade human SAMHD1 [65]. Virus-mediated degradation of SAMHD1 increases the

dNTP pool in the target cell, overcomes the viral restriction and enables viral RT activity. In cell culture experiments, SAMHD1 degradation can be mediated using transduction with virus-like particles (VLPs) containing Vpx (Vpx-VLPs).
In addition to the SAMHD1-dependent function of Vpx, the protein is also known to enhance the nuclear import of viral genomes [66]. In 2020, Singh *et al.* showed first mechanistic insights, where they demonstrated that Vpx is interacting with nucleoporin 153 (Nup153), a host protein known to facilitate the docking of complexes at the nuclear pore complex (NPC) [67]. The interaction between Vpx and Nup153 has been shown to be crucial for nuclear translocation of the viral genome, so that the reverse transcribed viral DNA can be integrated into the genome of the host cell [67]. In addition, this has been shown to depend on the phosphorylation of Vpx through the mitogen-activated protein kinase 1 (MAPK1 or ERK-2) [67].
In contrast to Vpx, the viral accessory protein R (Vpr) is encoded by most of the HIVs and SIVs, including HIV-1 [68]. Whereas it shows up to 50% sequence identity with Vpx, it is able to load proteins onto the degradation complex, but is can not target SAMHD1 for degradation and does not interfere with lentiviral infection in macrophages [50]. Instead, Vpr has been shown to encompass different functions: It mainly facilitates the nuclear import of the virus pre-integration complex, but also regulates the transcription of host genes, stabilizes the expression of the structural protein Env that is forming the viral envelope, induces cell cycle arrest/apoptosis and facilitates the degradation of other proteins than SAMHD1 [68].

1.2.7 Alternative roles of SAMHD1

SAMHD1's ability to cleave dNTPs serves as its best studied, major enzymatic activity. Besides that, other dNTPase-independent functions and activities of SAMHD1 are described in literature.
Firstly, SAMHD1 shows to have a role in retrotransposon regulation as it reduces the activity of long interspersed elements 1 (LINE-1) [69]. At least 17% of the human genome consists of LINE-1, the only retrotransposon that autonomously and actively creates insertions into the genome [69]. The mechanism by which SAMHD1 inhibits LINE-1 retrotransposons is not completely understood, but mutant SAMHD1 versions of Aicardi-Goutières syndrome patients (section 1.2.8) showed a reduced ability to inhibit LINE-1 compared to non-mutated SAMHD1 versions [69]. In line with this, truncated SAMHD1 versions were used to study the SAMHD1 regions that impact LINE-1 inhibition. These experiments indicated that the region between the SAM and the HD domain as well as the HD domain itself are sufficient for LINE-1 inhibition. On the other hand, the SAM-domain deficient version was still able to inhibit LINE-1 activity [69]. More recently, it has been shown that SAMHD1's LINE-1 inhibition is regulated through phosphorylation at residue T592 [70]. For instance, the SAMHD1 mutant T592A (unable to be phosphorylated) blocked LINE-1 activity, but not infection with a VSV-G-pseudotyped HIV-1 reporter in 293T cells. In this mutant, the dNTPase activity of SAMHD1 was not impaired, pointing to two different mechanisms for dNTPase and LINE-1 inhibiting activity [70].

Secondly, another study demonstrated a role of SAMHD1 in DNA damage response. Daddacha *et al.* showed that after DNA damage, SAMHD1 localizes to the site of damage and recruits DNA repair proteins, thereby promoting homologous recombination [14]. In detail, SAMHD1 complexes with CtIP, a DNA damage repair protein essential for DNA end resection, an important step in 5'-end processing for the repair of DSBs [14]. In addition, SAMHD1 also has another way of promoting genome stability. It blocks the formation of DNA:RNA hybrids, so-called R-loops that are byproducts of transcription [71]. Especially in regions where the transcription and the replication machinery collide with each other (transcription-replication conflicts (TRCs)), the R-loop blockage through SAMHD1 promotes genomic stability [71].
Thirdly, Coquel *et al.* showed that SAMHD1 co-localizes with components of replication foci and is involved in the stress response to DNA replication by promoting the restart of stalled replication folks for DNA synthesis [72]. SAMHD1 was shown to increase the degradation of single-stranded DNA (ssDNA) by promoting MRE11, an exonuclease that degrades nascent DNA, a step essential for replication fork restart. In SAMHD1-deficient cells, ssDNA can accumulate in the cytosol inducing type I IFN expression. Therefore, SAMHD1 is also able to participate in the inhibition of IFN induction [72].
In addition, SAMHD1 shows a connection to the STING pathway. SAMHD1 has been shown to mediate apoptosis in infection with human T cell leukemia virus type 1 (HTLV-1) through STING [73]. Another publication showed that SAMHD1 prevents innate sensing of viral infection through cGAS/STING [74]. STING as a downstream target of SAMHD1 was also described in lung adenocarcinoma cells [75].
Also, another way of blocking innate immune responses through SAMHD1 was suggested through inhibition of the nuclear factor κB (NF-κB) and IFN pathways. As a response to viral infections, SAMHD1 interacts with NF-κB1/2 and lowers the phosphorylation levels of IκBα, a protein that inhibits NF-κB [76].
Finally, SAMHD1 is known to bind nucleic acids with a preference for RNA over DNA [77, 78]. This binding has been shown to contribute to the antiviral activity of SAMHD1 [79]. In 2015, SAMHD1 was postulated to exhibit RNase activity, which degrades retroviral genomic RNA during infection [21, 80]. In contrast, other groups have provided strong data evidence that question a ribonuclease activity as one of SAMHD1's additional functions [78, 81].

1.2.8 SAMHD1, innate immune response and Aicardi–Goutières syndrome

Aicardi–Goutières syndrome (AGS) represents a rare neurological, inflammatory disorder with an elevated type I IFN response associated with mutations in genes that are somehow involved in nucleic acid metabolism. There are seven AGS subtypes described, which are categorized by the particular gene that inherits the mutations: 3'-5' exonuclease TREX1 (AGS1), parts of the endonuclease complex RNASEH2 A (AGS2), B (AGS3) and C (AGS4), dsRNA editing protein ADAR1 (AGS6) and dsRNA sensor MDA5 (encoded

by *IFIH1*, AGE7) [82, 83]. In addition, mutations in the *SAMHD1* gene (AGS5) were described to be associated with AGS [84, 85].
In contrast to that, mice deficient for SAMHD1 are viable, healthy and apparently do not develop any disease [86, 87]. Even though the expression of IFNs and ISGs as well as intracellular dNTP levels were increased in comparison to wildtype mice, *Samhd1* KO in mice did not result in neurological or autoimmunological damage. Understanding the connection between SAMHD1 and the innate immune system will shed more light on the SAMHD1 in AGS and HIV-1 restriction [11].

1.2.9 SAMHD1, its expression in cancer and cancer-associated mutations

SAMHD1 plays a major role in regulating the dNTP pool, contributing to dNTP homeostasis as well as genome stability in the cell. Changes in the *Samhd1* sequence and subsequently in SAMHD1 protein levels are frequently found in and connected with cancer development. The Catalogue of Somatic Mutations in Cancer (COSMIC), the cBioPortal for cancer genomics and the genomic data commons of the National Cancer Institute (NCI) of the National Institute of Health (NIH) currently report more than 300 SAMHD1 mutations found in patient samples from different types of cancers. In addition, an analysis with the database of the International Cancer Genome Consortium (ICGC) even revealed 1542 mutations in SAMHD1 associated with cancer projects [88].
In the literature, SAMHD1 expression and/or activity impairment has been described both for solid tumors such as lung adenocarcinoma [89] and colon carcinoma [90] as well as for liquid tumors such as chronic lymphocytic leukemia (CLL) [91], cutaneous T cell lymphoma (CTCL) [35] and T cell prolymphocytic leukemia (T-PLL) [92], described in detail in the following paragraphs.
Firstly, lung cancer is the leading cause of cancer mortality worldwide and lung adenocarcinoma represents its most common type. SAMHD1 protein as well as *Samhd1* mRNA expression levels showed to be lower in lung adenocarcinoma patient samples compared to healthy tissue. This downregulation was shown to be mediated by DNA methylation of the *Samhd1* promoter [89]. In addition, genome sequencing of lung cancer also listed SAMHD1 mutations [93].
Secondly, SAMHD1 is frequently mutated in colon carcinoma, with many of these mutations associated to the reduction of SAMHD1 dNTPase activity. Appearance of certain mutations in a heterozygous fashion already showed huge impacts on SAMHD1 functionality. Imbalances in the dNTP pool were shown to increase mutation rates in this type of cancer [90], which may elevate cell proliferation and tumor cell growth [2].
Thirdly, CLL represents a liquid tumor with abnormal amounts of lymphocyte production in the bone marrow. SAMHD1 protein as well as *Samhd1* mRNA expression levels were also downregulated in patient cells compared to cells from healthy individuals. This phenomenon could be connected with mutations in SAMHD1, which were found in 11% of patients where CLL relapsed or where it did not respond to treatment (refractory) [91].

Interestingly, one of this SAMHD1 mutations, L244F, is also found in GBM patient tissue [94].
Next, CTCL represents a cancer from the immune system, where malignant CD4 T cells infiltrate into the skin. SAMHD1 protein as well as *Samhd1* mRNA expression levels have been shown to be downregulated in Sézary syndrome patients, a very aggressive form of CTCL [35]. This phenomenon could be mechanistically linked to DNA methylation in the *Samhd1* promoter, a way of SAMHD1 expression regulation already observed in lung adenocarcinoma (section 1.2.3.2) [35, 89].
Finally, T-PLL is a leukemia originating from mature T cells. Significant downregulation of SAMHD1 protein as well as *Samhd1* mRNA expression levels has been also observed in T-PLL patient material including SAMHD1 mutations compared to those without SAMHD1 mutations. Interestingly, these mutations did not increase cytarabine (ara-C) sensitivity, which generally is not very potent in T-PLL [92].
In addition to these tumor types described in literature, SAMHD1 mutations are also found in sequencing data from tumor tissues of other cancer types such as pancreatic cancer [95], myeloma [96] as well as GBM [97], summarized in [98]. The functional relevance of these SAMHD1 mutations is not described yet and further investigations are important to get a better understanding of the SAMHD1-tumor interplay.

1.2.10 SAMHD1 and cancer chemotherapy

In general, tumor cells exhibit highly elevated proliferation rates, which represents one of the hallmarks of cancer [99]. Subsequently, this made nucleotide metabolism an attractive therapeutic target and especially nucleoside analogues promising drugs in the treatment of several types of cancer [2]. Nucleoside analogues are intensively used to induce cell death in cancer cells e.g. through incorporation into cellular RNA or DNA and mediating termination of DNA and RNA synthesis [100].
In 2016, Schneider *et al.* identified SAMHD1 as a modulator of ara-C cytotoxicity [101], a chemotherapeutic drug used to treat acute myeloid leukemia (AML) [102]. SAMHD1 can not only cleave triphosphates from dNTPs, but can also use the active form of ara-C, ara-CTP, as a substrate [103]. The strong structural similarities between the naturally occuring nucleotide deoxycytidine triphosphate and its isomer ara-CTP are depicted in figure 1.3. SAMHD1 converts the active metabolite ara-CTP back into its non-active prodrug, reducing the toxicity in leukemic cells. In a large variety of SAMHD1-deficient and down-regulated AML cell lines, the sensitivity to ara-C was increased compared to SAMHD1-proficient cells. In addition, in a retrospective analysis, AML patients treated with ara-C could be grouped into high SAMHD1 and no/low SAMHD1 expression in their leukemic cells. Patients with no/low SAMHD1 expressing leukemic cells showed significantly longer OS when treated with ara-C, compared to patients with high SAMHD1-expressing leukemic cells. Therefore, SAMHD1 was proposed as a predictive biomarker for the therapeutic response to ara-C [101].
Notably, ara-C is not the only SAMHD1-dependent nucleoside analogue that is used for cancer chemotherapy. Other nucleoside analogues including gemcitabine, nelarabine,

decitabine, vidarabine, cladribine, clofarabine, fludarabine and trifluridine showed SAMHD1-associated cytotoxicity and are summarized in table 1.3 [102, 103, 104, 105].
One central publication by Oellerich *et al.* in 2019 analyzed nucleoside analogues that work as hypomethylating agents in AML treatment. The active metabolite of decitabine, decitabine triphosphate (DAC-TP), is a substrate of SAMHD1 as they observed a negative correlation between SAMHD1 expression and decitabine treatment efficacy as well as the number of patients that reached complete remission (CR) in AML. This correlation was not observed in patients treated with the SAMHD1-independent hypomethylating agent azacytidine. These data emphasized a SAMHD1-dependent cytotoxicity for decitabine in AML. As a result, SAMHD1 can be also used as a predictive marker for decitabine treatment in AML [106].
More recently, Rothenburger *et al.* also characterized T-cell and B-cell acute lymphoblastic leukemias (T-ALL, B-ALL) [107]. They also showed a negative correlation between the nucleoside analogue nelarabine and SAMHD1 expression in B-ALL and T-ALL. SAMHD1 is able to convert the active metabolite of nelarabine, arabinosylguanine (ara-G), back into its inactive prodrug. In addition, they propose a connection between low SAMHD1 expression in T-ALL and DNA methylation in the *Samhd1* promoter [107]. These studies emphasize that the SAMHD1 dependency of treatment outcome is not a single standing phenomenon only observed with a certain nucleoside analogue or a specific type of cancer.
Besides SAMHD1 being a major player in the cytotoxicity of nucleoside analogues, there is a list of other factors that can also influence the efficacy of nucleoside analogues [108]. Firstly, there are additional factors besides SAMHD1 that regulate the dNTP pool in the cell such as the ribonucleotide reductase (RNR), which is important in the biosynthesis of dNTPs [108]. Secondly, there are factors that interfere with the conversion of the analogue into its metabolically active form such as cytidine deaminase (CDA) [109]. Also, insufficient membrane transport reduces the uptake and thus cytotoxicity of nucleoside analogues (e.g. equilibrative nucleoside transporter (ENT-1), section 1.5.1). Finally, elevated activities of chemically modifying enzymes like DNA methyltransferases (DNMT) can reduce the potency of nucleoside analogues in cancer treatment [108]. Besides internal factors, also sufficient delivery and stability of the nucleoside analogues is an essential requirement for treatment efficacy.
Concerning SAMHD1, likely many more chemotherapeutic treatments with nucleoside analogues might suffer from this mechanism of resistance at current state, resulting in a poor treatment outcome. Additional studies of SAMHD1-associated sensitivity to chemotherapeutics in other cancer models will advance not only the field of personalized medicine, but will open new treatment possibilities for cancer types with until now very limited treatment options such as GBM.

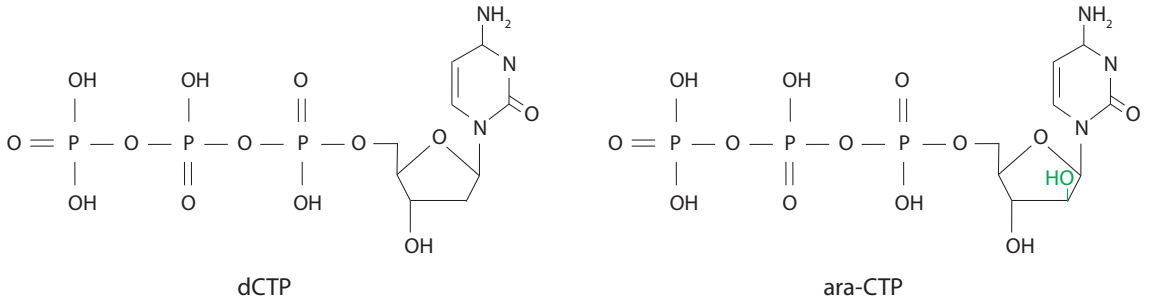

Figure 1.3: Structural similarity between physiological deoxycytidine triphosphate (dCTP) and arabinofuranosylcytosine triphosphate (ara-CTP), the active metabolite of the prodrug cytarabine (ara-C). In comparison to dCTP, ara-CTP carries a hydroxy group at the carbon 2 in the ribose ring [1, 103].

Table 1.3: Nucleoside analogues that are currently used as chemotherapeutic agents in tumor and other treatments as well as the respective substrate for SAMHD1, if SAMHD1 dependency is known. AML: acute myeloid leukemia, ALL: acute lymphocytic leukemia, MDS: myelodysplastic syndrome, CLL: chronic lymphocytic leukemia, T-ALL: T-cell acute lymphoblastic leukemia, NHL: Non-Hodgkin lymphoma [103, 104, 108, 110].

Analogues	Application	SAMHD1 substrate	Reference
Pyrimidine-based			
Azacytidine	MDS	not SAMHD1-dependent	[106]
Cytarabine	AML, ALL	ara-CTP	[101, 111]
Decitabine	MDS	DAC-TP	[105, 106]
Gemcitabine	pancreatic, lung, breast, bladder cancers	Gemcitabine-TP	[1]
Trifluridine	colorectal cancer	tF-dTP	[104]
Purine-based			
Cladribine	NHL, CLL	Cladribine-TP	[1]
Fludarabine	CLL	Fludarabine-TP	[1]
Nelarabine	T-ALL	ara-GTP	[107]
Vidarabine	epithelial keratitis	ara-ATP	[1, 104]
Fluoropyrimidine -based			
Capecitabine	relapsed breast, colorectal cancer	unknown SAMHD1 status	[108]
Clofarabine	ALL	Clofarabine-TP	[1, 102]
Fluorouracil	gastrointestinal, skin pancreatic, renal, head/neck, prostate, breast cancer	unknown SAMHD1 status	[108]

1.3 Glioblastoma multiforme

1.3.1 Classifications and cell origin

Glioblastoma multiforme (GBM, also referred to as grade IV astrocytoma or glioblastoma) represents the most common malignant primary tumor in the brain with a very poor prognosis [112, 113]. GBMs are classified as grade IV astrocytomas through the classification of tumors of the central nervous system (CNS) by the World Health Organization (WHO) [114]. GBMs can be distinguished into primary and secondary GBMs. Whereas primary GBMs develop directly from healthy tissue, secondary GBMs advance from lower-grade gliomas (LGG) I, II or III [115]. While most GBMs found in elderly patients classify as primary GBMs, secondary GBMs are more common in younger patients. GBMs can originate from three different cell types, i) neural stem cells (NSCs), ii) astrocytes that derived from NSCs and iii) oligodendrocyte precursor cells (OPCs) [116]. The major cell type from which the tumor originated from has been shown to have major impact on tumor development and prognosis, classifying GBMs into 3 subtypes: classical, proneural and mesenchymal. In general, a GBM of the proneural subtype is associated with a better prognosis compared to classical or mesenchymal subtypes. It is important to mention here that genomic analysis of whole tumor material showed that all subtypes can co-exist in one GBM and relative proportions need to be assessed to determine the major subtype present in the particular tumor [117]. Interestingly, the origin of cells also showed to affect drug sensitivity in GBM [118].

1.3.2 Prevalence, risk factors and properties

The survival after diagnosis with current state of the art treatment regimens averages at 14.6 months, with a 5-year survival rate of only 5% of all patients [113, 115, 119]. Despite the research done in this field for the past 40 years, the prognosis for GBM could barely be improved. Therefore, there is an urgent need for therapy improvements and treatment alternatives to fight GBM.
Primary brain tumors are tumors that originate in the brain and did not develop due to metastasis from other tissues. Approximately one third of primary brain tumors is malignant, from which 48% appear to classify as a GBM, emphasizing GBMs as the most common type of malignant primary brain tumor. GBM occurs in 3.19 out of 100.000 people (numbers from US population in 2010-2016). The tumor has a higher prevalence on the elderly population, where incidence increases with age with an average age of 64 years, peaking at 79 years (figure 1.4) [112, 113].
Concerning risk factors favoring the development of GBM, little is known. Increasing age and male gender have shown to be factors where GBM presents with higher incidence [113, 120]. While for most patients, no particular risk factor can be determined, a few hereditary cancer predispositions have been reported. One example here represents the familial tumor syndrome neurofibromatosis type 1, where high-grade gliomas such as GBM are 10-15 times more frequent compared to the rest of the population [112]. Despite

genetically-based risk factors, ionising radiation represents the only environmental risk factor with sufficient evidence [112].
GBMs are highly angiogenic (high vascularization within the tumor in order to secure nutrient flow and tumor growth) adding to heterogeneity and tumor aggressiveness [119]. In addition, they are highly invasive and diffusive, as they have the ability to invade the neighboring brain tissue and thereby destroy it [115]. Additional features represent atypical nuclei compared to healthy tissue, elevated mitotic activity, necrosis and microvascular proliferation, which are described as clusters of endothelial and smooth muscle cells [112, 121]. Nevertheless, metastasis is found in only less than 2% of GBM patients. The many physical and anatomic barriers in the brain are suspected to be responsible for this phenomenon. Mainly, the outest brain membrane closest to the skull (dura mater) as well as larger blood vessel membranes likely act as physical barriers to the tumor spreading. In addition, extracellular matrix proteins necessary for invasion of connective tissues are not present in tumors of the CNS [115].

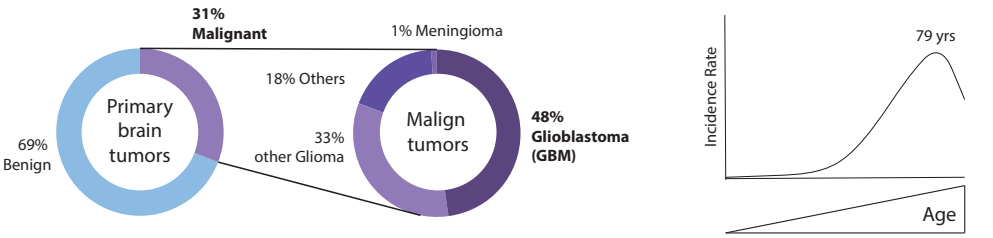

Figure 1.4: Primary brain tumors, GBMs and age distribution in adults from the central brain tumor registry of the United States of America (CBTRUS) 2010–2014 [112, 113].

1.3.3 Symptoms, diagnosis and biomarkers

Symptoms are very heterogeneous from patient to patient and are highly dependent on the location of the tumor [122]. In general, symptoms involve headache, nausea, vomiting, seizures, visual loss, general pain, cranial nerve disorders, weakness and numbness [122].
Diagnosis, prognosis and treatment strategies are closely connected in brain tumors. The more exact the diagnosis of the GBM is, the more predictable the course will be as well as more tailored and personalized the treatment can be. That is why, in addition to the WHO, an additional society called cIMPACT-NOW informs about molecular and practical approaches in CNS tumor taxonomy. They also introduced the terms NOS (Not Otherwise Specified) and NEC (Not Elsewhere Classified) for individual GBM cases that are difficult to categorize.
In general, biomarkers can be categorized into those that help to determine the exact glioma type (diagnostic biomarker), biomarkers that indicate the prognosis of the patient

(prognostic biomarker) and those biomarkers that predict how well a certain treatment will work (predictive biomarker).
Diagnosis is mainly performed through neuroimaging followed by intensive diagnostics of biopsy material or open tumor resection through histopathology and genomic/RNA/protein profiling [120]. Typical characteristics for a GBM obtained from resection diagnostics are chromosome aberrations such as gain of parts of chromosome 7 or loss of parts of chromosome 10. Aberrant expression of proteins (such as overexpression of the epidermal growth factor receptor (EGFR)) or gene mutations (e.g. in PTEN) represent another diagnostic approach for GBM [123].
The mutation status of the isocitrate dehydrogenase 1/2 (IDH1 at residue R132/IDH2 at residue R172) is crucial for GBM classification and prognosis. IDH is present mostly as wildtype in GBM [124], but in around 10% of diagnosed GBMs this gene is mutated resulting in an amino acid change to histidine (R132H/R172H), which is a marker for secondary GBM and correlated with prolonged overall survival (OS) [115].
The glioma GpG island methylator phenotype (G-CIMP) represents another characteristic that improved the classification and prediction process of GBMs within the last years [125]. The phenotype basically reflects the extent of DNA methylation in the tumor. Whereas G-CIMP-high tumors display more methylated promoter regions associated with gene silencing, G-CIMP-low tumors inherit loss of DNA methylation leading to chromatin reorganization and dysregulated gene expression. The G-CIMP-high phenotype has been shown to be enriched in the proneural subtype and associated with IDH-mutated gliomas, both indicators for a better prognosis. Also within IDH-mutated GBMs, patients with a G-CIMP-high status have a better prognosis in comparison to G-CIMP-low phenotypes [125].
In addition, the methylation status of the *MGMT* promoter (O^6-methylguanine-DNA methyltransferase) is a major prognostic marker for GBM. An unmethylated *MGMT* promoter is associated with *MGMT* gene expression, which reduces the treatment efficacy with the gold-standard chemotherapeutic temozolomide (TMZ, figure 1.6). The methylated form is quite common with 30-50% in primary GBMs; IDH wildtype GBMs show a methylated *MGMT* promoter, which is also favoring a better outcome [112]. The mode of action for TMZ as well as the influence of *MGMT* promoter methylation on TMZ efficacy is further described below in section 1.3.4. On the other hand, an example for a negative prognostic marker represents a mutation in the histone H3 K27M [112].
The glycoprotein antigen CD133 has been proposed as a marker for cells initiating the brain tumor [126]. Nevertheless, contradicting publications question this notion and show that CD133-negative cells can also initiate tumor growth [127].
Even though intensive research is done in finding blood-derived biomarkers contributing to a liquid biopsy (such as circulating tumor DNA (ctDNA), microRNAs and DNA mutations) in order to develop less invasive and early diagnosis possibilities, these technologies are not ready to substitute classical biopsy and diagnostics [123].

1.3.4 State of the art therapy

Despite the intense research and clinical trials performed in order to improve GBM therapy, the overall procedure after diagnosis has barely changed over the past years. The main procedure includes maximal tumor resection through surgery followed by radiation therapy and chemotherapy, mainly with TMZ [120]. The current state of therapy for GBM is summarized in figure 1.5, which shows again that detailed diagnostics before radiation and chemotherapy make a difference in treatment decisions and efficiencies. The following sections introduce the different current treatment options for GBM.

1.3.4.1 Surgical removal

As gold standard and first step after GBM diagnosis, surgery is being performed where the maximal tumor material is removed, but also on a maximal tissue safety level for intact healthy brain areas [120].
GBMs are found widespread throughout the brain. Nevertheless, the cerebrum of the brain (frontal, temporal, parietal and occipital lobes) represents the major location where GBMs are diagnosed. On the other hand, the cerebellum as well as the brain stem and the spinal cord rarely exhibit GBMs [115]. Depending on the location of the tumor and its closeness to particular brain areas, surgical resection may harbor difficulties.
In addition, the current state of the art visualization methods for tumor areas generally underestimate the tumor size and make it more difficult to resect as much tumor material as possible while not damaging healthy brain areas. Importantly, the higher the residual volume of the tumor after surgery, the worse the outcome is for the patient [120]. Current methods to localize and estimate the tumor size include magnetic resonance imaging (MRI), perfusion-assisted MRI and positron emission tomography (PET), which map a more realistic view of the tumor, including its heterogeneity [128]. Unfortunately, GBMs are diffusely infiltrative, which makes it nearly impossible to fully resect the tumor [123].

1.3.4.2 Radiation therapy

After surgical resection of the tumor material and intensive diagnostics, radiation therapy represents a standard treatment strategy for GBM (figure 1.5). The standard of care for over 15 years has been to treat with radiotherapy up to 60 Gy as fractions over a duration of 6 weeks adjuvanted with daily TMZ treatment (chemotherapy section below) [112]. The radiation frequency may be adjusted in an age-dependent manner or in patients with a poor profile for prognostic markers [120].

1.3.4.3 Chemotherapy

The major regimen used for chemotherapy in GBM is TMZ. It works as an alkylating agent that induces DNA DSBs resulting in cell cycle arrest and cell death [129]. As a standard of care since 2005, TMZ is given at the same time as radiation therapy with a TMZ extension of 6 *i.v.* infusion cycles (5 days over 21 days) after radiation therapy is completed [112, 120].

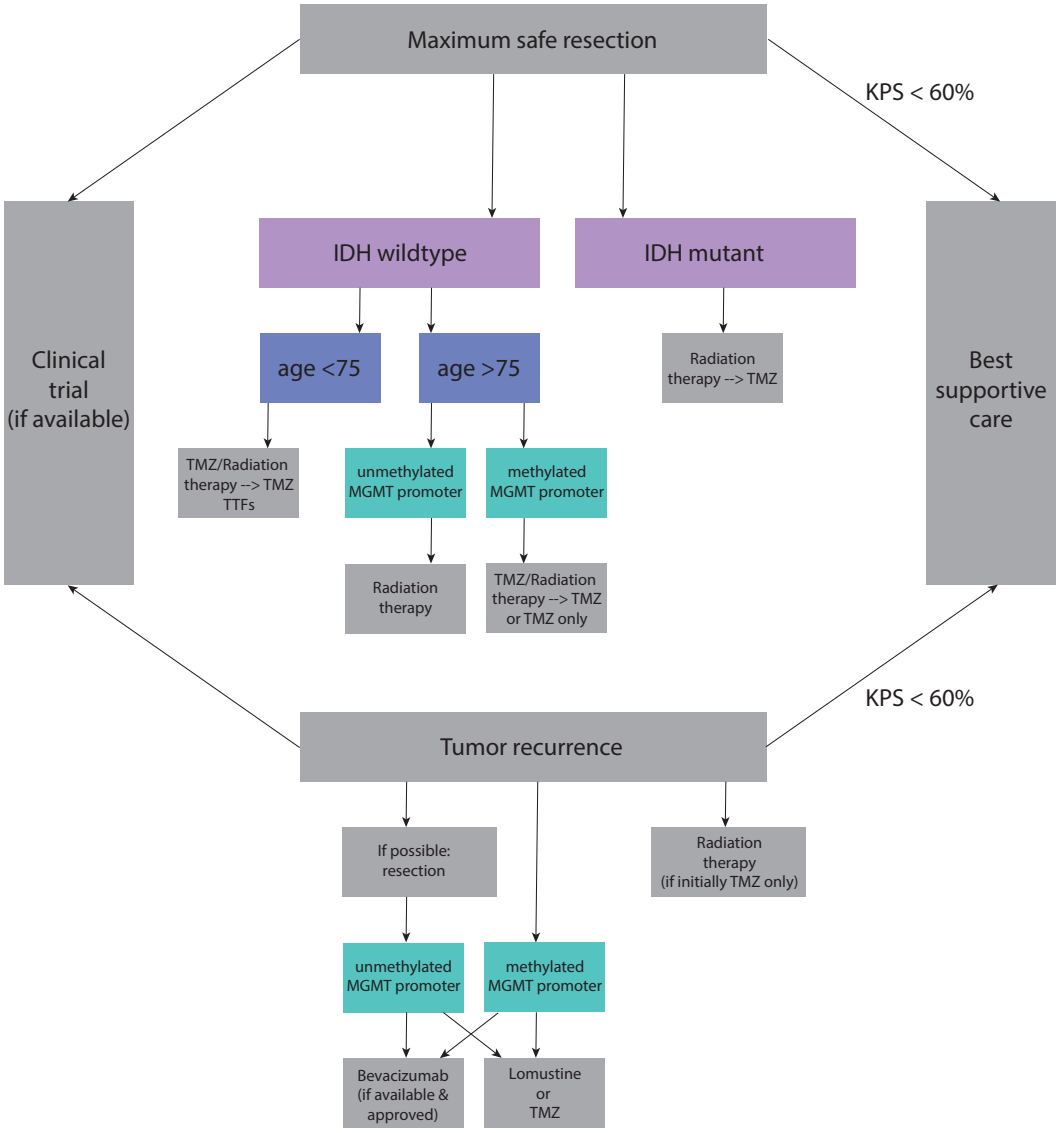

Figure 1.5: Current state of therapy approach for GBM. GTR: gross total resection, IDH: isocitrate dehydrogenase, KPS: karnofsky performance score, TTFs: tumor treating fields, MGMT: O^6-methylguanine-DNA methyltransferase, TMZ: temozolomide [120].

It has to be noted that while applied as a co-therapy to radiation, OS increases (so does the percentage of patients alive 2 years after first diagnosis), but it unfortunately has a very limited window of effect as compared to radiation therapy alone, as the median OS can only be extended by 2.6 months (from 12 to 14.6 months) [129]. In extreme cases, chemotherapy with TMZ alone might be the treatment of choice [120]. In addition, TMZ has a short half-life, making it necessary to apply with high dosages accompanying major side effects [129]. Notably, GBMs with a methylated *MGMT* promoter have been shown to be more sensitive to TMZ, whereas GBMs with an unmethylated *MGMT* promoter showed very limited TMZ treatment benefit [120]. TMZ methylates guanines at position O^6 amongst others, which gets repaired by MGMT. Low MGMT levels due to promoter methylation results in less repair and more mispairing leading to cell cycle arrest and cell death [130]. On the other hand, high MGMT levels due to an unmethylated promoter repairs the methylated guanines resulting in less efficient TMZ treatment (figure 1.6) [130]. Unfortunately, GBMs are incurable malignant brain tumors and will reoccur. In addition, the outcome after relapse is very poor and there are no treatment strategies that provide a better prognosis [120]. According to the current state of treatment, illustrated in figure 1.5, radiation therapy is applied if initial therapy was TMZ chemotherapy alone. In addition to TMZ for recurring GBM, two more chemotherapeutics are used: bevacizumab and lomustine (CCNU).
Bevacizumab is an anti-angiogenesis agent that is mainly used to treat recurrent GBM [120]. While it is Food and Drug Administration (FDA)-approved in the United States of America since 2009, it can not be used in the European Union, as it showed to only extent progression-free (PFS), but not overall survival (OS) [120].
CCNU is an alkylating agent. It is FDA-approved in the United States of America since 2017 and increases progression-free survival (PFS) in combination with bevacizumab [112]. Similar to TMZ, also treatment with lomustine does not show any benefit for patients with tumors that showed an unmethylated *MGMT* promoter [120].
The fact that the most effective and gold standard chemotherapeutic in GBM is a drug that shows really limited effect in terms of survival benefit, emphasizes that the development of alternative and improved treatment strategies for chemotherapy in GBM are essential and urgent.

1.3.4.4 Tumor treating fields

Tumor treating fields (TTFs) represent a low-intensity alternating electric field therapy that can be used to complement radiation- and chemotherapy, where intermediate frequencies around 200 kHz are used to inhibit tumor cell division [120, 131]. In 2017, a randomized clinial trial showed that adding TTFs to chemotherapy maintenance with TMZ significantly improved overall (OS) and progression-free survival (PFS) [131]. In order for it to be effective, the device needs to be worn and active for a minimal of 18 hours per day. Importantly, the positive effect could be seen in all patients independently of their age, sex, KPS, *MGMT* DNA promoter methylation status or the degree of their resection [112]. Since 2018, this treatment strategy is approved and used in Europe, Israel, Japan,

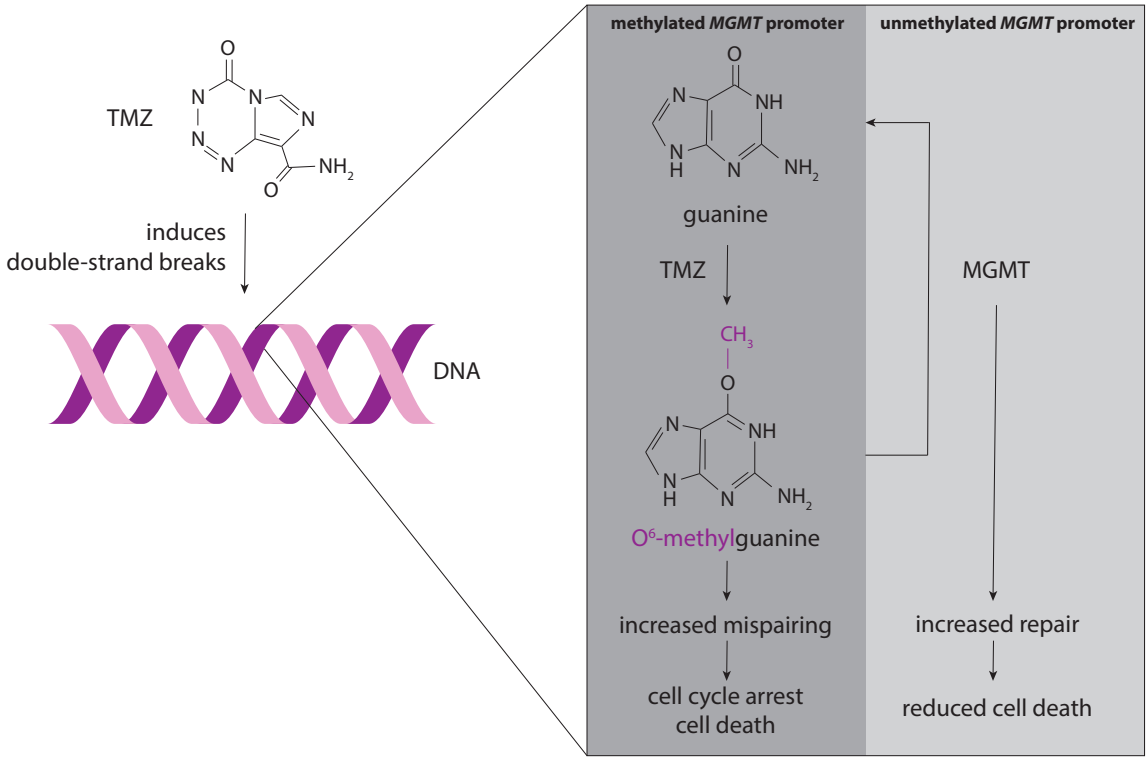

Figure 1.6: Mode-of-action for temozolomide (TMZ) and O^6-methylguanine-DNA methyltransferase (MGMT). TMZ induces double-strand breaks by methylating guanines at position O^6, which increases mispairing and leads to cell cycle arrest and cell death. In case the promoter of the *MGMT* gene is unmethylated, MGMT removes the methyl-group again from guanine, DNA repair can take place and cell death is reduced [130].

Australia and the United States of America (FDA-approved since 2011) [112].

1.3.5 Intra-, intertumoral heterogeneity and chemoresistance

While GBMs originate from astrocytes, NSCs or OPCs, they tumor consists of many more cell types besides tumor cells, including macrophages, microglia and a small portion of T cells [132, 133]. Together with stromal cells such as GBM-associated endothelial cells (ECs) and vascular cells, they form the tumor microenvironment (TME) that surround and interact with the cancer stem cells (CSCs) within the tumor. This contributes to the high levels of heterogeneity within the tumor [119, 130, 134]. Intratumoral heterogeneity in GBM occurs also because of selective pressures on the tumor cells including competition between cell clones and limited access to nutrients, which leads to optimal tumor cell growth in the microenvironment [134].

In addition to the high intratumoral heterogeneity, GBMs also differ immensely within each and every patient. Intertumoral heterogeneity arises due to the different properties of the cell from which the tumor originated from as well as the genetic and mutational shape of the cell [135]. The different microenvironment, in which the tumor resides, also strongly influences the individual tumor development [135].
Chemoresistance is a major issue in GBM treatment. In general, a tumor can be resistant to a chemotherapeutic treatment due to its genetic features and pro-tumor mutations already before the beginning of the treatment, e.g. *MGMT* promoter DNA methylation [130, 134]. On the other hand, chemoresistance can occur as a response to treatment [130]. In the TME, a more acidic pH (acidosis) and lower oxygen levels (hypoxia) play an important role in radio- and chemoresistance [130, 134]. In addition, one of the hallmarks of the TME is a strong immunosuppression eliminating a major self-protection mechanism and promoting tumor progress [130].
Another major phenomenon responsible for therapy resistance in GBMs is the constant formation of new blood vessels (angiogenesis) together with vascular collapse [115]. Constant proliferation leads to a non-optimal environment for the cells. Low oxygen levels result in both angiogenesis and migration of cells into a more optimal environment, which shapes in a strongly dynamic tumor that is changing over time and difficult to treat [115]. In addition, the ability of the tumor cells to migrate leads to movement of cells within the tumor and deep infiltration into neighboring brain areas [115, 119]. The large diversity of cells within the tumor as well as their high chemoresistance towards drugs represents a key issue in successful and effective therapy. Finally, the blood-brain barrier (BBB) blocks chemotherapeutics with certain characteristics from entering the brain, which rules out many possible treatment regimen when not applied intracranially [130].
All this taken together emphasizes how diverse and dynamic GBMs are, which makes it very difficult to correctly identify the tumor as well as to find an appropriate, successful treatment for it.

1.3.6 Current research on potential treatment strategies

In order to develop new and improved treatment strategies for GBM, many obstacles have to be overcome. The BBB represents a major barrier for the development of working therapeutics as it carefully selects, which molecules can penetrate the brain. This makes drug development and non-invasive application of chemotherapeutics an immense challenge for the treatment of GBM [112]. In addition, the heterogeneity of the tumor, the chemoresistance and the absence of well-established biomarkers represent major challenges for the development of alternative treatment strategies [112].
Unfortunately, very few clinical trials for GBM treatment made it into phase III so far, which is essential in the process of drug approval [112, 136]. The clinical trial database of the National Institute of Health (NIH) listed 1661 clinical trials for interventional GBM treatment, from which only 38 trials completed a phase III trial (https://clinicaltrials.gov/, 21st of December 2021). The trials contained both new therapeutic agents for GBM and combinatory therapies with radiation therapy or TMZ.

Using the patient's immune system for immunotherapy is currently an emerging field of research. One major branch here are oncolytic viruses [112]. Herpesvirus-based G207 or adenovirus-based DNX-2401 are two examples for approaches in GBM therapy that have been investigated in clinical trials, although with thus far very limited efficacy [137]. In addition, targeting specific genes and pathways through chemotherapy have been shown to be successful in the treatment of many cancers [112]. In the case of GBM treatment, promising candidates were molecules that inhibited tyrosine-kinase pathways as well as targeted angiogenesis, but unfortunately did not show significant clinical improvement [138]. Moreover, gene therapy to specifically modify cancer cells has been suggested as a promising alternative for GBM treatment [112].
In order to overcome the BBB, but also to be able to provide non-invasive applications for treatment, new technologies are developed that include the ability to bypass the BBB and deliver the chemotherapeutic agent directly into the tumor site [112]. Packaging the chemotherapeutically active component into a delivery system that can penetrate the BBB represents a major branch in research for brain tumor treatment. It has been shown that treatment with synthetic protein nanoparticles carrying the treatment regimen resulted in sufficient concentrations in the brain and increased OS and long-term survival in mice [139].
Whereas we more and more understand the biological mechanisms of oncogenesis in a GBM, a major challenge will be to transform this new knowledge into effective treatment strategies [112]. As common consent, it has to be emphasized that no single therapy alone will most likely be able to improve treatment for this complex tumor with dismal prognosis [112].

1.4 Acute myeloid leukemia

1.4.1 Prevalence, risk factors and cell origin

Acute myeloid leukemia (AML) is a malignant blood cancer originating from myeloid progenitor cells [140]. It includes genomic changes in the hematopoietic stem cells (HSCs) resulting in atypical cell proliferation and impaired myeloid cell differentiation [141]. While AML represents the most common type of acute leukemia, it is also the leukemia with the shortest survival rate (24% of patients alive 5 years after diagnosis) [140]. AML occurs in 4.3 out of 100.000 people (numbers from US population in 2016) and is with a median age of 68 years mainly a cancer disease of the elderly [140].
Even though the individual cause of AML development cannot be identified, known risk factors include exposure to radiation and mutagenic agents, such as alkylating drugs [141]. In addition, AML may develop from myelodysplastic syndrome (MDS), a bone marrow disease with impaired maturation and production of blood cells (hematopoiesis) [141].

1.4.2 State of the art chemotherapy

Ara-C represents the gold standard for chemotherapy of AML for over 40 years and is usually administered intravenously (*i.v.*) [142]. Low-dose (LD) treatments with ara-C represent the standard procedure and range of 100 to 200 mg/m^2 leading to plasma concentrations of 0.5-1 μM [109]. High-dose (HD) treatments with ara-C (2-3 g/m^2) can reach plasma concentrations higher than 10 μM [109]. While intravenous standard LD treatments for ara-C are not associated with CNS symptoms, HD ara-C can lead to severe side effects such as neurological toxicity [142]. On the other hand, HD ara-C has been associated with higher rates of relapse-free survival [143]. LD ara-C is used as a standard dosage for induction therapy of AML, whereas HD ara-C is mainly administered as a post-remission consolidation therapy [143]. Ara-C displays a very short half-life so that its concentration in the blood drops under the therapeutic range already 3 hours post-infusion [142].
Other chemotherapeutics used to treat AML include the intercalating agent daunorubicin or idarubicin (both anthracyclines), which show synergistic effects when given in combination with ara-C [144]. This therapy is usually referred to as 7+3 chemotherapy, where ara-C is infused for 7 days in combination with an anthracycline, daunorubicin or idarubicin, for the first three days [141]. In order to target tumor cells more specifically and to make sure that the majority of the drug concentration reaches the tumor cells, ara-C is now also approved to be formulated into liposomal formations together with daunorubicin [144].
Within the last years, a whole list of new chemotherapeutics were FDA-approved and partly European Medicines Agency (EMA)-approved for AML treatment [144]. Many of these newly approved therapies act as inhibitors and can be grouped into targeted therapy approaches, such as IDH or kinase inhibitors. In addition, a monoclonal antibody conjugated to a chemotherapeutically active metabolite is now approved against CD33, a major antigen expressed on the surface of leukemic cells [144]. Which chemotherapeutic strategy is optimal for the individual depends on age and general fitness of the patient, diagnostic analysis and the differentiation between newly diagnosed, relapsed or refractory AML [144].
After chemotherapy, a stem cell transplantation of hematopoietic stem cells can be an additional treatment strategy and needs to be considered according to the characteristics above as well as the donor-recipient fit [141].

1.4.3 Current research on potential treatment strategies

Even though many newly approved drugs for AML treatment entered the market over the last years, major challenges in the treatment of AML remain, specifically targeting the tumor cells, administration of the drug, chemoresistance and side effects arising from the treatments [141].
At the moment, researchers are developing more alternative strategies to fight AML [141, 144]. For example, manipulating a certain factor in the target cells in order to sensitize tumor cells to the chemotherapeutic treatment has been also shown by the example of

SAMHD1 protein expression in AML cells. As described before in section 1.2.10, SAMHD1 expression in target cells lowers the effectivity of ara-C in the treatment of AML [101] and therefore contributes to the ara-C chemoresistance [145]. Temporarily inhibiting or depleting SAMHD1 through combinational treatment with SAMHD1 inhibitors, Vpx-containing VLPs or *Samhd1* small interfering RNAs (siRNAs) represent a promising way to block the tumor's own influence on drug effectivity [101]. In addition, epigenetic therapy including hypomethylating agents such as the nucleoside analogue decitabine represent promising drug alternatives [105]. Whereas decitabine is still only FDA-approved for myelodysplastic syndrome (MDS), it is EMA-approved since 2012 for the treatment of *de novo* AML in elder patients [141].
Even though many chemotherapeutics target especially highly proliferating cells in the body (such as tumor cells, but also rapidly dividing healthy cells), most drugs in AML are given intravenously and thus systemically [141]. In order to increase the targeting of tumor cells, drugs conjugated with antibodies targeting specific tumor surface factors are developed such as the approved antibody conjugate for CD33 [144]. Basic research and clinical trials are being conducted to identify additional tumor surface markers, for example for the CD123 surface receptor [141]. In addition, antibody-conjugated, tumor-targeted drugs may reduce the currently massive side effects in AML.
Another major branch in AML treatment research is represented by nanocarrier technologies that can improve the contact between the compound and the target cells by increasing the half-life of the drug [141]. Packaging drugs into liposomes constitutes by far the most advanced technology, but other nanoparticles based on polymers or lipids are under development [141].
Finally, drug resistance remains a major issue in AML [146]. Major sources for chemoresistance in AML are proteins, including SAMHD1, that lower the effectivity of drugs. In addition, overexpressed/repressed/altered genes that code for proteins relevant in targeted therapy, impaired expression of miRNA that regulate cell division and DNA damage of the cells as well as impaired signal pathways are favoring the treatment survival of individual clones [145, 146]. Specific factors involved in ara-C chemoresistance are described in more detail in section 1.5.1.

1.5 Cytarabine

1.5.1 Mode of action and chemoresistance

Cytarabine (also 1'-β-d-arabinofuranosylcytosine, cytosine arabinoside or ara-C) is a nucleoside analogue of the physiological nucleoside cytidine (figure 3.1). Concerning chemoresistance to ara-C, there are many factors that can influence its effectivity. Sufficient expression of certain proteins is essential in the target cell. The expression of the equilibrative nucleoside transporter (ENT-1), for example, is very important for the treatment of target cells as it facilitates the uptake of ara-C to the cell [109]. Ara-C is a prodrug, which needs to be processed into the active metabolite ara-CTP through cellular factors: the deoxycytidine

kinase (dCK) phosphorylates ara-C into ara-C monophosphate (ara-CMP); pyrimidine kinases phophorylate ara-CMP into the metabolically active ara-CTP, which is cytotoxic in cells as it has the ability to incorporate into DNA and thereby competes with dCTP (figure 1.3 and 1.7) [109]. As a result, DNA synthesis terminates, DNA and RNA synthesis are blocked and cell death is triggered [109]. If ENT-1 and dCK are not expressed or only in low protein levels in target cells, ara-C is less effective [109].
On the other hand, there are cellular factors that reduce ara-C efficacy when expressed at high levels. Ara-CMP can be dephosphorylated back to ara-C by the enzyme 5'-nucleotidase II (NT5C2), which hinders ara-C of being processed into ara-CTP and lowers treatment efficacy [109]. In addition, the enzymes cytidine deaminase (CDA) and deoxycytidylate deaminase (DCTD) also lower ara-C efficacy; while CDA converts ara-C into the ara-U, DCTD converts ara-CMP into the ara-UMP and therefore removes ara-C molecules from the conversion pipeline into active metabolites (figure 1.7) [109]. Finally, also high levels of adenylate kinase isoenzyme 1 (AK1) reduce the efficacy of ara-C as it lowers the levels of the active ara-CTP by transferring a phosphate group from ara-CTP to ara-CMP [147]. High levels of intracellular dCTP itself also contribute to ara-C resistance. It competes with ara-CTP during the incorporation into DNA as well as inhibits dCK in a feedback loop [142]. Another point why chemotherapy with ara-C can be insufficient is the rather long time window of 12 hours between infusions. Ara-C is mostly active in the S phase during DNA replication [142]. While it has been shown that the S phase of AML cells from certain patients can last only 8 hours, there is a high likelihood that a certain fraction of AML cells will undergo their S phase during the treatment pause and thereby escape ara-C treatment [142].

1.5.2 Cytarabine in glioblastoma multiforme treatment

The chemotherapeutic agent ara-C is originally FDA-approved for treatment of AML. Taking an existing, approved drug and repurposing it for the treatment of another disease setting has many advantages: Toxicological studies have been completed, safety profiles have been established through already completed clinical trials and extensive data for patient applications are available. In the early 70s, a publication studied ara-C treatment of 5 different human GBM cell cultures isolated from different patients. The study indicated an effective ara-C-mediated growth inhibition in GBM cells that was dose-dependent [148]. Interestingly, ara-C has been shown to penetrate the BBB successfully [149]. In the past years, one clinical trial aimed to investigate the effect of ara-C treatment in recurrent GBM. Under the clinical trial number NCT01044966, ara-C encapsulated in liposomes (DepoCyt) was administered directly into a brain ventricle. Unfortunately, the study was terminated due to low recruitment numbers. In a case report from 2020, data was presented for two of these patients. MR imaging of the brain before and after DepoCyt treatment cycles showed promising results as the tumor volume was largely decreased after treatment and not longer detected through MR imaging [150]. This state was prolonged by constant treatment with a potential survival benefit, whereas repeated tumor progression was observed 4-6 weeks after termination of treatment [150].

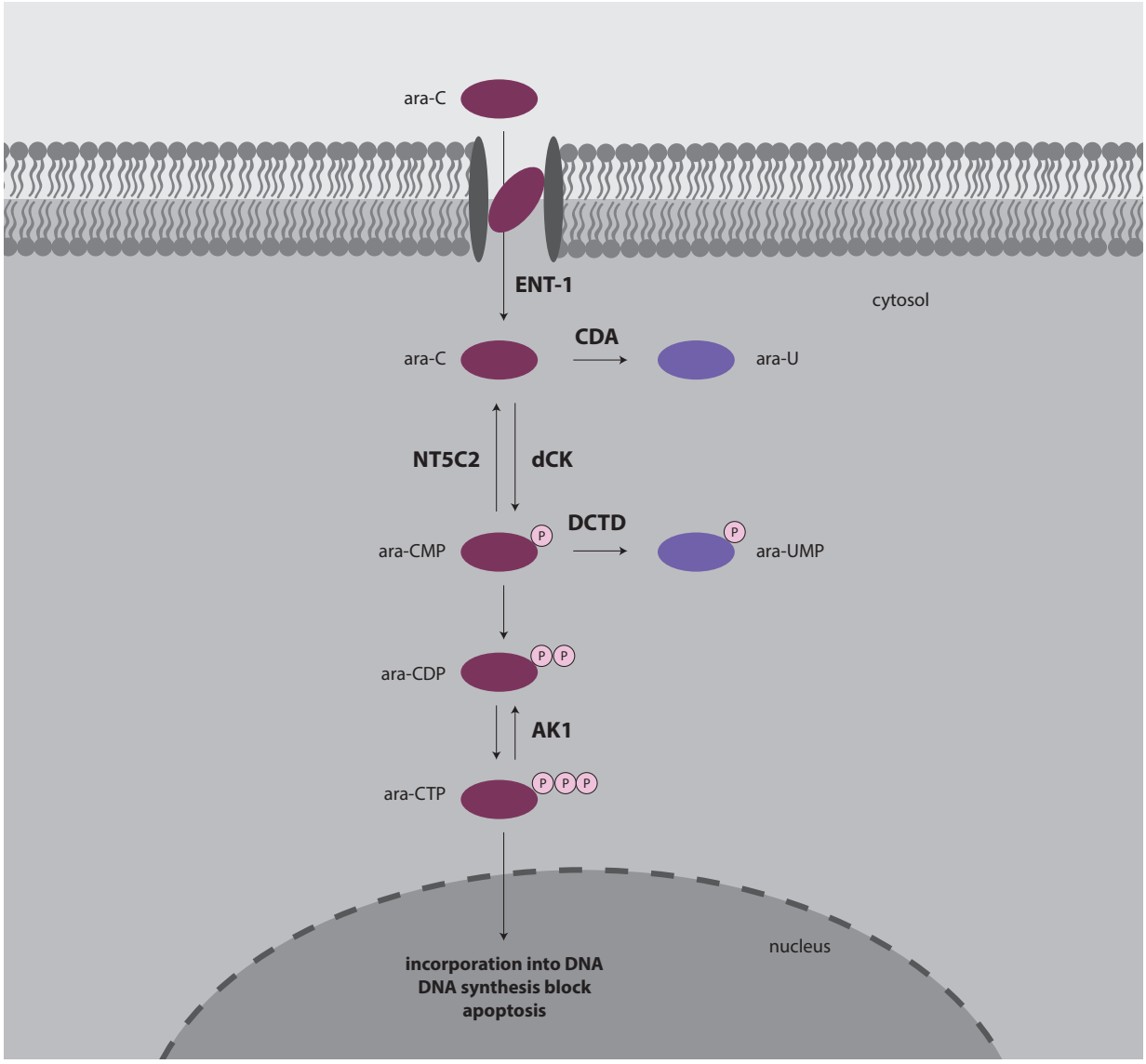

Figure 1.7: Metabolic pathway of the prodrug ara-C into its active metabolite ara-CTP. The prodrug ara-C is taken up into the cell by the equilibrative nucleoside transporter (ENT-1). The deoxycytidine kinase (dCK) phosphorylates ara-C into ara-C monophosphate (ara-CMP) and then pyrimidine kinases phophorylate ara-CMP into the metabolically active ara-CTP. On the other hand, 5'-nucleotidase II (NT5C2) dephosphorylates ara-CMP back to ara-C. In addition, cytidine deaminase (CDA) converts ara-C into ara-U, deoxycytidylate deaminase (DCTD) converts ara-CMP into ara-UMP and adenylate kinase isoenzyme 1 (AK1) converts ara-CTP into ara-C diphosphate (ara-CDP) [147]. The active metabolite ara-CTP then enters the nucleus, incorporates into DNA, DNA synthesis gets blocked and the cell enters apoptosis [101, 109].

Chapter 2

Aim of the Thesis

Glioblastoma multiforme (GBM) represents the most common, malignant tumor with origin in the brain [112, 113]. Despite the effort in research and clinical trials within the past centuries, treatment of GBM has remained very limited and ineffective - barely increasing the overall survival. In terms of GBM chemotherapy, TMZ still represents the gold standard, a chemotherapeutic which barely improves overall survival when administered together with radiotherapy in comparison to radiotherapy alone [129]. This emphasizes an essential need for advancing the chemotherapy options with additional treatment strategies in GBM. The absence of the dNTPase SAMHD1, a restriction factor well known in HIV-1 and other retro- and DNA viruses [53], has been shown to sensitize to cytarabine (ara-C) treatment in the chemotherapy of acute myeloid leukemia (AML) [101]. By recognizing the nucleoside analogue ara-C's active metabolite ara-CTP as a substrate, SAMHD1 converts ara-CTP back into its inactive prodrug ara-C, thus reducing its antitumoral efficacy [103].

The aim of this thesis is to validate whether SAMHD1 affects ara-C treatment also in the context of GBM. Therefore, we first analyze the protein expression profile of SAMHD1 in GBM cell lines, patient-derived xenografts (PDXs) and primary GBM tumor material. In addition, the *Samhd1* promoter methylation status is studied as a modulator for SAMHD1 expression in the context of GBM. Then, the role of SAMHD1 and its importance in the chemosensitization to the nucleoside analogue ara-C in the context of GBM chemotherapy is investigated. Therefore, different SAMHD1-proficient and -deficient GBM models are examined for ara-C toxicity. Finally, SAMHD1 mutant studies including mutations with relevance in SAMHD1 function and cancer as well as mutations found in GBM patients are studied for their impact on ara-C sensitivity and potential clinical relevance.

Chapter 3

Material and Methods

3.1 Material

3.1.1 Chemicals and reagents

Product	Article number	Vendor
Acetic acid, glacial	2234.1000	Chemosolute, Th. Geyer
Agarose	3810.3	Carl Roth
Albumin fraction V (BSA)	8076.3	Carl Roth
Ampicillin (D-α-Aminobenzylpenicilline sodiumsalt)	K029.4	Carl Roth
Calcium chloride	A119.1	Carl Roth
Carbenicillin (α-Carboxypenicilline disodiumsalt)	6344.3	Carl Roth
CellTiter-Glo® 2.0 assay	G9243	Promega
Ciprofloxacin Kabi, solution for infusion, 200 mg/100 ml	PZN: 3506088	Fresenius Kabi Austria GmbH
Clarity western ECL substrate	1705061	Biorad
Dimethylsulfoxide (DMSO)	4720.2	Carl Roth
dNTP mix, 10 mM	R0192	Thermo Fisher Scientific
1,4-Dithiothreit (DTT)	6908.2	Carl Roth
Dulbecco's phosphate buffered saline (PBS)	P04-36050P	Pan-Biotech
EDTA-free protease inhibitor cocktail cOmplete, Mini	11836170001	Roche
Ethylenediaminetetraacetic acid disodiumsalt-dihydrate (EDTA)	2216.1000	Chemsolute, Th. Geyer
Fetal bovine serum (FBS)	F7524	Sigma-Aldrich

Continued on next page

Product	Article number	Vendor
Gel loading dye purple, 6x	B7024S	New England Biolabs
Gylcerin	2050.1011	Th. Geyer
Human methylated and non-methylated (WGA) DNA set	D5013	Zymo Research
Hydrochloride acid (HCl, 32%)	P074.3	Carl Roth
Kanamycinsulfate	T832.2	Carl Roth
Linear polyethylenimine (PEI)	23966	Polysciences
Lipofectamine™ 2000 transfection reagent	11668019	Thermo Fisher Scientific
Lipopolysaccharides (LPS) from *Escherichia coli*	L6529-1MG	Sigma-Aldrich
Lysogenic broth (LB) acc. Miller powder	8885.0500	ChemSolute, Th. Geyer
Magnesium chloride hexahydrate	105833	Merck
Methanol, 100%	1437.2511	ChemSolute, Th. Geyer
Milk powder	T145.3	Carl Roth
Nonidet P40 (NP-40)	A1694	PanReac Applichem
Nuclease-free H_2O	129114	Qiagen
NucleoZOL	740404.200	Macherey-Nagel
PageRuler™ plus prestained protein ladder, 10 to 250 kDa	26619	Thermo Fisher Scientific
Paraformaldehyde (PFA)	A3813.1000	Applichem
Penicillin/Streptomycin (P/S), 10.000U/ml	P0781-100ml	Sigma-Aldrich
Proteinase K (recombinant PCR grade), 20 mg/ml	EO0491	Thermo Fisher Scientific
Recombinant human M-CSF	300-25-50μg	Peprotech
RNase-free H_2O	B-003000-WB-100	Dharmacon
SmartLadder, 200 to 10000 bp	MW-1700-10	Eurogentec
Sodium azide (NaN_3)	4221.1	Carl Roth
Sodium chloride (NaCl)	9265.2	Carl Roth
Sodium hydroxide (NaOH, 50%)	8655.1	Carl Roth
SuperSignal™ west pico PLUS chemiluminescent substrate	34577	Thermo Fisher Scientific
SYBR safe DNA gel stain	S33102	Thermo Fisher Scientific
TaqMan fast advanced master mix	44-449-64	Applied Biosystems
Terrific broth (TB) medium	8049.0500	ChemSolute, Th. Geyer
Tris(hydroxymethyl)aminomethane (Tris)	T1503-1KG	Sigma-Aldrich

Continued on next page

Product	Article number	Vendor
Triton X-100	39795.01	Serva
Trypsin-EDTA solution, 10x	T4174-100ml	Sigma-Aldrich

3.1.2 Buffers and solutions

3.1.2.1 Commercial buffers

Product	Article number	Vendor
BD cytofix fixation buffer	554655	BD Biosciences
BD perm buffer III	558050	BD Biosciences
BD perm/wash Buffer	554723	BD Biosciences
CutSmart buffer, 10x	B7204S	New England Biolabs
NuPAGE LDS sample buffer, 4x	NP0007	Thermo Fisher Scientific
NuPAGE MOPS SDS running buffer, 20x	NP0001	Thermo Fisher Scientific
NuPAGE Transfer Buffer, 20x	NP0006	Thermo Fisher Scientific
Phusion HF buffer, 5x	F518L	Thermo Fisher Scientific
Phusion GC buffer, 5x	F519L	Thermo Fisher Scientific
T4 DNA ligase reaction buffer, 10x	B0202S	New England Biolabs

3.1.2.2 Buffer preparations

Buffer	Composition
Direct lysis buffer	10 mM Tris pH 7.5, 1 mM $CaCl_2$, 3 mM $MgCl_2$, 1 mM EDTA, 1% Triton X-100
FACS buffer	1xPBS, 1% inactivated, sterile-filtered FBS, 2 mM EDTA
Hunt lysis buffer	20 mM Tris-HCl pH 8.0, 100 mM Sodium chloride, 1 mM EDTA, 0.5% NP-40
Tris-acetate-EDTA (TAE) buffer, 50x	242 g Tris, 57.1 ml Acetic acid, 18.6 g EDTA
Tris buffered saline (TBS) buffer, 10x, pH 7.5	121 g Tris, 175.2 g Sodium chloride

3.1.2.3 Solution preparations

Solution	Composition
Antibody solution	1xTBS, 1% BSA, 0.09% Sodium azide
50 mg/ml Antibiotic stocks	2 g of antibiotic in 40 ml Milli-Q H_2O, sterile filtered
4% Paraformaldehyde (PFA), pH 7.2	20 g PFA in 450 ml 60°C warm Milli-Q H_2O under constant stirring for 10 minutes, 50 ml of 10xPBS at room temperature, sterile filtered
1 mg/ml Polyethylenimine (PEI, linear), pH 7.0	250 mg PEI in 250 ml 70°C warm Milli-Q H_2O, sterile filtered

3.1.3 Media

3.1.3.1 Commercial media

Product	Article number	Vendor
Dulbecco's modified eagle medium (DMEM), high glucose, GlutaMAX™ supplement, pyruvate	31966047	Thermo Fisher Scientific
Iscove's liquid medium with stable glutamine (IBM)	FG0465	Merck
Iscove's modified dulbecco's medium (IMDM), GlutaMAX™ supplement	31980048	Thermo Fisher Scientific
Opti-MEM™ I reduced serum medium	31985070	Thermo Fisher Scientific
Roswell park memorial institute medium 1640 (RPMI), GlutaMAX™ Supplement	64870-010	Thermo Fisher Scientific
SOC outgrowth medium (super optimal broth with catabolite repression)	B9020S	New England Biolabs

3.1.3.2 Media preparations

Bacterial media	Composition
Agar plates	6.25 g Agar in 500 ml LB medium, 1:500 50 mg/ml antibiotic stocks
Lysogenic broth (LB) medium	25 g in 1000 ml heated Milli-Q H_2O, autoclaved at 121°C for 15 minutes, 1:1000 50 mg/ml antibiotic stocks
Terrific broth (TB) medium	47.6 g in 1000 ml heated Milli-Q H_2O, 4 ml Glycerin, autoclaved at 121°C for 15 minutes, 1:1000 50 mg/ml antibiotic stocks

Freezing media for cell lines	Composition
AML cell lines	IBM/IMDM (no additives), 20% FBS, 5% DMSO
Jurkat	RPMI (no additives), 20% FBS, 10% DMSO
LN-18	DMEM (no additives), 5% FBS, 5% DMSO
All other GBM cell lines	DMEM (no additives), 20% FBS, 10% DMSO

Special cell culture media	Composition
Collection medium for sorting	Respective cell culture medium, 20% FBS, 1% Penicillin/Streptomycin, 1:500 200 mg/ 100 ml Ciprofloxacin Kabi solution

3.1.4 Commercial kits

Product	Article number	Vendor
CloneJET PCR cloning kit	K123	Thermo Fisher Scientific
DNeasy blood and tissue kit	69506	Qiagen
EZ DNA methylation kit	D5002	Zymo Research
High-capacity RNA-to-cDNA kit	4387406	Thermo Fisher Scientific

Continued on next page

Product	Article number	Vendor
NucleoBond xtra midi plasmid DNA purification	740410.100	Macherey-Nagel
NucleoBond xtra maxi plasmid DNA purification	740414.100	Macherey-Nagel
Neon™ transfectionsystem 100 μl Kit	MPK10025	Invitrogen, Thermo Fisher Scientific
NucleoSpin® gel and PCR clean-up	740609.250	Macherey-Nagel
Pierce bicinchoninic acid (BCA) protein assay kit	23227	Thermo Fisher Scientific
QIAprep spin miniprep kit	27106	Qiagen
TaqMan™ RNase P control reagents kit, 20x	4316844	Thermo Fisher Scientific

3.1.5 Enzymes

Product	Article number	Vendor
Antarctic phosphatase, 5 units/μl	M0289S	New England Biolabs
BamHI-HF, 20 units/μl	R3136S	New England Biolabs
DpnI, 20 units/μl	R0176S	New England Biolabs
EcoRI-HF, 20 units/μl	R3101S	New England Biolabs
HotStarTaq DNA polymerase, 5 units/μl	203203	Qiagen
Phusion high fidelity DNA polymerase, 2 units/μl	F530L	Thermo Fisher Scientific
SbfI-HF, 20 units/μl	R3642S	New England Biolabs
SpeI-HF, 20 units/μl	R3133S	New England Biolabs
T4 DNA ligase, 400 units/μl	M0202S	New England Biolabs

3.1.6 Drugs

Product	Article number	Vendor
Cytosine β-D-arabinofuranoside hydrochloride (cytarabine, ara-C)	C6645-500MG	Sigma-Aldrich

Continued on next page

Product	Article number	Vendor
$^{13}C_3$ ara-C	C998102	Toronto Research Chemicals

3.1.7 Cell lines

3.1.7.1 Bacterial cell lines

Name	Description	Source
DH5α	chemical competent *Escherichia coli* for cloning	MAX efficiency™ DH5α competent cells, 18258012, Thermo Fisher Scientific
STBLII	chemical competent *Escherichia coli* for cloning with unstable inserts	MAX efficiency™ Stbl2™ competent cells, 10268019, Thermo Fisher Scientific

3.1.7.2 Human cell lines

All GBM and AML parental cell lines used in this thesis were provided by Jindrich Cinatl laboratories (University Hospital Frankfurt, Germany). THP-1 *Samhd1* KO B7 was generated in collaboration with the Veit Hornung laboratories (LMU Munich, Germany) for the publication Schneider *et al.* [101]. All PDX lines were cultivated by the Prof. Rainer Glaß laboratories (LMU Munich, Germany) for Line11, NCH421k, NCH441 and NCH644 as well as by the Dr. Massimo Squatrito laboratory (CNIO, Madrid, Spain) for H543, H561, BTSC268, BTSC409, BTSC349, BTSC380 and BTSC407.

GBM cell lines	Description	Cultivation
A-172	Grade IV	
G62	Grade IV	
GMS-10	Grade IV	
GOS-3	Grade IV	
HROG17	Grade IV	

Continued on next page

GBM cell lines	Description	Cultivation
LN-18	Grade IV from right temporal lobe	DMEM, 10% FBS, 1% P/S for all lines
LN-229	Grade IV	
LN-405	Grade IV	
MZ-18	Grade IV	
T98-G	Grade IV	
TU132	Grade IV	
TU140	Grade IV	
U-87 MG	Grade IV	
U-138 MG	Grade IV	
U-251 MG	Grade IV	

AML cell lines	Description	Cultivation
HEL	Acute erythroid leukemia	
HL-60	Adult AML	
Jurkat	T lymphocyte cells derived from T cell leukemia	
Monomac6	Adult acute monocytic leukemia (AMOL)	IBM/IMDM, 10% FBS, 1% P/S for all lines
MV4-11	Pediatric AMOL	
OCI-AML3	Adult AML	
THP-1	Monocytic cell line derived from AMOL	

Other cell lines	Description	Cultivation
ANA-1	Murine macrophage cell line	DMEM, 10% FBS, 1% P/S
HEK 293T	Embryonic kidney cells encoding SV40 T-antigen and neomycin resistance	DMEM, 10% FBS, 1% P/S

3.1.8 Plasmids

Name of construct	Description	Source/Publication
pMini_U6_gRNA 1 SAMHD1_CMV_mCherry _T2A_Cas9	Mammalian expression vector containing Cas9 and gRNA for KO generation in Samhd1 gene	Veit Hornung laboratories (LMU Munich, Germany)
pCMVΔ8.9	Packaging vector for lentiviral vector production	Wolfgang Hammerschmidt laboratories (Helmholtz Center Munich, Germany)
pMD2.G VSV-G	VSV-Glycoprotein, Envelope vector for lentiviral vector production	Wolfgang Hammerschmidt laboratories (Helmholtz Center Munich, Germany)
pDEST.H2B.iRFP670	HIV transfer vector expressing iRFP670 localized in nucleus	Wolfgang Hammerschmidt laboratories (Helmholtz Center Munich, Germany)
pCDH-EF1α-BFP-1	HIV transfer vector expressing mtagBFP	Wolfgang Hammerschmidt laboratories (Helmholtz Center Munich, Germany)
pGEX-4T-1 His-SAMHD1	Bacterial expression vector expressing human SAMHD1	Yong Xiong laboratories (Yale School of Medicine, USA)
pCDH-EF1α-SAMHD1 WT-BFP-1 natural sequence	HIV transfer vector expressing SAMHD1 wildtype	Cloned within this thesis
pCDH-EF1α-SAMHD1 mutations-BFP-1 natural sequence	HIV transfer vector expressing SAMHD1 mutations	Cloned within this thesis
SIV-3+ R-	SIV packaging vector containing Vpx	Thomas Gramberg laboratories (University Hospital Erlangen, Germany) [151]
SIV-3+ R-X-	Empty SIV packaging vector	Thomas Gramberg laboratories (University Hospital Erlangen, Germany) [151]

3.1.9 Primers

3.1.9.1 Primers for bisulfite sequencing

Primer	Sequence 5' → 3'	T_M (°C)
STS19_SAMHD1_3_fwd	AGGTTTTTTTTAAGTTTGGGGTATTT	55.5
STS20_SAMHD1_3_rev	CAAACTCACTAACAATTAAACCCTTC	55.5

3.1.9.2 Primers for cloning

Primer	Sequence 5' → 3'	T_M (°C)
STS27_fwd	CCTAGGATCCCTTCATTGGGTCATCT TTAAAAAGCTGG	62.0
STS28_rev	CCTAGAATTCGCCACCATGCAGCGAG CCGATTCCG	62.0

3.1.9.3 Primers for directed mutagenesis

For the annealing temperatures indicating a "gradient pooled", the temperatures 62-72°C were used.

Primer	Sequence 5' → 3'	T_M (°C)
STS85_D311A_fwd	GAGATAGTATCTAATAAAAGAAATGG CATTGATGTGGCCAAATGGGATTATT TTGCCAGGGACTG	gradient pooled
STS86_D311A_rev	CAGTCCCTGGCAAAATAATCCCATTT GGCCACATCAATGCCATTTCTTTTAT TAGATACTATCTC	
STS42_D137N_fwd	CTCTCCTCGTCCGAATCATTAATACA CCTCAATTTCAACGTCTTC	gradient pooled
STS43_D137N_rev	GAAGACGTTGAAATTGAGGTGTATTA ATGATTCGGACGAGGAGAG	
STS44_T592A_fwd	CGATGTTATAGCCCCACTCATAGCAC CTCAAAAAAAGGAATGGAACG	gradient pooled
STS45_T592A_rev	CGTTCCATTCCTTTTTTTGAGGTGCT	

Continued on next page

Primer	Sequence 5' → 3'	T_M (°C)
	ATGAGTGGGGCTATAACATCG	
STS46_T592E_fwd	CGATGTTATAGCCCCACTCATAGAAC	gradient
	CTCAAAAAAAGGAATGGAACG	pooled
STS47_T592E_rev	CGTTCCATTCCTTTTTTTGAGGTTCT	
	ATGAGTGGGGCTATAACATCG	
STS48_T592D_fwd	GGCGATGTTATAGCCCCACTCATAGA	58.7
	TCCTCAAAAAAAGGAATGGAACGACAG	
STS49_T592D_rev	CTGTCGTTCCATTCCTTTTTTTGAGG	
	ATCTATGAGTGGGGCTATAACATCGCC	
STS50_D207N_fwd	CAGATTGCTGGACTTTGTCATAATCT	gradient
	CGGTCATGGGCCATTTTC	pooled
STS51_D207N_rev	GAAAATGGCCCATGACCGAGATTATG	
	ACAAAGTCCAGCAATCTG	
STS52_Q548A_fwd	CTGCCAGAGAAATTTGCAGAGGCGCT	58.7
	GATTCGAGTATATTGTAAGAAGGTGG	
STS53_Q548A_rev	CCACCTTCTTACAATATACTCGAATC	
	AGCGCCTCTGCAAATTTCTCTGGCAG	
STS54_K405R_fwd	GAGATTACAGGTGCTGGAGGAAGAAA	gradient
	GTATCGCATTTCTACAGCAATTG	pooled
STS55_K405R_rev	CAATTGCTGTAGAAATGCGATACTTT	
	CTTCCTCCAGCACCTGTAATCTC	
STS56_K484T_fwd	CAAAAGAGGTTGCCAGTGCTACACCC	58.7
	AAAGTATTGCTAGACGTG	
STS57_K484T_rev	CACGTCTAGCAATACTTTGGGTGTAG	
	CACTGGCAACCTCTTTTG	
STS58_R451A/L453A	GCACGAGAGATTTTAAAACAAATTGA	gradient
_fwd	ATACGCTAATGCATTCAAGTATGTGG	pooled
	GTGAGACG	
STS59_R451A/L453A	CGTCTCACCCACATACTTGAATGCAT	
_rev	TAGCGTATTCAATTTGTTTTAAAATC	
	TCTCGTGC	
STS60_V133I_fwd	GAGCTCCACCCTCTCCTCATCCGAAT	55.5
	CATTGATACACCTCAATTTCAAC	
STS61_V133I_rev	GTTGAAATTGAGGTGTATCAATGATT	
	CGGATGAGGAGAGGGTGGAGCTC	
STS62_A338T_fwd	CAAAATAATTTTGATTACAAGCGCTT	gradient
	TATTAAGTTTACCCGTGTCTGTGAAG	pooled
	TAGACAATGAG	
STS63_A338T_rev	CTCATTGTCTACTTCACAGACACGGG	
	TAAACTTAATAAAGCGCTTGTAATCA	

Continued on next page

Primer	Sequence 5' → 3'	T_M (°C)
	AAATTATTTTG	
STS64_R366H_fwd	CTGTATGACATGTTCCACACTCACAA	gradient
	CTCTTTACACCGTAGAGCTTATC	pooled
STS65_R366H_rev	GATAAGCTCTACGGTGTAAAGAGTTG	
	TGAGTGTGGAACATGTCATACAG	
STS66_D497Y_fwd	GACGTGAAACTGAAGGCTGAATATTT	gradient
	TATAGTGGATGTTATCAACATGGATT	pooled
	ATGG	
STS67_D497Y_rev	CCATAATCCATGTTGATAACATCCAC	
	TATAAAATATTCAGCCTTCAGTTTCA	
	CGTC	
STS68_R145Q_fwd	GATACACCTCAATTTCAACGTCTTCA	gradient
	ATACATCAAACAGCTGGGAGG	pooled
STS69_R145Q_rev	CCTCCCAGCTGTTTGATGTATTGAAG	
	ACGTTGAAATTGAGGTGTATC	
STS82_S33A_fwd	CCGCAGAGGCAGACTGGGCCCCGGGC	gradient
	CTGGAACTCC	pooled
STS83_S33A_rev	GGAGTTCCAGGCCCGGGGCCCAGTCT	
	GCCTCTGCGG	
STS125_L244F_fwd	CAGTTATGATGTTTGAGCACTTTATT	gradient
	AATTCTAATGGAATTAAG	pooled
STS126_L244F_rev	CTTAATTCCATTAGAATTAATAAAGT	
	GCTCAAACATCATAACTG	
STS147_A30T _fwd	CAAACACCCCTTCCGCAGAGACAGAC	gradient
	TGGTCCCCGGGCCTGG	pool
STS148_A30T _rev	CCAGGCCCGGGGACCAGTCTGTCTCT	
	GCGGAAGGGGTGTTTG	
STS129_R531S_fwd	CCCCAACAGAGCAATCAGCATTACTA	gradient
	AAAACCAGG	pooled
STS130_R531S_rev	CCTGGTTTTTAGTAATGCTGATTGCT	
	CTGTTGGGG	
STS131_A565T_fwd	GAAAGAGTTTGTATGCCACAAGACAA	gradient
	TATTTTGTTCAG	pooled
STS132_A565T_rev	CTGAACAAAATATTGTCTTGTGGCAT	
	ACAAACTCTTTC	
STS133_F578L_fwd	GTGTGCAGACAGAAATTTGACCAAGC	gradient
	CGCAGGATG	pooled
STS134_F578L_rev	CATCCTGCGGCTTGGTCAAATTTCTG	
	TCTGCACAC	
STS135_L620H_fwd	CAAAAGCAGAGTCCAGCATTTTAAAG	gradient

Continued on next page

Primer	Sequence 5' → 3'	T_M (°C)
STS136_L620H_rev	ATGACCCAATG CATTGGGTCATCTTTAAAATGCTGGA CTCTGCTTTTG	pooled

3.1.9.4 Primers for deep sequencing

Primer	Sequence 5' → 3'	T_M (°C)
STS1_SAMHD1 1_fwd	ACACTCTTTCCCTACACGACGCTCTTC CGATCTTTCTTGACTGCTGTGCCGGAC	60.0
STS2_SAMHD1 1_rev	TGACTGGAGTTCAGCGTGTGCTCTTCC GATCTGCCGCTACCTCGGATGTTCTTCA	60.0

3.1.9.5 Primers for sanger sequencing

Primer sequences for primers STS113 and STS114 were taken from CloneJET PCR Cloning Kit.

Primer	Sequence 5' → 3'
STS32_pCDH_fwd	GTTACAGATCCAAGCTGTG
STS33_pCDH_rev	CAGCTCGCTCATATGCATA
STS113_pJET1.2_fwd	CGACTCACTATAGGGAGAGCGGC
STS114_pJET1.2_rev	AAGAACATCGATTTTCCATGGCAG

3.1.10 Antibodies and dyes

Antibody and dye dilutions labeled with IB were used for immunoblotting, Wes for quantitative immunoblotting, FC for flow cytometry and IHC for immunohistochemistry.
For α-SAMHD1 antibodies, the regions that each of the antibody recognizes are not known. All of them were generated by immunization with the whole human SAMHD1 protein. For the 5 customized α-SAMHD1 antibodies made by Eurogentec, the purified SAMHD1 protein from the vector pGEX-4T-1 His-SAMHD1 was used to generate the antibodies. For the commercial antibodies, the immunogen for the α-SAMHD1 antibody from Origene

was full length human recombinant protein of human SAMHD1 (NP-056289) produced in HEK 293T cells. For the α-SAMHD1 antibody from Proteintech, the immunogen was not specified.

Primary antibody	**Species**	**Dilution**	**Article number**	**Vendor**
α-GAPDH	mouse	1:500 (IB)	sc-365062	Santa Cruz Biotechnology
α-Phospho SAMHD1 Thr592	rabbit	1:10.000 (IB)	8005	ProSci
α-Rabbit IgG Isotype control	rabbit	1:3760 (FC)	02-6102	Thermo Fisher Scientific
α-SAMHD1	rabbit	1:1000 (IB), 1:100 (FC), 1:50 (IHC)	12586-1-AP	Proteintech
α-SAMHD1 1FG	mouse	1:1000 (IB)	TA501953	OriGene Technologies
α-SAMHD1 EGT986-11G6E8	mouse	1:250 (IB), 1:200 (Wes), 1:50 (FC)	Customized	Eurogentec
α-SAMHD1 rb1245	rabbit	1:2000 (IB), 1:100 (FC)	Customized	Eurogentec
α-SAMHD1 rb1246	rabbit	1:2000 (IB), 1:100 (FC)	Customized	Eurogentec
α-SAMHD1 H153	chicken	1:2000 (IB)	Customized	Eurogentec
α-SAMHD1 H154	chicken	1:4000 (IB), 1:100 (IHC)	Customized	Eurogentec
α-tRFP (mtagBFP)	rabbit	1:500 (IB)	AB233-EV	Evrogen, Biocat
α-Vinculin	mouse	1:2000 (IB, Wes)	V9264-100μl	Sigma-Aldrich

Secondary antibody	Species	Dilution	Article number	Vendor
α-Chicken-Biotin IgY (H and L)	goat	1:300 (IHC)	ab6876	Abcam
α-Chicken-HRP IgY (H and L)	goat	1:10.000 (IB)	ab6877	Abcam
α-Chicken IgY (H and L) Alexa Fluor® 488nm	goat	1:200 (FC)	ab150169	Abcam
α-Mouse-HRP IgG (H and L)	goat	1:10.000 (IB)	115-035-062	Jackson Immuno Research, Dianova
α-Mouse-IgG (H and L) cross-adsorbed Alexa Fluor® 488nm	goat	1:200 (FC)	A11001	Life Technologies
α-Rabbit IgG (H and L)	goat	1:10.000 (IB)	111-035-144	Jackson Immuno Research, Dianova
α-Rabbit IgG (H and L) cross-adsorbed Alexa Fluor® 488nm	goat	1:200 (FC)	A11008	Life Technologies

Dyes	Species	Dilution	Article number	Vendor
LIVE/DEAD™ fixable near infrared dead cell dye, excitation 633/635 nm	-	1:50 (FC)	L10119	Invitrogen

3.1.11 Plastics and other material

Product	Article number	Vendor
Amersham protran® transfer membrane, 0.45 μm NC	4675.1	Carl Roth

Continued on next page

Product	Article number	Vendor
Bolt™ bis tris gel 4-12%, 10 well and 17 well	NW04120BOX, NW04127BOX	Thermo Fisher Scientific
Neubauer improved counting chamber	0640010	Marienfeld Superior
Polyallomer tube for ultracentrifugation	5052	Beranek Laborgeräte
Round bottom high clarity PP test	352063	Falcon, Omnilab
Stericup-HV sterile vacuum filtration system, 0.22 μm	S2GPU05RE	Sigma-Aldrich
Stericup-HV sterile vacuum filtration system, 0.45 μm	S2HVU05RE	Sigma-Aldrich
Tube with cell filter cap with 35 μm nylon mesh	10585801	Corning, Omnilab
24-well plate (flat bottom)	83.3922	Sarstedt
96-well plate (flat bottom)	83.3924	Sarstedt
96-well plate (round bottom)	83.3925	Sarstedt
10 cm dish	83.3902	Sarstedt
15 cm dish	83.3903	Sarstedt
T25 flask	83.3910.002	Sarstedt
T75 flask	83.3911.002	Sarstedt
T175 flask	83.3912.002	Sarstedt
SafeSeal 1.5 ml tube	72.706.400	Sarstedt
SafeSeal 2.0 ml tube	72.695.400	Sarstedt
CyroPure 2.0 ml cryotube	72.380	Sarstedt

3.1.12 Analytical devices and software

All illustrations in this thesis were created autonomously with Adobe Illustrator CC 2019. Background references are indicated in the figure legends.

Device	Vendor
BD FACS Aria Fusion (5 laser configuration)	BD Biosciences
BD FACS Lyric (3 laser configuration, red 640 nm, blue 488 nm, violet 405 nm)	BD Biosciences
BD FACS Melody cell sorter	BD Biosciences
Biometra compact DNA gel electrophoresis (846-025-100)	Analytik Jena
Eclipse Ti2 microscope with DS-Qi2 camera	Nikon

Continued on next page

Device	Vendor
Mantis liquid handler	Formulatrix
Mastercycler Vapo.protect	Eppendorf
Mini gel tank for immunoblotting (A25977)	Invitrogen, Thermo Fisher Scientific
Microplate reader CLARIOstar plus	MGG Labtech
MiSeq benchtop sequencing system	Illumina
Nanodrop One	Thermo Fisher Scientific
Neon transfection system	Thermo Fisher Scientific
Quantstudio 3 real-time PCR-system, 96 Well 0.1 ml Block	Thermo Fisher Scientific
Rotor SW28	Beckman Coulter
Sorvall WX+ ultracentrifuge	Thermo Fisher Scientific
UVP UVsolo touch	Analytik Jena
Vi-Cell XR cell viability analyzer	Beckman Coulter
Vilber fusion FX	Vilber
Wes quantitative western blot device	ProteinSimple

Software	Vendor/Publication
Adobe Illustrator CC 2019 (Version 23.0.1)	Adobe
BiQ Analyzer for DNA methylation analysis	[152]
Compass for SW	ProteinSimple Analysis
Epidesigner	Agena Bioscience
Excel 2016	Microsoft Office
FlowJo flow cytometry analysis (Version 10.4.2)	FlowJo
GraphPad Prism (Version 6.01)	GraphPad
Outknocker (Version 2.0)	[153]
Quantstudio Design and Analysis Software 2016 (Version 1.4.3)	Thermo Fisher Scientific
PyMOL (Version 2.4.1)	Schrödinger
SnapGene (Version 2.6.2)	SnapGene

3.2 Methods

3.2.1 Cell culture conditions and maintenance

Cells were cultivated in corresponding cell culture medium with 10% FBS (heat-inactivated at 65°C for 30 minutes and filtered to remove protein aggregates) and 1% P/S at 37°C with 5% CO_2 and were split according to confluence or experimental setup. For splitting of adherent cell lines, medium was removed, cells were washed with 1x PBS, detached by 1x Trypsin-EDTA solution in 1x PBS. Trypsinization was stopped using at least the double amount of complete, appropriate medium volume and cell suspensions were seeded into new cell culture ware for maintenance. Cells were counted using a Neubauer improved counting chamber.

3.2.2 Thawing and freezing of mammalian cells

For thawing, cells stored in liquid nitrogen tanks were incubated in a water bath (37°C) for 1-2 minutes, transferred into complete, corresponding cell culture medium (adding to a volume of 5 ml) and centrifuged at 500 g for 5 minutes. Supernatants were removed, cells were resuspended in complete cell culture medium and plated onto a cell culture dish.
For freezing, cells were trypsinized (for adherent cell lines), resuspended in complete cell culture medium and centrifuged at 500 g for 5 minutes. Supernatants were removed, cells were resuspended in freezing medium (section 3.1.3) and frozen down 1 degree/min at -80°C as 1 ml aliquots in cryo-vials. The next day, cells were transferred into liquid nitrogen tanks for long-time storage.

3.2.3 Plasmid DNA amplification

3.2.3.1 Transformation into STBII/DH5α cells

50 μl STBII/DH5α cells were thawn slowly on ice, mixed with 1 μl plasmid DNA and incubated on ice for 20 minutes. Cells were heat-shocked at 42°C for 2 minutes and cooled-down on ice for 5 minutes. The mix was added to 500 μl SOC outgrowth medium and shaken at 37°C for a minimum of 30 minutes. After incubation, samples were centrifuged at 13.000 rpm for 1 minute. Supernatant was removed and cells were resuspended in the residual supernatant. The cell suspension was then plated on prewarmed LB agar plates containing 100 μg/ml of the respective antibiotic solution and kept overnight at 37°C to allow growth of single colonies.

3.2.3.2 Plasmid DNA preparation

For plasmid DNA preparation, a single clone colony was picked from transformation plates, inoculated in 3 ml LB medium containing 50 μg/ml of the respective antibiotic solution and incubated overnight at 37°C under constant shaking. The next day, the small bacterial culture was transferred into 300 ml TB medium containing 50 μg/ml of the respective

antibiotics in a 2 l Erlenmeyer flask in order to shake overnight at 37°C. Plasmid DNA preparation was performed using Nucleobond Xtra midi or maxi plasmid DNA purification kit according to the manufacturer's procedure.

3.2.4 DNA gel electrophoresis

PCR quality was validated through DNA gel electrophoresis. Therefore, 1% agarose in 1x TAE buffer were mixed and shortly heated in a microwave in order to dissolve the powder completely. SYBR safe DNA gel stain was added 1:10.000, the solution was filled into an electrophoresis chamber with inserting combs and cooled down for solidification. Samples were loaded after being mixed with 6x gel loading dye purple for a final concentration of 1x and 5 μl SmartLadder was used as size reference. Electrophoresis was performed at 80 V for 30 minutes and gels were documented with UVP UVsolo Touch.

3.2.5 Bisulfite sequencing

Total DNA from cell cultures was extracted using the silica-based DNeasy blood and tissue kit according to the manufacturer's procedure. Sample quality and DNA concentration was measured photometrically with Nanodrop One.
Bisulfite conversion of 1 μg total DNA/sample was performed using the EZ DNA methylation kit according to the manufacturer's procedure. A human methylated and non-methylated (WGA) DNA set was used as methylated and non-methylated control, respectively. A representative part of the endogenous promoter of the *Samhd1* gene was amplified by polymerase chain reaction (PCR, tables 3.28 and 3.29). The PCR reaction was loaded on a 1% agarose gel (section 3.2.4), the respective band was cut out of the gel and purified using the NucleoSpin® gel and PCR clean-up kit according to the manufacturer's procedure. Samples were eluted in 20 μl sterile, nuclease-free H_2O and the sample quality was assured photometrically with Nanodrop One.
The purified PCR fragment was cloned into the vector pJET1.2 using the sticky end cloning protocol for Taq polymerase with the CloneJET PCR cloning kit. Therefore, the reaction was pipetted according to the pipetting scheme in table 3.30. Reactions were vortexed, spun down and incubated at 70°C for 5 minutes. After cooling down on ice, the ligation reaction was prepared by adding 1 μl pJET1.2 (50 ng/μl) and 1 μl T4 DNA ligase to the reaction mixture. Reactions were vortexed, spun down and incubated at room temperature for 5 minutes. Ligations were transformed into STBLII cells according to the description in section 3.2.3. The isolated DNA from different clones was sent for Sanger sequencing to Eurofins Genomics. Sequences were analyzed using BiQ Analyzer Software [152].

Table 3.28: Pipetting scheme for *Samhd1* promoter amplification

Amount	Substance
10 μl	Reaction buffer, 10x
2 μl	Primer fwd, 100 μM
2 μl	Primer rev, 100 μM
2 μl	10 mM dNTP mix
0.5 μl	HotStarTaq DNA polymerase
ad 100 μl	Nuclease-free H_2O
x μl	Bisulfite converted DNA

Table 3.29: PCR program for *Samhd1* promoter amplification

Step	Temp.	Time
1	95 °C	15 minutes
2	95 °C	60 seconds
3	55.5 °C	60 seconds, increasing 1°C/cycle for first 5 cycles
4	72 °C	60 seconds, return to step 2, 18 cycles
5	72 °C	10 minutes
6	12 °C	Infinite

3.2.6 Cloning and directed mutagenesis

3.2.6.1 Cloning of *Samhd1* sequence into transfer vector pCDH-EF1α-BFP-1

For cloning the natural *Samhd1* sequence from the bacterial expression plasmid pGEX-4T-1 GST SAMHD1 into the transfer vector pCDH-EF1α-BFP-1, the *Samhd1* sequence was amplified by the PCR reaction shown in table 3.31 and 3.32. A clear PCR product was validated through DNA gel electrophoresis (section 3.2.4) and purified using the NucleoSpin® gel and PCR clean-up kit according to the manufacturer's procedure with an elution volume of 20 μl nuclease-free H_2O. The purified PCR product as well as the target vector pCDH-EF1α-BFP-1 were digested separately by the restriction enzymes BamHI-HF and EcoRI-HF at 37°C for 1 hour according to table 3.33 and the reaction with the PCR product was stopped at 65°C for 20 minutes. The target vector pCDH-EF1α-BFP-1 was dephosphorylated by addition of 2 μl antarctic phosphatase buffer and 1 μl antarctic phosphatase and incubated at 37°C for at least 15 minutes followed by inactivation at 65°C for 5 minutes. Whereas the target vector was gel extracted, the insert reaction was purified directly using the NucleoSpin® gel and PCR clean-up kit according to the manufacturer's procedure with an elution volume of 20 μl nuclease-free H_2O. Target vector and insert were ligated at 16°C overnight followed by inactivation of the ligation reaction at 65°C for 10 minutes (table 3.34). In order to remove self-ligated target vectors that do not

Table 3.30: Pipetting scheme for sticky end cloning of PCR fragment into pJET1.2 vector

Amount	Substance
10 μl	Reaction buffer, 2x
1 μl	Purified PCR fragment
6 μl	Nuclease-free H_2O
1 μl	DNA blunting enzyme

Table 3.31: Pipetting scheme for cloning of *Samhd1* sequence into transfer vector pCDH-EF1α-BFP-1

Amount	Substance
5 μl	Phusion GC buffer, 10x
5 μl	Phusion HF buffer, 10x
1 μl	10 mM dNTP mix
2.5 μl	Primer STS27_fwd, 10 μM
2.5 μl	Primer STS28_rev, 10 μM
1.5 μl	DMSO, 100%
1 μl	Phusion high fidelity DNA polymerase
1 μl	10 ng/μl pGEX-4T-1 GST SAMHD1 as template
ad 50 μl	Nuclease-free H_2O

contain the insert, the reaction was additionally digested by 0.5 μl AgeI-HF with 1.5 μl 10x CutSmart buffer at 37°C for 1 hour. AgeI-HF only cuts in the Luc2 cassette of the original target vector, a part that the final vector will not longer contain. Afterwards the reaction was transformed into STBLII cells according to section 3.2.3. Clones were validated with Sanger sequencing using Eurofins Genomics and the primer pair STS32/STS33.

3.2.6.2 Directed mutagenesis of *Samhd1* wildtype sequence

For directed mutagenesis of the *Samhd1* gene, overlapping primers with the mutated nucleotides in the middle of the primers were used in order to introduce the mutation (section 3.1.9). Amplification was checked by DNA gel electrophoresis (section 3.2.4) and purified using the NucleoSpin® gel and PCR clean-up kit according to the manufacturer's procedure. The PCR product was eluted in 21 μl nuclease-free H_2O. 2.5 μl CutSmart buffer as well as 1.5 μl DpnI was added and the sample was incubated overnight at 37°C followed by transformation into STBLII competent bacteria (section 3.2.3). DNA was isolated from 6 ml bacterial cultures with the QIAprep spin miniprep kit and successful mutagenesis was determined by Sanger sequencing through Eurofins Genomics. From the successfully mutated clones, larger cultures were inoculated and DNA extracted for further procedures described in section 3.2.9 and 3.2.12.

Table 3.32: PCR program for cloning of *Samhd1* sequence into transfer vector pCDH-EF1α-BFP-1

Step	Temp.	Time
1	95°C	30 seconds
2	98°C	15 seconds
3	55°C	30 seconds
4	72°C	90 seconds, return to step 2, 5 cycles
5	98°C	15 seconds
6	gradient*	30 seconds
7	72°C	90 seconds, return to step 5, 30 cycles
8	72°C	120 seconds
9	12°C	Infinite

*62-72°C Gradient PCR was used for optimal annealing and condition 62°C was used for further proceeding after validation with DNA gel electrophoresis.

Table 3.33: Restriction digest of PCR product and transfer vector pCDH-EF1α-BFP-1

Amount	Substance
2 μl	CutSmart buffer, 10x
1 μl	BamHI-HF
1 μl	EcoRI-HF
10 μg	Target vector or
1 μg	Purified PCR product
ad 20 μl	Nuclease-free H_2O

3.2.7 Drug treatments and cell viability assay

Cells were counted and seeded in duplicates into 384-well white multiwell plates (27 μl cell-medium suspension). Control wells with medium or cells only were included. 3 μl/well ara-C (figure 3.1) in 1xPBS with 5% DMSO was added using the Mantis Liquid Handler in a dilution series of 1:3 with a starting concentration of 2.5 mM (highest final concentration in well 250 μM). The number of viable cells was determined using the CellTiter-Glo® 2.0 assay by quantification of ATP, indicating metabolically active cells [154]. The Ultra-Glo luciferase converts luciferin to oxyluciferin using ATP, resulting in a luminescent signal, illustrated in figure 3.2 [154]. Therefore, 10 μl/well CellTiter-Glo® 2.0 assay was added using the Mantis Liquid Handler, samples were shaken at room temperature for 2 minutes and incubated in the dark for an additional 10 minutes. Afterwards, plates were centrifuged at full speed for 5 minutes, followed by luminescence-based measurement with Microplate Reader CLARIOstar Plus according to the manufacturer's procedure.

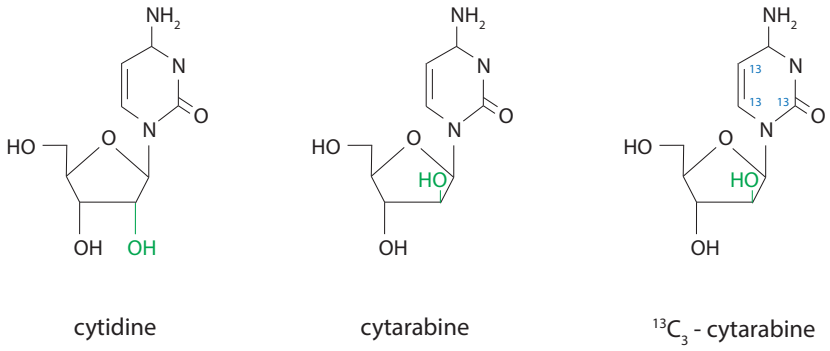

Figure 3.1: Structure of physiological cytidine, the prodrug cytarabine (ara-C) and its labeled version $^{13}C_3$ ara-C. Ara-C represents an isomer of the physiological nucleoside cytidine, where the hydroxy group at carbon 2 is flipped in the ribose ring. $^{13}C_3$ ara-C contains three 13-carbon atoms instead of the regular 14-carbon atoms in the cytosine ring [1, 103].

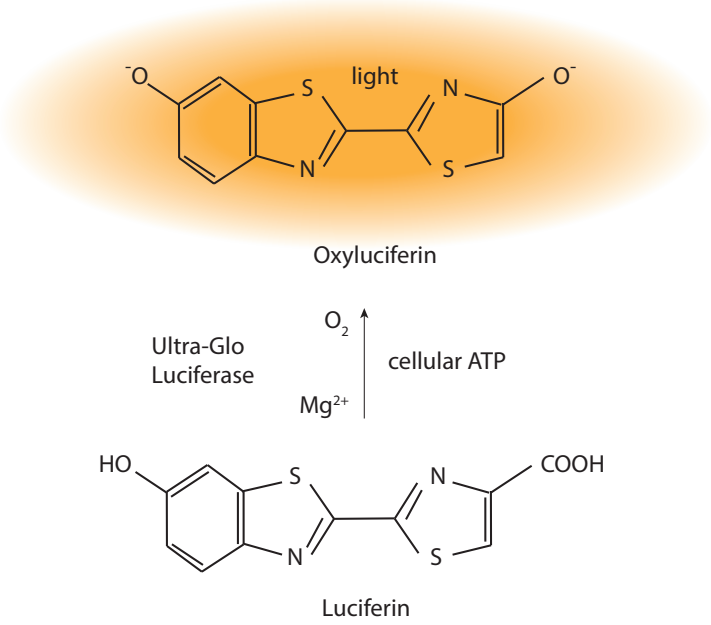

Figure 3.2: CellTiter-Glo® 2.0 assay to determine cell viability. The Ultra-Glo luciferase converts luciferin to oxyluciferin using ATP, resulting in a luminescent signal that can be measured by a plate reader [154]. The measured luminescence directly indicates the viable cells in the sample and can be used to determine the cytotoxicity of a drug treatment and its effective dose 50 (ED_{50}).

Table 3.34: Ligation of insert *Samhd1* and target vector pCDH-EF1α-BFP-1

Amount	Substance
1 μl	T4 DNA ligase reaction buffer, 10x
50 ng	Digested, dephosphorylated, purified target vector
30 ng	Digested, purified insert
1 μl	T4 DNA ligase
ad 10 μl	Nuclease-free H_2O

Table 3.35: Pipetting scheme for directed mutagenesis

Amount	Substance
5 μl	Phusion GC buffer, 10x
5 μl	Phusion HF buffer, 10x
1 μl	10 mM dNTP mix
2.5 μl	Primer fwd, 10 μM
2.5 μl	Primer rev, 10 μM
2.5 μl	DMSO, 100%
1 μl	Phusion high fidelity DNA polymerase
50 ng	pCDH-EF1α-SAMHD1-WT-BFP-1 natural sequence as template
ad 50 μl	Nuclease-free H_2O

3.2.8 Liquid chromatography–tandem mass spectrometry (LC–MS/MS)

In order to determine the ara-CTP levels in cells, equal cell numbers were seeded and treated with 40 μM $^{13}C_3$ ara-C for 6 hours at 37°C. Afterwards cells were counted, equal cell numbers were harvested in SafeSeal 1.5 ml tubes and frozen at -80°C. In order to be able to measure ara-CTP levels, three carbon atoms in the ara-C are replaced with three 13-carbon atoms instead of the regular 14-carbon atoms (figure 3.1). For determination of dNTP levels, equal cell numbers of untreated cells were harvested. Samples were processed and measured in collaboration with the laboratory of Prof. Gerd Geißlinger (University Hospital of the Goethe University, Frankfurt am Main, Germany). Shortly, samples were extracted and the solvent was evaporated using nitrogen. Samples were directly reconstituted in the adequate mobile phase. For determination of dNTP levels, reconstitution of the samples was done using alkaline medium containing ammoniac.

3.2.9 Production of lentiviral vectors

For production of lentiviral vectors, HEK 293T cells were seeded 1 day before transfection in 12x 15 cm dishes (2x 10^7 cells/dish). On the day of transfection, the DNA/PEI mix was prepared as shown in table 3.38, incubated at room temperature for 20 minutes and

Table 3.36: PCR program for directed mutagenesis

Step	Temp.	Time
1	98°C	2.5 minutes
2	98°C	45 seconds
3	T_M	60 seconds
4	72°C	5 minutes, return to step 2, 18 cycles
5	72°C	10 minutes
6	12°C	Infinite

Table 3.37: Cell seeding and incubation times for cell viability assay

Cell line	Cell number per well	Incubation time until analysis
LN-18	1000 cells	4 days
U-87 MG	750 cells	4 days
THP-1	7500 cells	3 days

added dropwise onto the cells (2 ml/dish). Three days after transfection, medium containing lentiviral vectors was harvested and filtered through a Stericup-HV sterile vacuum filtration system with the pore size 0.45 μm. Polyallomer tubes for ultracentrifugation were filled with 6 ml 25% sucrose and then carefully overlayed with 28 ml of lentiviral supernatant, tubes were balanced with a scale and samples were centrifuged at 28.000 rpm at 4°C for 1.5 hours in a Sorvall WX+ ultracentrifuge with the rotor SW28. After ultracentrifugation, the supernatant was discarded and lentiviral vectors were resuspended in 100 μl 1xPBS/tube. Lentiviral vectors were dissolved at 4°C for at least 1 hour, aliquoted and stored at -80°C. In case lentiviral vectors were not concentrated, viral supernatants were centrifuged at 1.200 rpm for 10 minutes followed by a second centrifugation at 5.000 rpm for 20 minutes and aliquots were stored at -80°C.

Table 3.38: Pipetting scheme for lentiviral vector production

Amount	Substance
7 μg	pCMVΔ8.9 (packaging vector)
8 μg	pMD2.G (VSV-G, envelope vector)
11 μg	Transfer vector
2 ml	DMEM (no additives)
104 μl	1 mg/ml Polyethylenimine (PEI)

3.2.10 Transfections with Lipofectamine™ 2000

For transfection with Lipofectamine™ 2000 transfection reagent, adherent cells were seeded in a 12-well plate one day prior transfection to achieve 80% confluence. For suspension cells, cells were seeded on the day of transfection into a 96-well plate (u-shaped). 50 μl Opti-MEM were mixed with 1 μg plasmid in tube A, whereas additional 50 μl Opti-MEM were mixed with 2.5 μl Lipofectamine™ 2000 transfection reagent in tube B (plasmid to Lipofectamine™ 2000 ratio of 1:2.5). After incubation of 5 minutes, tube A and B were pooled, incubated for 25 minutes and the mixture was added to the culture. Cells were incubated at least 48 hours before analysis or further procedure.

3.2.11 *Samhd1* CRISPR/Cas9 knockout generation in cell lines

For CRISPR/Cas9-mediated *Samhd1* KO generation, the GBM cell lines LN-18, U-87 MG and U-251 MG were seeded at optimal cell density one day before. In order to KO *Samhd1*, the cells were transfected with a plasmid containing a *Cas9* cassette and the respective guideRNA (gRNA) for *Samhd1* (figure 3.3) together the fluorescence cassette for *mCherry* (section 3.2.10). 48 hours after transfection, cells were bulk sorted for the highest fluorescence positivity and single cell seeded into 96-well plates. Cells were incubated at least 2 weeks before wells were manually screened for cell colonies originating from 1 clone. Respective wells were marked, cell colonies were expanded and split into 2 wells when reaching confluence. One well was used for culture maintenance whereas the other well was used for deep sequencing. Therefore, the cell clones were lysed in 50 μl direct lysis buffer (section 3.1.2) containing 0.2 mg/ml proteinase K and incubated on ice for 10 minutes. For lysis, 20 μl of the mix per clone was incubated in the Mastercycler at 65°C for 10 minutes and at 95°C for 15 minutes. In order to amplify the edited region in the genome, PCR1 and PCR2 were performed according to table 3.39, 3.40 and 3.41. Primer sequences for PCR1 are listed in section 3.1.9 and primer sequences for PCR2 were taken from Schmid-Burke *et al.* [153]. Samples were processed by the laboratory of Prof. Veit Hornung (LMU Munich, Germany) and deep sequencing was performed using the MiSeq benchtop sequencing system [153]. Analysis was performed using Outknocker 2.0 [153].

3.2.12 Production of SAMHD1 wildtype and mutant reconstitutions in SAMHD1-deficient cell clones

3.2.12.1 Transductions of SAMHD1-deficient cell clones

In order to reconstitute SAMHD1-deficient cell clones with SAMHD1 wildtype or mutants, cells were transduced with lentiviral vectors with corresponding SAMHD1 wildtype and mutated sequences (sections 3.2.6 and 3.2.9, for a SAMHD1 mutation overview see table 4.1 in results section 4.5). SAMHD1-deficient cell clones were seeded according to table 3.42 and 24 hours later, cells were transduced with filtered, non-concentrated lentiviral supernatants followed by centrifugation at 1.200 g at 37°C for 90 minutes. Medium was

Figure 3.3: *Samhd1* gRNA sequence and CRISPR target site for CRISPR/Cas9-mediated KO generation of *Samhd1*. The gRNA sequence is indicated in blue, followed by the respective protospacer adjacent motif (PAM) sequence 5'-NGG-3' indicated in green and the CRISPR target site indicated in purple. The gRNA used for *Samhd1* in this study binds at the beginning of the *Samhd1* gene in Exon 1.

Table 3.39: Pipetting scheme for PCR1

Amount	Substance
0.6 μl	Phusion GC buffer, 10x
0.6 μl	Phusion HF buffer, 10x
0.12 μl	10 mM dNTP mix
0.03 μl	Primer fwd, 100 μM
0.03 μl	Primer rev, 100 μM
0.06 μl	Phusion high fidelity DNA polymerase
1 μl	Lysis as template
ad 6 μl	Nuclease-free H_2O

changed the next day and cells were expanded for up to two weeks.

3.2.12.2 Bulk sort of transductions

Transduced cell populations were bulk sorted for mtagBFP positivity using fluorescence-activated cell sorting (FACS) by BD FACS Melody cell sorter and BD FACS Aria Fusion cell sorter. On the day of sorting, cells were prepared in FACS buffer (section 3.1.2), incubated on ice and meshed through a 70 μm cell strainer prior to sorting. Collection tubes were pre-coated with serum over night at 4°C to reduce surface charge and filled with 0.5 ml fresh collection medium before sorting. Cells were gated and sorted for viable, single and mtagBFP-positive cells using the BV421 channel. Sorted cells were seeded and expanded in sorting medium for 1 week and then cultivation was continued with standard, complete medium. The mtagBFP positivity was confirmed by flow cytometry analysis using BF FACS Lyric flow cytometer. Heterogeneous cell populations were resorted until a homogeneous, mtagBFP positive cell population was obtained. Cell populations were monitored for mtagBFP positivity throughout the cultivation process to assure stable protein expression.

Table 3.40: Pipetting scheme for PCR2

Amount	Substance
2 μl	Phusion GC buffer, 10x
2 μl	Phusion HF buffer, 10x
0.4 μl	10 mM dNTP mix
2 μl	Primer fwd, 100 μM
2 μl	Primer rev, 100 μM
0.2 μl	Phusion high fidelity DNA polymerase
2 μl	PCR product from PCR1
ad 20 μl	Nuclease-free H_2O

Table 3.41: PCR program for PCR1/PCR2

Step	Temp.	Time
1	98°C	3 minutes
2	98°C	20 seconds
3	60°C	20 seconds
4	72°C	30 seconds, return to step 2
		18 cycles (PCR1), 25 cycles (PCR2)
5	72°C	3 minutes
6	12°C	Infinite

3.2.13 Production and validation of virus-like particles

For production of virus-like particles (VLPs), HEK 293T cells were seeded 1 day before transfection in 12 x 15 cm dishes (5.6x 10^6 cells/dish). On the day of transfection, the DNA/PEI mix was prepared as shown in table 3.43, vortexed, incubated at room temperature for 45 minutes and added dropwise into the dish (2 ml/dish). 48 hours after transfection, medium containing VLPs was harvested and filtered through a Stericup-HV sterile vacuum filtration system with the pore size 0.45 μm. VLPs were concentrated using sterile-filtered 25% sucrose. 6 ml 25% sucrose were provided into a polyallomer tube for ultracentrifugation, overlayed carefully with 28 ml of viral supernatant, tubes were balanced with a scale and samples were centrifuged at 28.000 rpm at 4°C for 1.5 hours in a Sorvall WX+ ultracentrifuge with the rotor SW28. After ultracentrifugation, the supernatant was discarded and VLPs were resuspended in 100 μl 1xPBS/tube. VLPs were dissolved at 4°C for at least 1 hour, aliquoted and stored at -80°C.
To titrate the VLPs containing Vpx (Vpx-VLPs), the Vpx-dependent SAMHD1 degradation capacity was determined by ara-C toxicity analysis. For this, a SAMHD1-proficient cell line (e.g. LN-18 parental) was seeded into a 384-well plate (1000 cells in 21 μl per well) and six different volumes of Vpx-VLPs (0.15 μl/0.1 μl/0.075 μl/0.05 μl/0.025 μl/0.0 μl) in 6 μl total volume were added in duplicate rows onto the cells. As an additional, non-treated con-

Table 3.42: Cell seeding for SAMHD1 reconstitutions

Cell clone	Format	Cell number per well
LN-18 SAMHD1 KO SKO1	12-well plate	120.000
U-87 MG SAMHD1 KO KO1	24-well plate	40.000
U-251 MG SAMHD1 KO H3	24-well plate	60.000
THP-1 -/- SAMHD1 KO B7	96-well plate (u-shaped)	500.000

trol, a corresponding SAMHD1-deficient line (e.g. LN-18 SAMHD1 KO SKO1) was seeded in duplicate rows. Plates were centrifuged at 500 g at room temperature for 5 minutes. 24 hours later, ara-C was added in a dilution series of 1:3 with a starting concentration of 2.5 mM (highest final concentration in well 250 μM) and plates were processed 4 days later with CellTiter-Glo® 2.0 assay according to section 3.2.7. The amount of Vpx-VLPs that showed a similar ara-C toxicity phenotype to the corresponding SAMHD1-deficient line was chosen for future Vpx-VLP treatment with this stock.

Table 3.43: Pipetting scheme for VLP production

Amount	Substance
198 μg	SIV3+ vector
54 μg	VSV-G envelope vector
29.52 ml	DMEM (no additives)
751 μl	1 mg/ml Polyethylenimine (PEI)

3.2.14 Quantitative mRNA expression analysis

3.2.14.1 RNA isolation

Total RNA isolation was performed using NucleoZOL according to the manufacturer's procedure. Shortly, the cell pellets were lysed in 1 ml NucleoZOL/sample by pipetting up and down. Contaminants (e.g. DNA, proteins) were precipitated with 400 μl RNase-free H_2O/1 ml NucleoZOL in the lysate. Samples were shaken for 15 seconds, incubated at room temperature for 15 minutes and centrifuged at 12.000 g at 4°C for 15 minutes. 1 ml of supernatant was transferred into a fresh 2.0 ml SafeSeal 2.0 ml tube, 400 μl 75% ethanol was added and samples were incubated at room temperature for 10 minutes. Afterwards, samples were centrifuged at 12.000 g at 4°C for 8 minutes, the RNA was washed by adding 500 μl 75% ethanol/1ml supernatant. After centrifugation at 8.000 g at 4°C for 3 minutes, the supernatant was removed and the RNA was reconstituted in 20 μl RNase-free H_2O. To ensure efficient reconstitution of the RNA, samples were vortexed 2 minutes and then put on ice.

3.2.14.2 Reverse transcription

Reverse transcription of total RNA was performed using the high-capacity RNA-to-cDNA kit. Reactions were prepared according to table 3.44 and incubated at 37°C for 60 minutes followed by incubation at 95°C for 5 minutes. Reactions were either stored at -20°C or processed for quantitative PCR right away.

Table 3.44: Pipetting scheme for reverse transcription

Amount	Substance
10.0 μl	2x RT buffer mix
1.0 μl	20x RT enzyme mix
Up to 9.0 μl	1 μg of RNA sample
ad 20.0 μl	RNase-free H_2O

3.2.14.3 Quantitative PCR

Quantitative PCR (qPCR) was performed using Quantstudio 3 real-time PCR-system with a 96-well/0.1 ml block. Reactions were prepared and run according to table 3.45 and 3.46. Data was analyzed using Quantstudio Design and Analysis Software as well as Excel 2016.

Table 3.45: Pipetting scheme for qPCR

Amount	Substance
5 μl	TaqMan fast advanced master mix, 2x
0.5 μl	TaqMan gene expression assay of target gene, 20x or
0.5 μl	TaqMan RNase P control reagents kit, 20x
1.0 μl	cDNA
3.5 μl	RNase-free H_2O

Table 3.46: PCR program for qPCR

Step	Temp.	Time
1	50°C	2 minutes
2	95°C	20 seconds
3	95°C	1 second
4	60°C	20 seconds, return to step 2, 40 cycles
5	12°C	Infinite

3.2.15 Immunoblotting

3.2.15.1 Total protein extraction and concentration measurement

Cell samples were harvested, washed once with 1xPBS and pellets were frozen at -80°C. Total protein extraction was performed by resuspension of the cell pellet with hunt lysis buffer (section 3.1.2) with freshly added 1x EDTA-free protease inhibitor cocktail cOmplete. For physical disruption and cell lysis, the samples were frozen in liquid nitrogen and thawed again at room temperature. The freeze-thaw procedure was repeated twice and cells were centrifuged at full speed at 4°C for 30 minutes. Supernatants were transferred into fresh SafeSeal 1.5 ml tube and stored at -20°C. Purified protein controls such as His-SAMHD1 and GST-SAMHD1 protein were kindly provided by Dr. Paul R. Song Wratil (in-house) and His-SS19 protein was provided by Saskia Schmitt (Hopfner laboratory, Gene Center Munich, Germany).
Protein concentrations were measured using Pierce bicinchoninic acid (BCA) protein assay kit. Therefore, a standard using different concentrations of bovine serum albumin (BSA) from 0 to 2.0 mg/ml was pipetted into a flat bottom 96-well plate. For sample measurement, 10 μl of protein lysis samples (or 1:10 dilution in H_2O respectively) were pipetted into free wells. 100 μl/well of solution A and B was added in a 50:1 dilution, the plate was incubated at 37°C for 20 minutes and total protein quantification was colorimetrically measured using the Microplate Reader CLARIOstar Plus.

3.2.15.2 Conventional immunoblot analysis

Equal protein amounts from each sample (for cell lysates 25 μg if not indicated otherwise and for purified protein 0.05 μg) were mixed with 4x NuPAGE LDS sample buffer to a final concentration of 1x and DTT was added to a final concentration of 50 mM. To achieve equal volumes, H_2O was added to 20 μl. The mix was incubated at 70°C for 10 minutes. Precast gels with neutral pH using bis-tris chemistry were used for SDS gel electrophoresis, e.g. Bolt™ bis tris gel 4-12% with 10 well and 17 wells. Samples were loaded onto the gel and 5 μl of PageRuler™ plus prestained protein ladder were loaded as size reference. SDS gel electrophoresis was performed at 150 V for 1.5 hours in 1x NuPAGE MOPS SDS running buffer. Then, the proteins were blotted from the gel to a 0.45 μm nitrocellulose membrane at 30 V for 1 hour in 1x NuPAGE transfer buffer with 10% methanol. After blotting, the membrane was blocked in 5% milk in 1xTBS at room temperature for 30 minutes and washed three times in 1xTBS for 10 minutes. The membrane was incubated overnight at 4°C in the primary antibody diluted in antibody solution (section 3.1.2). On the next day, the membrane was washed three times in 1xTBS for 10 minutes and incubated with the corresponding secondary antibody conjugated with horseradish peroxidase (HRP) diluted in 5% milk in 1xTBS (1:10.000) at room temperature for 1 hour. The membrane was washed three times in 1xTBS for 10 minutes and developed using the Clarity western ECL substrate kit. Digital imaging was proceeded using the Vilber Fusion FX. To increase the protein detection sensitivity, the SuperSignal west pico PLUS chemiluminescent substrate was used for development. After development, the membrane was washed three times in

1xTBS for 10 minutes and incubated in the next primary antibody, respectively.

3.2.15.3 Quantitative immunoblot analysis using Wes

Quantitative immunoblot analysis was performed using Wes according to the manufacturer's procedure. 0.3 μg protein lysate in 3 μl per sample was used for loading. 10x sample buffer was diluted 1:10 with H_2O and used to dilute the lysates accordingly. Data was analyzed using Compass for SW analysis software.

3.2.16 Immunohistochemistry (IHC)

Sample preparation, immunohistochemical staining and histopathological evaluation was performed by Dr. Rupert Egensperger and colleagues (Center for Neuropathology Munich, Germany). Shortly, tissue from first-diagnosed glioma and GBM patients (grades II, III and IV) was fixed with 4% buffered formalin and embedded in paraffin. 3 μm sections were stained with rabbit α-SAMHD1 12586-1-AP from Proteintech or chicken α-SAMHD1 #H154 antibody (section 3.1.10) with the UltraView DAB (3,3'-Diaminobenzidine) detection system of Roche-Ventura on a Benchmark Ultra staining system and routinely stained with hematoxylin and eosin. The histological diagnosis of all tissue specimen was made according to the WHO classification of tumors of the CNS, 4^{th} Edition, 2007 [114]. Pictures were taken with an Eclipse Ti2 microscope.
For analysis of SAMHD1 protein expression in the glioma and GBM tissue sections, the intensity of SAMHD1 nuclear staining for protein expression levels was blindly scored using the following criteria: 0 = no staining, 1 = 5 - 35% staining, 2 = 36 - 70% staining and 3 > 70% staining compared to highly SAMHD1-positive cells at blood vessels, which were taken as a positive control.

3.2.17 Flow cytometry analysis

3.2.17.1 Preparation of cells for flow cytometry

For analysis of cells by flow cytometry, cells were pipetted into a 96-well plate (v-shaped), centrifuged at 500 g for 5 minutes, washed once with 1xPBS followed by staining with LIVE/DEAD^{TM} fixable near infrared dead cell dye (1:50 dilution in 1xPBS) at 4°C for 20 minutes. Afterwards, cells were centrifuged at 500 g for 5 minutes, supernatant was removed, cells were resuspended in 100 μl 4% PFA and incubated at 37°C for 10 minutes (biosafety 1) or 90 minutes (biosafety 2) for fixation. Cells were centrifuged at 500 g for 5 minutes, supernatant was removed and cells were resuspended in FACS Buffer for flow cytometry measurement. Data was analyzed using FlowJo flow cytometry analysis software.

3.2.17.2 SAMHD1 staining for flow cytometry

In order to analyze SAMHD1 protein expression by flow cytometry, cells were prepared as described above, but fixed with prewarmed BD cytofix fixation buffer at room temperature for 10 minutes (biosafety 1) or 90 minutes (biosafety 2). Cells were centrifuged at 600 g at 4°C for 7.5 minutes, put on ice, supernatant was removed and cells were resuspended thoroughly in 100 μl BD perm buffer III per well followed by incubation on ice for 10 minutes. 150 μl BD perm/wash buffer was added per well and cells were centrifuged at 600 g at 4°C for 7.5 minutes. Cells were washed with 150 μl BD perm/wash buffer and centrifugation was repeated. The supernatant was removed and cells were incubated in an α-SAMHD1 primary antibody (section 3.1.10) in BD perm/wash buffer at 4°C for 30 minutes. Extra wells were incubated with respective α-species IgG control primary antibody, secondary antibody only and unstained with BD perm/wash buffer only. 150 μl BD perm/wash buffer was added for washing, cells were centrifuged at 600 g at 4°C for 7.5 minutes and incubated in the dark at 4°C in the respective secondary antibody conjugated with an fluorophore for 30 minutes. 150 μl BD perm/wash buffer was added for washing, cells were centrifuged at 600 g at 4°C for 7.5 minutes, supernatant was removed and cells were resuspended in 100 μl FACS buffer for flow cytometry measurement.

3.2.18 Statistical analysis

The significant differences between samples were determined using an unpaired Student's t-test with GraphPad Prism 6. P- and r^2-values were also determined with GraphPad Prism 6, standard deviation (s.d.) is shown. P-values are defined as following: *P < 0.05, **P < 0.01, ***P < 0.001. P values higher than 0.05 were termed not significant (ns).
For qPCR analysis, values were normalized with the respective parental sample set to 1 if not indicated otherwise. Relative quantification R_Q is defined as $2^{-\Delta\Delta C_T}$. Therefore, target values are divided by the mean of the corresponding values of the housekeeping gene RNase P and the parental value is subtracted for normalization. Then the negative potence 2 of this value is calculated to receive the relative quantification R_Q.
For quantitative immunblotting by Wes, a standard curve for SAMHD1 protein expression was generated using 1:2 dilutions of SAMHD1 protein starting from 10 ng and used to normalize SAMHD1 protein expression of lysate inputs in ng/μl.
For the correlation dot plots, data was analyzed in R (version 4.1.1) by Prof. Lars Kaderali (University Medicine Greifswald, Germany). Values were log-transformed, linear regression modeling was used to analyze dependencies between variables. Pearson's correlation was used to analyze linear correlations.

Chapter 4

Results

4.1 Establishment of customized α-SAMHD1 antibodies

As SAMHD1 is an important protein of interest to study in the Keppler laboratory, custom α-SAMHD1 antibodies were produced together with Eurogentec. Customized antibodies have lots of advantages in comparison to commercially available antibodies, but mainly, they are very cost-effective and can possibly cover a broad spectrum of assay applications (e.g. immunoblotting, flow cytometry analysis, immunohistochemistry analysis). Three different species were selected for antibody production: rabbit, chicken and mouse. For all species, the bacterially produced human His-SAMHD1 full length protein from the vector pGEX-4T-1 His-SAMHD1 (section 3.1.8) was used for immunization. Whereas for rabbit and chicken, a polyclonal approach was followed, the SAMHD1 antibody production in mice was done monoclonally by generating hybridoma cells.
Figure 4.1 summarizes the validation of the generated antibodies in conventional immunoblotting as well as flow cytometry analysis. Whereas the commercially available mouse α-SAMHD1 antibody TA501953 from OriGene Technologies (figure 4.1A) served as a positive control for conventional immunoblotting, the commercially available rabbit α-SAMHD1 antibody 12586-1-AP from Proteintech (figure 4.1D) served as a control for flow cytometry analysis. The figure shows the validation of the customized α-SAMHD1 antibodies using the above described full length SAMHD1 as an immunogen for rabbit #1245 (figure 4.1B and E), rabbit #1246 (figure 4.1C and F), mouse (figure 4.1G and J), chicken H153 (figure 4.1H and K) and chicken H154 (figure 4.1I and L). Cell lysates from SAMHD1-deficient and -proficient THP-1 and LN-18 cells as well as purified, tagged SAMHD1 proteins were used to validate the antibodies.
For conventional immunoblotting, antibody dilution series revealed antibody working concentrations of 1:500 - 1:4.000 (data not shown). Respective antibody concentration used is indicated in figure 4.1. In order to validate α-SAMHD1 antibody performance with cell lysates, SAMHD1-deficient and -proficient cell lysates from THP-1 were used. The *Samhd1* KO clone showed no band in all tested antibodies, whereas a single band at the molecular

weight of 72.2 kDa for SAMHD1 was detected in the lysate of SAMHD1-proficient THP-1 cells. In addition, when loading purified His-SAMHD1 and GST-SAMHD1 protein, single bands were detected at the predicted molecular weight for every tested antibody and condition. On the other hand, the α-SAMHD1 antibodies did not react with His-SS19 protein, a His-tagged control protein, but a band at the respective molecular weight for His-SS19 was visible when an α-His antibody was used. Unspecific, faint bands were detected at 120 kDa height for rabbit α-SAMHD1 #1245 antibody in both SAMHD1-proficient and -deficient THP-1 cell lysates and at about 100 kDa for rabbit α-SAMHD1 #1245, #1246 and chicken α-SAMHD1 #H153 in the GST-SAMHD1 sample. These results verified the α-SAMHD1 antibodies for sufficient use to detect SAMHD1 in conventional immunoblotting.

All α-SAMHD1 antibodies were also validated for their use as primary antibodies in flow cytometry analysis in combination with an α-IgG or IgY-Alexa Fluor 488nm-conjugated secondary antibody. Primary antibody dilution series revealed antibody working concentrations for flow cytometry staining of 1:50 - 1:200 (data not shown). Respective antibody concentration used is indicated in figure 4.1. SAMHD1-deficient and proficient LN-18 cells were used to verify antibody performance for flow cytometry staining. All antibodies were able to distinguish between SAMHD1-positive and negative cell populations, for the rabbit α-SAMHD1 control antibody from Proteintech (figure 4.1D), for rabbit α-SAMHD1 #1245 and #1246 from Eurogentec (figure 4.1E and F) as well as for mouse α-SAMHD1 from Eurogentec (figure 4.1J) and for chicken α-SAMHD1 #H153 and #H154 antibodies from Eurogentec (figure 4.1K and L). These results indicated the utility of these antibodies for sufficient use to detect SAMHD1 in flow cytometry analysis.

Alternatively to the immunization with the whole SAMHD1 protein, a synthetic peptide-based antigen approach for SAMHD1 was carried out in rabbit using the peptide sequence 5'-VSNKRNGIDVDKWDY-3'. The 15 amino acid long sequence from SAMHD1 was determined through algorithm-based *in silico* analysis. Unfortunately, both antibodies produced in two rabbits (#1243 and #1244) were insufficient for analysis with both low specificity and sensitivity (data not shown) and were therefore excluded in further analysis.

In addition, the antibody sets were tested for their ability to detect murine SAMHD1. For that purpose, a cell lysate from the mouse macrophage cell line ANA-1 was used for immunoblotting together with the human SAMHD1-proficient cell line THP-1. α-SAMHD1 antibodies chicken #H153 and #H154 as well as two commercially available antibodies from Proteintech and Origene were able to detect murine SAMHD1 in ANA-1 cells, rabbit 1245 and 1246 showed weaker bands (figure 4.2). On the contrary, the mouse α-SAMHD1 antibody produced by Eurogentec was not able to detect murine SAMHD1 (figure 4.2).

Taken together, the customized α-SAMHD1 antibodies generated together with Eurogentec performed well compared to the commercially available α-SAMHD1 antibodies in both conventional immunoblotting and flow cytometry analysis. In addition, all α-SAMHD1 antibodies, except the mouse monoclonal α-SAMHD1 antibody from Eurogentec, were able to detect murine SAMHD1 by immunoblotting.

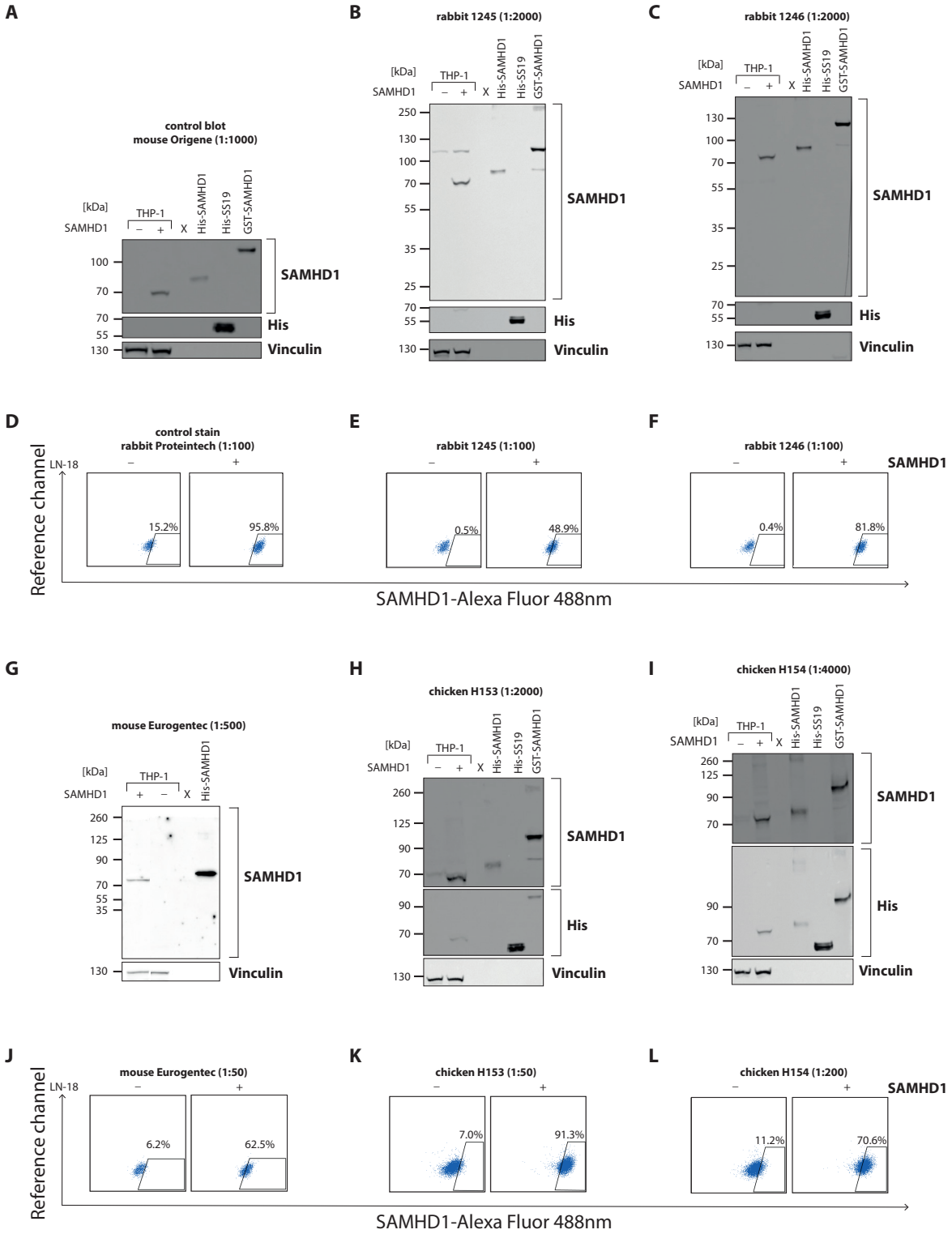

Figure 4.1: Continued on next page.

Figure 4.1: Customized α-SAMHD1 antibody validation with purified, tagged SAMHD1 and SAMHD1-deficient and -proficient THP-1 and LN-18 cells for immunoblotting and flow cytometry analysis, respectively. (A) Immunoblot with commercially available, monoclonal α-SAMHD1 TA501953 clone 1FG from Origene Technologies as well as flow cytometry analysis with polyclonal rabbit α-SAMHD1 antibody 12586-1-AP from Proteintech (D) were used as controls. Conventional immunoblotting as well as flow cytometry analysis is shown for the polyclonal rabbit α-SAMHD1 antibodies #1245 (B and E) and #1246 (C and F) as well as monoclonal mouse α-SAMHD1 antibody from Eurogentec EGT986 clone 11G6E8 (G and J) and polyclonal chicken α-SAMHD1 antibodies #H153 (H and K) and #H154 (I and L). His-SAMHD1 and GST-SAMHD1 proteins served as a control to verify antibody binding to the bacterial expressed human SAMHD1 protein. As a specificity control, the His-tagged protein His-SS19 was used. Flow cytometric analysis of SAMHD1 protein expression was performed using a secondary α-IgG or IgY antibody conjugated with the fluorophore Alexa Fluor 488nm. APC served as a reference channel. Immunoblots were loaded with 15 μg per cell lysate and 0.05 μg per purified protein. Immunoblots were performed by Katharina Hofmann (in-house) under my supervision.

4.2 *Samhd1* promoter DNA methylation as a modulator for expression and activity

After evaluating SAMHD1 protein detection with the series of new α-SAMHD1 antibodies, the regulation of SAMHD1 itself was investigated in more detail. DNA methylation of the promoter represents a major regulation mechanism for expression of *Samhd1*, introduced in section 1.2.3.2 [34]. In this section, AML cell lines facilitated the establishment of the assay and then, GBM cells were used in addition to determine the DNA methylation of the *Samhd1* promoter. Whereas all parental GBM cell lines used in this thesis showed positive SAMHD1 protein expression, AML cell lines included high SAMHD1 expressors (Monomac6, MV4-11, OCI-AML3) as well as those with no detectable SAMHD1 expression (HL-60, HEL).

4.2.1 Establishment of bisulfite sequencing to determine *Samhd1* promoter methylation status

In order to be able to determine the DNA methylation status of the *Samhd1* promoter, a bisulfite sequencing strategy was established that allowed to quantitatively determine the DNA methylation status in single CpG resolution.
Figure 4.3A shows the workflow for the procedure. As described in section 3.2.5, genomic DNA isolated from cell lines was bisulfite-converted and a region in the CpG island of the *Samhd1* promoter was amplified by PCR. The region was cloned into a bacterial expression plasmid and Sanger-sequenced to analyze the DNA methylation status of the *Samhd1*

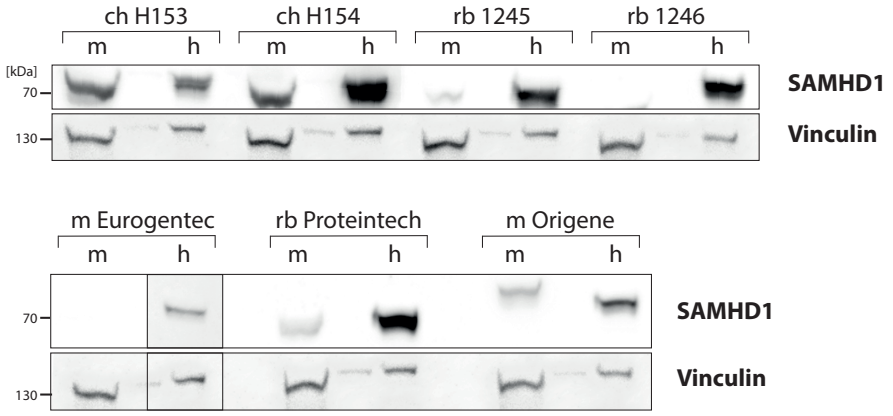

Figure 4.2: Customized α-human-SAMHD1 antibodies detect murine SAMHD1. Cell lysates from the murine macrophage cell line ANA-1 were used as murine SAMHD1 source (labeled as m) for SAMHD1 protein expression analysis by conventional immunoblotting, whereas the human SAMHD1-proficient monocytic cell line THP-1 served as a positive control (labeled as h). ch: chicken, rb: rabbit, m: mouse. The following α-SAMHD1 antibodies were used: polyclonal chicken H153 and H154, polyclonal rabbit 1245 and 1246, monoclonal mouse from Eurogentec, polyclonal rabbit from Proteintech and monoclonal mouse from Origene.

promoter. The human T cell leukemia cell line Jurkat showed no detectable SAMHD1 protein expression whereas THP-1 cells were highly SAMHD1-positive. In these cell lines, the link between promoter methylation and SAMHD1 protein expression was documented [34] used as positive and negative control for the SAMHD1 promoter methylation assay, respectively (figure 4.3B). In addition, commercial human methylated as well as unmethylated DNA was used to determine PCR conditions, where methylated and unmethylated DNA are amplified equally to assure that no specific methylation status is favored during PCR amplification. Figure 4.3C shows the agarose gel with the loaded PCR promoter amplification for all four samples, with different annealing temperatures. As the methylated and unmethylated controls showed similar band intensities with the annealing temperature 55°C, these samples were further processed.

The amplified DNA was sequenced at the single bacterial clone level through Sanger sequencing and analyzed with BiQ analyzer software [152]. The methylated control as well as the SAMHD1-negative cell line Jurkat were confirmed as methylated. On the other hand, the unmethylated control and the SAMHD1-positive cell line THP-1 were shown to be unmethylated in the assay (figure 4.3D), mirroring the literature [34]. These experiments verified the workflow for bisulfite sequencing for further evaluations.

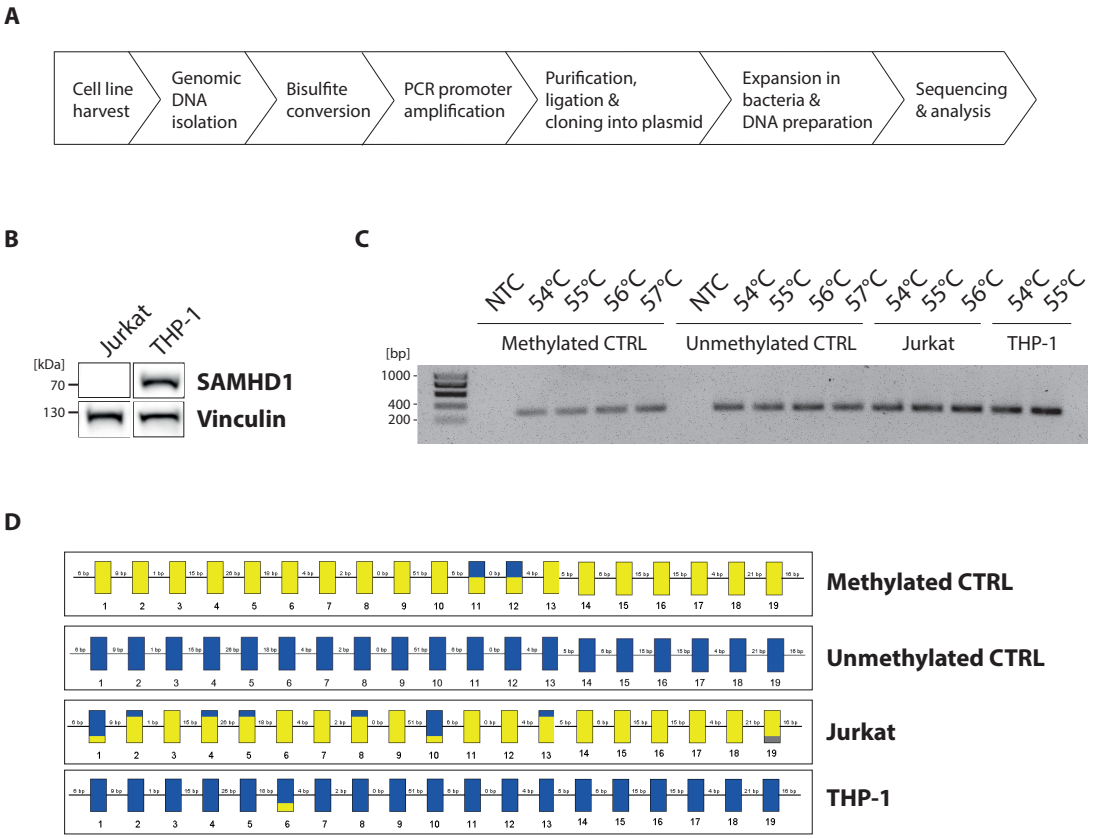

Figure 4.3: Establishment of bisulfite sequencing to determine SAMHD1 promoter methylation status. (A) Workflow to determine the promoter DNA methylation status. (B) SAMHD1 protein expression in Jurkat and THP-1 determined by conventional immunoblotting using the α-SAMHD1 antibody EGT986-11G6E8. (C) Agarose gel showing the PCR promoter amplification using different annealing temperatures. NTC: non-target control. (D) *Samhd1* promoter DNA methylation status on the CpG level. The numbers 1-19 indicate the individual CpG positions evaluated in the *Samhd1* promoter. Methylated CpGs are indicated in yellow, unmethylated CpGs in blue. Insufficient determination for unmethylated or methylated state at a certain CpG is indicated in grey. The methylation status of 5 sequences from 5 individual clones per condition are shown. Mix-colored status means that there were both unmethylated and methylated CpGs detected at this position. Sanger sequences were analyzed with BiQ analyzer software [152].

4.2.2 SAMHD1 promoter is methylated in SAMHD1-negative and unmethylated in SAMHD1-positive parental glioblastoma multiforme and acute myeloid leukemia cell lines

In order to profile DNA methylation in the promoter as a modulator of SAMHD1 expression and activity, the DNA methylation status of the *Samhd1* promoter was determined in AML and GBM cell lines. Figure 4.4 shows DNA methylation in the *Samhd1* promoter on the CpG level. For AML cell lines, the SAMHD1-negative cell line HL-60 was methylated in this specific sequence, whereas the SAMHD1-positive cell lines Monomac6, MV4-11 and OCI-AML3 were unmethylated (figure 4.4A). In addition, two GBM cell lines, MZ-18 and U-87 MG, were evaluated. Both are SAMHD1-positive with MZ-18 as a rather low SAMHD1 protein expressor and U-87 MG as a rather high SAMHD1 protein expressor. Despite these quantitative differences, both MZ-18 and U-87 MG showed unmethylated CpGs in the CpG island of the *Samhd1* promoter (figure 4.4B). Cell's SAMHD1 protein expression status is indicated on the right.
Figure 4.4A shows one exception: the AML cell line HEL showed no detectable SAMHD1 protein expression in conventional immunoblotting, but appeared to have an unmethylated *Samhd1* promoter, which does not go in line with an exclusively methylation-regulated expression regulation pattern. These experiments indicated that, besides a well established expression regulation by DNA methylation in the promoter, SAMHD1 protein expression can most likely be regulated by additional mechanisms. It is not known whether the *Samhd1* gene in HEL is intact, whereas undetectable SAMHD1 protein levels in this cell line are confirmed in various publications [101, 107].
Taken together, bisulfite sequencing was successfully established in the lab and quantitatively recapitulated the known regulation basis for SAMHD1 expression through DNA methylation in the *Samhd1* promoter in AML cell lines. In addition, the *Samhd1* promoter was unmethylated in the tested SAMHD1-positive GBM cell lines.

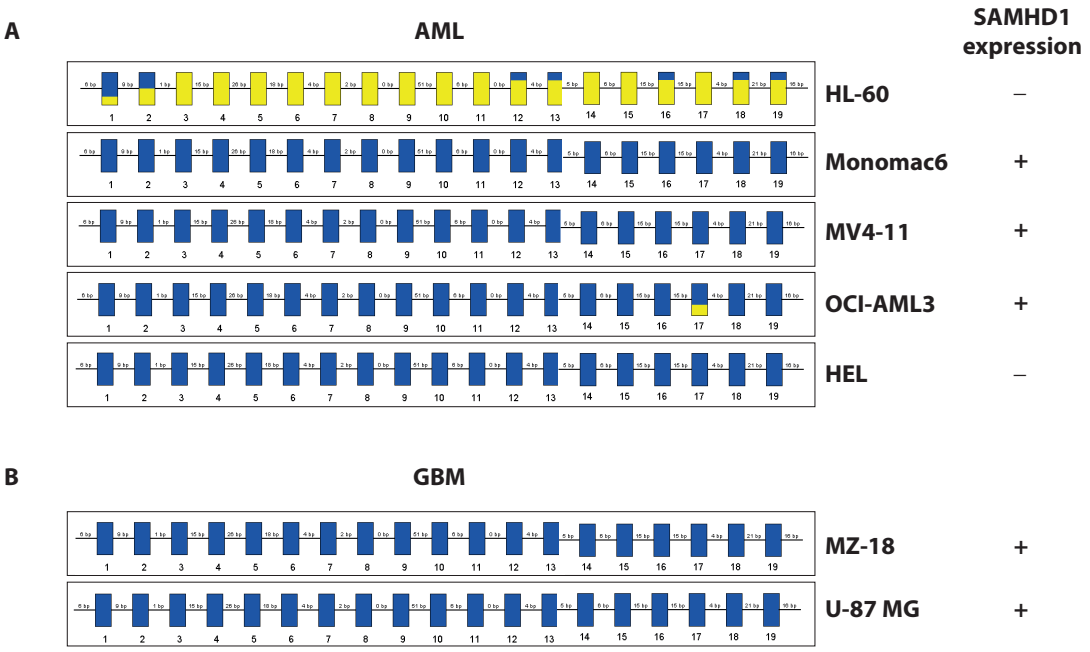

Figure 4.4: DNA methylation status in the *Samhd1* promoter on the CpG level. (A) AML cell lines HL-60, Monomac6, MV4-11, OCI-AML3 and HEL were analyzed for their *Samhd1* promoter DNA methylation status. (B) *Samhd1* promoter DNA methylation status in GBM cell lines MZ-18 and U-87 MG. Numbers 1-19 indicate the individual CpG positions evaluated in the *Samhd1* promoter. Methylated CpGs are indicated in yellow, unmethylated CpGs in blue. Insufficient determination for unmethylated or methylated state at a certain CpG is indicated in grey. Mix-colored status means that there were both unmethylated and methylated CpGs detected at this position. Sanger sequences were analyzed with BiQ analyzer software [152]. SAMHD1 protein expression for each cell line was evaluated by conventional immunoblotting by Dr. Ernesto Mejías Pérez (in-house) and is indicated on the right.

4.3 SAMHD1 expression in glioblastoma multiforme

4.3.1 SAMHD1 is abundantly expressed in glioblastoma multiforme cell lines

In order to obtain a broad SAMHD1 protein expression profile in GBM, SAMHD1 protein expression was determined in GBM cell lines. Therefore, 15 different, in the neuro-oncology field widely excepted, cell lines were analyzed for *Samhd1* mRNA expression through quantitative PCR (shown at the top, figure 4.5A) and SAMHD1 protein expression through immunoblotting (shown at the bottom, figure 4.5A). All tested cell lines showed detectable *Samhd1* mRNA and SAMHD1 protein expression levels, but differences in the intensity of SAMHD1 expression levels. Whereas some cell lines (e.g. MZ-18 and

U-138 MG) looked like low SAMHD1 expressors, others like GMS-10, LN-18 and TU140 showed higher SAMHD1 protein levels. Of note, blotting *Samhd1* mRNA and SAMHD1 protein levels showed no statistically significant correlation ($r^2 = 0.1824$, $P = 0.0717$, figure 4.5B).

4.3.2 SAMHD1 is expressed in patient-derived xenografts of glioblastoma multiforme

Patient-derived xenografts (PDXs) are isolated cells from GBM tumor patient tissue. They grow in spheres and mimic the primary tumor better than conventional, immortal cell lines [155]. In collaboration with Prof. Rainer Glaß (LMU Munich, Germany) and Dr. Massimo Squatrito (CNIO, Madrid, Spain), we were able to test 11 different GBM PDXs for SAMHD1 protein expression by immunoblotting (figure 4.5C and D). Except for "Line11", all tested GBM PDXs showed detectable SAMHD1 protein expression levels. Whereas the PDXs from Prof. Rainer Glaß in figure 4.5C differed in SAMHD1 protein levels, the PDXs from Dr. Massimo Squatrito showed comparable levels (figure 4.5D).

4.3.3 SAMHD1 is expressed in glioma and glioblastoma multiforme patient tissue

In order to elucidate SAMHD1 expression in the *in vivo* context, tumor biopsy sections from 30 different first diagnosed GBM/glioma patients (10 with grade IV, 10 with grade III and 10 with grade II) were stained for SAMHD1 and histologically analyzed for SAMHD1 protein expression in collaboration with Dr. Rupert Egensperger and colleagues (LMU Munich, Germany). This analysis served as a first step to profile SAMHD1 protein expression *in vivo*. Figure 4.6A shows the percentages of SAMHD1-stained cells for each tumor sample - categorized with the grading system of the World Health Organisation (WHO) [114]. All of the stained sections showed SAMHD1-positive cells in the tumor mass. With increasing WHO grade, there were statistically significant higher numbers of SAMHD1-positive cells in the tumor mass of grade IV GBM compared to grade II glioma ($P = 0.0246$). On the other hand, when we looked at the intensity of SAMHD1 nuclear staining, significantly higher SAMHD1 staining was observed in the nucleus of grade IV GBM in comparison to grade II glioma ($P = 0.0340$, figure 4.6B).
Also, representative pictures of grade IV GBM sections are shown in figure 4.6C. These pictures as well as the bar graph in figure 4.6A showed that the fraction of strongly SAMHD1-positive cells varied among the different grade IV patients (2 - 20% SAMHD1-positive cells). This observation emphasizes an intertumoral heterogeneity of SAMHD1 protein expression in GBM. In addition, we saw that the intensity of SAMHD1 expression differed within the tumor mass, reflecting intratumoral heterogeneity.
Taken together, we created a SAMHD1 expression profile in the context of GBM and showed that SAMHD1 is broadly expressed in GBM, shown with GBM cell lines, PDXs and primary tumor tissue.

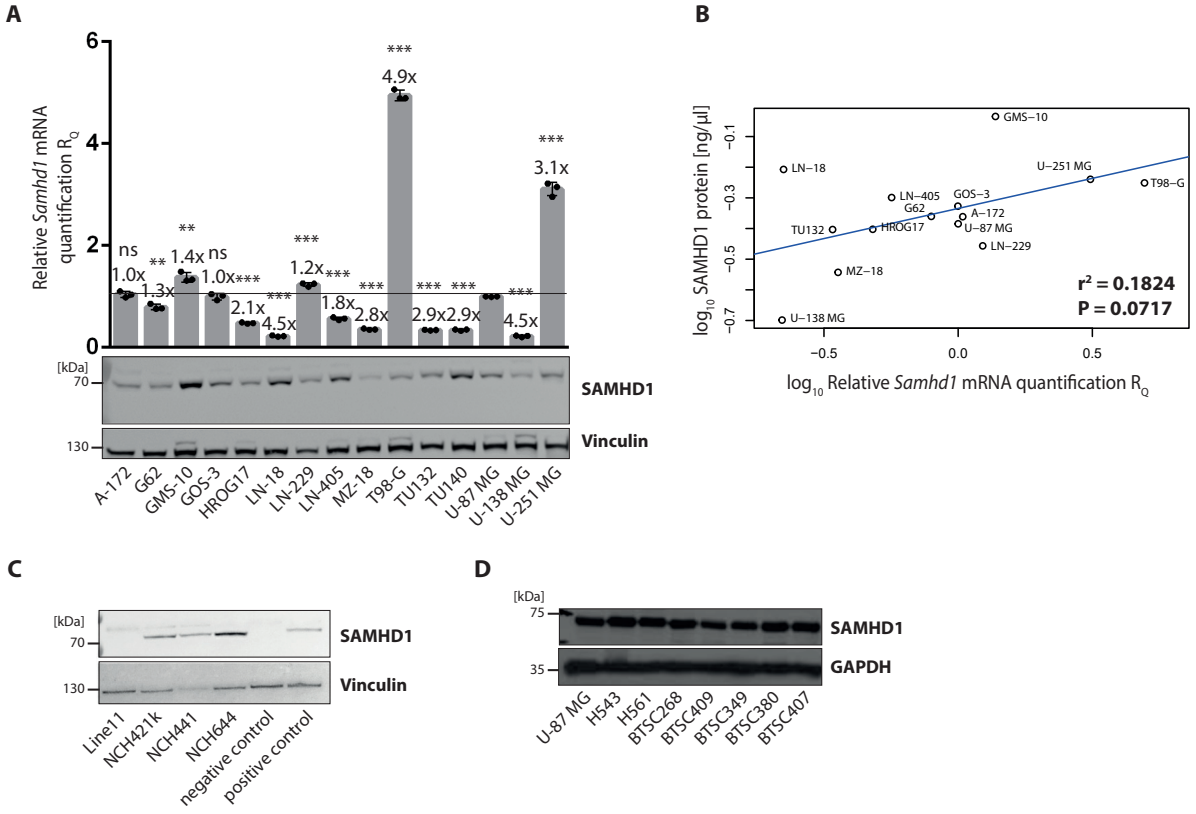

Figure 4.5: SAMHD1 is expressed in established GBM cell lines and PDXs. (A) Top: *Samhd1* mRNA expression levels for 15 different GBM cell lines were determined by qPCR. RNaseP was used as a housekeeping gene and samples were normalized to U-87 MG, which was set to 1. Factor of difference to U-87 MG parental is shown. Statistical analysis: Student's unpaired t-test: ***P $<$ 0.001, **P $<$ 0.01, *P $<$ 0.05, ^{ns}P $>$ 0.05. Bottom: SAMHD1 protein expression levels for the 15 GBM cell lines were determined with conventional immunoblotting and was performed by Dr. Ernesto Mejías Pérez (in-house). (B) Dot plot comparing *Samhd1* mRNA levels (x-axis) with SAMHD1 protein levels (y-axis). (C,D) SAMHD1 protein expression levels were determined in GBM PDXs with immunoblotting using the α-SAMHD1 antibody EGT986-11G6E8. PDX samples from (C) were kindly provided by Prof. Rainer Glaß (LMU Munich, Germany). LN-18 SAMHD1 KO clone SKO1 served as negative control, LN-18 parental cells as positive control for SAMHD1 expression. Immunoblotting in (D) was performed by Dr. Massimo Squatrito (CNIO, Madrid, Spain). U-87 MG parental cells were loaded as a positive control for SAMHD1 expression.

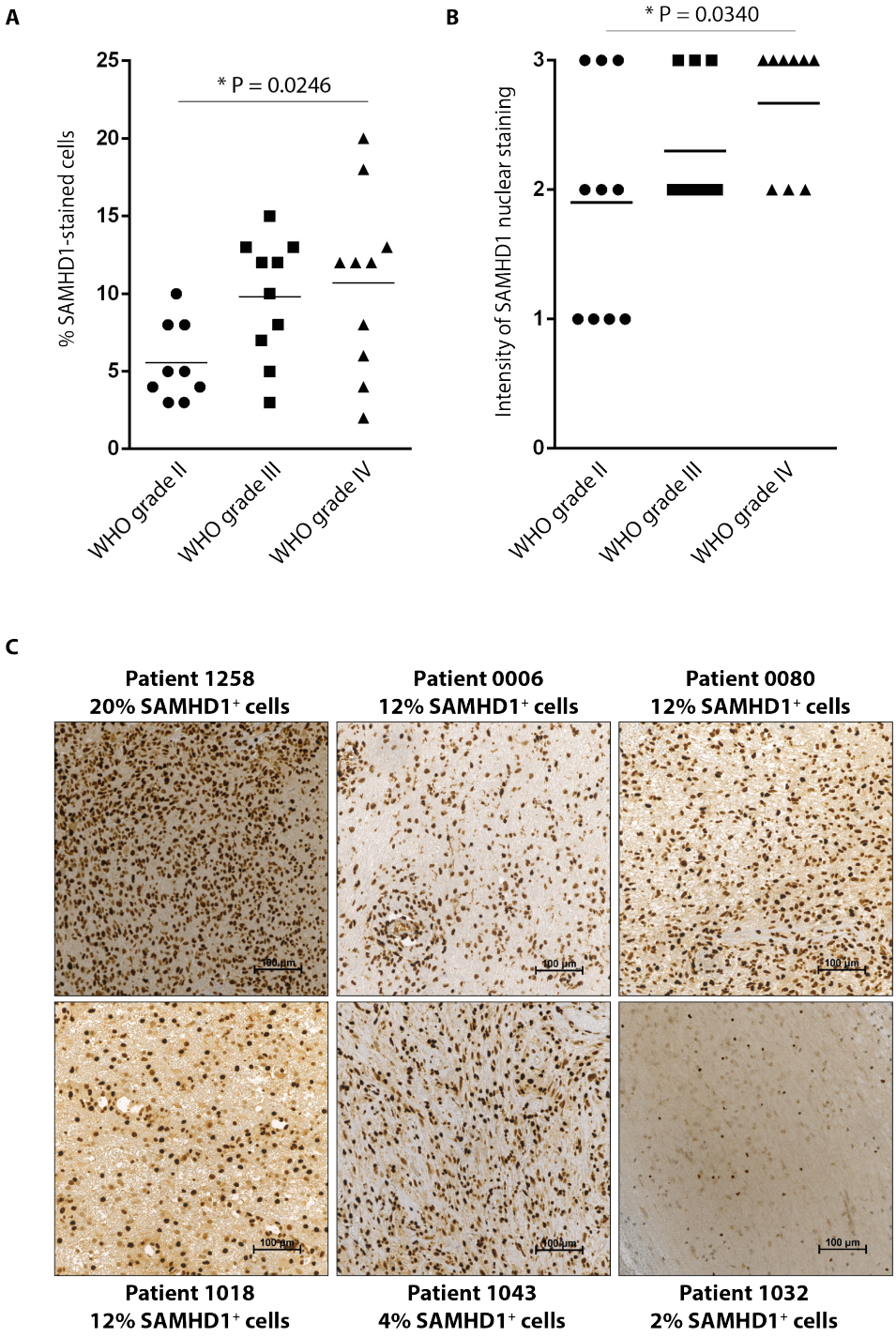

Figure 4.6: Continued on next page.

Figure 4.6: SAMHD1 is expressed in grade IV GBM patient tissue, is higher in WHO grade IV GBM compared to grade II and III glioma and varies between patients in grade IV GBMs. (A,B) Tumor sections of grade II and III gliomas as well as grade IV GBM were stained for SAMHD1 protein expression and are shown as percentage of SAMHD1-stained cells in (A) and intensity of SAMHD1 nuclear staining in (B). The percentages show strongly SAMHD1-stained cells in the section: 0 = no staining, 1 = 3-35%, 2 = 36-70%, 3 $\geq$ 70%. Statistical analysis: Student's unpaired t-test: *P < 0.05. (C) Tumor sections of 6 different grade IV GBM first-diagnosed patients stained with the rabbit α-SAMHD1 antibody 12586-1-AP from Proteintech verified SAMHD1-positive cells in the tumor mass. The DAB (3,3'-Diaminobenzidine) staining and the histological analysis was performed by Dr. Rupert Egensperger and colleagues (LMU Munich, Germany). Brown staining represents SAMHD1 expression. Analysis in (A,B) was performed by Dr. Ernesto Mejías Pérez (in-house). All shown material is classified according to the guidelines for classification of CNS tumors by the WHO, 4th Edition from 2007 [114]. Objective: 20x.

4.3.4 Characterizing SAMHD1-positive cells in glioblastoma multiforme tumor mass

For further characterization of SAMHD1-positive cells in sections of the tumor mass, neighboring slices of the same section were stained for cell identification markers of major cell types in GBM, namely CR3-43 (for microglia and macrophages), CD68 (for macrophages), CD8 (for T cells) and NeuN (for neurons, figure 4.7). Firstly, an image of the whole section stained with chicken α-SAMHD1 antibody #H154 was created and assembled by merged consecutive recording in order to choose a representative area in the section (figure 4.7A). In figure 4.7B, a zoom into a representative section shows staining of SAMHD1 and cell identification markers for the same position. Whereas microglia and macrophages were frequently present in the tumor mass [132], cells from neighboring tissue are known to not infiltrate immensely into the GBM tumor site [115] and therefore can not account for the complete SAMHD1-positive cells. As expected, CD8 T cells and neurons were barely present in the tumor mass [132].
Notably, the customized antibody chicken α-SAMHD1 #H154 (SAMHD1 (ch)) showed a good sensitivity in immunohistochemical staining and less background compared to the commercially available rabbit α-SAMHD1 antibody (SAMHD1 (rb)) used in parallel (figure 4.7B).
Taken together, even though a specific tumor cell marker is not available in the GBM field, the stainings of neighboring slides with standard cell identification markers mirrored the cell types known in GBM [132] and gave a first hint to the SAMHD1-expressing cell composition in GBM tissue. Whereas CD8 T cell marker and NeuN neuron marker were negative in the sections, a high fraction of microglia and macrophages was detected, which may explain partly but not entirely the SAMHD1-positive cells in the tumor mass. Nevertheless, if the tumor cells in GBM patient tissue are indeed SAMHD1-positive can not be concluded from these sections.

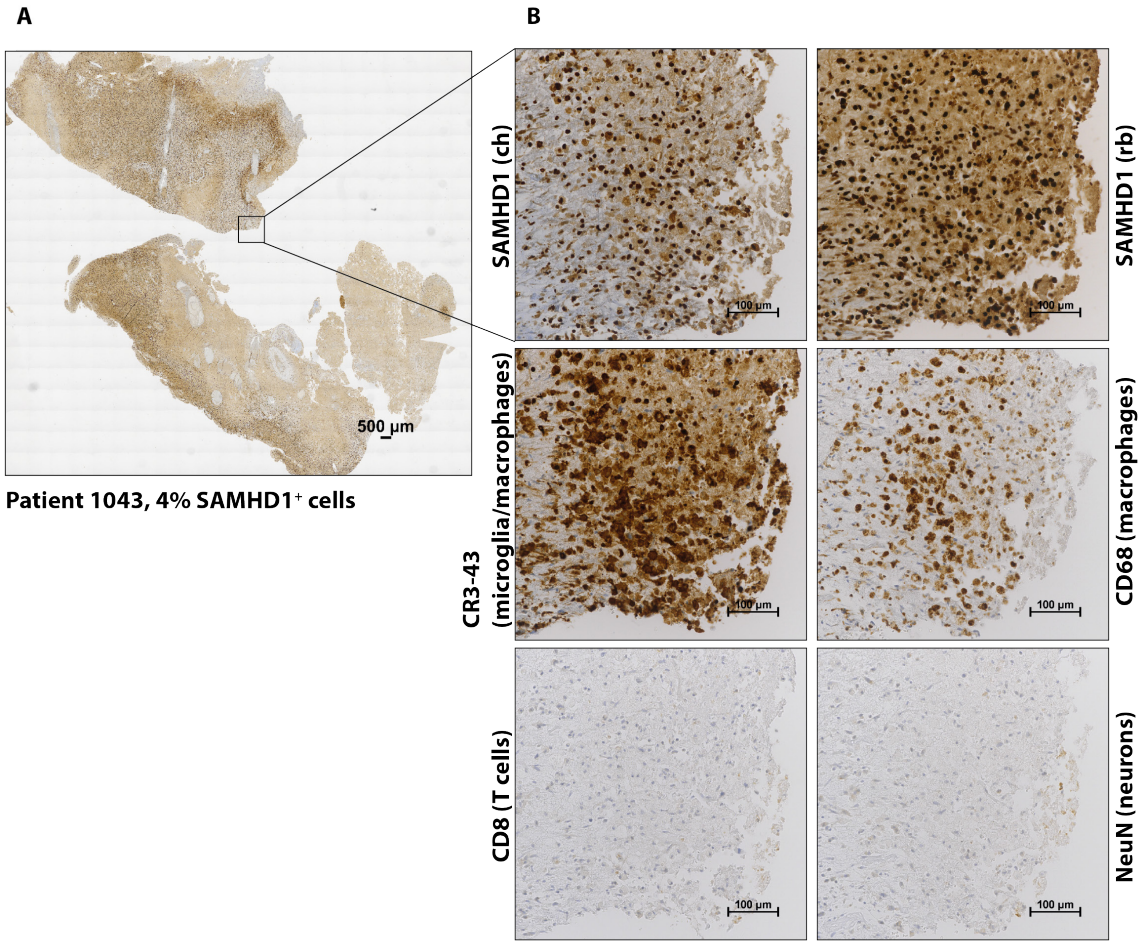

Figure 4.7: Profiling of SAMHD1-positive cells in the GBM tumor mass. (A) Whole tumor section from grade IV GBM patient 1043, stained for SAMHD1 with the chicken α-SAMHD1 antibody #H154. Objective: 10x. (B) A representative section from the whole tumor section shown in (A); neighboring slices of the same section were stained for different cell markers in order to further characterize the origin of the SAMHD1-positive cells in the tumor mass. Parallel sections were stained for SAMHD1 with two different antibodies as well as the cell markers CR3-43 (microglia and macrophages), CD68 (macrophages), CD8 (T cells) and NeuN (neurons). ch: chicken α-SAMHD1 antibody #H154, rb: rabbit α-SAMHD1 antibody 12586-1-AP from Proteintech. Objective: 20x.

4.4 Manipulation of SAMHD1 protein expression in glioblastoma multiforme cell lines

4.4.1 Vpx-containing virus-like particles sensitizes glioblastoma multiforme cell lines to cytarabine

First, we were interested whether sensitivity to ara-C correlated with SAMHD1 protein levels in GBM cell lines. Therefore, we treated parental GBM cell lines with a dilution series of ara-C and analyzed culture viability 4 days later using the luminescence-based viability assay Cell Titer Glo 2.0. Figure 4.8A shows the dot plot for ara-C sensitivity against SAMHD1 protein expression, which showed no statistically significant correlation (r^2 = -0.04542, P = 0.4865). As all GBM cell lines were SAMHD1-positive (figure 4.5A), we reasoned that the differences in SAMHD1 levels may be too small in contrast to AML cells [101] to establish a significant correlation.
To further test for SAMHD1-dependent ara-C sensitivity and to see whether the absence of SAMHD1 in GBM cell lines may sensitize to ara-C treatment, we employed the tool to temporarily degrade SAMHD1 in cell culture by treatment with Vpx-VLPs (section 1.2.6). Therefore, GBM cell lines were pre-treated with either Vpx-VLPs or medium only (mock) for 24 hours before initiation of ara-C treatment. Figure 4.8B shows that all cell lines displayed significantly lower effective dose 50 (ED_{50}) values for ara-C when treated with Vpx-VLPs in comparison to mock-treated cells. Successful Vpx-dependent SAMHD1 degradation was verified by immunoblotting (data not shown). This means that the absense of SAMHD1 sensitized GBM cells to ara-C, which goes along with the SAMHD1 dependency observed for ara-C treatment in AML [101]. Depending on the cell line, the difference of treatment with either Vpx-VLPs or mock showed factors of ara-C sensitization ranging from 6- to 63-fold.
These results report SAMHD1-associated ara-C sensitivity in GMB context for the first time. In addition, we establish that SAMHD1-associated ara-C sensitivity is not limited to a certain cell line, but rather a broad phenomenon.

4.4.2 CRISPR/Cas9 indels result in *Samhd1* knockout in glioblastoma multiforme cell lines

In order to study SAMHD1-dependent ara-C sensitivity in a KO setting, *Samhd1* KO clones of three different GBM cell lines, LN-18, U-251 MG and U-87 MG, were generated using CRISPR/Cas9-mediated genome editing. Figure 4.9A shows the workflow including cell seeding and transfection with a vector-based *Samhd1* gRNA, *Cas9* and a *mCherry* fluorescence cassette. After mCherry-positive sort and single cell seeding, single clones were picked 2 weeks later, lysed and the target site was amplified through PCR. The successful generation of *Samhd1* KO monoclones was validated by MiSeq sequencing [153]. Figure 4.9 shows *Samhd1* KO validation for (B) LN-18, (C) U-251 MG and (D) U-87 MG represented in pie charts. Whereas *Samhd1* KO clones displayed two different out-of-frame mutations

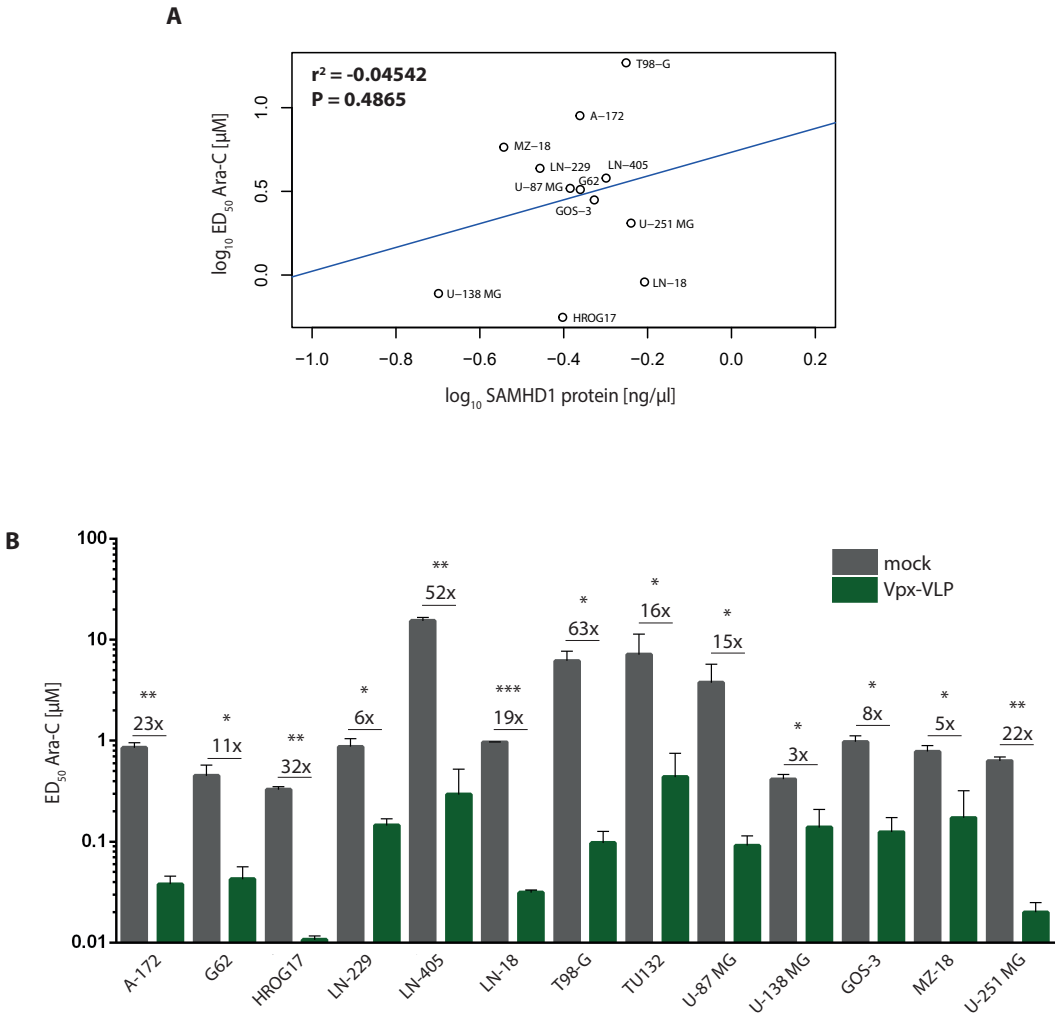

Figure 4.8: GBM cell lines are sensitized to ara-C treatment when pre-treated with SAMHD1 degrading Vpx-containing virus-like particles. (A) Cell viability of 13 GBM cell lines was analyzed 4 days after ara-C treatment and is shown as a dot plot together with SAMHD1 protein levels established by Wes immunoblotting. ED_{50} of ara-C is shown in μM. (B) Cells were treated with Vpx-VLPs for 24 hours prior to ara-C treatment. Cell viability was analyzed 4 days later. Error bars indicate standard deviation (s.d.). n=2 (technical duplicates). A representative experiment from 5 biological replicates is shown. Statistical analysis: Student's unpaired t-test: *P $<$ 0.05; **P $<$ 0.01; ***P $<$ 0.001. Experiments were performed by Dr. Ernesto Mejías Pérez (in-house).

at the gRNA binding site in the *Samhd1* exon 1, indicating both alleles were successfully edited, *Samhd1* control (CTRL) clones, which went through the same KO generation procedure as the KO clones, showed no indels at the side of editing. The following number of individual clones were generated: for LN-18, 9 *Samhd1* KO and 6 CTRL clones; for U-251 MG, 7 *Samhd1* KO and 3 CTRL clones and for U-87 MG, 1 *Samhd1* KO and 1 CTRL clone.
Samhd1 KO and CTRL clones were also validated at the protein level. Conventional immunoblotting showed complete loss of SAMHD1 protein in all monoclonal *Samhd1* KO clones, whereas all respective *Samhd1* CTRL clones displayed detectable levels of SAMHD1 protein expression. As these cells were monoclonal, SAMHD1 protein levels varied somewhat between the different CTRL clones.
All in all, CRISPR/Cas9-mediated *Samhd1* KO generation was validated on the genomic and protein level and established a set of monoclonal SAMHD1-deficient KO and SAMHD1-proficient CTRL GBM monoclones.

4.4.3 Sensitivity to cytarabine is significantly increased in *Samhd1* knockout cell lines of glioblastoma multiforme

In order to further examine the SAMHD1-dependent ara-C sensitivity observed upon Vpx-VLP treatment in section 4.4.2, CRISPR/Cas9-generated *Samhd1* KO and CTRL clones were treated with increasing concentrations of ara-C. Figure 4.10 displays the ED_{50} values for ara-C and shows that knocking out *Samhd1* markedly sensitizes all three GBM cell lines to ara-C treatment compared to *Samhd1* CTRL cells. The individual clones showed slightly different ED_{50} values within the groups of *Samhd1* KO or CTRL clones, respectively. If possible, a minimum of three different clones was included in these studies to exclude clonal, SAMHD1-independent effects. E.g. LN-18 *Samhd1* KO clone D7 displayed a higher ED_{50} value than the other *Samhd1* KO clones and would thus not be a good choice for a representative KO clone. Taken together, these data validated that absence of SAMHD1 protein significantly sensitized GBM cells to ara-C.

4.4.4 SAMHD1 reconstitution in SAMHD1-deficient glioblastoma multiforme cell lines reduces sensitivity to cytarabine

Based on the *Samhd1* KO validation at DNA and protein level as well as their sensitivity to ara-C described in section 4.4.2 and 4.4.3, representative clones were chosen to be used for SAMHD1 reconstitution. LN-18 *Samhd1* KO clone SKO1 as well as U-251 MG *Samhd1* KO clone H3 and U-87 MG *Samhd1* KO clone SKO1 showed a clear *Samhd1* KO in both alleles on the DNA level and no detectable protein in immunoblotting. In addition, they show average sensitivity enhancement to ara-C compared to all *Samhd1* KO clones (figure 4.9 and 4.10).
In order to reintroduce SAMHD1 into the KO clones, the natural *Samhd1* cDNA sequence from the bacterial expression vector pGEX-4T-1 His-SAMHD1 was cloned into the plas-

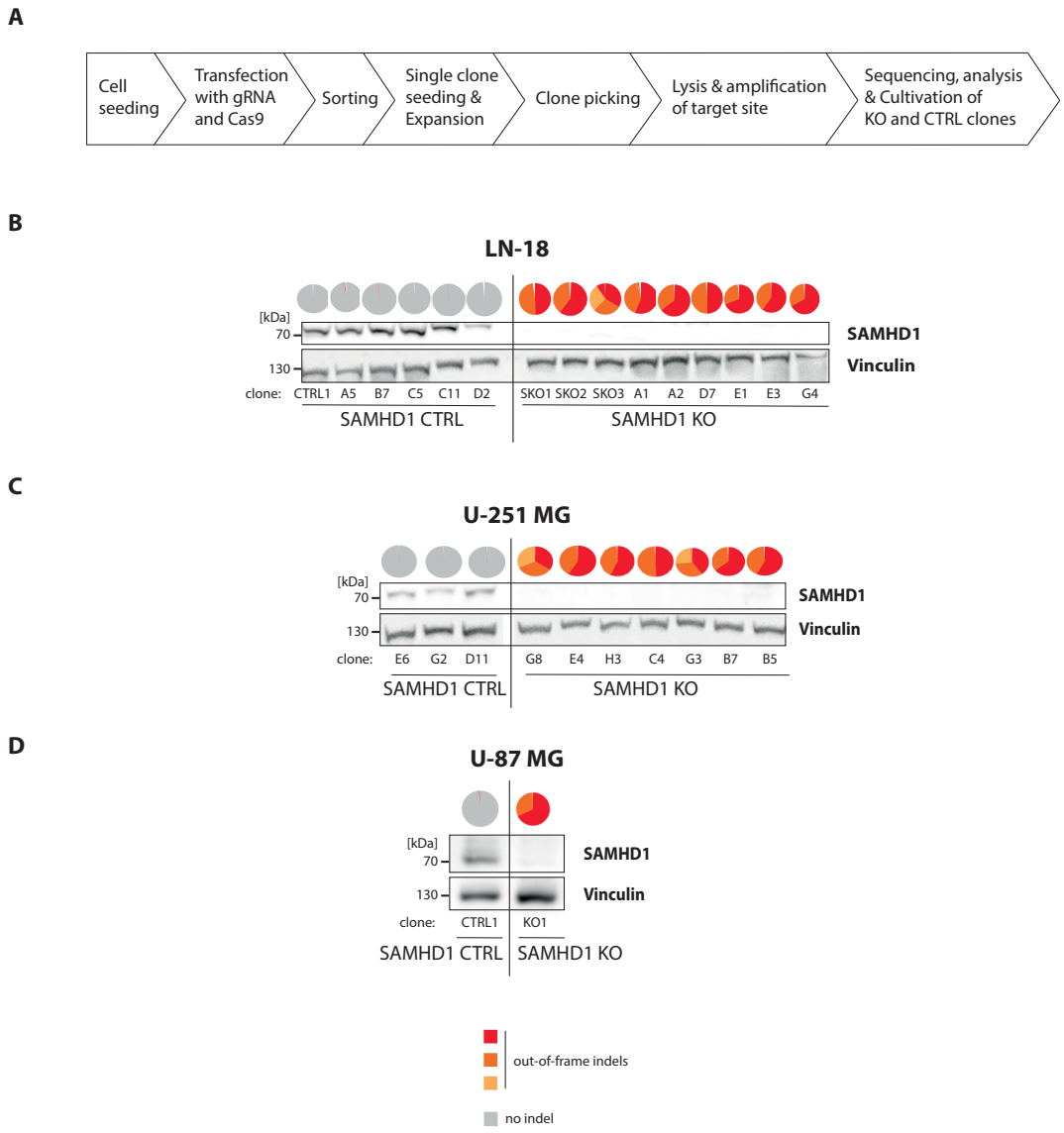

Figure 4.9: CRISPR/Cas9-generation of *Samhd1* KO clones in GBM cell lines. (A) Workflow of *Samhd1* KO generation through CRISPR/Cas9. (B-D) Characterization of *Samhd1* KO and CTRL clones (B) LN-18, (C) U-251 MG and (D) U-87 MG by next generation sequencing (NGS) analysis and immunoblotting. The pie charts represent the editing efficiencies at the gRNA target site in the *Samhd1* gene for each clone indicated. Grey charts show *Samhd1* CTRL clones with no indels at this site; red/orange charts show *Samhd1* KO clones with two different out-of-frame mutations for the two alleles; red/orange/yellow charts represent *Samhd1* KO clones with three different out-of-frame mutations detected. For KO validation on the DNA level, pie charts were generated with Outknocker 2.0 based on Miseq data [153]. For *Samhd1* KO verification on the protein level, SAMHD1 expression levels were analyzed by immunoblotting using the commercially available α-SAMHD1 antibody 1FG TA501953 from OriGene Technologies. *Samhd1* KOs were partially established together with Dr. Ernesto Mejías Pérez and Dr. Paul R. Song Wratil (in-house).

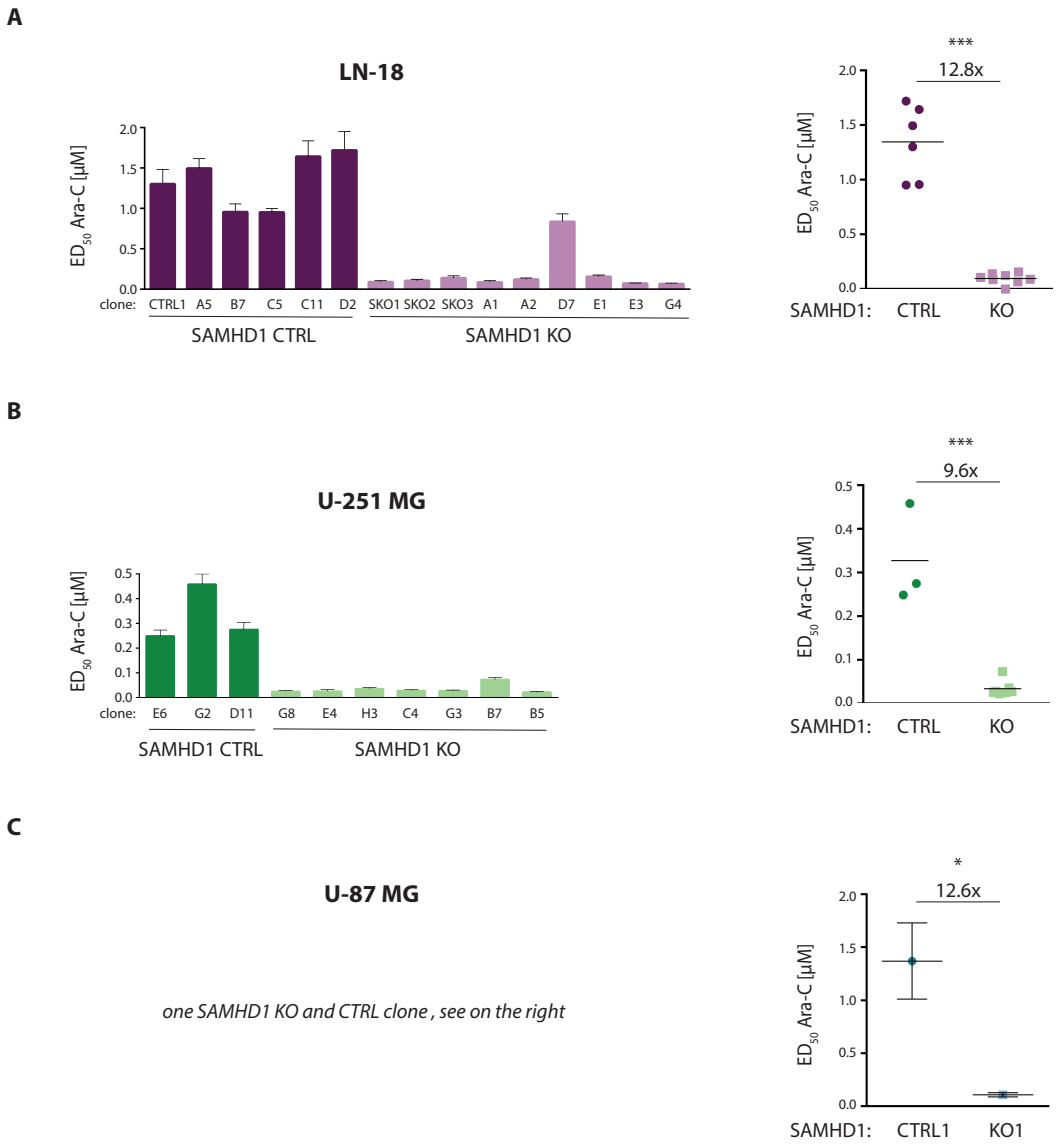

Figure 4.10: *Samhd1* KO in GBM cells increases sensitivity to ara-C. Cytotoxicity assay for *Samhd1* KO and CTRL clones in GBM cell lines (A) LN-18, (B) U-251 MG and (C) U-87 MG. Bar charts show the ED_{50} of ara-C in μM for individual clones (on the left) and group analysis for *Samhd1* KO and CTRL clones (on the right). Cell viability was analyzed 4 days after ara-C treatment. Error bars indicate standard deviation (s.d.). Statistical analysis: Student's unpaired t-test: *P $<$ 0.05; ***P $<$ 0.001. The experiment in B was performed by Dr. Ernesto Mejías Pérez (in-house).

mid pCDH-EF1α-BFP-1, a lentiviral transfer vector expressing mtagBFP that was kindly provided by Prof. Wolfgang Hammerschmidt (Helmholtz Center Munich, Germany).
In the pCDH-EF1α-SAMHD1-BFP-1 plasmid, the *Samhd1* wildtype sequence is followed by a self-cleaving T2A-site and a mtagBFP fluorescence cassette. Both genes are under the same promoter, the EF1α promoter. After the transfer vector was successfully cloned, the *Samhd1* wildtype sequence was mutated in a site-directed manner at position D311 to generate a *Samhd1* D311A mutant plasmid. *Samhd1* D311A represents a dNTPase-inactive mutant [6] and is used as an additional control in the following experiments.
The *Samhd1* KO clones from LN-18, U-251 MG and U-87 MG were then transduced with lentiviral vectors containing either pCDH-EF1α-SAMHD1 WT-BFP-1 (+ SAMHD1 WT) or pCDH-EF1α-SAMHD1 D311A-BFP-1 (+ SAMHD1 D311A), sorted for mtagBFP-positivity, expanded and validated in order to have a stable SAMHD1/mtagBFP protein expressing population for further characterization (workflow in figure 4.11A).
Figure 4.11B shows mtagBFP protein levels analyzed by flow cytometry. Whereas the untransduced parental and *Samhd1* KO clones are negative for mtagBFP, the transduced populations for SAMHD1 wildtype and D311A showed almost 100% mtagBFP positivity in all three cell lines. For the U-251 MG *Samhd1* KO reconstituted with SAMHD1 D311A, the majority of cells were mtagBFP-positive (83.8%) and 16.2% of cells still showed no mtagBFP signal in flow cytometry. As already this somewhat impure U-251 MG +SAMHD1 D311A mirrored the dNTPase-function-dependent ara-C sensitivity, undergoing another sorting round was not pursued at this point of evaluation.
Looking at their cytotoxicity to ara-C, *Samhd1* KO cells reconstituted with pCDH-EF1α-SAMHD1 WT-BFP-1 mimicked the parental cells' ara-C sensitivity, while *Samhd1* KO cells reconstituted with pCDH-EF1α-SAMHD1 D311A-BFP-1 mirrored the *Samhd1* KO sensitivity for ara-C in all three GBM cell lines (figure 4.11C, top).
In addition, conventional immunoblotting confirmed the SAMHD1 protein reintroduction through transduction with the transfer vector pCDH-EF1α-SAMHD1 WT/D311A-BFP-1 (figure 4.11, bottom). mtagBFP protein was also detected by immunoblotting and confirmed the mtagBFP expression levels obtained by flow cytometry (figure 4.11, bottom).
Taken together, SAMHD1 wildtype reconstitution markedly reduced sensitivity to ara-C in all three *Samhd1* KO GBM cell lines, whereas reconstitution with the dNTPase-inactive SAMHD1 mutant D311A recapitulated the phenotype of the *Samhd1* KO cells. This demonstrated that the sensitivity to ara-C is not only dependent on SAMHD1, but directly associated to its dNTPase function.

4.4.5 Ara-CTP levels are higher in *Samhd1* knockout cells compared to parental glioblastoma multiforme cell lines

To confirm whether the higher ara-C cytotoxic sensitivity in SAMHD1-deficient compared to SAMHD1-proficient GBM cells is due to the dNTPase activity of SAMHD1 against the metabolically active, toxic form of ara-C (ara-CTP), ara-CTP levels were quantified by LC–MS/MS in collaboration with Prof. Gerd Geißlinger's laboratory (University Hospital

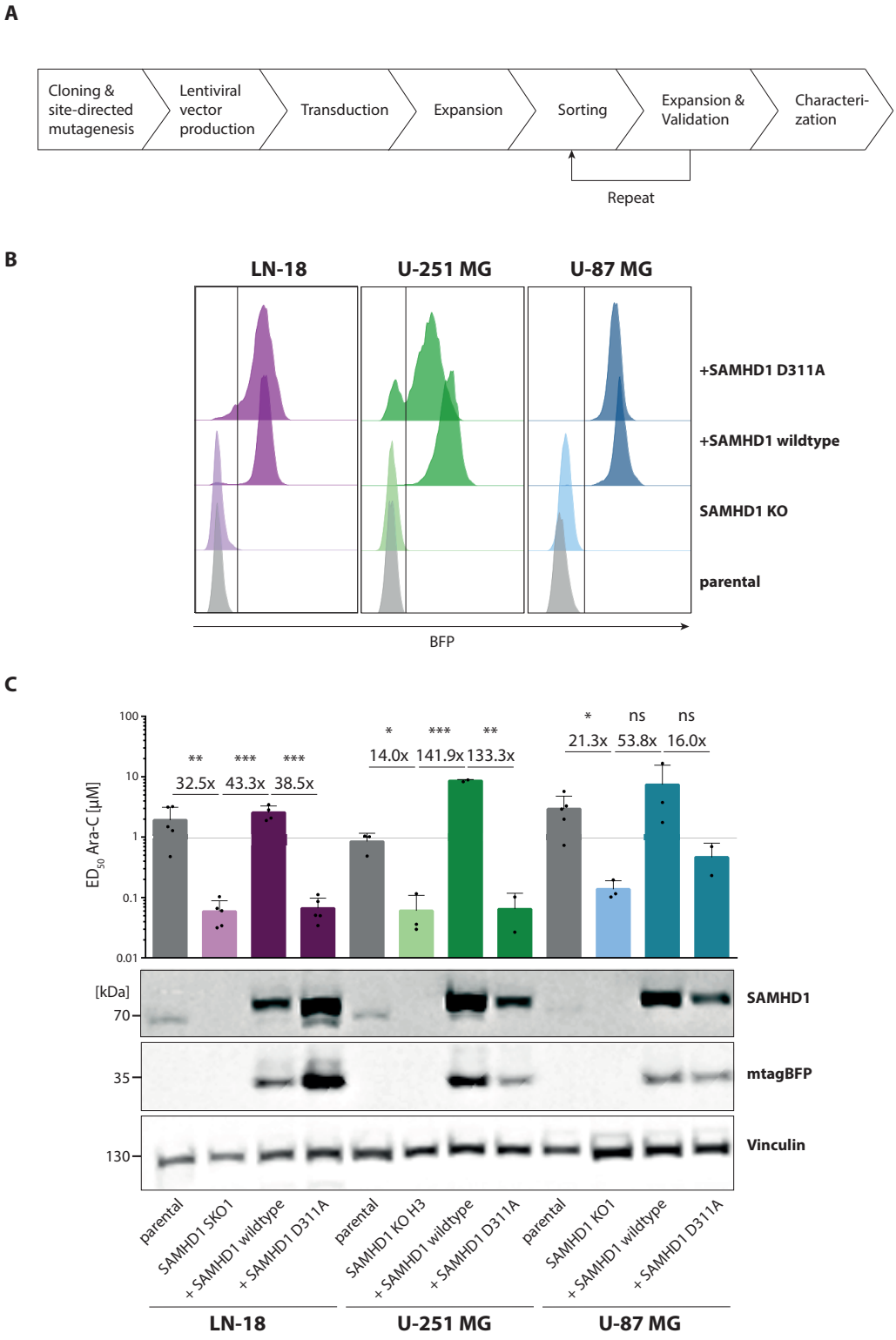

Figure 4.11: Continued on next page.

Figure 4.11: Reconstitution of *Samhd1* KO with SAMHD1 wildtype decreases sensitivity to ara-C in LN-18, U-251 MG and U-87 MG GBM cells. (A) Workflow for reconstitution of *Samhd1* KO clones. (B) Flow cytometry analysis for mtagBFP, measured in the BFP channel. LN-18 and U-251 MG cells were sorted twice, U-87 MG cells were sorted three times. The vertical line in the flow cytometry plots separates mtagBFP-negative from positive events. (C) Top: Cell viability was analyzed 4 days after ara-C treatment. ED_{50} of ara-C is shown in μM. Error bars indicate standard deviation (s.d.). $n \geq 3$ (biological replicates). Statistical analysis: Student's unpaired t-test: ***P < 0.001, **P < 0.01, *P < 0.05, ^{ns}P > 0.05. Bottom: SAMHD1 and mtagBFP protein expression levels were analyzed by immunoblotting.

of the Goethe University, Frankfurt am Main, Germany). Figure 4.12 shows significantly elevated Ara-CTP levels in the GBM LN-18, U-251 MG and U-87 MG *Samhd1* KO cells compared to parental cell lines, which goes along with their ara-C sensitivity displayed in figure 4.11. Importantly, it reinforces that the increased cytotoxicity of ara-C in SAMHD1-deficient GBM cells was associated with increased levels of ara-CTP and confirms [101] that SAMHD1 recognizes ara-CTP as a substrate.

4.5 SAMHD1 mutant reconstitutions as a toolbox to study SAMHD1

After reintroducing SAMHD1 wildtype and the dNTPase-inactive mutant D311A into *Samhd1* KO clones of different cell lines, SAMHD1 mutants with functional and cancer-related relevance were studied. In order to select meaningful SAMHD1 mutants, an extensive literature research was performed. SAMHD1 mutations were included that have been shown to be relevant for dNTPase-dependent and alternative functions, activity regulation through phosphorylation, tetramer formation as well as single nucleotide polymorphisms (SNPs) found in colon carcinoma (table 4.1).
The monocytic cell line THP-1 as well as GBM cell lines LN-18 and U-87 MG were chosen to be used for SAMHD1 mutant reconstitutions. Firstly, THP-1 was chosen, because the phenotype of SAMHD1-dependent chemosensitization to ara-C was very strong in this cell line (with a factor of difference between *Samhd1* parental and *Samhd1* KO cells of approximately 200-fold). This dynamic range made THP-1 the ideal cell line to screen SAMHD1 mutants for effects on ara-C cytotoxicity. Secondly, we were interested to study SAMHD1 mutations also in a GBM background. That is why we decided to include LN-18 and U-87 MG for SAMHD1 mutant reconstitutions.

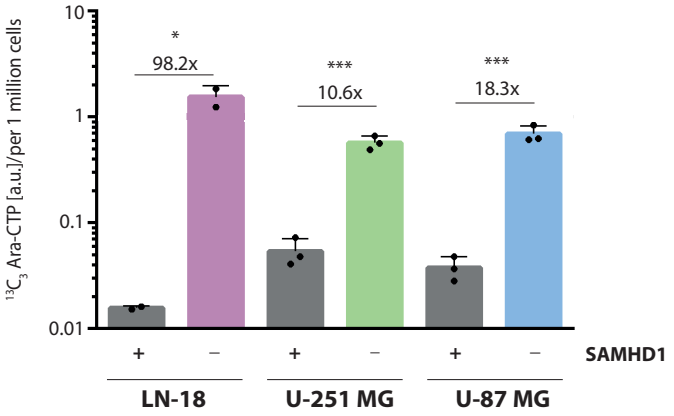

Figure 4.12: $^{13}C_3$ Ara-CTP levels are increased in SAMHD1-deficient LN-18, U-251 MG and U-87 MG GBM cells compared to the parental cell lines. LC–MS/MS analysis of Ara-CTP in LN-18 *Samhd1* KO clone SKO1, U-251 MG *Samhd1* KO clone C4 and U-87 MG *Samhd1* KO clone SKO1 as well as their parental counterparts. Cells were treated with 40 μM $^{13}C_3$ ara-C for 6 hours at 37°C. Equal cell numbers were harvested and frozen at -80°C. Nucleotides were measured in collaboration with the Prof. Gerd Geißlinger laboratory (University Hospital of the Goethe University, Frankfurt am Main, Germany). Error bars indicate standard deviation (s.d.). n=3 (biological triplicates). Statistical analysis: Student's unpaired t-test: ***P $<$ 0.001, *P $<$ 0.05. Experiment was performed by Dr. Ernesto Mejías Pérez (in-house).

4.5.1 Reconstitutions with SAMHD1-mtagBFP mutants are stable over time

After reintroducing different mutant versions of SAMHD1 into representative *Samhd1* KO clones of THP-1, LN-18 and U-87 MG cells and subsequently sorting for mtagBFP-positive cells, clones were analyzed by flow cytometry for mtagBFP protein expression. Figure 4.13A shows histogram blots of mtagBFP expression for all 16 SAMHD1 mutants including SAMHD1 wildtype reconstitution and untransduced *Samhd1* KO cells (negative control shown in light colors). Overall, the mutants showed a clear shift into mtagBFP-positive protein expression with mostly one population detected (exception: U-87 MG *Samhd1* KO +SAMHD1 T592E and R366H displayed two distinct populations, but both mtagBFP-positive). While sorting, a more narrow gating strategy for high expressors may have prevented biphasic reconstituted cell lines. Unfortunately, THP-1 *Samhd1* KO + SAMHD1 T592D reconstitution still remained mostly mtagBFP-negative in the flow cytometry analysis. As the THP-1 set was sorted only once, an additional round of sorting would likely enhance the fraction of mtagBFP-positive cells in this mutant. Also, many LN-18 *Samhd1* KO SAMHD1 reconstitutions showed a small fraction of mtagBFP-negative cells after 2 rounds of sorting. We decided here that as the great majority of cells was mtagBFP-positive, it was sufficient for our initial functional assessment.

Table 4.1: SAMHD1 mutants with direct functional and cancer-related relevance that were used in this study. Mutants were described in the literature and publications are indicated on the right.

SAMHD1 mutation	Description	Publication/Source
D311A	dNTP-inactive mutant	[6]
D137N	Allosteric mutant	[21]
T592A	Phosphorylation mutant	[37]
T592E	Phosphomimetic mutant	[38]
T592D	Phosphomimetic mutant	[38]
D207N	Allosteric mutant	[21]
Q548A	Allosteric mutant	[21]
K405R	Acetylation mutant	[44]
K484T	DNA damage mutant	[14]
R451A/L453A	Cyclin-binding mutant	[12]
V133I	Colorectal cancer SNP	[90]
A338T	Colorectal cancer SNP	[90]
R366H	Colorectal cancer SNP	[90]
D497Y	Colorectal cancer SNP	[90]
R145Q	AGS-associated mutant	[156]
S33A	LINE-1 retrotransposon SNP	[157]

Next, it was tested whether the mtagBFP signal remained stable over time during cell cultivation. Therefore, we monitored mtagBFP expression levels by flow cytometry over a period of 2 months. Figure 4.13B shows representative flow cytometry plots at 1, 2 and 8 weeks of cultivation. Here, the percentage of mtagBFP-positive cells remained stable at nearly 100%. Looking at the mean fluorescent intensity (MFI), also this parameter was stable in the mtagBFP-positive populations over the observation period (figure 4.13C). Therefore, it was concluded that the cell lines generated stably expressed mtagBFP from the SAMHD1 mutant-expressing vector and that their maintenance in culture (up to 2 months) did not markedly alter their mtagBFP expression in the reconstituted cell populations.

4.5.2 Uncoupling of mtagBFP and SAMHD1 in stable SAMHD1 mutant reconstituents from *Samhd1* knockout cells displays in part mutant-specific expression levels

After stable mtagBFP expression linked to co-encoded expression of the respective SAMHD1 mutants was achieved, SAMHD1 protein expression was evaluated extensively. Therefore, both quantitative immunoblotting through Wes and conventional immunoblotting were used to obtain a comprehensive picture of SAMHD1 protein expression. Figure 4.14 shows

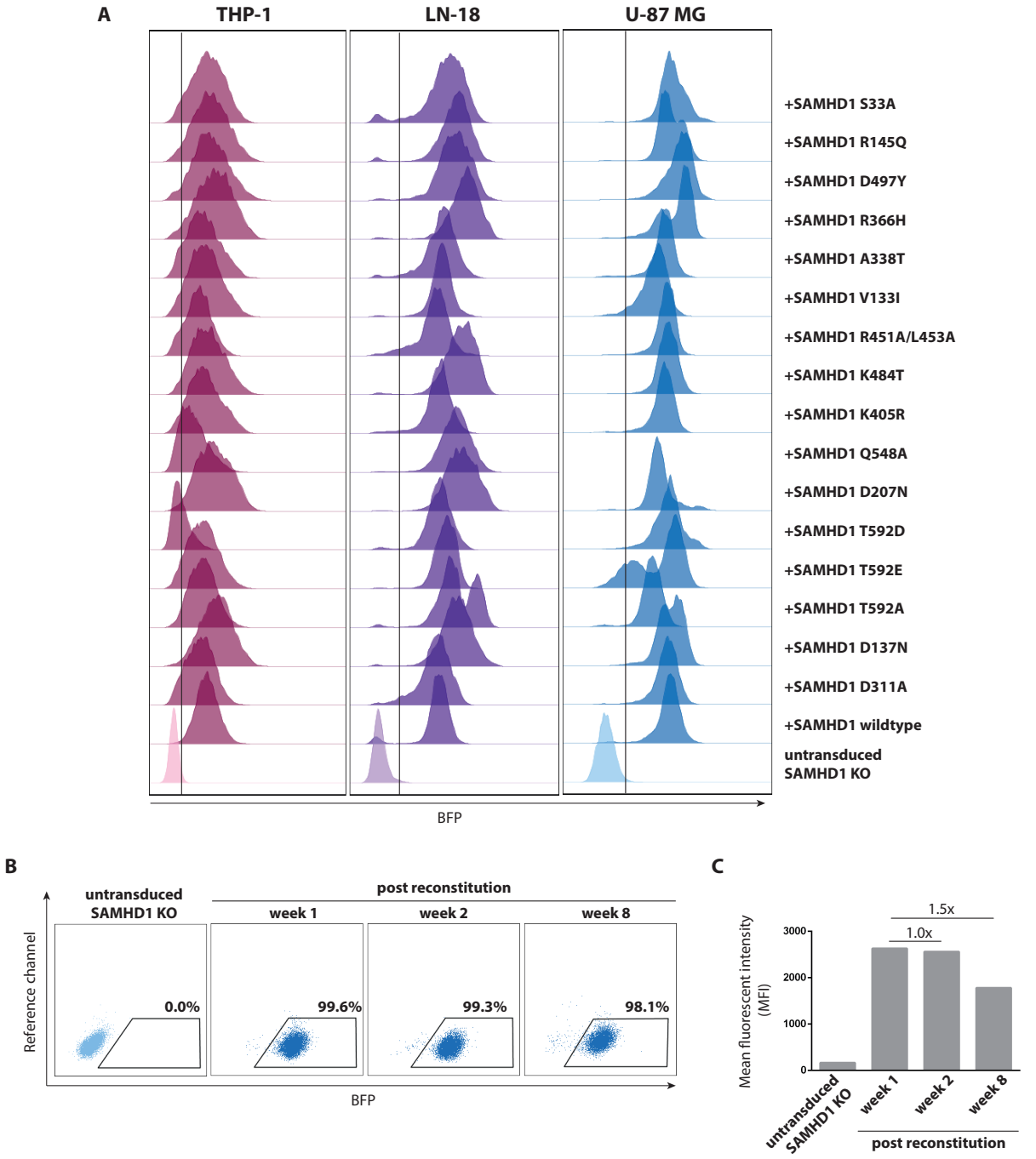

Figure 4.13: Continued on next page.

Figure 4.13: SAMHD1 mutant reconstitutions with functional and cancer-related relevance show positive and comparable mtagBFP protein expression within each cell line. (A) Flow cytometry analysis of THP-1 , LN-18 and U-87 MG *Samhd1* KO cells after transduction with a lentiviral vector expressing SAMHD1/mtagBFP following mtagBFP-positive sorting. mtagBFP expression was measured in the BFP channel. Untransduced LN-18 *Samhd1* KO cells served as negative control. The vertical line in the histogram blots divides mtagBFP negative from positive cells. (B) Flow cytometry blot showing mtagBFP protein expression levels in U-87 MG *Samhd1* KO +SAMHD1 wildtype reconstitution as a representative example for the mtagBFP levels over time. Percentages indicate mtagBFP-positive cells. APC was used as reference channel. Time points: untransduced *Samhd1* KO cells before transduction and transduced, sorted and stably mtagBFP-expressing cells at 1, 2 and 8 weeks of cell cultivation. (C) Mean fluorescent intensity (MFI) corresponding to (B). Median of MFI and factor of difference relative to week 1 is shown.

the expression analysis for the SAMHD1 mutants analyzed by quantitative Wes (shown at the top) and conventional immunoblotting (shown at the bottom) in (A) THP-1, (B) LN-18 and (C) U-87 MG cells. It could be observed that SAMHD1 protein expression levels varied between different SAMHD1 mutants within a cell line. Factors of difference describe SAMHD1 protein expression compared to the SAMHD1 wildtype reconstitution. Also, the differences in SAMHD1 protein expression were in part mutant-specific and differed between cell lines. This can be observed when plotting the SAMHD1 protein expression of the different cell lines relative to each other. The dot plots show a trend that is statistically significant, but the positive correlation was not very strong ($r^2 = 0.3146/0.159/0.2679$, figure 4.14D).

Despite similarly high mtagBFP levels, some SAMHD1 mutants exhibited low SAMHD1 levels, including D311A, T592A, Q548A, R451A/L453A, A338T, D497Y and R145Q for THP-1 cells, D311A, R451A/L453A and V133I for LN-18 cells and T592A, R451A/L453A, V133I, D497Y and R145Q for U-87 MG cells. Whereas the mutant R451A/L453A showed low SAMHD1 levels in all three cell lines tested, other mutants like T592A showed SAMHD1 levels comparable to SAMHD1 wildtype in LN-18 cells, but not in THP-1 and U-87 MG cells.

Reassuringly, analyzing the mtagBFP expression using conventional immunoblotting recapitulated the levels observed by flow cytometry (figure 4.14A-C at the bottom). This can be seen especially with the reconstituted cell line THP-1 *Samhd1* KO + SAMHD1 T592D, which showed low mtagBFP expression in both assays compared to the rest of the SAMHD1 mutants studied.

Notably, LN-18 parental and LN-18 *Samhd1* KO +SAMHD1 K405R showed no detectable Vinculin band in conventional immunoblotting, which likely originates from a sample-specific issue in this particular assay. Therefore, the SAMHD1 protein expression for these samples was mainly assessed through quantitative immunoblotting.

Taken together, this analysis of the SAMHD1 mutant reconstitutions showed that SAMHD1 expression levels differed among each other as well as among the different cell lines.

4.5.3 Evaluation of SAMHD1 mutants with 7 different α-SAMHD1 antibodies

We observed different SAMHD1 protein expression levels among the set of SAMHD1 mutants reconstituted in *Samhd1* KO cell lines. As for both quantitative and conventional immunoblotting, the same α-SAMHD1 antibody was used (mouse α-SAMHD1 antibody EGT986-11G6E8), we wondered whether some of the SAMHD1 mutations might have impaired the binding of the antibody. To test this, the detection patterns of all 7 α-SAMHD1 antibodies available in the laboratory were analyzed with a subset of THP-1 SAMHD1 mutant reconstitutions. Figure 4.15 shows a conventional immunoblot of THP-1 SAMHD1 mutants incubated with all 7 α-SAMHD1 antibodies. Notably, the different antibodies displayed similar SAMHD1 band patterns and intensities. We realized, however, that rabbit α-SAMHD1 antibody #1245 had troubles detecting the SAMHD1 S33A mutant in comparison to the other 6 antibodies. In addition, we saw that chicken α-SAMHD1 antibody #H153 seemed to be more unspecific as it showed an apparent SAMHD1 band in the *Samhd1* KO clone as well as for SAMHD1 D497Y and R145Q mutants, which turned out to be low SAMHD1 expressors with the other α-SAMHD1 antibodies tested. As mouse α-SAMHD1 from Origene also detected the SAMHD1 D497Y and R145Q mutants more intensely, we cannot exclude that both of these antibodies may specifically detect these mutants with higher sensitivity. It is important to mention here that for all of the α-SAMHD1 antibodies tested, the epitope(s) which are recognized are unknown as all of them were generated by immunizing with the whole SAMHD1 protein (section 3.1.10).
It is necessary to stress that the α-SAMHD1 antibodies rb #1246 and ch #H154 showed faint shadows in the *Samhd1* KO clone. Size-wise the band at α-SAMHD1 antibody rb #1246 looked like a slightly lower, unspecific band, whereas the band for α-SAMHD1 antibody ch #H154 has the predicted molecular weight. Comparing this with the validation of the antibodies in figure 4.1C and G, which showed no detectable band in the THP-1 *Samhd1* KO cell lysate, supported a potential spillover as an explanation for the faint bands.
Even though this immunoblot did not include all SAMHD1 mutants used in this study and only the THP-1 set of reconstitutions, we established that band intensities and thus steady-state protein levels are recapitulated by different α-SAMHD1 antibodies. As no distinct abnormalities in band detection and intensities were observed using the mouse α-SAMHD1 antibody from Eurogentec for all mutants and cell line sets, we concluded that this blot was appropriate to exclude differential antibody binding as a factor for the low SAMHD1 protein levels determined for a variety of mutants.

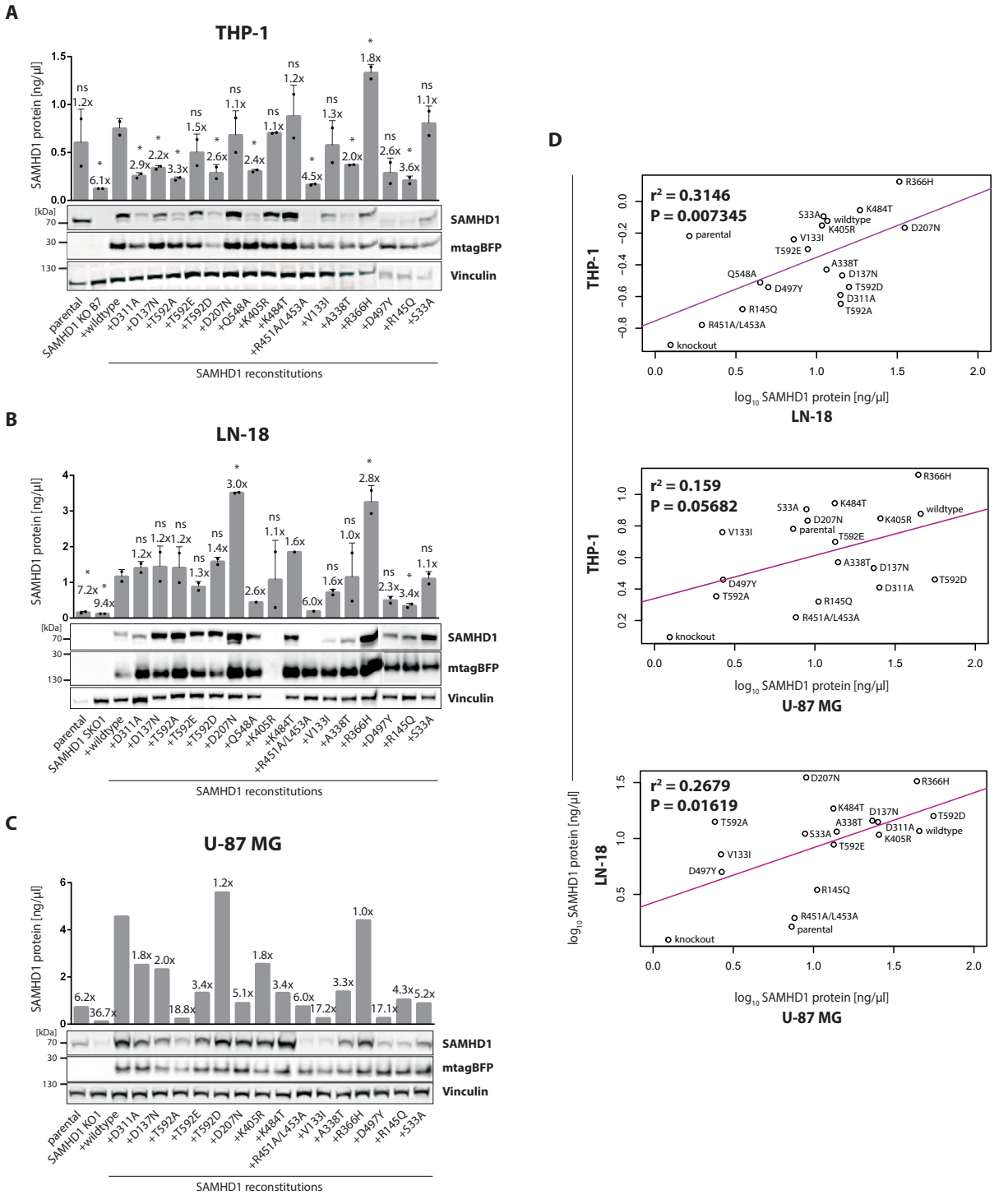

Figure 4.14: Continued on next page.

Figure 4.14: SAMHD1 mutant reconstitutions display different SAMHD1 protein levels. SAMHD1 protein expression was analyzed in (A) THP-1, (B) LN-18 and (C) U-87 MG cells using Wes quantitative immunoblotting - bar graph on the top - ($n \geq 2$ (biological replicates) for THP-1 and LN-18, n=1 for U-87 MG cells) as well as conventional immunoblotting - pictures on the bottom. The customized mouse α-SAMHD1 antibody EGT986-11G6E8 was used in both assays. Statistical analysis: Student's unpaired t-test: ***P < 0.001, **P < 0.01, *P < 0.05, ^{ns}P > 0.05. Error bars indicate standard deviation (s.d.). (D) Dot plots comparing the mean of SAMHD1 protein expression determined by Wes among the different cell line sets. Bioinformatical analysis in (D) was performed in collaboration with Prof. Lars Kaderali (University Medicine Greifswald, Germany).

4.5.4 SAMHD1 mutant reconstitutions display different *Samhd1* mRNA levels that do not correlate with protein levels

After showing that the different SAMHD1 protein levels in the SAMHD1 mutant reconstitutions are not a result of a mutant-specific impairment of binding of the specific α-SAMHD1 antibody, we were wondering whether the *Samhd1* mRNA levels would mirror the different SAMHD1 protein levels. Therefore, *Samhd1* mRNA levels of all SAMHD1 mutant reconstitutions were evaluated by qPCR. Figure 4.16 shows the respective data for (A) THP-1, (B) LN-18 and (C) U-87 MG cells. We observed that also *Samhd1* mRNA expression levels differed both among the SAMHD1 mutant reconstitutions within a cell line and comparing the same SAMHD1 mutant in different cell lines. Importantly, comparing *Samhd1* mRNA with SAMHD1 protein levels, no statistically significant correlation could be observed ($r^2 = 0.08846$, P = 0.1158, figure 4.16D).
Taken together, this expression analysis reveals that along with SAMHD1 protein expression, also *Samhd1* mRNA expression significantly differs among the SAMHD1 reconstitutions. For functional assays of mutants, this indicates a complex scenario where the observed differences will need to be studied in detail.

4.5.5 SAMHD1 mutant reconstitutions show heterogeneous sensitivity to cytarabine and segregate into specific groups

After characterizing the SAMHD1 mutant reconstitutions for their expression levels of mtagBFP, SAMHD1 protein and *Samhd1* mRNA, the set of SAMHD1 mutants were analyzed with functional assays. One of the main questions was how the different SAMHD1 mutants affect the sensitivity to the chemotherapeutic drug ara-C. In addition, ara-CTP levels were measured for the THP-1 set only as this technique is costly and the dynamic range of the SAMHD1-dependent ara-C cytotoxicity was biggest in this cell line. SAMHD1 mutants were also analyzed for their phosphorylation status at residue T592. In addition, transduction efficiencies and dCTP levels were analyzed in the THP-1 reconstituents.
Finally, transient Vpx-VLP-mediated degradation (LN-18 cells) or SIK0001-mediated inhibition (THP-1 cells) of SAMHD1 was performed, respectively. In THP-1 cells, overex-

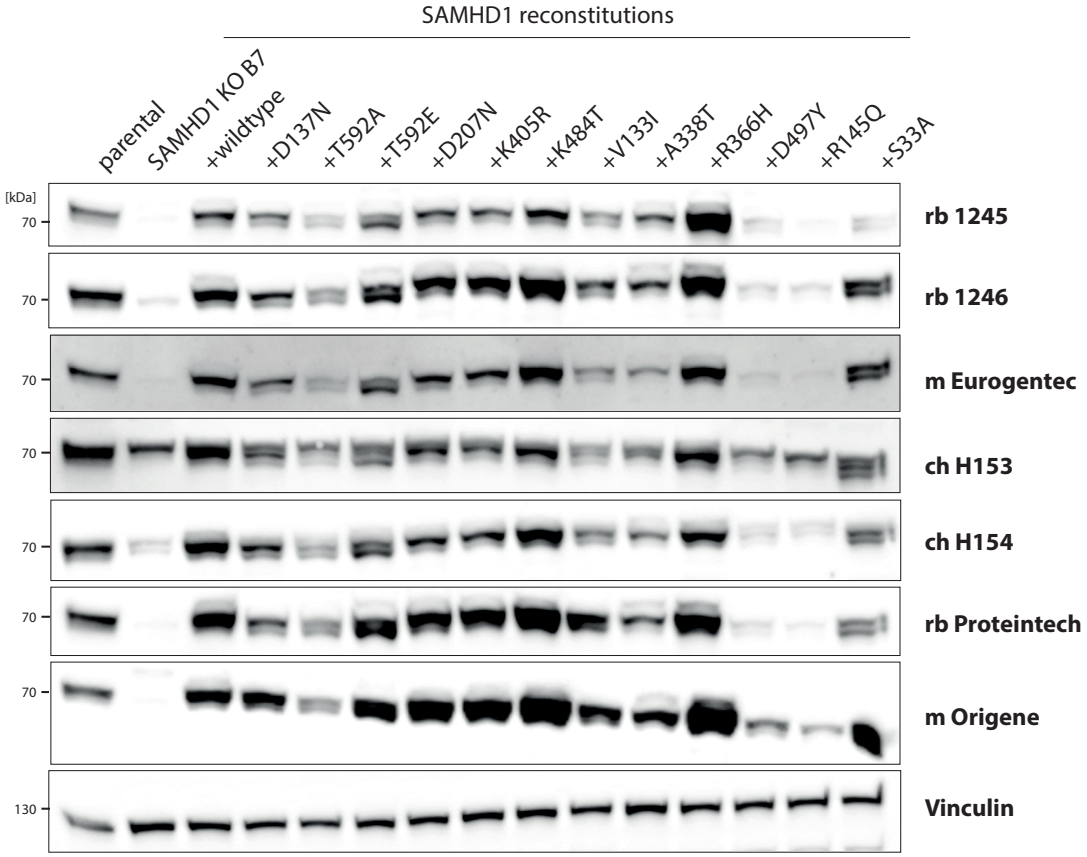

Figure 4.15: Differences in steady state expression levels of SAMHD1 mutants are largely recapitulated by 7 different α-SAMHD1 antibodies. SAMHD1 protein expression was tested in THP-1 lysates from the same harvest using 7 different α-SAMHD1 antibodies. The loading control Vinculin was incubated on all blots and showed a comparable loading pattern. The displayed Vinculin signal was obtained by reprobing the blot incubated with the mouse α-SAMHD1 antibody from Origene.

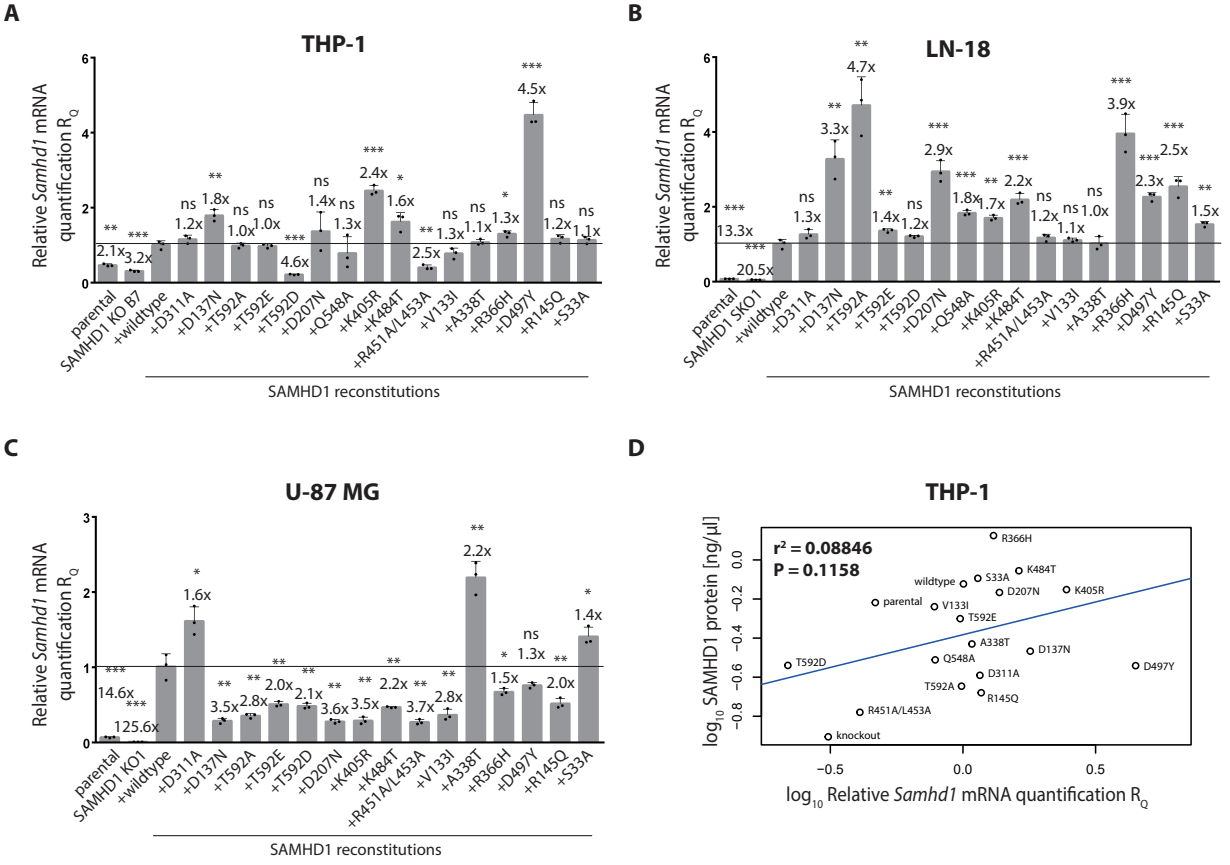

Figure 4.16: *Samhd1* mRNA expression in SAMHD1 mutant reconstitutions differs within and between the cell lines. *Samhd1* mRNA expression was analyzed by qPCR in (A) THP-1, (B) LN-18 and (C) U-87 MG cells. n=3 (technical triplicates). (D) Dot plot comparing *Samhd1* mRNA (x-axis) and SAMHD1 protein expression levels (y-axis). Sample values were normalized to the SAMHD1 wildtype reconstitution, which was set to 1, and is indicated by the horizontal line. Factor of difference to the SAMHD1 wildtype reconstitution is shown. Error bars indicate standard deviation (s.d.). Statistical analysis: Student's unpaired t-test: ***P < 0.001, **P < 0.01, *P < 0.05, ^{ns}P > 0.05. Bioinformatical analysis in (D) was performed in collaboration with Prof. Lars Kaderali (University Medicine Greifswald, Germany).

pressed SAMHD1 protein levels turned out to be too high for sufficient Vpx-VLP-mediated degradation, seen by remaining SAMHD1 protein levels in immunoblotting and insufficient sensitization to ara-C (data not shown). On the other hand, SIK0001 did not inhibit SAMHD1 activity in LN-18 cells (data not shown). As the SAMHD1 protein levels differed among the same mutant in different cell lines, the mutants are represented as groups by the respective cell lines.

4.5.5.1 SAMHD1 mutant reconstitutions in THP-1 cells

As mentioned before, the SAMHD1 mutant set in the monocytic cell line THP-1 had high priority in this project as the SAMHD1-dependent ara-C chemosensitization was most pronounced. For evaluating ara-C sensitivity, equal cell numbers were treated with different drug concentrations and incubated for 3 days before luminescence-based viability analysis. Figure 4.17A shows ED_{50} values for ara-C in the set of THP-1 SAMHD1 mutants. The 4 first displayed cell lines from the left, i.e. THP-1 parental, *Samhd1* KO B7, SAMHD1 wildtype and D311A reconstitutions, followed the described pattern of ara-C sensitivity (figure 4.11) [101]: Whereas the KO of *Samhd1* significantly reduced the ED_{50} value, reconstitution with SAMHD1 wildtype elevated the ED_{50} value again to a parental cell-like value. The dNTPase-inactive mutant SAMHD1 D311A, expectedly, behaved like *Samhd1* KO in ara-C chemosensitization [101]. The rest of the SAMHD1 mutants showed ara-C sensitivity within the phenotypic range between *Samhd1* KO and SAMHD1 wildtype reconstitution/parental cells.
In order to be able to interpret the data in a meaningful way, the SAMHD1 protein expression levels were included in this data set. In figure 4.17B, the relation between ara-C sensitivity (by μM ED_{50}) and the SAMHD1 protein expression levels (by ng/μl SAMHD1 protein) is represented. Bioinformatical analysis revealed no strong positive correlation between the two parameters ($r^2 = 0.2695$). Even though the P-value showed significance ($P = 0.01327$), the weak positive correlation might be due to the outliers D207N and R366H that behaved differently than the rest of the SAMHD1 mutants.
In addition, we grouped the mutants into the following categories: "neutral" mutations that behaved like the SAMHD1 wildtype reconstitution, including T592E, V133I, S33A, K484T and K405R, "medium" phenotypic mutants that showed highly reduced SAMHD1 protein expression and ED_{50} levels that range between those of *Samhd1* KO and wildtype reconstitution, including A338T, D137N, T592D and Q548A, and "weak" phenotype mutants that showed low SAMHD1 protein expression and low ED_{50} levels comparable to the *Samhd1* KO, including R451A/L453A, R145Q, T592A, D311A and D497Y.
The two SAMHD1 mutations R366H and D207N showed high SAMHD1 protein expression but low ED_{50} levels, which groups them into a loss-of-function phenotype. If SAMHD1 in cells inherits one of these mutations, these cells sensitize to ara-C, making the drug more efficient in chemotherapeutic treatment.
In addition to the ara-C toxicity assays, we wanted to show that the increased cytotoxicity is associated with increased levels of ara-CTP. Therefore, we treated the mutant panel with labeled ara-C and determined ara-CTP levels in cells 6 hours after incubation. Figure 4.17C

shows labeled ara-CTP levels of all SAMHD1 mutants in THP-1 cells. Again the 4 cell lines from the left, i.e. THP-1 parental, *Samhd1* KO B7, SAMHD1 wildtype and D311A reconstitutions showed the expected pattern [101] of ara-CTP levels in the cells. Whereas cell lines that include wildtype SAMHD1, including parental and the SAMHD1 wildtype reconstitution, displayed low levels of ara-CTP due to their dNTPase activity, *Samhd1* KO and the dNTPase-inactive SAMHD1 D311A reconstitution showed significantly higher ara-CTP levels. The rest of the SAMHD1 mutants showed ara-CTP levels within this dynamic range. Figure 4.17D combines the ara-CTP levels with SAMHD1 protein expression levels indicating a modest inverse correlation ($r^2 = 0.2274$) with statistical significance ($P = 0.0225$), similar to figure 4.17B.
The dot plot in figure 4.17E establishes the relationship between ara-CTP levels and ED_{50} values and emphasizes a strong negative correlation between the two parameters ($r^2 = 0.6415$) with high statistical significance ($P = 2.299e\text{-}05$). These results underline that the toxicity observed in the viability assay correlates with ara-CTP levels in the cell as well as SAMHD1's capacity to recognize ara-CTP as a substrate.
In order to estimate whether the mutations of SAMHD1 affect PTMs such as phosphorylation, the SAMHD1 mutants were examined for their phosphorylation status at threonine 592 (T592). Whereas the SAMHD1 mutant T592A can no longer be phosphorylated and served as negative control, the mutants T592E and T592D display phosphomimetic mutants that can no longer block HIV-1 infection compared SAMHD1 wildtype reconstitution. It can be concluded that the phosphorylation levels of SAMHD1 mirrored the total SAMHD1 protein expression levels and no marked alterations in phosphorylation at T592 were detected.
To sum up, the intense characterization of THP-1 SAMHD1 mutants showed that the interpretation of functional assays needs specific care as the SAMHD1 expression levels between the SAMHD1 mutants were highly variable. In addition, the screening process for ara-C sensitivity revealed two SAMHD1 mutants, R366H and D207N, that may serve as relevant biomarkers in ara-C chemotherapy as they showed a similarly high sensitization to drug treatment as the SAMHD1-deficient cell line. In the end, SAMHD1 phosphorylation at residue T592 could be largely excluded as an explanation for different enzyme activities of the mutants.

4.5.5.2 SAMHD1 mutant reconstitutions in LN-18 cells

In order to see how the SAMHD1 mutants behave in a GBM setting, the LN-18 SAMHD1 mutants were analyzed for their sensitivity to ara-C. Therefore, same as for THP-1, equal cell numbers were treated with different drug concentrations and incubated over a period of 4 days before luminescence-based analysis. Figure 4.18A displays the sensitivity to ara-C shown as ED_{50} values in combination with the SAMHD1 protein expression information through conventional immunoblotting in figure 4.18B. As before with THP-1 cells, also in the GBM cell line LN-18, ara-C sensitivity of the first 4 displayed cell lines from the left behaved like expected [101]. Whereas SAMHD1 wildtype containing cell lines, like parental and SAMHD1 wildtype reconstitution, showed high ED_{50} values for ara-C, sensitivity to

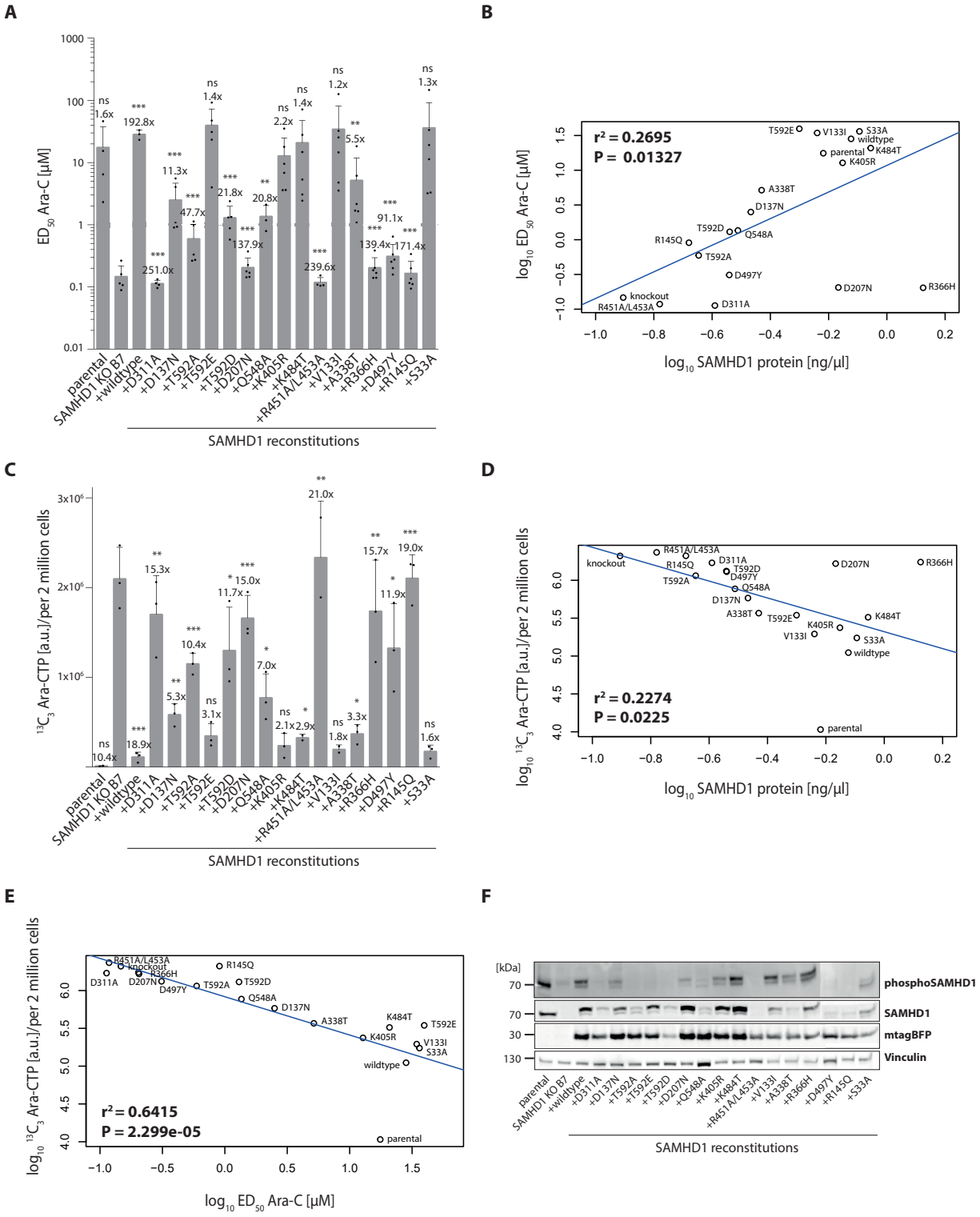

Figure 4.17: Continued on next page.

Figure 4.17: Characterization of THP-1 SAMHD1 mutant set for ara-C sensitivity, SAMHD1 protein expression, ara-CTP levels and SAMHD1 phosphorylation status. (A) Cell viability of THP-1 cells was analyzed 3 days after ara-C treatment. ED_{50} of ara-C is shown in μM. Error bars indicate standard deviation (s.d.), $n \geq 4$ (biological replicates). Factor of difference to SAMHD1 wildtype reconstitution is shown. (B) Dot plot comparing SAMHD1 protein expression (x-axis) and ED_{50} levels for ara-C (y-axis). (C) LC–MS/MS analysis of $^{13}C_3$-labeled ara-CTP. n=3 (biological triplicates). Error bars indicate s.d. Statistical analysis: Student's unpaired t-test: ***P < 0.001, **P < 0.01, *P < 0.05, ^{ns}P > 0.05. (D) Dot plot comparing SAMHD1 protein expression (x-axis) and $^{13}C_3$ ara-CTP levels (y-axis). (E) Dot plot comparing ED_{50} levels for ara-C (x-axis) and $^{13}C_3$ ara-CTP levels (y-axis). (F) Conventional immunoblot using α-phospho SAMHD1 T592 as well as α-SAMHD1 and α-mtagBFP antibodies. Bioinformatical analysis in (B), (D) and (E) was performed in collaboration with Prof. Lars Kaderali (University Medicine Greifswald, Germany).

ara-C was significantly increased by 38.5 to 43.3-fold in *Samhd1* KO and dNTPase-inactive SAMHD1 mutant D311A. The ara-C sensitivity of the other SAMHD1 mutants could be found in this dynamic range. The 7.1-fold higher ara-C ED_{50} value in the SAMHD1 K484T reconstitution exhibited high variety between the biological replicates and was not statistically significant.
The dot plot in figure 4.18C compares SAMHD1 protein expression (x-axis) obtained from Wes analysis and ED_{50} levels for ara-C (y-axis) with no strong statistical significant correlation ($r^2 = 0.0071$, $P = 0.303$). In contrast to the THP-1 set, it was more difficult to clearly group the LN-18 SAMHD1 mutants into phenotypic categories. One explanation might have been the smaller dynamic range between *Samhd1* KO and SAMHD1 wildtype reconstitution in LN-18 (43.3-fold) compared to THP-1 cells (192.8-fold). When trying to group LN-18 reconstituents, we identified "neutral" mutations that behaved like SAMHD1 wildtype, including T592D, Q548A, K405R, K484T, A338T and S33A, mutants that showed "medium" SAMHD1 protein expression and ED_{50} levels between the ones from *Samhd1* KO and SAMHD1 wildtype reconstitution, including V133I, T592E and D137N and hints for "weak" ED_{50} phenotypes that showed low SAMHD1 protein expression and low ED_{50} levels like the *Samhd1* KO, including R451A/L453A, R145Q, D311A, T592A and D497Y. Nevertheless, this categorization needs to be handled with caution, as SAMHD1 protein levels showed a high variance among the same SAMHD1 mutants in the different cell lines (figure 4.14D).
Same as in the THP-1 set of SAMHD1 mutants, also LN-18 cells reconstituted with SAMHD1 D207N and R366H showed significantly higher sensitivity to ara-C compared to the SAMHD1 wildtype reconstitution (21.0-fold for D207N and 14.1-fold for R366H). This showed that SAMHD1 mutants D207N and R366H were sensitizing to ara-C treatment in two different cell lines, excluding a cell line-specific phenomenon. In addition, the dot plot in figure 4.18C emphasizes that sensitivity to ara-C did not correlate with

SAMHD1 protein expression in the mutants in LN-18 cells (r^2 = -0.004822) and was not statistically significant (P = 0.3526).
LN-18 SAMHD1 mutant K484T also stood out from the dot plot in figure 4.18C as it showed decreased sensitivity to ara-C compared to the SAMHD1 wildtype reconstitution, although this difference did not reach statistical significance.
Also in the LN-18 set, SAMHD1 mutants were investigated for their phosphorylation status at T592. The phosphorylation mutant SAMHD1 T592A, which can no longer be phosphorylated, was used as a negative control, whereas T592E and T592D are phosphomimetic mutants that mimic a constant phosphorylated state at T592. Different to THP-1 cells, the SAMHD1 mutant T592A in LN-18 cells showed a band with the respective molecular weight for the α-phospho SAMHD1 T592 antibody, but this band was most likely the result of a spillover from the neighboring lanes as repeated verification of the sample showed no band for the SAMHD1 phosphorylation mutant T592A in LN-18 cells (data not shown). In general, the phosphorylation levels of SAMHD1 mirrored the total SAMHD1 protein levels. SAMHD1 mutant R145Q was an exception, which showed very low SAMHD1 phosphorylation levels but higher overall SAMHD1 protein levels (figure 4.14B), an observation that could not be recapitulated in the THP-1 set of SAMHD1 mutants.
Notably, the SAMHD1 mutants in the second GBM cell line U-87 MG showed high variance for sensitivity to ara-C between the biological replicates (data not shown). This phenomenon in combination with the different SAMHD1 protein expression levels among the mutants made it difficult to conclusively evaluate this data set, which was therefore excluded for sensitivity analysis of ara-C.

4.5.6 SAMHD1 mutant reconstitutions show heterogeneous transduction efficacies with a lentiviral vector

Next, we wanted to know whether the viral restriction associated with SAMHD1 and retro-/lentiviruses is affected by the SAMHD1 mutants. For LN-18 cells, we saw no statistically significant difference in transduction levels between LN-18 parental, *Samhd1* KO, SAMHD1 wildtype and D311A reconstitution (data not shown), excluding LN-18 cells as a suitable model for lentiviral vector transduction evaluation in the context of the SAMHD1 mutants. As parental, *Samhd1* KO, SAMHD1 wildtype and D311A reconstitution in THP-1 cells, on the other hand, showed statistically significant differences in transduction efficacies, we decided to proceed with THP-1 cells as the model to study lentiviral vector transduction in SAMHD1 mutant reconstitutions.
Therefore, we used a VSV-G-pseudotyped lentiviral vector coding for GFP, transduced THP-1 SAMHD1 mutants and analyzed GFP protein expression by flow cytometry 48 hours later. In figure 4.19A, the percentage of GFP-positive cells after transduction with the pLenti-based lentiviral vector coding for GFP is shown. When wildtype SAMHD1 was present (either in the parental or in the SAMHD1 wildtype reconstitution), the percentage of GFP-positive cells was significantly lower compared to the SAMHD1-deficient KO clone. When SAMHD1 was knocked out or the dNTPase-inactive SAMHD1 mutant

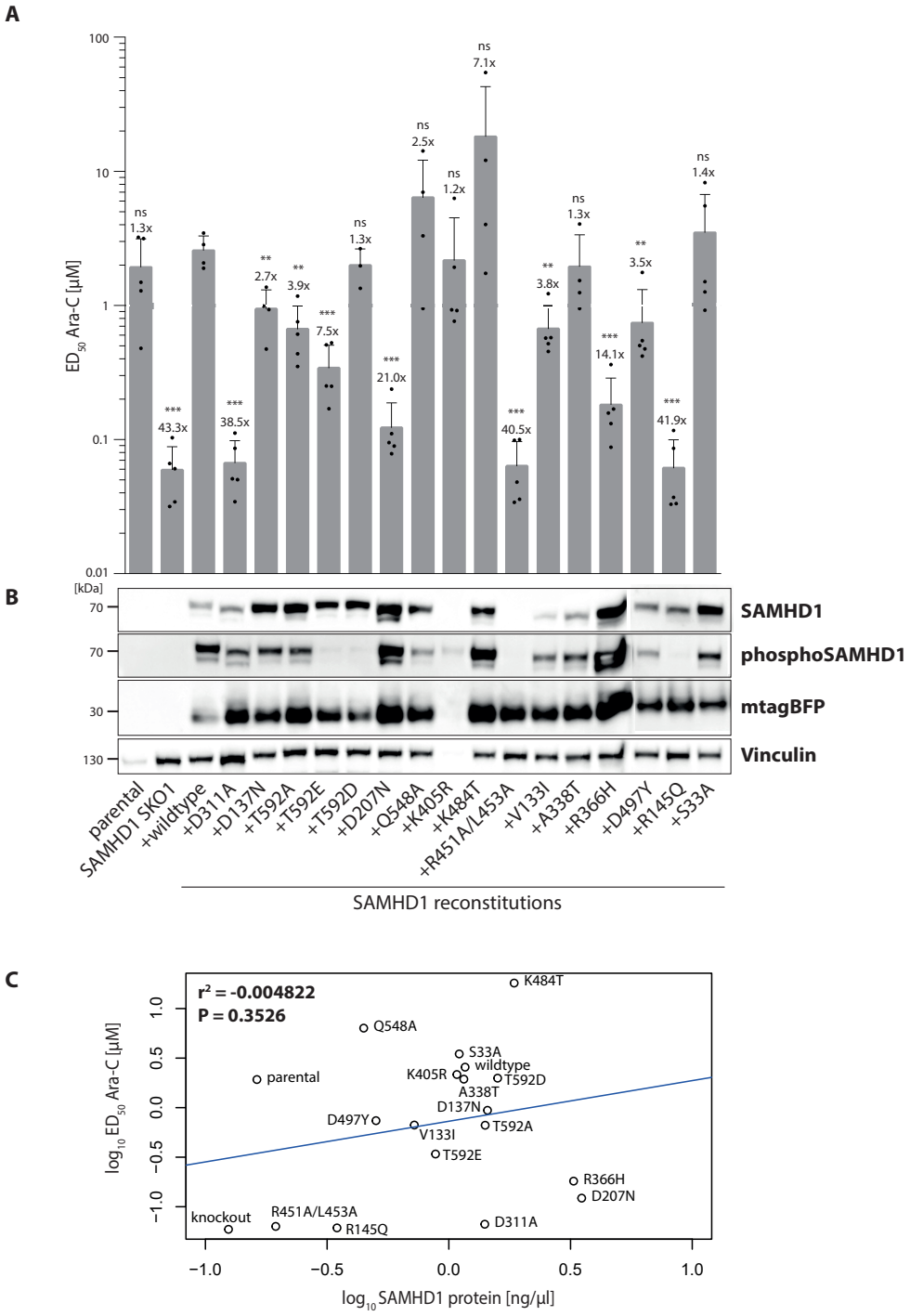

Figure 4.18: Continued on next page.

Figure 4.18: Characterization of LN-18 SAMHD1 mutants for ara-C sensitivity, SAMHD1 protein expression and SAMHD1 phosphorylation status. (A) Cell viablity of LN-18 cells was analyzed 4 days after ara-C treatment. ED_{50} of ara-C is shown in μM. Error bars indicate standard deviation (s.d.), $n \geq 4$ (biological replicates). Statistical analysis: Student's unpaired t-test: ***P < 0.001, **P < 0.01, ^{ns}P > 0.05. Factor of difference to SAMHD1 wildtype reconstitution is shown. (B) Conventional immunoblot using α-phospho SAMHD1 T592 as well as α-SAMHD1 and α-mtagBFP antibodies. (C) Dot plot comparing SAMHD1 protein expression (x-axis) and ED_{50} levels for ara-C (y-axis). Bioinformatical analysis in (C) was performed in collaboration with Prof. Lars Kaderali (University Medicine Greifswald, Germany).

D311A was expressed [6], the transduction lead to significantly higher GFP-positive cells compared to parental or SAMHD1 wildtype reconstitution (3.5-fold for *Samhd1* KO and 2.7-fold for *Samhd1* KO +SAMHD1 D311A, respectively). These experiments recapitulated the already known restriction of lentiviral vector transduction through SAMHD1 and its dNTPase activity [53]. For the rest of the SAMHD1 mutants, lentiviral transduction efficacies positioned within this dynamic range of the *Samhd1* KO and the parental or SAMHD1 wildtype reconstituted population (figure 4.19A).
As the lentiviral restriction by SAMHD1 is mainly facilitated through its dNTPase activity, a low dNTP pool in the cell due to high SAMHD1 dNTPase activity will likely limit reverse transcription and restrict the transduction with the lentiviral vector. Therefore, the level of dNTPs in the cell presents a surrogate of SAMHD1's dNTPase activity and, in turn, the restriction potential of the SAMHD1 mutants. Looking at the dCTP concentrations in the cells, we observed 2.0-fold higher levels in the *Samhd1* KO cells compared to SAMHD1 wildtype reconstitution, which was not statistically significant due to high variance in the biological replicates (figure 4.19B). Also here, parental and SAMHD1 wildtype reconstitution showed lower dCTP levels in comparison to *Samhd1* KO cells and the dNTPase-inactive SAMHD1 mutant D311A. For the rest of the SAMHD1 mutants, dCTP levels fell into this small dynamic range. Of note, the ara-CTP levels (figure 4.17C) showed much higher differences and a broader dynamic range than the dCTP levels (i.e. 18.9-fold for ara-CTP compared to 2.0-fold for dCTP). The other dNTPs, namely dGTP, dATP and dTTP, resembled the differences seen with dCTP (data not shown). In figure 4.19C, a dot blot with dCTP levels (x-axis) and the percentage of VSV-G GFP-positive cells (y-axis) shows no statistically significant correlation between the two parameters (r^2 = -0.004822, P = 0.3526).
All in all, SAMHD1 mutant reconstitutions transduced with a lentiviral vector expressing GFP revealed higher transduction efficacies in *Samhd1* KO compared to SAMHD1 parental and wildtype reconstitution in THP-1 cells. Transduction efficiencies of the SAMHD1 mutant reconstitutions were found to lie within this dynamic range. In line with this finding, dCTP levels inversely mirrored the transduction efficacies, but were not statistically significant.

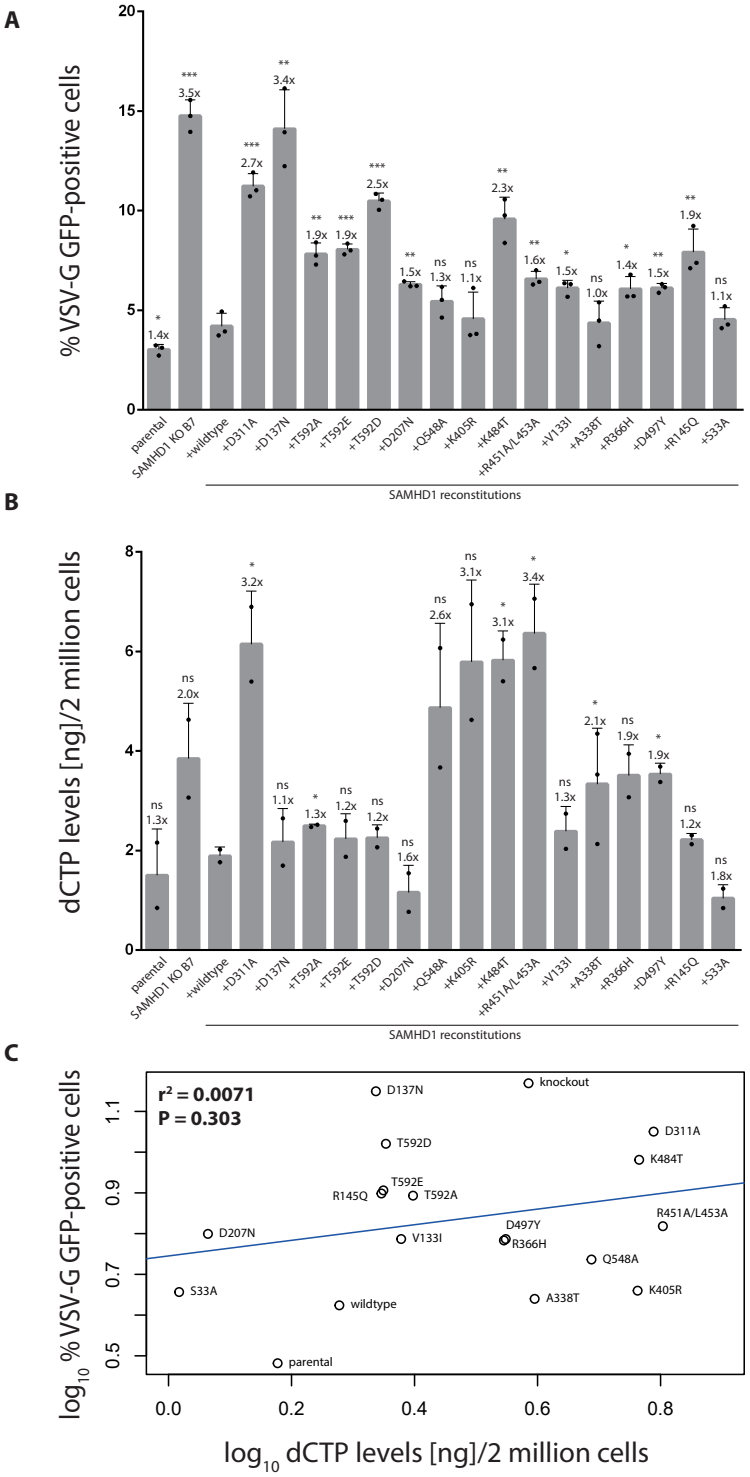

Figure 4.19: Continued on next page.

Figure 4.19: Transduction of SAMHD1 mutant reconstitutions with a VSV-G-pseudotyped lentiviral vector shows a small functional dynamic range. (A) THP-1 cells were seeded in triplicates and transduced with a VSV-G-enveloped lentiviral vector encoding GFP. Cells were cultivated for 48 hours before flow cytometric analysis. Shown is the percentage of pLenti VSV-G GFP-positive cells. n=3 (technical triplicates). (B) LC–MS/MS analysis of dCTP levels in ng per 2 million cells. n=2 (biological duplicates). Factor of difference to SAMHD1 wildtype reconstitution is shown. Error bars indicate standard deviation (s.d.). Statistical analysis: Student's unpaired t-test: ***P < 0.001, **P < 0.01, *P < 0.05, ^{ns}P > 0.05. (C) Dot plot comparing dCTP levels (x-axis) and the percentage of VSV-G GFP-positive cells (y-axis). Bioinformatical analysis in (C) was performed in collaboration with Prof. Lars Kaderali (University Medicine Greifswald, Germany).

4.5.7 Vpx-VLP-mediated degradation and small molecule-mediated inhibition of SAMHD1 mutant reconstitutions sensitize to cytarabine treatment

After assessing the transduction efficacy, we wanted to know whether Vpx is able to target SAMHD1 mutants for degradation. Therefore, equal cell numbers were transduced with VLPs containing Vpx. Empty VLPs and 1xPBS only-treated (mock) cells served as controls. Cells were incubated for 24 hours before treatment with an ara-C dilution series. Figure 4.20A shows ED_{50} values 4 days after ara-C treatment in the LN-18 SAMHD1 mutants. In low SAMHD1 expressors or mutants with a low ED_{50} value, also Vpx treatment could not significantly reduce the ED_{50}, including D311A, D207N, R451A/L453A and R145Q. The rest of the mutants were sensitized to ara-C upon Vpx-VLP treatment compared to the SAMHD1 wildtype reconstitution. To sum up, all SAMHD1 mutants with SAMHD1 protein levels comparable to SAMHD1 wildtype reconstitution were able to be degraded by Vpx-VLPs, whereas Vpx-VLP treatment of SAMHD1 mutants with low SAMHD1 protein levels and/or reduced ara-C ED_{50} values could not be sensitized further to ara-C.

Another way of transiently reducing SAMHD1 activity is by treatment with a small molecule SAMHD1 inhibitor. As part of another project in the Keppler group, a large-scale SAMHD1 interactor screen revealed a small molecule that inhibits SAMHD1, named SIK0001. Interestingly, SIK0001 treatment itself does not effect SAMHD1 protein expression (data not shown). Thus, in order to see whether SIK0001 is able to inhibit the different SAMHD1 mutants, THP-1 SAMHD1 mutants were seeded the same day in equal cell numbers and treated with 25 μM SIK0001 or 1xPBS only (mock) together with a dilution series of ara-C. Figure 4.20B shows the ED_{50} values after 3 days of incubation. SIK0001 was able to inhibit SAMHD1 wildtype reconstitution potently with a factor of difference of 200-fold compared to 1xPBS-treated (mock) cells. On the other hand, SIK0001 treatment in the *Samhd1* KO cells was not able to further sensitize cells to ara-C. Concerning

the SAMHD1 mutants, if SAMHD1 expression was low, including D311A, T592A, T592D, Q548A, R451A/L453A, D497Y and R145Q, or the sensitivity to ara-C was high, including D207N and R366H, then the sensitivity to ara-C could not be enhanced by SIK0001 treatment. For the rest of the SAMHD1 mutants tested in this setting, including T592E, K405R, K484T, V133I, A338T and S33A, SIK0001 was able to sensitize cells to ara-C to levels comparable to the *Samhd1* KO clone.
Taken together, both Vpx-VLP-mediated SAMHD1 protein degradation as well as SIK0001-mediated inhibition of SAMHD1 activity are potent tools to transiently reduce its protein expression or activity, respectively, and therefore to increase the sensitivity to ara-C.
All in all, the generated toolbox is able to recapitulate already published phenotypes, which makes the workflow trustworthy and suitable to study novel SAMHD1 mutants. In a next step, this workflow was used to investigate SAMHD1 mutants and their dNTPase activity not described in literature thus far (section 4.6).

4.6 Studying SAMHD1 mutations found in patients with glioblastoma multiforme

After the characterization of already described SAMHD1 mutations, the methodological approach was used to study SAMHD1 mutations that have not been described in literature yet. A database search was performed in the cancer genomics cBIOPortal, the catalogue of somatic mutations in cancer (COSMIC) and the genomic data commons (GDC) data portal of the national cancer institute (NCI). The search revealed mutations in the *Samhd1* gene that were found in whole genome sequencing (WGS) analyzes of GBM patient tissues (table 4.2). As these SAMHD1 mutations are found in GBM patient tissue, they were primarily studied in the GBM cell line LN-18 for their impact on ara-C chemoresistance.

Table 4.2: SAMHD1 mutants that were found in GBM patients and were used in this study. WGS: whole genome sequencing.

SAMHD1 mutation	Publication/Source
L244F	WGS [94]
A30T	WGS [158]
R531S	Cancer genomics cBIOPortal
A565T	WGS [158]
F578L	Cancer genomics cBIOPortal
L620H	Cancer genomics cBIOPortal

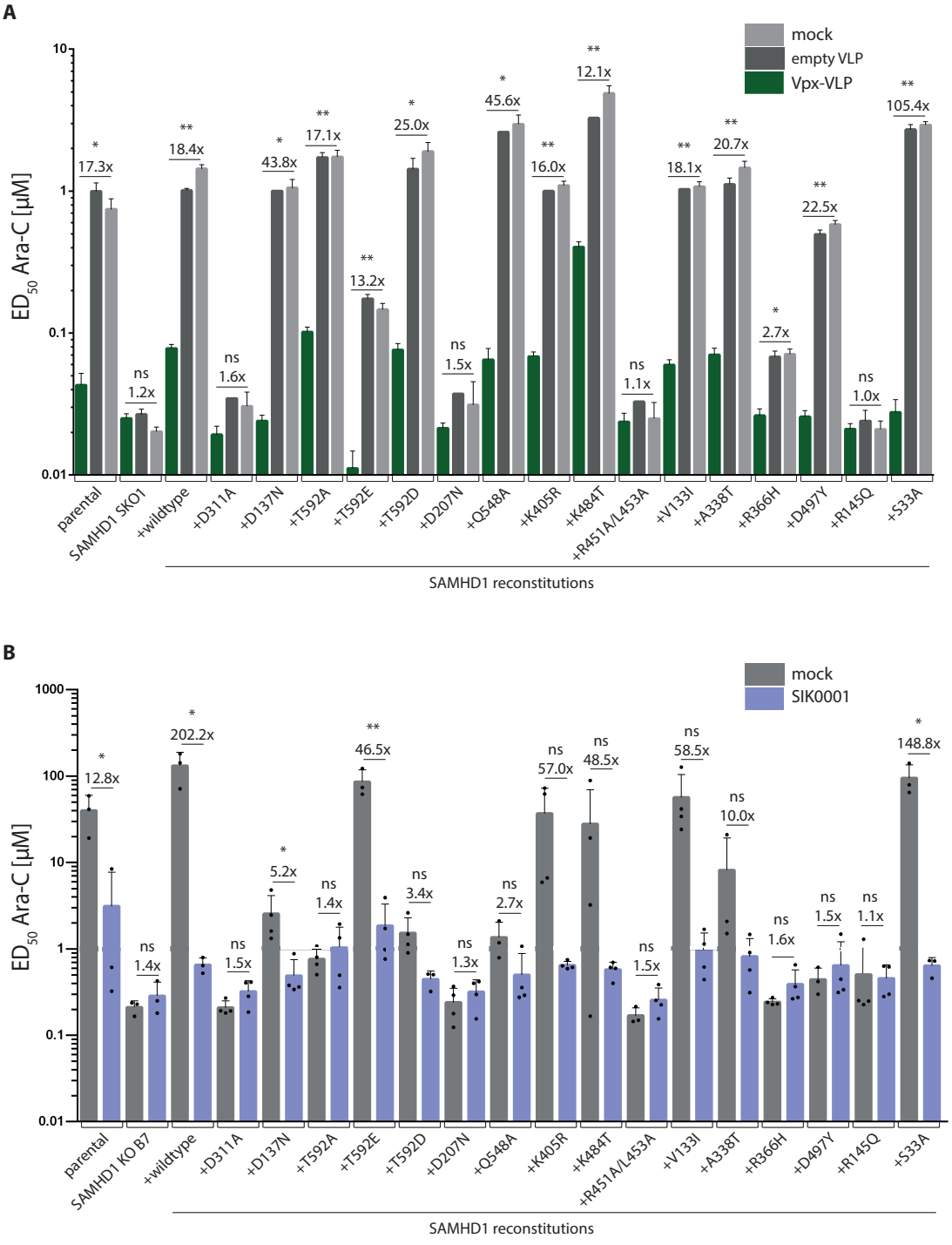

Figure 4.20: Continued on next page.

Figure 4.20: Vpx-VLP transduction and SIK0001-treatment in SAMHD1 mutants show different levels of SAMHD1 degradation and inhibition. (A) LN-18 cells were seeded and treated with Vpx-VLPs for 24 hours prior to ara-C treatment and cell viability was analyzed 4 days after ara-C treatment. ED_{50} values of ara-C are shown in μM. Vpx-VLP treatment is indicated in green, treatment with empty VLPs in dark grey and treatment with 1xPBS (mock) in light grey. n=2 (technical duplicates). (B) THP-1 cells were seeded and treated with the SAMHD1 inhibitor SIK0001 with a final concentration of 25 μM in the well. On the same day, ara-C was added. Cell viability was analyzed using the CellTiter-Glo® 2.0 Assay 3 days later. ED_{50} values of ara-C are shown in μM. Purple: treatment with SIK0001, grey: treatment with 1xPBS (mock). $n \geq 3$ (biological replicates). Error bars indicate standard deviation (s.d.). Factor of difference for Vpx-VLP or 25 μM SIK0001 compared to mock is shown. Statistical analysis: Student's unpaired t-test: **P < 0.01, *P < 0.05, ^{ns}P > 0.05.

4.6.1 Reconstitution of cancer-related SAMHD1 mutants shows variable SAMHD1 expression

In order to study SAMHD1 mutants first described in GBM patient tissue, they were reconstituted in GBM LN-18 *Samhd1* KO cells according to the first set described earlier (section 3.2.12). SAMHD1 mutations L244F [94], A30T [158], A565T [158], R531S, F578L and L620H were used for reconstitution. The flow cytometric analysis in figure 4.21A mainly shows two things: firstly, the two-times sorted cell populations showed homogeneous mtagBFP-positive protein expression; and secondly, the SAMHD1 mutant reconstitutions displayed consistent and comparable mtagBFP-positive signals. Untransduced *Samhd1* KO cells were used as negative control. Analyzing mtagBFP expression by conventional immunoblotting mirrored the comparable mtagBFP expression throughout the panel of SAMHD1 mutations (figure 4.21B). Also shown in figure 4.21B, a SAMHD1 protein expression analysis by both conventional and quantitative immunoblotting showed equal mtagBFP expression, but significantly different SAMHD1 expression among the mutants. While SAMHD1 mutants A30T, R531S, F578L and L620H displayed expression levels comparable to SAMHD1 wildtype reconstitution, the SAMHD1 mutation L620H showed lower expression signal in the conventional immunoblotting. A α-SAMHD1-antibody comparison could later show that the low band intensity for SAMHD1 in L620H may be due to the recognition of the α-SAMHD1-antibody used in this assay (data not shown). Importantly, SAMHD1 mutations L244F and A565T showed significantly lower SAMHD1 expression levels compared to SAMHD1 wildtype, but similar expression levels as the parental cell line.
Finally, the phosphorylation status of SAMHD1 at T592 was estimated by conventional immunoblotting (figure 4.21B). The band pattern for the α-phospho SAMHD1 T592 antibody mirrored the SAMHD1 general protein expression band pattern.
Taken together, whereas consecutive mtagBFP expression-based sorting of *Samhd1* KO cells transduced with a lentiviral vector containing SAMHD1/mtagBFP resulted in equally

mtagBFP-positive cell populations, SAMHD1 protein expression in these reconstituted cell populations differed among the SAMHD1 mutants.

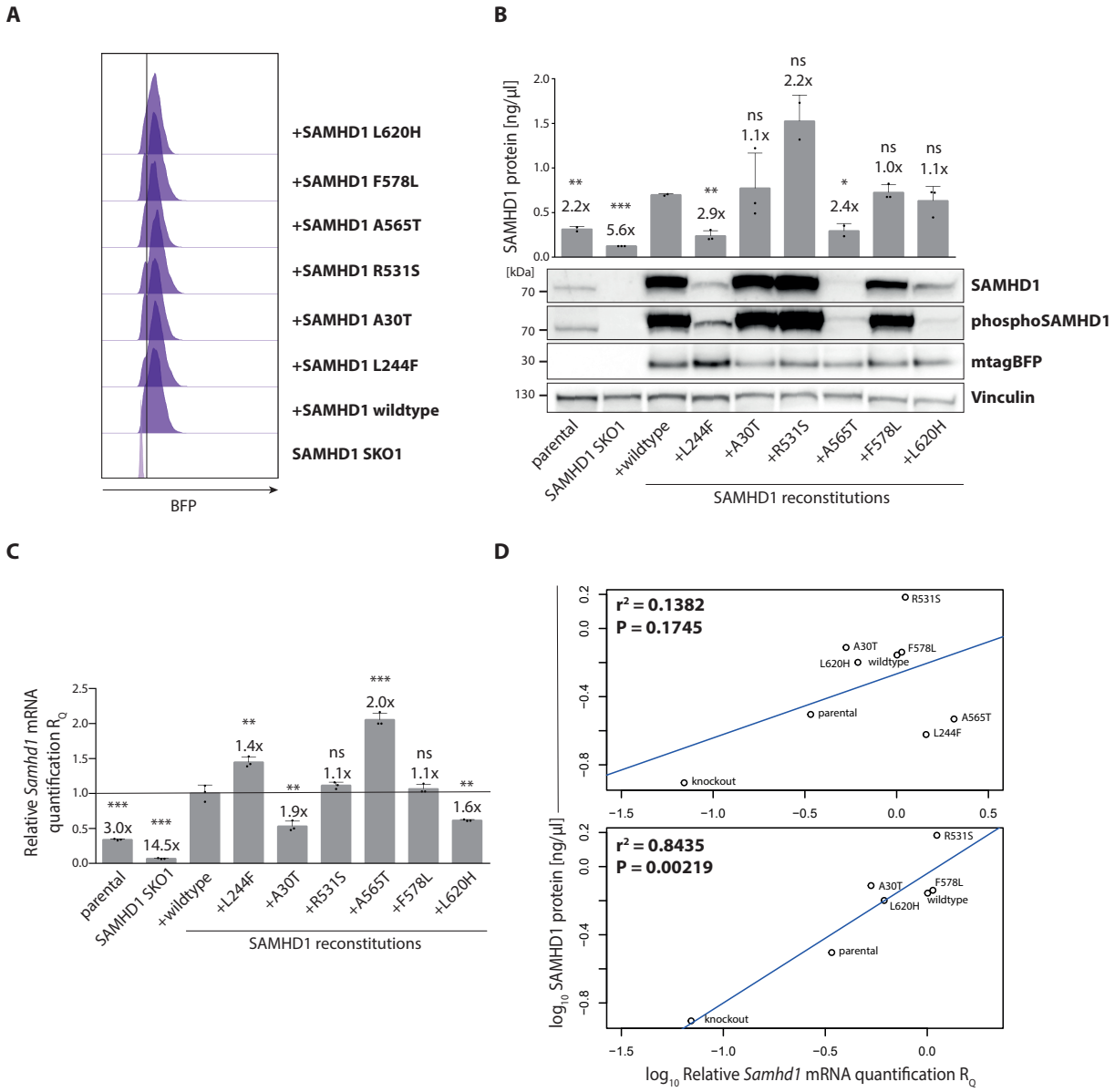

Figure 4.21: Continued on next page.

Figure 4.21: Reconstitution of LN-18 *Samhd1* KO cells with SAMHD1 mutants found in GBM patient tissue. (A) Flow cytometry analysis of LN-18 cells after transduction with lentiviral vectors expressing SAMHD1/mtagBFP and two rounds of mtagBFP-positive cell sorting. mtagBFP expression was measured in the BFP channel. Untransduced LN-18 *Samhd1* KO cells served as negative control. (B) Top: SAMHD1 protein expression analysis using Wes quantitative immunoblotting. n=3 (biological triplicates). Bottom: One representative out of three independent experiments was also analyzed by conventional immunoblotting using α-SAMHD1, α-phospho SAMHD1 T592 and α-mtagBFP antibodies. (C) *Samhd1* mRNA expression levels were measured by qPCR. Samples were normalized to the SAMHD1 wildtype reconstitution, which was set to 1. The horizontal line indicates *Samhd1* mRNA levels for the SAMHD1 wildtype reconstitution. Factor of difference to SAMHD1 wildtype reconstitution is shown. n=3 (technical triplicates). (D) Top: Dot plot comparing *Samhd1* mRNA expression levels (x-axis) and SAMHD1 protein expression (y-axis). Bottom: Same plot, but without SAMHD1 mutants L244F and A565T. Error bars indicate standard deviation (s.d.). Statistical analysis: Student's unpaired t-test: ***P $<$ 0.001, **P $<$ 0.01, *P $<$ 0.05, ^{ns}P $>$ 0.05. Wes immunoblots in B on the top were performed by Johanna Döring (in-house) under my supervision. Bioinformatical analysis in (D) was performed in collaboration with Prof. Lars Kaderali (University Medicine Greifswald, Germany).

4.6.2 *Samhd1* mRNA expression levels are elevated in low-SAMHD1 protein-expressing mutants L244F and A565T

After observing different SAMHD1 protein levels in the mutant reconstitutions, we decided to study *Samhd1* mRNA expression in these cells. Interestingly, *Samhd1* mRNA expression levels mirrored the SAMHD1 protein expression levels in general, but both low-SAMHD1 protein-expressing mutants L244F and A565T had significantly higher *Samhd1* mRNA expression levels compared to wildtype (figure 4.21C). Figure 4.21D compares SAMHD1 protein and *Samhd1* mRNA levels with no statistically significant correlation (shown at the top, $r^2 = 0.1382$, $P = 0.1745$). When plotting the same data without SAMHD1 mutants L244F and A565T, all other mutants lined up together in a statistically significant positive correlation (shown at the bottom, $r^2 = 0.8435$, $P = 0.00219$). Taken together, whereas SAMHD1 protein and *Samhd1* mRNA levels showed a positive correlation for most SAMHD1 mutants, L244F and A565T displayed lower SAMHD1 levels and higher *Samhd1* mRNA levels compared to wildtype and other SAMHD1 mutant reconstitutions.

4.6.3 Cytarabine sensitivity is dependent on SAMHD1 protein levels in cancer-related SAMHD1 mutants

After expression analysis, we wanted to study the mutants and their effect on ara-C sensitization in the GBM cell line LN-18. Cytotoxicity studies in the reconstituted SAMHD1 mutants showed ara-C sensitivities similar to SAMHD1 wildtype for SAMHD1 mutants

A30T, R531S and F578L, which goes in line with their comparable SAMHD1 protein expression levels and groups them as "neutral" ara-C sensitivity phenotypes (figure 4.22A). Sensitivity to ara-C reflected by ED_{50} levels (y-axis) positively correlated with SAMHD1 protein levels (x-axis) with statistical significance (figure 4.22B; $r^2 = 0.4966$, $P = 0.0205$). On the other hand, the SAMHD1 mutations L244F and A565T showed significantly lower ED_{50} levels compared to SAMHD1 wildtype reconstitution. As described above, the SAMHD1 protein levels of these two mutants were significantly lower compared to SAMHD1 wildtype reconstitution (2.9-fold for L244F and 2.4-fold for A565T, figure 4.21B), but showed SAMHD1 expression levels comparable with the parental cell line, grouping them as loss-of-function phenotypes compared to the parental cell line. In addition, the fact that the parental cell line showed similar ED_{50} levels, but much lower SAMHD1 protein levels compared to SAMHD1 wildtype reconstitution, indicated that even low amounts of SAMHD1 wildtype protein were sufficient to desensitize to ara-C in LN-18 cells.
Interestingly, SAMHD1 mutation L620H showed significantly increased sensitivity to ara-C while SAMHD1 protein levels did not significantly differ compared to the wildtype reconstitution. Whereas *Samhd1* KO cells were 24.8-fold more sensitive to ara-C, mutant L620H showed 8.0-fold more sensitivity to ara-C compared to the wildtype reconstitution and can therefore be grouped as a medium loss-of-function phenotype compared to the SAMHD1 wildtype reconstitution.
In addition to the ara-C toxicity assay, we wanted to show that the increased cytotoxicity is associated with increased levels of ara-CTP in the cells. In line with previous reports, figure 4.22C shows that ara-CTP levels significantly increased in SAMHD1-deficient KO cells (figure 4.12) [101] as well as SAMHD1 L244F, A565T and L620H mutants compared to wildtype reconstitution. Plotting ara-CTP levels and SAMHD1 protein levels showed a statistically significant inverse correlation (figure 4.22D, $r^2 = 0.5588$, $P = 0.01248$). Comparing ara-CTP and ED_{50} levels in figure 4.22E emphasized a strong inverse correlation between these two parameters ($r^2 = 0.9487$), which was statistically highly significant ($P = 5.666e\text{-}06$), proving that the cytotoxicity observed in figure 4.22A strongly correlated with ara-CTP levels in the cells.
Taken together, whereas the SAMHD1 mutants A30T, R531S and F578L found in GBM patient tissue displayed ara-C sensitivity comparable to the wildtype reconstitution, the SAMHD1 mutants L244F and A565T showed SAMHD1 protein levels comparable to the parental cell line, but ED_{50} levels were comparable to *Samhd1* KO cells. On the other hand, SAMHD1 mutant L620H showed comparable SAMHD1 protein levels, but a significantly higher sensitivity to ara-C compared to the wildtype reconstitution. Finally, ara-CTP levels inversely correlated with ED_{50} levels in the SAMHD1 mutant reconstitutions with statistical significance.

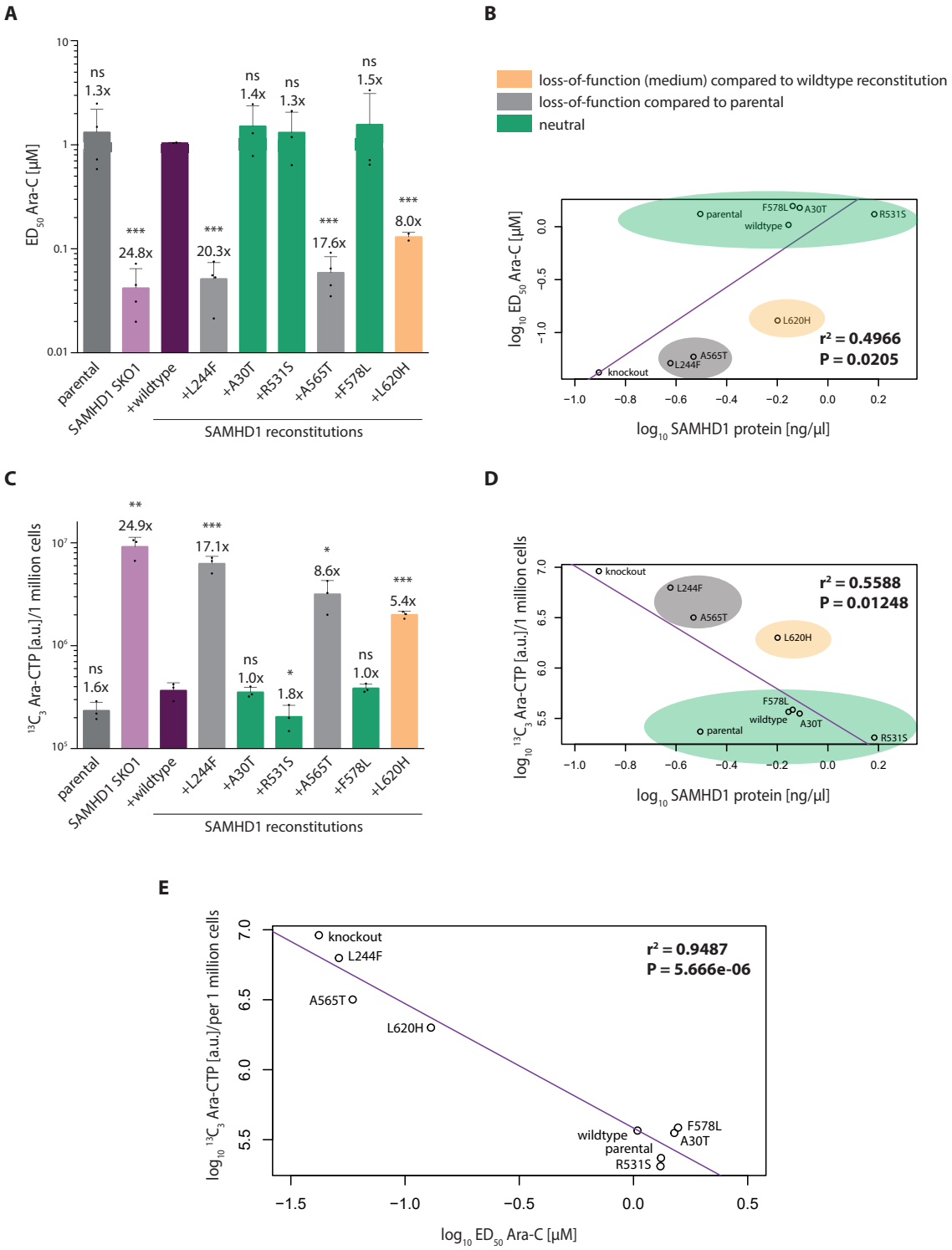

Figure 4.22: Continued on next page.

Figure 4.22: SAMHD1 mutants found in GBM patient tissue show different sensitivity to ara-C which correlates with ara-CTP levels in cells. (A) Cell viability of LN-18 cells was analyzed 4 days after ara-C treatment. ED_{50} of ara-C is shown in μM. Error bars indicate standard deviation (s.d.), n=4 (biological replicates). (B) Dot plot comparing SAMHD1 protein expression (x-axis) and ED_{50} levels for ara-C (y-axis). (C) LC–MS/MS analysis of ara-CTP using labeled $^{13}C_3$ ara-CTP. Factor of difference to the SAMHD1 wildtype reconstitution is shown. n=3 (biological triplicates). Error bars indicate standard deviation (s.d.). Statistical analysis: Student's unpaired t-test: ***P < 0.001, **P < 0.01, *P < 0.05, ^{ns}P > 0.05. (D) Dot plot comparing SAMHD1 protein expression (x-axis) and $^{13}C_3$ ara-CTP levels (y-axis). (E) Dot plot comparing ED_{50} levels for ara-C (x-axis) and $^{13}C_3$ ara-CTP levels (y-axis). Bioinformatical analysis in (B), (D) and (E) was performed in collaboration with Prof. Lars Kaderali (University Medicine Greifswald, Germany).

4.6.4 Vpx-VLP transduction and small molecule inhibitor treatment in SAMHD1 mutants show different sensitivity to SAMHD1 degradation and inhibition, respectively

To investigate whether SAMHD1 protein expression or activity of the thus far unreported SAMHD1 mutants can be manipulated transiently, cells were transduced with Vpx-VLPs or treated with the SAMHD1 inhibitor SIK0001 followed by ara-C toxicity evaluation as an endpoint readout. SAMHD1 mutants categorizing for the "neutral" ara-C phenotype, including A30T, R531S and F578L, could be downregulated by Vpx-VLPs (figure 4.23A), seen by reduced SAMHD1 protein levels (at the bottom) and increased ara-C sensitivity (at the top) for the Vpx-VLP-treated cells in comparison to cells treated with 1xPBS (mock). On the other hand, in SAMHD1 mutants L244F and A565T, with the loss-of-function phenotype compared to the parental cell line, SAMHD1 protein levels could not be decreased further by Vpx-VLP treatment.
SAMHD1 mutant L620H exhibits a special role. Even though its starting ara-C ED_{50} value was similar compared to parental cells and the SAMHD1 wildtype reconstitution, SAMHD1 L620H could not be targeted for degradation by Vpx-VLP treatment and ED_{50} levels for ara-C consequently remained unchanged.
Finally, treatment with the SAMHD1 inhibitor SIK0001 showed a similar pattern. Whereas the activity of GBM SAMHD1 mutants A30T, R531S and F578L could be inhibited by SIK0001 treatment, the already low ara-C ED_{50} value in SAMHD1 L244F and A565T could not be further decreased by SIK0001 treatment (figure 4.23B). Remarkably, SIK0001 treatment did not lead to an increase in ara-C sensitivity in SAMHD1 mutant L620H compared to wildtype SAMHD1 reconstitution.
Taken together, Vpx-VLP or SIK0001 treatment sensitized to ara-C in parental cells, SAMHD1 wildtype reconstitution as well as SAMHD1 mutants A30T, R531S and F578L, but were not able to further sensitize SAMHD1 mutants L244F, A565T and L620H. In

addition, SAMHD1 mutant L620H showed higher SAMHD1 protein levels than L244F and A565T, but still could not be affected by Vpx-VLP-mediated SAMHD1 degradation or SIK0001-mediated SAMHD1 inhibition.

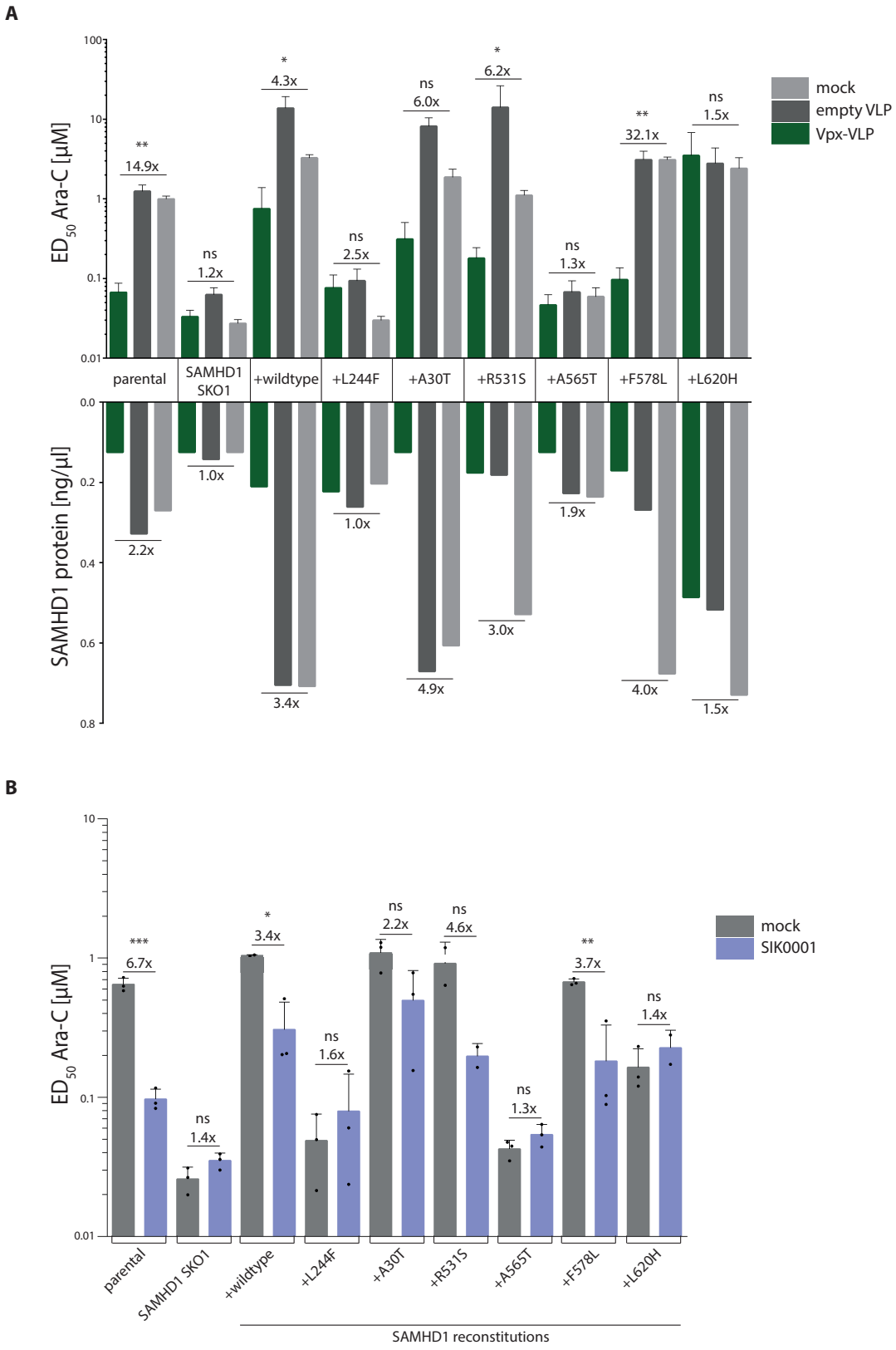

Figure 4.23: Continued on next page.

Figure 4.23: Vpx-VLP transduction and SIK0001-treatment in SAMHD1 mutants found in GBM patient tissue show different degrees of SAMHD1 degradation and inhibition. (A) LN-18 cells were treated with Vpx-VLPs for 24 hours prior to ara-C treatment. Cell viability was analyzed 4 days after ara-C treatment. ED_{50} of ara-C is shown in μM. The graph represents one out of two independent experiments. Vpx-VLP treatment is indicated in green, treatment with empty VLPs in dark grey, treatment with 1xPBS (mock) in light grey. (B) Cells were treated with the SAMHD1 inhibitor SIK0001 at a final concentration of 25 μM. On the same day, ara-C treatment was performed. Purple: treatment with SIK0001, grey: treatment with 1xPBS (mock). n=3 (biological triplicates). Error bars indicate standard deviation (s.d.). Factor of difference for Vpx-VLP or 25 μM SIK0001 compared to mock is shown. Statistical analysis: Student's unpaired t-test: ***P < 0.001, **P < 0.01, *P < 0.05, ^{ns}P > 0.05.

Chapter 5

Discussion

5.1 α-SAMHD1 antibody generation provides a broad application profile for SAMHD1 protein expression analysis

Within this thesis, customized α-SAMHD1 antibodies were generated by Eurogentec and validated by us for the usage in different immunological assays. The five α-SAMHD1 antibodies generated in mouse (EGT986), rabbit (#1245 and #1246) and chicken (#H153 and #H154) showed good performance in both immunoblotting as well as flow cytometric stainings compared to commercial α-SAMHD1 antibodies (figure 4.1). Also, the mouse α-SAMHD1 antibody EGT986 was optimized for quantitative immunoblotting by Wes and used extensively in this thesis. Moreover, most of the antibodies were also capable of detecting mouse SAMHD1, even though immunizations were performed against human SAMHD1 (figure 4.2). This is not surprising as human and mouse SAMHD1 exhibit a high degree of sequence similarity (72% (isoform 1) and 74% (isoform 2) compared to human) [9, 159]. In addition, both SAM and HD domain are quite conserved among the two species [9] and specific immunodominant regions of SAMHD1 are not described in literature yet. Chicken α-SAMHD1 #H154 was optimized to detect SAMHD1 expression in immunohistological stainings of GBM tumor sections with less background than commercial α-SAMHD1 antibodies (figure 4.7B). All in all, the customized α-SAMHD1 antibody generation broadened the applications for SAMHD1 protein evaluation and provided the protein detection tools for the upcoming years of SAMHD1 research in the Keppler lab.

5.2 The *Samhd1* promoter is unmethylated in glioblastoma multiforme cell lines

DNA methylation at the promoter of the *Samhd1* gene is an established regulatory mechanism for SAMHD1 protein expression in different cell models [34], which was also connected

to disease environment in CTCL [35] and lung cancer [36]. To be able to test this regulatory level for SAMHD1, a bisulfite sequencing assay was established within this thesis in order to determine the DNA methylation status in the *Samhd1* promoter in a quantitative manner. The method was successfully verified with SAMHD1-negative Jurkat cells, which have been reported to have a methylated *Samhd1* promoter [34] and with SAMHD1-positive THP-1 cells, which display an unmethylated *Samhd1* promoter [34] (figure 4.3). Crucial for this method was the PCR step, which amplifies the region in the *Samhd1* promoter as PCR conditions needed to be optimized to amplify unmethylated and methylated DNA to an equal extent. Due to the bisulfite conversion, the GC-content in the methylated samples is higher than in the unmethylated samples and so is the optimal melting temperature. Using a melting temperature for PCR, which for both methylated and unmethylated DNA assures comparable conditions for amplification, provided a solid technical foundation for the assay.
The correlation between positive SAMHD1 protein levels and an unmethylated *Samhd1* promoter was further validated in AML cell lines Monomac6, MV4-11 and OCI-AML3, whereas the SAMHD1-negative AML cell line HL-60 showed a methylated promoter status (figure 4.4A). In contrast to that, AML cell line HEL showed no detectable SAMHD1 protein expression, but an unmethylated *Samhd1* promoter profile (figure 4.4A), which points out that there are likely additional regulatory mechanisms that determine SAMHD1 protein levels besides *Samhd1* promoter methylation. A mutation in the *Samhd1* gene of HEL may interfere with this regulation mechanism, but is not confirmed yet.
As established in the SAMHD1 protein expression profile in GBM, all immortalized cell lines showed detectable SAMHD1 protein expression to a different extent (figure 4.5A). In this assay, the GBM cell lines MZ-18 and U-87 MG showed an unmethylated DNA methylation profile in the *Samhd1* promoter, demonstrating that promoter methylation is as a regulatory factor for its expression in these cell lines.

5.3 SAMHD1 is broadly expressed in glioblastoma multiforme

In this thesis, the SAMHD1 expression in the GBM context was analyzed in detail. For this purpose, GBM material from different sources was used to generate a broad SAMHD1 expression profile. In total 15 GBM immortalized cell lines, 11 GBM PDXs and 30 tumor tissues from first-diagnosed glioma and GBM patients were analyzed for SAMHD1 protein levels and emphasized that SAMHD1 is broadly expressed in GBM (figure 4.5 and 4.6). In literature, such a broad SAMHD1 expression characterization for GBM does not exist until now and elucidates the expression landscape of the protein SAMHD1 in this highly malignant solid tumor.
In general, SAMHD1 has been shown to be expressed in most human tissues [18]. Concerning its expression specifically in cancer cells, a downregulation of SAMHD1 compared to healthy tissue was observed in different types of leukemia [91, 107], lymphoma [35],

melanoma [160] and lung cancer [89, 161]. On the other hand, upregulation of SAMHD1 expression compared to healthy tissue was reported for colorectal cancer [161, 162]. The fact that SAMHD1 was broadly expressed in the tested material allowed the deeper characterization of SAMHD1's role in ara-C toxicity in the GBM context.
Beyond that, the SAMHD1 levels varied among the different cell lines, PDXs and patient tissues. In order to represent SAMHD1 expression in GBM properly, large numbers of each cell model were used to exclude cell line- and patient-specific phenomena. The differences observed for SAMHD1 levels also reflected the heterogeneic nature of the tumor itself [135]. In addition, patient tissue from different glioma grades was evaluated for SAMHD1 expression. For this purpose, tissue samples from 10 different patients each for grade II, III and IV were stained for SAMHD1 protein expression by IHC. In general, grade II gliomas belong to the low-grade gliomas (LGGs), whereas grade III and IV gliomas (GBMs) are described as high-grade gliomas (HGGs) [115]. This classification was made due to the proliferative nature of the tumors; LGGs exhibit a low proliferative potential in comparison to the highly proliferative HGGs [115]. Interestingly, the percentage of SAMHD1-positive cells as well as the intensity of SAMHD1 nuclear staining significantly increased with the glioma grade (figure 4.6A and B). In addition, a database evaluation by Dr. Ernesto Mejías Pérez revealed that SAMHD1 protein levels were significantly increased in GBM tumor cells compared to healthy brain tissue (data not shown). Both data sets indicate that SAMHD1 is altered in GBM tumor cells, which motivated us to further investigate SAMHD1's role in GBM chemotherapy.

Whereas working with GBM cell lines revealed many insights into ara-C sensitivity, these cell lines do not mirror the tumor environment *in vivo*. Also, the heterogeneity displayed in the *in vivo* tumors is better maintained in primary cells compared to immortal cell lines, which display more homogeneity over time [116]. In terms of immortal cell lines, including a high number of different cell lines was essential to get a representative overview. That is why 15 different GBM cell lines, all well accepted in the field, were chosen to perform in initial experiments. In addition, *in cellula* monolayers display significantly reduced malignancy compared to the *in vivo* scenario [119]. Even though sphere-growing GBM PDXs showed more complex cultivation conditions and the access to *in vivo* immunohistological sections of first-diagnosed GBM patients was limited, these two models immensely supported the SAMHD1 protein expression analysis in the GBM context.

For the SAMHD1 expression profile, resected tumor tissue from GBM patients was histologically stained for SAMHD1 protein expression; large differences within each tissue sample were observed regarding the SAMHD1 expression in cells (figure 4.6C). Now, besides tumor cells, there are many different cell types found in the tumor mass of GBMs [119]. The question therefore is whether the heterogeneous SAMHD1 expression, determined within each GBM, points to different cell types in the tumor, which express different levels of SAMHD1 (e.g. tumor cells and macrophages) or tumor cells with different SAMHD1 levels. In order to shed light on the identity of the SAMHD1-positive cells in the histological material, neighboring slides stained for common cell types found in GBM identified microglia and macrophages in the tumor section and could largely exclude T cells and

neurons in the tissue sections analyzed (figure 4.7B). This detected cell composition in the GBM patient tissues mirrors the finding by other groups [132, 133]. Very recently, shown through single-cell RNA transcriptomics, Cui *et al.* sequenced tumor biopsies from 9 different GBM patients and reported following cell type composition in percentages: 62.31% tumor cells, 20.29% macrophages, 16.10% microglia and 1.30% T cells [132]. Same as for our immunohistological stainings, they also excluded T cells as a major cell type in GBM, but detected high fractions of macrophages and microglia [132]. Whereas the single-cell RNA sequencing identified tumor cells through their distinct oncogenic expression profile [132], there is thus far no histological tumor marker available to specifically visualize and detect tumor cells in GBM tissue. Nevertheless, with tumor cells being the major cell type in GBM tissue [132], GBM being a cold tumor [115] with rather low infiltration of cells and a high majority of SAMHD1-positive cells in the tumor mass (seen in our immunohistological stainings in figure 4.7 as well as RNA sequencing databases (data not shown)), we expect most of the SAMHD1-positive cells to be tumor cells. Consequently, this data provides a hint at the composition of the individual GBM patient material. Co-staining with SAMHD1 and the already used (e.g. CR3-43 for macrophages/CD8 for macrophages) as well as other cell identification markers (e.g. GFAP for astrocytes) will determine the individual cell identity of SAMHD1-positive cells on a single cell basis. This will verify the hypothesis of SAMHD1-positive tumor cells in the GBM tumor mass, which will help to understand how a SAMHD1-depleting agent can be efficiently implemented in GBM treatment.

5.4 SAMHD1 depletion sensitizes glioblastoma multiforme cells to cytarabine

In this thesis, the influence of SAMHD1 on the cytotoxicity of ara-C in the context of GBM was investigated. In a variety of approaches to compare SAMHD1-deficient to SAMHD1-proficient GBM cells, SAMHD1 deficiency sensitized to ara-C treatment. Transient SAMHD1 degradation mediated by Vpx-VLPs (figure 4.5) and SAMHD1 inhibition by SIK0001 treatment (figure 4.23) as well as stable *Samhd1* KOs (figure 4.10) resulted in a higher sensitivity to ara-C. Conversely, this sensitization could be decreased by SAMHD1 wildtype reconstitution in *Samhd1* KO clones (figure 4.11).
Additional experiments with *Samhd1* KO clones reconstituted with dNTPase inactive SAMHD1 D311A emphasized that the observed difference in ara-C toxicity is associated with the dNTPase activity of SAMHD1 (figure 4.11) [6]. Also, LC-MS/MS measurements emphasized that a *Samhd1* KO resulted in increased levels of the active metabolite ara-CTP supporting that SAMHD1 recognizes ara-CTP as a substrate in GBM cells (figure 4.12), in line with previous reports [101].
Importantly, the GBM cell line LN-18 exhibited generally low SAMHD1 expression levels, but in comparison to LN-18 *Samhd1* KO cells, the endogenous SAMHD1 in the parental cell line was still able to significantly decrease ara-C sensitivity. In comparison to the

highly SAMHD1-positive monocytic cell line THP-1, in cell lines like LN-18, already low levels of SAMHD1 were enough to have a significant effect on ara-C sensitivity. This direct negative correlation between SAMHD1 levels and ara-C toxicity has not been described for GBM thus far and opens the possibility for future GBM treatment approaches in the context of SAMHD1.

In addition to SAMHD1, also other factors can influence the toxicity to ara-C. In AML, SAMHD1 protein levels correlated with the sensitivity to ara-C in the parental cell lines [101]. In GBM, there was no direct correlation between ara-C toxicity and SAMHD1 levels in parental cell lines (figure 4.5A), but when manipulating *Samhd1* by CRISPR/Cas9 KO generation or Vpx-VLP treatment, a strong positive correlation between ara-C sensitivity and SAMHD1 levels was observed (figure 4.5B and 4.10). In contrast to the more homogenous cancer AML, GBMs have a more heterogenic profile, which makes it more difficult to determine mono-specific correlations. In addition, it shows that, whereas SAMHD1 deficiency in GBM sensitizes to ara-C treatment, there are other factors also influencing ara-C effectivity among GBM parental cell lines. One example might be a diverse expression profile of ara-C entry and processing factors. In order for ara-C to be effective in the target cells, the entry factor ENT-1 and processing factor dCK need to be expressed and functional [109]. On the other hand, low or no protein expression of processing factors CDA, NT5C2 and DCTD help to increase the concentration and toxicity of the active metabolite ara-CTP in the cancer cells (figure 1.7) [109]. Differential expression of these factors may influence ara-C toxicity, which makes it more difficult to establish a general correlation between SAMHD1 protein levels and ara-C toxicity in GBM parental cell lines.

5.5 Combinatory SAMHD1 manipulation and cytarabine treatment are proposed as a glioblastoma multiforme treatment strategy

Until now, the chemotherapy landscape for GBM is very limited. The alkylating agent TMZ is mainly used as an adjuvant to radiation therapy, which barely improves overall survival of patients compared to radiation therapy alone [129]. Concerning SAMHD1, the efficacy of TMZ was shown to not correlate with SAMHD1 expression in T-ALL cell lines [107], which was also confirmed by us (data not shown). In addition, due to the extensive heterogeneity of GBMs, most chemotherapy approaches have failed their clinical trials [116]. The data in this thesis indicates that SAMHD1 depletion sensitizes to ara-C treatment in the context of GBM. Therefore, ara-C treatment in combination with a SAMHD1-degrading/inhibiting factor such as Vpx-VLPs, SAMHD1 inhibitors or *Samhd1* siRNAs is being proposed as an alternative treatment strategy for GBM to sensitize GBM cells to ara-C (figure 5.1). Very few is known about ara-C treatment in the context of GBM [148, 150]. A publication from the 70ies [148] as well as a more recent case study [150] provided first hints to an ara-C treatment in GBM, but without the context of SAMHD1.

Determining the SAMHD1 levels in the tumor material prior to treatment decision will be essential and can be performed by either α-SAMHD1 antibody-based immunohistological stainings of tumor sections or SAMHD1 protein level evaluation using minced tumor material. The findings in this thesis will act as the groundwork for alternative treatment implementations in GBM and will, together with further experiments *in vivo* as well as clinical trials, help to develop SAMHD1 as a therapeutic target combined with ara-C or other SAMHD1-dependent nucleoside analogues as alternative treatment to fight GBMs.

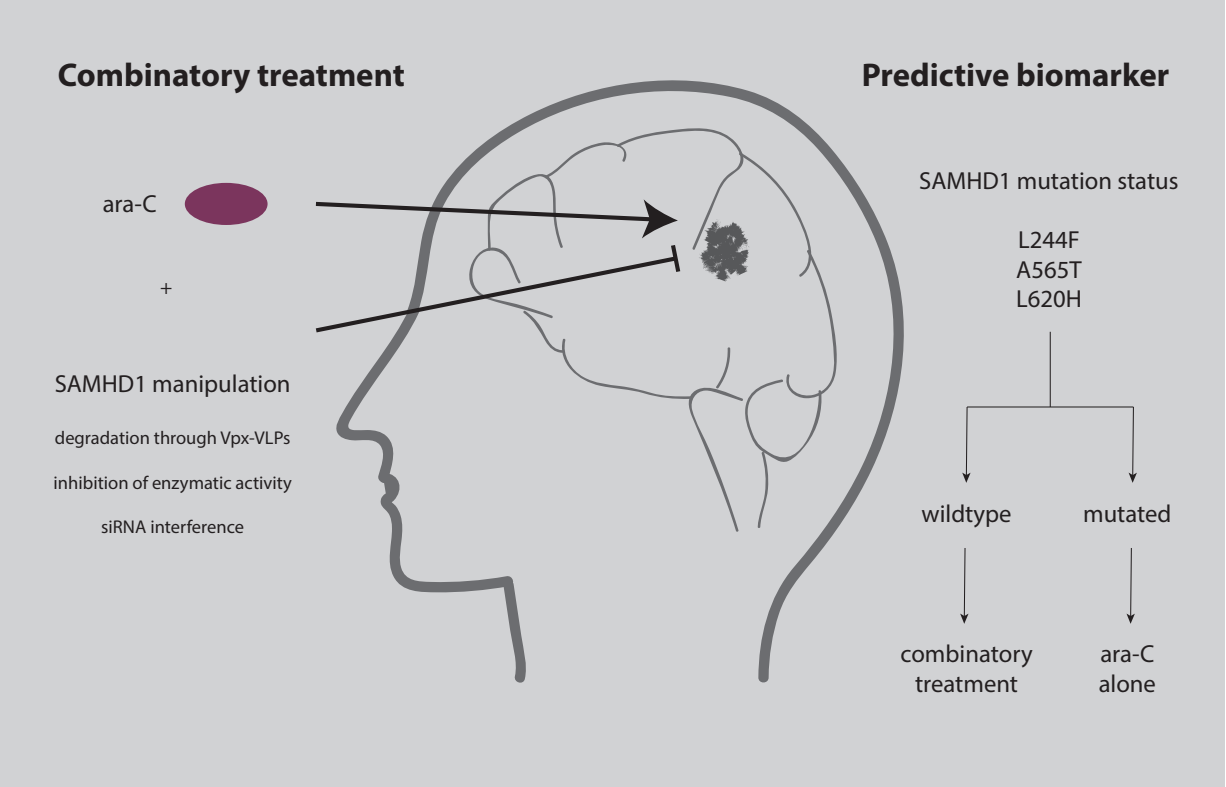

Figure 5.1: Potential predictive biomarker and novel treatment strategy in GBM. On the left: A combinational treatment proposal of ara-C together with a compound that temporarily reduces SAMHD1 protein levels or activity for GBM treatment is being proposed. For the manipulation of SAMHD1, several strategies are possible, ranking from SAMHD1 degradation through Vpx-VLPs, inhibition of SAMHD1's enzymatic activity through small molecules like SIK0001 and with *Samhd1* expression interference using siRNAs. On the right: SAMHD1 mutations as potential predictive biomarkers for the combinatory treatment stratification. In case of a wildtype status at the residues L244, A565 and L620, the combinatory treatment is proposed, whereas in case of one of the mutations L244F, A565T or L620H, SAMHD1-manipulating compounds might not further improve ara-C treatment.

Whereas the side effects for intravenous administration of ara-C are already well as-

sessed in the case of AML treatment (high dose ara-C is known to lead to severe neurological toxicity [142]), depleting SAMHD1 as part of a chemotherapeutical treatment represents a novel strategy and needs to be assessed in a clinical setting.
Firstly, targeting SAMHD1 may lead to general genomic instability in cells where ara-CTP is active [163]. This can increase mutational rates in ara-C-surviving cells through long term treatments. SAMHD1 depletion likely also increases the dNTP pool in ara-C-surviving tumor cells. As a consequence, DNA replication, already elevated in the tumor cells, might even more increase as more building material is available in the cell. This could lead to an elevated tumor cell proliferation in the remaining tumor cells [2] as THP-1 *Samhd1* KO cells have been shown to exhibit elevated proliferation rates [23]. This enforces treatment resistance and acts against successful elimination of all tumor cells. Nevertheless, tumor biology is very complex and such monocausal relationships might not apply directly. In addition, contradicting both elevated genomic instability and tumor cell proliferation, *Samhd1* KO mice do not develop any associated pathologies [86, 87]. These mice are viable and healthy, which indicates that even though SAMHD1 exhibits diverse functions in the body, cells are capable to overcome the lack of SAMHD1, which may not lead to major disadvantages of a transiently SAMHD1-inhibiting treatment.
Secondly, in AML treatment, ara-C is mostly administered intravenously and distributes into the whole body [141]. Depleting SAMHD1 also in other cells of the body may contribute to more severe side effects of the treatment. A local delivery approach targeting the tumor will contribute to reduce possible side effects of overall SAMHD1 depletion in non-cancerous cells. Intracranial injection, administration after surgery or intrathecal injection into the spinal canal are possible local administration routes that are also already licensed for ara-C [164, 165].
Finally, another side effect of depleting SAMHD1 might be a higher risk for viral infections that are usually restricted by the antiviral role of SAMHD1. This may affect in particular the infection with HIV-1 [20, 46, 47, 48], but also for other viruses, for which SAMHD1 acts antivirally, including HSV-1 [54, 55], HCMV [56], EBV [57], HPV16 [58], vaccinia virus [54] and HBV [59, 60]. Nevertheless, cancer patients undergoing chemotherapy are in a very controlled and closely monitored environment, which by itself will reduce the risk of an infection exposure. In addition, the risk-benefit ratio might be beneficial towards the treatment. In this particular treatment strategy, the risk of a viral infection, which mostly exhibits a time-delayed disease development, might be negligible in contrast to the treatment benefit and the option of possible prolongation of overall survival.
Even though we do not know yet how SAMHD1 depletion as part of a cancer treatment will affect a patient, we currently believe that the beneficial effects of SAMHD1 depletion in combination with ara-C administration outweigh possible side effects. Advanced preclinical and early clinical studies should help to clarify this.

Efficient and non-invasive drug delivery systems for ara-C and SAMHD1-depleting compounds in GBM will be also important when proposing an alternative strategy for brain tumor chemotherapy. The BBB represents a major obstacle in the chemotherapy of tumors in the brain and complicates non-invasive drug administration techniques. Importantly,

ara-C has been shown to penetrate the BBB successfully [149]. Whereas BBB permeability is a crucial compound characteristic when using non-invasive administration of drugs treating GBM (such as oral or intravenous administration), it is important that the drug reaches concentrations at the site of treatment that are clinically effective [139]. In the case of AML, low dose ara-C treatments through *i.v.* infusions are standard (100-200 mg/m^2) and lead to plasma concentrations of 0.5-1 μM [109]. Effective and realistic working concentrations of ara-C for GBM treatment will need to be assessed.
In general, SAMHD1 depletion can be achieved by different approaches such as Vpx-VLP-mediated SAMHD1 protein degradation, SIK0001-mediated SAMHD1 activity inhibition or *Samhd1* siRNA interference. For these compounds to overcome the BBB through non-invasive treatment applications, new technologies are currently under development that bypass the BBB, enter the brain and deliver the chemotherapeutic agent to the tumor site [112]. Packing such components into a delivery system that can penetrate the BBB represents a major branch in research for brain tumor treatment. It has been shown that treatment with synthetic protein nanoparticles from polymerized human serum albumin, that carry the treatment regimen resulted in sufficient concentrations in the brain and increased overall survival as well as long-term survival in mice, making them a promising source for compound delivery to the brain in the future [139].

5.6 Reconstitution of *Samhd1* knockout with SAMHD1 mutants is a powerful tool to study SAMHD1 function and regulation

In this thesis, a workflow was established that allowed the *in cellula* study of mutations in the *Samhd1* gene, with special focus on functional and regulatory relevance. Implementing the workflow of *Samhd1* KO reconstitution using lentiviral vectors including a fluorescence-based transfer vector and consecutive enrichment of reconstituted cells by sorting provided an approach with many technical advantages (figure 4.11A).
Firstly, SAMHD1 expression under the constitutively active promoter EF1α allowed the *Samhd1* gene as well as the *mtagBFP* gene after it to be continuously transcribed, but a self-cleaving T2A peptide derived from thosea asigna virus was expressed between the two sequences. Expressing SAMHD1 and mtagBFP right next to each other, but cleaving them after transcription ensures that both proteins are expressed under the same promoter and that the majority of the SAMHD1 protein will be present in an unmodified form, without fusion to another protein. From prior evaluations in literature, we know that none of the 2A peptides cleaves the fusion proteins completely, but that the T2A peptide, which was used in this study, is the most efficient among them [166]. A classical fusion protein of SAMHD1 and mtagBFP would have created additional questions as how the relatively large 26.7 kDa mtagBFP protein might influence the function and activity of SAMHD1. In addition, the presence of the fluorophore mtagBFP allows the enrichment of transduced cells through sorting, which both selects for transduced cells as well as avoids possible side

effects associated with a selection through drugs.
Secondly, directed mutagenesis enabled us to generate a transfer vector with any mutation of interest in the *Samhd1* sequence in a fast and cost-effective manner. Also, this method is not limited to SAMHD1, but can be used to clone any gene sequence of interest into the pCDH-EF1α-BFP-1 transfer vector.
Finally, with this approach, it was possible to generate uniform, stably reconstituted cell populations in cell lines even with unconcentrated lentiviral stocks that showed low initial transduction efficiencies (data not shown).

When characterizing SAMHD1 mutants, one part was to quantitatively determine SAMHD1 protein and *Samhd1* mRNA levels in the SAMHD1 mutant reconstitutions. As shown in figure 4.14 and 4.16, the SAMHD1 mutant reconstitutions displayed both different SAMHD1 protein as well as *Samhd1* mRNA expression levels. Interestingly, the expression parameters of SAMHD1 protein and *Samhd1* mRNA did not correlate with each other (figure 4.16D). Within these cell sets, mutants were generated and handled identically. In particular, seeding, lentiviral transduction and sorting was performed in parallel among the mutants in a set. Subsequent monitoring of the SAMHD1 mutants also assured comparable mtagBFP expression levels (figure 4.13). Nevertheless, both SAMHD1 protein and *Samhd1* mRNA levels differed significantly. Reasons for this phenomenon can be diverse:
Firstly, the question arose whether the percentage of mtagBFP-positive cells actually was a sufficient quantitative parameter for sorting and monitoring the expression of SAMHD1 mutants. Due to SAMHD1 and mtagBFP being expressed under the same promoter, it was assumed that mtagBFP levels will directly reflect SAMHD1 levels. Similar mtagBFP levels, but different SAMHD1 protein levels might suggest mutation-specific SAMHD1 regulation on the translational or post-translational level.
Secondly, simultaneous sorting of the mutants may not have been sufficient enough to unify expression levels. When sorting the transduced cells, differences in the percentage of mtagBFP-positive cells were seen (data not shown), emphasizing that the lentiviral vector productions showed different levels of transduction efficiencies. For transduction of SAMHD1-deficient cell clones, non-concentrated lentiviral supernatants in medium with identical volumes were used when applied for all SAMHD1 mutations from the same cell line (200 μl in 96-well plate for the suspension cell line THP-1 and 500 μl in 24-well plate for the adherent cell lines LN-18, U-251 MG and U-87 MG). Nevertheless, using non-concentrated lentiviral supernatants without any further evaluation of potency lacks the information of a lentiviral titer. Even though comparable and narrow gating throughout sorting was ensured, determining the RT activity using SYBR Green I-based product-enhanced reverse transcription (SG-PERT) [167] as well as titrating the lentiviral stocks [168] prior to transduction may have helped to unify protein expression levels.
Thirdly, the different SAMHD1 protein levels might be a result of different stability and possible proteasomal degradation of certain SAMHD1 mutants, which could explain low SAMHD1 expression levels compared to wildtype reconstitution (figure 4.14) and was also described by Bowen *et al.* [169]. Treatments with components inhibiting key players in

proteosomal degradation such as MG-132, ALLN and clasto-lactacystin *beta*-lactone [170] as well as cellular thermal shift assays (CETSA) [171] will elucidate stability and degradation processes for the SAMHD1 mutants.
Finally, SAMHD1 mutants might localize differently in the cell. An aberrant SAMHD1 localization or a different ratio of distribution between cytoplasm and nucleus ratio might also affect proteosomal degradation [172]. In addition, ara-C is processed into its active metabolic ara-CTP mainly in the cytoplasm (figure 1.7). Elevated cytosolic SAMHD1 protein levels due to increased cytoplasmic localization might also further decrease ara-C sensitivity to an even higher extent than "regularly" localized SAMHD1. Immunofluorescent stainings of SAMHD1 will therefore shed light on the subcellular localization of SAMHD1 mutants.

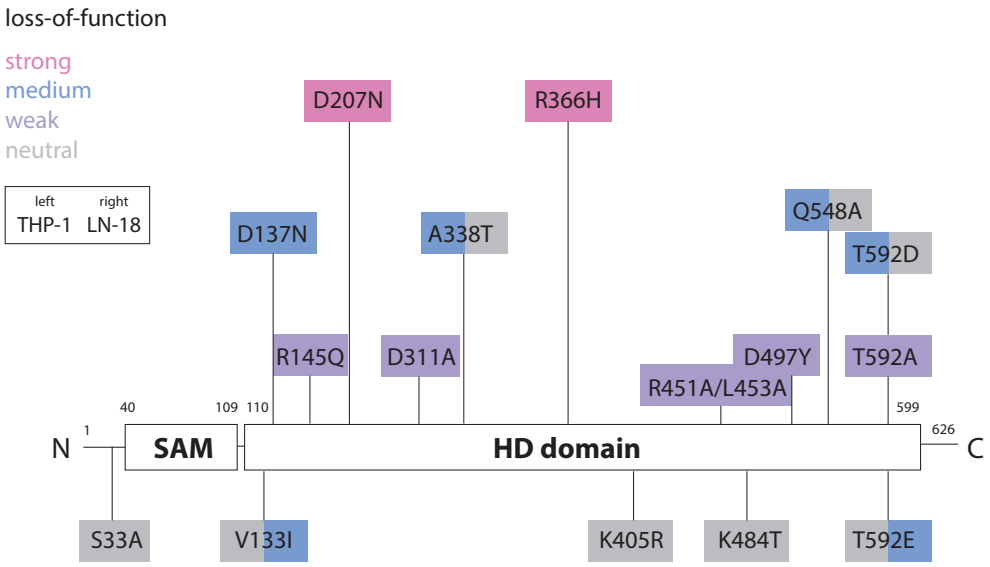

Figure 5.2: Schematic representation of SAMHD1 with the mutations investigated in this thesis. Mutations indicated in grey on the bottom were "neutral" mutations in terms of ara-C toxicity compared to the SAMHD1 wildtype reconstitution. Mutations indicated in purple were grouped into "weak", mutations indicated in blue into "medium" and mutations indicated in pink into "strong" loss-of-function phenotypes. In case mutations behaved differently in the two cell lines tested, this is indicated by the two different colors for THP-1 on the left and LN-18 on the right, respectively.

Beyond that, this study was able to recapitulate mutational phenotypes that have been reported in literature, which further validated the system established. Whereas the SAMHD1 mutants showed phenotypes in diverse settings and output assays in literature, for this project, the influence of the particular SAMHD1 mutation was investigated especially for the sensitization of ara-C. Table 4.1 summarizes the SAMHD1 mutants investigated in this study. The SAMHD1 mutant D311A was the optimal control as it is known

to be dNTPase-inactive [6]. In the sensitization model for ara-C, whose efficacy negatively correlates with the dNTPase activity of SAMHD1 (figures 4.11 and 4.12) [101], SAMHD1 D311A behaved like the *Samhd1* KO cells and validated the workflow on a functional level. Categorizing the different SAMHD1 mutants was more difficult due to the different SAMHD1 expression profiles. All mutations from this set are summarized in figure 5.2 for their sensitivity to ara-C. Concerning the THP-1 SAMHD1 mutants, T592E [38], V133I [90], S33A [157], K484T [14] and K405R [44] were grouped as a "neutral" ara-C toxicity phenotype as the sensitivity to ara-C was not significantly increased compared to the wildtype reconstitution (figure 4.17A,B). Also, "medium" ara-C sensitization phenotypes that showed intermediate SAMHD1 protein expression and intermediate ED_{50} levels in comparison to *Samhd1* KO could be seen for A338T [90], D137N [21], T592D [38] and Q548A [21] (figure 4.17A,B). Other SAMHD1 mutations displayed such low SAMHD1 protein expression levels that the SAMHD1 present was not able to sensitize to ara-C and a statement about an ED_{50} decrease due to SAMHD1-mediated sensitization was not possible (figure 4.17A,B). This was seen for SAMHD1 mutations R451A/L453A [12], R145Q [156], D497Y [90], T592D [38] and D311A [6] in THP-1 cells (figure 4.17A,B).
For LN-18 cells, grouping into ara-C sensitization phenotypes was more difficult as the dynamic range was not as broad as in THP-1 cells. Preliminary assessment suggests that some mutants behaved similar in LN-18 and THP-1 cells, including K405R, K484T and S33A for the "neutral" phenotype, D137N for the "medium" phenotype and R451A/L453A, D311A, T592A, R145Q and D497Y for the "weak" phenotype. Importantly, not all mutants behaved similarly in the two mutant sets for both SAMHD1 protein levels as well as ara-C sensitivity.
Finally, two SAMHD1 mutations stood out in both THP-1 and LN-18 cells: SAMHD1 D207N [21] as well as R366H [90] displayed significantly elevated ara-C sensitivity paired with similar SAMHD1 protein levels compared to the SAMHD1 wildtype reconstitution (D207N: 137.9-fold in THP-1 cells and 21.0-fold in LN-18 cells; R366H: 139.4-fold in THP-1 cells and 14.1-fold in LN-18 cells, figure 4.17A,B and 4.18) - ED_{50} levels similar to the sensitization phenotype of both *Samhd1* KO clones.
SAMHD1 mutation D207N was described by Ryoo *et al.* in 2015 as an allosteric mutant that could no longer restrict HIV-1 infection and did not longer cleave dNTP levels compared to wildtype SAMHD1 in U937 cells [21]. Interestingly, dNTP level measurements in the THP-1 SAMHD1 D207N mutant showed no significantly reduced dCTP levels compared to the wildtype reconstitution (figure 4.19B), which did not go in line with the findings by Ryoo *et al.* Nevertheless, dNTP levels in the THP-1 mutants generally showed a small dynamic range. For example, in the dNTPase-inactive SAMHD1 mutant D311A, dCTP levels only increased by 3.2-fold compared to SAMHD1 wildtype reconstitution. As a result, even when the dNTPase activity of SAMHD1 is impaired, the cell may balance the additional load of dNTPs through alternative mechanisms to assure counter cell homeostasis.
The SAMHD1 mutation R366H was described by Rentoft *et al.* in 2016 as a single nucleotide polymorphism (SNP) in colorectal cancer [90]. The purified protein SAMHD1 R366H inherited decreased dNTPase activity and increased dN levels *in vitro* [90]. The

data in this thesis recapitulated R366H's decreased dNTPase activity *in cellula* in the two different cancer cell models. Nevertheless, dCTP measurements also showed no significant differences between SAMHD1 R366H and the wildtype reconstitution (figure 4.19B). In addition, very recently, Bowen *et al.* published structural and functional insights about the loss of dNTPase activity in the SAMHD1 mutation R366H [169]. Here, they demonstrate that SAMHD1 R366H looses its dNTPase activity through the absence of the dGTP substrate in its active site, but preserves dNTPase-independent, alternative functions of SAMHD1 [169]. The publication recapitulated our results as they showed abundant and comparable SAMHD1 R366H protein levels as well as sensitization to ara-C relative to the wildtype reconstitution due to the lack of dNTPase activity of SAMHD1 R366H [90].
Taken together, reconstitutions of *Samhd1* KO with SAMHD1 mutants using lentiviral vectors is a powerful tool to study SAMHD1 function and regulation. Concerning the impact of single nucleotide changes in SAMHD1 on ara-C chemosensitivity, the carefully performed correlation and statistical analysis helped to group SAMHD1 mutants and in part recapitulated mutant characteristics already reported. The SAMHD1 mutations D207N and R366H sensitized to ara-C in both AML cell line THP-1 as well as GBM cell line LN-18.

5.7 SAMHD1 mutations L244F, A565T and L620H found in glioblastoma multiforme patients may have clinical relevance

In this thesis, the SAMHD1 mutations L244F, A30T, R531S, A565T, F578L and L620H have been selected for ara-C sensitization studies due to their occurrence in WGS analysis of GBM patient material (figure 4.2) [94, 158]. Therefore, the mutant SAMHD1 versions were stably overexpressed in GBM LN-18 *Samhd1* KO cells and evaluated for sensitization to ara-C.
All six SAMHD1 mutations and their sensitivity to ara-C are summarized in figure 5.3. The three SAMHD1 mutants A30T, R351S and F578L showed no difference in ara-C sensitivity compared to wildtype reconstitution with similar SAMHD1 protein levels ("neutral" ara-C sensitization phenotype, figure 4.22). SAMHD1 mutations L244F and A565T showed SAMHD1 protein levels comparable to the parental cells, but ED_{50} values comparable to *Samhd1* KO (figure 4.21B and 4.22). Interestingly, the SAMHD1 mutation L620H was shown to partly sensitize GBM cells to ara-C as it displayed a statistically significant, 8-fold lower ED_{50} value compared to the SAMHD1 wildtype reconstitution (figure 4.22A, B). SAMHD1 protein levels have been shown to be slightly lower in SAMHD1 L620H compared to the wildtype reconstitution, but the difference was not statistically significant in the quantitative expression analysis (figure 4.21B). As the investigated SAMHD1 mutations were found in GBM patient tissue, this could be a first hint that ara-C alone might be sufficient to have therapeutic relevance in GBM patients carrying the SAMHD1 mutations L244F, A565T or L620H in their tumor. In addition, the SAMHD1 mutation L244F has been also reported in CLL, indicating that this mutation might be inherent to a wider

range of cancers [91].

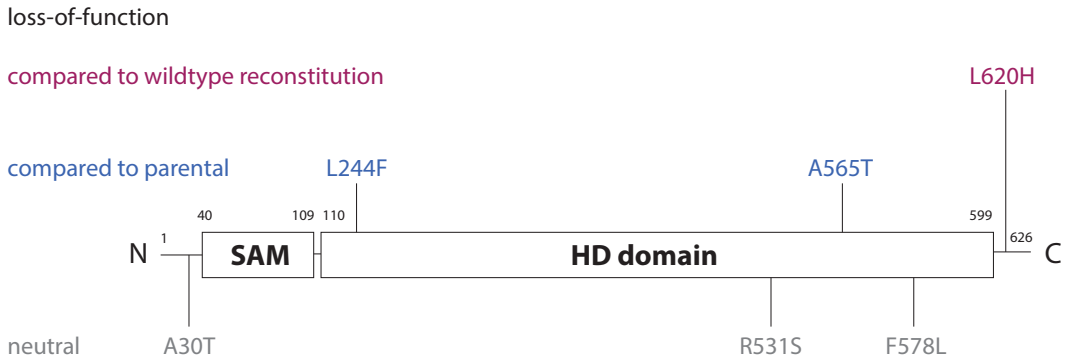

Figure 5.3: Schematic representation of SAMHD1 with the mutations found in GBM patients that were investigated in this thesis in LN-18 cells. Mutations indicated in grey on the bottom were "neutral" mutations in terms of ara-C toxicity compared to SAMHD1 wildtype reconstitution. Mutations indicated in blue on the top were loss-of-function mutations compared to the parental population and the L620H mutation indicated in red was a loss-of-function mutation compared to SAMHD1 wildtype reconstitution.

Treatment with either Vpx-VLP or SIK0001 revealed that, in comparison to SAMHD1 A30T, R351S and F578L, these interventions were not able to further sensitize to ara-C in the SAMHD1 mutants L244F, A565T and L620H. This was demonstrated in the GBM cell line LN-18, where SAMHD1 protein/activity of these mutant versions could not further be reduced by Vpx-VLP-mediated degradation or SIK0001-mediated inhibition, respectively (figure 4.23). In contrast to L244F and A565T, which already displayed significantly lower SAMHD1 protein levels compared to the wildtype reconstitution, the SAMHD1 mutant L620H showed protein levels comparable to wildtype, but still could not be degraded by Vpx-VLPs or inhibited through SIK0001. As the residues essential for the interaction of SAMHD1 with Vpx are very close to residue R620, namely R617, V618 and K622, we speculate that the mutation R620H impairs this interaction [64]. It is important to mention that the protein Vpx from SIV_{mac251} was used in this thesis [151]. The question arises as to which extent Vpx proteins of other origin would be able to mediate SAMHD1 L620H degradation. These experiments will be essential to elucidate the Vpx-mediated degradation of this SAMHD1 mutant.
Concerning the small molecule SIK0001, colleagues (in-house) showed that SIK0001 treatment does not alter SAMHD1 protein expression itself (data not shown), indicating a regulatory mechanism likely targeting the dNTPase activity of the enzyme. Nevertheless, the mode-of-action of how SIK0001 is inhibiting SAMHD1 activity and therefore increases sensitivity to ara-C is still under study. *In vitro* binding assays and *in silico* analysis will shed light on the SAMHD1-inhibitoring mechanism of SIK0001 and contribute to the understanding of the role of the SAMHD1 residues L244, A565 and L620.

These findings in SAMHD1 mutations L244F, A565T and L620H found in GBM patients point at them as possible predictive biomarkers for ara-C combinatory treatment in GBM, as patients carrying these SAMHD1 mutations in their tumor may not need an additional Vpx/SIK0001 treatment to sensitize for ara-C (figure 5.1).

5.8 Methodical limitation of the thesis

Whereas the lentiviral vector-based SAMHD1 reintroduction of SAMHD1 in *Samhd1* KO clones including a mtagBFP expression cassette divided by a self-cleaving T2A site was the optimal available decision for our project at the particular time, the different protein expression levels among the SAMHD1 mutants in comparison to wildtype SAMHD1 as well as the overexpressed system with a constitutively active promoter EF1α were limitations we had to face. An overexpressed system does not fully represent the natural endogenous state of the cell, as highly overexpressed SAMHD1 might misrepresent phenotypes. Especially in the Vpx-VLP treatments, the high SAMHD1 expression levels in the reconstituted cell populations technically limited the assay as the maximal amount of concentrated Vpx-VLPs added to the cells was not able to fully degrade SAMHD1.
An alternative to our approach would be to introduce the desired mutation directly in the endogenous *Samhd1* gene. This is possible through a CRISPR/Cas9-based knock-in (KI) strategy where the mutation is introduced by a specific gRNA for the mutational region and a Cas9 protein that cuts directly at the desired mutation site [173]. One advantage of this system is that we most likely would fear less SAMHD1 protein expression differences as there would be no differences in transduction efficiencies. We would expect SAMHD1 expression levels to be more comparable to each other than in the overexpressed system as most importantly, all the mutants would be expressed under the control of the natural promoter. In addition, the generation of the endogenous mutation KI would be faster as it can be performed directly from the parental population and no *Samhd1* KO needs to be generated beforehand. Finally, the system would remain endogenous and polyclonal from the start. As we would only edit single nucleotides in the endogenous *Samhd1* sequence, we would work with the natural parental polyclonal population and avoid the more artificial overexpressed system based on a monoclonal *Samhd1* KO clone.

5.9 Outlook

Even though a multitude of research publications and clinical trials have been executed to understand and successfully treat GBM within the last decades, state of the art chemotherapy in GBM and corresponding survival rates have barely improved. Finding and implementing new chemotherapeutic strategies to improve survival of GBM patients is therefore crucial to fight this malignant brain tumor.
This thesis showed that depletion of *Samhd1* sensitizes GBM to ara-C. Ara-C in combination with SAMHD1 manipulation is therefore proposed as an effective treatment strategy

in GBM. Besides SAMHD1 acting as a potential predictive biomarker for ara-C treatment, it would also broaden the drug portfolio for the thus far very limited chemotherapeutic strategies in GBM. As a result, this thesis provides a solid foundation towards the path of an alternative treatment strategy to fight GBM.
In addition, the SAMHD1 mutants established provide a basis for many future projects and can be used to approach different scientific questions. In this thesis, the focus was on ara-C cytotoxicity, but SAMHD1 was firstly described as an antiviral factor and the SAMHD1 mutants could also be used e.g. in infection studies with different SAMHD1-dependent viruses, including e.g. HIV-1 [20, 46, 47, 48], HSV-1 [54, 55] or ZIKV [61].
In order to shed more light on the functional effects of the single nucleotide changes, SAMHD1 mutations could also be introduced into a bacterial expression vector for human SAMHD1 such as pGEX-4T-1 His-SAMHD1. Mutant SAMHD1 protein could be purified and investigated *in vitro* through SAMHD1 activity assays in order to collect valuable information e.g. whether the particular SAMHD1 mutation interferes with the dNTPase activity of SAMHD1. In order to use a human background to produce human SAMHD1, it would be also possible to use human cell lines for protein production of SAMHD1 mutants. In addition, cellular thermal shift assays (CETSA) [171] can be performed in order to investigate the protein stability of the SAMHD1 mutants as well their interaction capability with SIK0001.
In order to advance these studies towards more *in vivo*-like systems, the SAMHD1 mutations can be also studied in the GBM PDXs by either reintroducing the SAMHD1 mutations into already generated *Samhd1* KO clones of PDX line H561 or directly mutating endogenous SAMHD1 using the CRISPR/Cas9 KI strategy [173]. In addition, *in vivo* experiments using intracranial injection of human GBM cells with either SAMHD1 wildtype or SAMHD1 mutations into mouse brains followed by ara-C and Vpx-VLP/SIK0001-single and combinatory treatment will help to shed more light on therapeutic relevance. In the future, a treatment decision towards a combinatory ara-C and SAMHD1-degrading/inhibiting molecule could be proposed by determining the mutation state in the tumor of the patient for SAMHD1 residues L244, A565 and L620 prior to treatment start (figure 5.1). As the SAMHD1 L620H mutant already showed partial increased sensitivity to ara-C (figure 4.22A, B), ara-C might be also effectively administered without Vpx-VLP or SIK0001 in this particular case. Additional experiments are required in order to estimate the SAMHD1 mutations L244F, A565T and L620H as predictive markers for combinatory treatment of ara-C with a SAMHD1-manipulating compound.
Taken together, this thesis provides the groundwork for the role of SAMHD1 in the context of ara-C toxicity in GBM for future research studies and clinical trials in the fight against one of the deadliest brain tumors that currently challenge human health. In addition, SAMHD1 mutants were established as a useful tool that will benefit various SAMHD1-focused projects in the future and will enhance the functional knowledge about SAMHD1.

Bibliography

[1] K. M. Knecht, O. Buzovetsky, C. Schneider, D. Thomas, V. Srikanth, L. Kaderali, F. Tofoleanu, K. Reiss, N. Ferreirós, G. Geisslinger, V. S. Batista, X. Ji, J. Cinatl, O. T. Keppler, and Y. Xiong. The structural basis for cancer drug interactions with the catalytic and allosteric sites of SAMHD1. *Proc Natl Acad Sci U S A*, 115(43): E10022–E10031, 2018.

[2] R. Kohnken, K. M. Kodigepalli, and L. Wu. Regulation of deoxynucleotide metabolism in cancer: novel mechanisms and therapeutic implications. *Mol. Cancer*, 14:176, 2015.

[3] R. Buj and K. M. Aird. Deoxyribonucleotide Triphosphate Metabolism in Cancer and Metabolic Disease. *Front Endocrinol (Lausanne)*, 9:177, 2018.

[4] T. W. Traut. Physiological concentrations of purines and pyrimidines. *Mol. Cell. Biochem.*, 140(1):1–22, 1994.

[5] N. Li, W. Zhang, and X. Cao. Identification of human homologue of mouse IFN-gamma induced protein from human dendritic cells. *Immunol. Lett.*, 74(3):221–224, 2000.

[6] D. C. Goldstone, V. Ennis-Adeniran, J. J. Hedden, H. C. Groom, G. I. Rice, E. Christodoulou, P. A. Walker, G. Kelly, L. F. Haire, M. W. Yap, L. P. de Carvalho, J. P. Stoye, Y. J. Crow, I. A. Taylor, and M. Webb. HIV-1 restriction factor SAMHD1 is a deoxynucleoside triphosphate triphosphohydrolase. *Nature*, 480(7377): 379–382, 2011.

[7] X. Ji, Y. Wu, J. Yan, J. Mehrens, H. Yang, M. DeLucia, C. Hao, A. M. Gronenborn, J. Skowronski, J. Ahn, and Y. Xiong. Mechanism of allosteric activation of SAMHD1 by dGTP. *Nat. Struct. Mol. Biol.*, 20(11):1304–1309, 2013.

[8] C. Zhu, W. Gao, K. Zhao, X. Qin, Y. Zhang, X. Peng, L. Zhang, Y. Dong, W. Zhang, P. Li, W. Wei, Y. Gong, and X. F. Yu. Structural insight into dGTP-dependent activation of tetrameric SAMHD1 deoxynucleoside triphosphate triphosphohydrolase. *Nat Commun*, 4:2722, 2013.

[9] O. Buzovetsky, C. Tang, K. M. Knecht, J. M. Antonucci, L. Wu, X. Ji, and Y. Xiong. The SAM domain of mouse SAMHD1 is critical for its activation and regulation. *Nat Commun*, 9(1):411, 2018.

[10] J. Ahn. Functional organization of human SAMHD1 and mechanisms of HIV-1 restriction. *Biol. Chem.*, 397(4):373–379, 2016.

[11] S. A. Coggins, B. Mahboubi, R. F. Schinazi, and B. Kim. SAMHD1 Functions and Human Diseases. *Viruses*, 12(4), 2020.

[12] C. St Gelais, S. H. Kim, L. Ding, J. S. Yount, D. Ivanov, P. Spearman, and L. Wu. A Putative Cyclin-binding Motif in Human SAMHD1 Contributes to Protein Phosphorylation, Localization, and Stability. *J. Biol. Chem.*, 291(51):26332–26342, 2016.

[13] J. Yan, C. Hao, M. DeLucia, S. Swanson, L. Florens, M. P. Washburn, J. Ahn, and J. Skowronski. CyclinA2-Cyclin-dependent Kinase Regulates SAMHD1 Protein Phosphohydrolase Domain. *J. Biol. Chem.*, 290(21):13279–13292, 2015.

[14] W. Daddacha, A. E. Koyen, A. J. Bastien, P. E. Head, V. R. Dhere, G. N. Nabeta, E. C. Connolly, E. Werner, M. Z. Madden, M. B. Daly, E. V. Minten, D. R. Whelan, A. J. Schlafstein, H. Zhang, R. Anand, C. Doronio, A. E. Withers, C. Shepard, R. K. Sundaram, X. Deng, W. S. Dynan, Y. Wang, R. S. Bindra, P. Cejka, E. Rothenberg, P. W. Doetsch, B. Kim, and D. S. Yu. SAMHD1 Promotes DNA End Resection to Facilitate DNA Repair by Homologous Recombination. *Cell Rep*, 20(8):1921–1935, 2017.

[15] A. Brandariz-Nuñez, J. C. Valle-Casuso, T. E. White, N. Laguette, M. Benkirane, J. Brojatsch, and F. Diaz-Griffero. Role of SAMHD1 nuclear localization in restriction of HIV-1 and SIVmac. *Retrovirology*, 9:49, 2012.

[16] J. Yan, S. Kaur, M. DeLucia, C. Hao, J. Mehrens, C. Wang, M. Golczak, K. Palczewski, A. M. Gronenborn, J. Ahn, and J. Skowronski. Tetramerization of SAMHD1 is required for biological activity and inhibition of HIV infection. *J. Biol. Chem.*, 288(15):10406–10417, 2013.

[17] E. C. Hansen, K. J. Seamon, S. L. Cravens, and J. T. Stivers. GTP activator and dNTP substrates of HIV-1 restriction factor SAMHD1 generate a long-lived activated state. *Proc. Natl. Acad. Sci. U.S.A.*, 111(18):E1843–1851, 2014.

[18] S. Schmidt, K. Schenkova, T. Adam, E. Erikson, J. Lehmann-Koch, S. Sertel, B. Verhasselt, O. T. Fackler, F. Lasitschka, and O. T. Keppler. SAMHD1's protein expression profile in humans. *J. Leukoc. Biol.*, 98(1):5–14, 2015.

[19] G. I. Rice, J. Bond, A. Asipu, R. L. Brunette, I. W. Manfield, I. M. Carr, J. C. Fuller, R. M. Jackson, T. Lamb, T. A. Briggs, M. Ali, H. Gornall, L. R. Couthard, A. Aeby, S. P. Attard-Montalto, E. Bertini, C. Bodemer, K. Brockmann, L. A.

Brueton, P. C. Corry, I. Desguerre, E. Fazzi, A. G. Cazorla, B. Gener, B. C. Hamel, A. Heiberg, M. Hunter, M. S. van der Knaap, R. Kumar, L. Lagae, P. G. Landrieu, C. M. Lourenco, D. Marom, M. F. McDermott, W. van der Merwe, S. Orcesi, J. S. Prendiville, M. Rasmussen, S. A. Shalev, D. M. Soler, M. Shinawi, R. Spiegel, T. Y. Tan, A. Vanderver, E. L. Wakeling, E. Wassmer, E. Whittaker, P. Lebon, D. B. Stetson, D. T. Bonthron, and Y. J. Crow. Mutations involved in Aicardi-Goutieres syndrome implicate SAMHD1 as regulator of the innate immune response. *Nat. Genet.*, 41(7):829–832, 2009.

[20] H. M. Baldauf, X. Pan, E. Erikson, S. Schmidt, W. Daddacha, M. Burggraf, K. Schenkova, I. Ambiel, G. Wabnitz, T. Gramberg, S. Panitz, E. Flory, N. R. Landau, S. Sertel, F. Rutsch, F. Lasitschka, B. Kim, R. Koenig, O. T. Fackler, and O. T. Keppler. SAMHD1 restricts HIV-1 infection in resting CD4(+) T cells. *Nat. Med.*, 18(11):1682–1687, 2012.

[21] J. Ryoo, J. Choi, C. Oh, S. Kim, M. Seo, S. Y. Kim, D. Seo, J. Kim, T. E. White, A. Brandariz-Nuñez, F. Diaz-Griffero, C. H. Yun, J. A. Hollenbaugh, B. Kim, D. Baek, and K. Ahn. The ribonuclease activity of SAMHD1 is required for HIV-1 restriction. *Nat. Med.*, 20(8):936–941, 2014.

[22] A. Sze, D. Olagnier, R. Lin, J. van Grevenynghe, and J. Hiscott. SAMHD1 host restriction factor: a link with innate immune sensing of retrovirus infection. *J Mol Biol*, 425(24):4981–4994, 2013.

[23] S. Bonifati, M. B. Daly, C. St Gelais, S. H. Kim, J. A. Hollenbaugh, C. Shepard, E. M. Kennedy, D. H. Kim, R. F. Schinazi, B. Kim, and L. Wu. SAMHD1 controls cell cycle status, apoptosis and HIV-1 infection in monocytic THP-1 cells. *Virology*, 495:92–100, 2016.

[24] S. Batalis, L. C. Rogers, W. O. Hemphill, C. H. Mauney, D. A. Ornelles, and T. Hollis. SAMHD1 Phosphorylation at T592 Regulates Cellular Localization and S-phase Progression. *Front Mol Biosci*, 8:724870, 2021.

[25] Z. Wang, A. Bhattacharya, T. White, C. Buffone, A. McCabe, L. A. Nguyen, C. N. Shepard, S. Pardo, B. Kim, S. T. Weintraub, B. Demeler, F. Diaz-Griffero, and D. N. Ivanov. Functionality of Redox-Active Cysteines Is Required for Restriction of Retroviral Replication by SAMHD1. *Cell Rep*, 24(4):815–823, 2018.

[26] R. Kohnken, K. M. Kodigepalli, A. Mishra, P. Porcu, and L. Wu. MicroRNA-181 contributes to downregulation of SAMHD1 expression in CD4+ T-cells derived from Sèzary syndrome patients. *Leuk Res*, 52:58–66, 2017.

[27] S. Pilakka-Kanthikeel, A. Raymond, V. S. Atluri, V. Sagar, S. K. Saxena, P. Diaz, S. Chevelon, M. Concepcion, and M. Nair. Sterile alpha motif and histidine/aspartic acid domain-containing protein 1 (SAMHD1)-facilitated HIV restriction in astrocytes is regulated by miRNA-181a. *J Neuroinflammation*, 12:66, 2015.

[28] M. Riess, N. V. Fuchs, A. Idica, M. Hamdorf, E. Flory, I. M. Pedersen, and R. Koenig. Interferons Induce Expression of SAMHD1 in Monocytes through Down-regulation of miR-181a and miR-30a. *J Biol Chem*, 292(1):264–277, 2017.

[29] M. Li, D. Zhang, M. Zhu, Y. Shen, W. Wei, S. Ying, H. Korner, and J. Li. Roles of SAMHD1 in antiviral defense, autoimmunity and cancer. *Rev. Med. Virol.*, 27(4), 2017.

[30] M. Statzu, L. Santinelli, A. Viscido, C. Pinacchio, G. Ceccarelli, C. Rotondo, G. Corano Scheri, I. Mezzaroma, O. Turriziani, G. Antonelli, G. d'Ettorre, and C. Scagnolari. Increased SAMHD1 transcript expression correlates with interferon-related genes in HIV-1-infected patients. *Med Microbiol Immunol*, 208(5):679–691, 2019.

[31] A. Martinez-Lopez, M. Martin-Fernandez, S. Buta, B. Kim, D. Bogunovic, and F. Diaz-Griffero. SAMHD1 deficient human monocytes autonomously trigger type I interferon. *Mol Immunol*, 101:450–460, 2018.

[32] C. Oh, J. Ryoo, K. Park, B. Kim, M. B. Daly, D. Cho, and K. Ahn. A central role for PI3K-AKT signaling pathway in linking SAMHD1-deficiency to the type I interferon signature. *Sci Rep*, 8(1):84, 2018.

[33] A. Portela and M. Esteller. Epigenetic modifications and human disease. *Nat Biotechnol*, 28(10):1057–1068, 2010.

[34] S. de Silva, H. Hoy, T. S. Hake, H. K. Wong, P. Porcu, and L. Wu. Promoter methylation regulates SAMHD1 gene expression in human CD4+ T cells. *J. Biol. Chem.*, 288(13):9284–9292, 2013.

[35] S. de Silva, F. Wang, T. S. Hake, P. Porcu, H. K. Wong, and L. Wu. Downregulation of SAMHD1 expression correlates with promoter DNA methylation in Sezary syndrome patients. *J Invest Dermatol*, 134(2):562–565, 2014.

[36] J. L. Wang, F. Z. Lu, X. Y. Shen, Y. Wu, and L. T. Zhao. SAMHD1 is down regulated in lung cancer by methylation and inhibits tumor cell proliferation. *Biochem Biophys Res Commun*, 455(3-4):229–233, 2014.

[37] A. Cribier, B. Descours, A. L. Valadão, N. Laguette, and M. Benkirane. Phosphorylation of SAMHD1 by cyclin A2/CDK1 regulates its restriction activity toward HIV-1. *Cell Rep*, 3(4):1036–1043, 2013.

[38] T. E. White, A. Brandariz-Nuñez, J. C. Valle-Casuso, S. Amie, L. A. Nguyen, B. Kim, M. Tuzova, and F. Diaz-Griffero. The retroviral restriction ability of SAMHD1, but not its deoxynucleotide triphosphohydrolase activity, is regulated by phosphorylation. *Cell Host Microbe*, 13(4):441–451, 2013.

[39] C. Tang, X. Ji, L. Wu, and Y. Xiong. Impaired dNTPase activity of SAMHD1 by phosphomimetic mutation of Thr-592. *J. Biol. Chem.*, 290(44):26352–26359, 2015.

[40] K. Schott, N. V. Fuchs, R. Derua, B. Mahboubi, E. Schnellbaecher, J. Seifried, C. Tondera, H. Schmitz, C. Shepard, A. Brandariz-Nuñez, F. Diaz-Griffero, A. Reuter, B. Kim, V. Janssens, and R. Koenig. Dephosphorylation of the HIV-1 restriction factor SAMHD1 is mediated by PP2A-B55α holoenzymes during mitotic exit. *Nat Commun*, 9(1):2227, 2018.

[41] R. Geiss-Friedlander and F. Melchior. Concepts in sumoylation: a decade on. *Nat Rev Mol Cell Biol*, 8(12):947–956, 2007.

[42] C. Martinat, A. Cormier, J. Tobaly-Tapiero, N. Palmic, N. Casartelli, B. Mahboubi, S. A. Coggins, J. Buchrieser, M. Persaud, F. Diaz-Griffero, L. Espert, G. Bossis, P. Lesage, O. Schwartz, B. Kim, F. Margottin-Goguet, A. Saïb, and A. Zamborlini. SUMOylation of SAMHD1 at Lysine 595 is required for HIV-1 restriction in non-cycling cells. *Nat Commun*, 12(1):4582, 2021.

[43] F. Saiada, K. Zhang, and R. Li. PIAS1 potentiates the anti-EBV activity of SAMHD1 through SUMOylation. *Cell Biosci*, 11(1):127, 2021.

[44] E. J. Lee, J. H. Seo, J. H. Park, T. T. L. Vo, S. An, S. J. Bae, H. Le, H. S. Lee, H. J. Wee, D. Lee, Y. H. Chung, J. A. Kim, M. K. Jang, S. H. Ryu, E. Yu, S. H. Jang, Z. Y. Park, and K. W. Kim. SAMHD1 acetylation enhances its deoxynucleotide triphosphohydrolase activity and promotes cancer cell proliferation. *Oncotarget*, 8 (40):68517–68529, 2017.

[45] E. O. Freed. HIV-1 assembly, release and maturation. *Nat. Rev. Microbiol.*, 13(8): 484–496, 2015.

[46] N. Laguette, B. Sobhian, N. Casartelli, M. Ringeard, C. Chable-Bessia, E. Segeral, A. Yatim, S. Emiliani, O. Schwartz, and M. Benkirane. SAMHD1 is the dendritic- and myeloid-cell-specific HIV-1 restriction factor counteracted by Vpx. *Nature*, 474 (7353):654–657, 2011.

[47] H. Lahouassa, W. Daddacha, H. Hofmann, D. Ayinde, E. C. Logue, L. Dragin, N. Bloch, C. Maudet, M. Bertrand, T. Gramberg, G. Pancino, S. Priet, B. Canard, N. Laguette, M. Benkirane, C. Transy, N. R. Landau, B. Kim, and F. Margottin-Goguet. SAMHD1 restricts the replication of human immunodeficiency virus type 1 by depleting the intracellular pool of deoxynucleoside triphosphates. *Nat. Immunol.*, 13(3):223–228, 2012.

[48] B. Descours, A. Cribier, C. Chable-Bessia, D. Ayinde, G. Rice, Y. Crow, A. Yatim, O. Schwartz, N. Laguette, and M. Benkirane. SAMHD1 restricts HIV-1 reverse transcription in quiescent CD4(+) T-cells. *Retrovirology*, 9:87, 2012.

[49] C. H. Yu, A. Bhattacharya, M. Persaud, A. B. Taylor, Z. Wang, A. Bulnes-Ramos, J. Xu, A. Selyutina, A. Martinez-Lopez, K. Cano, B. Demeler, B. Kim, S. C. Hardies, F. Diaz-Griffero, and D. N. Ivanov. Nucleic acid binding by SAMHD1 contributes to the antiretroviral activity and is enhanced by the GpsN modification. *Nat Commun*, 12(1):731, 2021.

[50] K. Hrecka, C. Hao, M. Gierszewska, S. K. Swanson, M. Kesik-Brodacka, S. Srivastava, L. Florens, M. P. Washburn, and J. Skowronski. Vpx relieves inhibition of HIV-1 infection of macrophages mediated by the SAMHD1 protein. *Nature*, 474 (7353):658–661, 2011.

[51] S. K. Van Cor-Hosmer, D. H. Kim, M. B. Daly, W. Daddacha, and B. Kim. Restricted 5'-end gap repair of HIV-1 integration due to limited cellular dNTP concentrations in human primary macrophages. *J. Biol. Chem.*, 288(46):33253–33262, 2013.

[52] B. Mahboubi, C. Gavegnano, D. H. Kim, R. F. Schinazi, and B. Kim. Host SAMHD1 protein restricts endogenous reverse transcription of HIV-1 in nondividing macrophages. *Retrovirology*, 15(1):69, 2018.

[53] T. Gramberg, T. Kahle, N. Bloch, S. Wittmann, E. Muellers, W. Daddacha, H. Hofmann, B. Kim, D. Lindemann, and N. R. Landau. Restriction of diverse retroviruses by SAMHD1. *Retrovirology*, 10:26, 2013.

[54] J. A. Hollenbaugh, P. Gee, J. Baker, M. B. Daly, S. M. Amie, J. Tate, N. Kasai, Y. Kanemura, D. H. Kim, B. M. Ward, Y. Koyanagi, and B. Kim. Host factor SAMHD1 restricts DNA viruses in non-dividing myeloid cells. *PLoS Pathog.*, 9(6): e1003481, 2013.

[55] E. T. Kim, T. E. White, A. Brandariz-Nñez, F. Diaz-Griffero, and M. D. Weitzman. SAMHD1 restricts herpes simplex virus 1 in macrophages by limiting DNA replication. *J. Virol.*, 87(23):12949–12956, 2013.

[56] E. T. Kim, K. L. Roche, K. Kulej, L. A. Spruce, S. H. Seeholzer, D. M. Coen, F. Diaz-Griffero, E. A. Murphy, and M. D. Weitzman. SAMHD1 Modulates Early Steps during Human Cytomegalovirus Infection by Limiting NF-kappaB Activation. *Cell Rep*, 28(2):434–448, 2019.

[57] K. Zhang, D. W. Lv, and R. Li. Conserved Herpesvirus Protein Kinases Target SAMHD1 to Facilitate Virus Replication. *Cell Rep*, 28(2):449–459, 2019.

[58] C. D. James, A. T. Prabhakar, R. Otoa, M. R. Evans, X. Wang, M. L. Bristol, K. Zhang, R. Li, and I. M. Morgan. SAMHD1 Regulates Human Papillomavirus 16-Induced Cell Proliferation and Viral Replication during Differentiation of Keratinocytes. *mSphere*, 4(4), 2019.

[59] Z. Chen, M. Zhu, X. Pan, Y. Zhu, H. Yan, T. Jiang, Y. Shen, X. Dong, N. Zheng, J. Lu, S. Ying, and Y. Shen. Inhibition of Hepatitis B virus replication by SAMHD1. *Biochem. Biophys. Res. Commun.*, 450(4):1462–1468, 2014.

[60] G. U. Jeong, I. H. Park, K. Ahn, and B. Y. Ahn. Inhibition of hepatitis B virus replication by a dNTPase-dependent function of the host restriction factor SAMHD1. *Virology*, 495:71–78, 2016.

[61] S. Wichit, R. Hamel, A. Zanzoni, F. Diop, A. Cribier, L. Talignani, A. Diack, P. Ferraris, F. Liegeois, S. Urbach, P. Ekchariyawat, A. Merits, H. Yssel, M. Benkirane, and D. Misse. SAMHD1 Enhances Chikungunya and Zika Virus Replication in Human Skin Fibroblasts. *Int J Mol Sci*, 20(7), 2019.

[62] H. Hofmann, E. C. Logue, N. Bloch, W. Daddacha, S. B. Polsky, M. L. Schultz, B. Kim, and N. R. Landau. The Vpx lentiviral accessory protein targets SAMHD1 for degradation in the nucleus. *J Virol*, 86(23):12552–12560, 2012.

[63] J. Ahn, C. Hao, J. Yan, M. DeLucia, J. Mehrens, C. Wang, A. M. Gronenborn, and J. Skowronski. HIV/simian immunodeficiency virus (SIV) accessory virulence factor Vpx loads the host cell restriction factor SAMHD1 onto the E3 ubiquitin ligase complex CRL4DCAF1. *J. Biol. Chem.*, 287(15):12550–12558, 2012.

[64] T. Schaller, H. Bauby, S. Hué, M. H. Malim, and C. Goujon. New insights into an X-traordinary viral protein. *Front Microbiol*, 5:126, 2014.

[65] Y. Wu, L. M. Koharudin, J. Mehrens, M. DeLucia, C. H. Byeon, I. J. Byeon, G. Calero, J. Ahn, and A. M. Gronenborn. Structural Basis of Clade-specific Engagement of SAMHD1 (Sterile alpha Motif and Histidine/Aspartate-containing Protein 1) Restriction Factors by Lentiviral Viral Protein X (Vpx) Virulence Factors. *J. Biol. Chem.*, 290(29):17935–17945, 2015.

[66] M. Fujita, M. Nomaguchi, A. Adachi, and M. Otsuka. SAMHD1-Dependent and -Independent Functions of HIV-2/SIV Vpx Protein. *Front Microbiol*, 3:297, 2012.

[67] S. P. Singh, S. Raja, and S. Mahalingam. Viral protein X unlocks the nuclear pore complex through a human Nup153-dependent pathway to promote nuclear translocation of the lentiviral genome. *Mol Biol Cell*, 31(4):304–317, 2020.

[68] H. Fabryova and K. Strebel. Vpr and Its Cellular Interaction Partners: R We There Yet? *Cells*, 8(11), 2019.

[69] K. Zhao, J. Du, X. Han, J. L. Goodier, P. Li, X. Zhou, W. Wei, S. L. Evans, L. Li, W. Zhang, L. E. Cheung, G. Wang, H. H. Kazazian, and X. F. Yu. Modulation of LINE-1 and Alu/SVA retrotransposition by Aicardi-Goutieres syndrome-related SAMHD1. *Cell Rep*, 4(6):1108–1115, 2013.

[70] A. Herrmann, S. Wittmann, D. Thomas, C. N. Shepard, B. Kim, N. Ferreiros, and T. Gramberg. The SAMHD1-mediated block of LINE-1 retroelements is regulated by phosphorylation. *Mob DNA*, 9:11, 2018.

[71] K. Park, J. Ryoo, H. Jeong, M. Kim, S. Lee, S. Y. Hwang, J. Ahn, D. Kim, H. C. Moon, D. Baek, K. Kim, H. Y. Park, and K. Ahn. Aicardi-Goutières syndrome-associated gene SAMHD1 preserves genome integrity by preventing R-loop formation at transcription-replication conflict regions. *PLoS Genet*, 17(4):e1009523, 2021.

[72] F. Coquel, M. J. Silva, H. Techer, K. Zadorozhny, S. Sharma, J. Nieminuszczy, C. Mettling, E. Dardillac, A. Barthe, A. L. Schmitz, A. Promonet, A. Cribier, A. Sarrazin, W. Niedzwiedz, B. Lopez, V. Costanzo, L. Krejci, A. Chabes, M. Benkirane, Y. L. Lin, and P. Pasero. SAMHD1 acts at stalled replication forks to prevent interferon induction. *Nature*, 557(7703):57–61, 2018.

[73] A. Sze, S. M. Belgnaoui, D. Olagnier, R. Lin, J. Hiscott, and J. van Grevenynghe. Host restriction factor SAMHD1 limits human T cell leukemia virus type 1 infection of monocytes via STING-mediated apoptosis. *Cell Host Microbe*, 14(4):422–434, 2013.

[74] J. Maelfait, A. Bridgeman, A. Benlahrech, C. Cursi, and J. Rehwinkel. Restriction by SAMHD1 Limits cGAS/STING-Dependent Innate and Adaptive Immune Responses to HIV-1. *Cell Rep*, 16(6):1492–1501, 2016.

[75] Y. Wu, Y. Niu, Y. Wu, X. Chen, X. Shen, and W. Gao. SAMHD1 can suppress lung adenocarcinoma progression through the negative regulation of STING. *J Thorac Dis*, 13(1):189–201, 2021.

[76] S. Chen, S. Bonifati, Z. Qin, C. St Gelais, K. M. Kodigepalli, B. S. Barrett, S. H. Kim, J. M. Antonucci, K. J. Ladner, O. Buzovetsky, K. M. Knecht, Y. Xiong, J. S. Yount, D. C. Guttridge, M. L. Santiago, and L. Wu. SAMHD1 suppresses innate immune responses to viral infections and inflammatory stimuli by inhibiting the NF-kappaB and interferon pathways. *Proc Natl Acad Sci U S A*, 115(16):E3798–E3807, 2018.

[77] A. Goncalves, E. Karayel, G. I. Rice, K. L. Bennett, Y. J. Crow, G. Superti-Furga, and T. Buerckstuemmer. SAMHD1 is a nucleic-acid binding protein that is mislocalized due to aicardi-goutières syndrome-associated mutations. *Hum Mutat*, 33(7): 1116–1122, 2012.

[78] K. J. Seamon, Z. Sun, L. S. Shlyakhtenko, Y. L. Lyubchenko, and J. T. Stivers. SAMHD1 is a single-stranded nucleic acid binding protein with no active site-associated nuclease activity. *Nucleic Acids Res*, 43(13):6486–6499, 2015.

[79] C. H. Yu, A. Bhattacharya, M. Persaud, A. B. Taylor, Z. Wang, A. Bulnes-Ramos, J. Xu, A. Selyutina, A. Martinez-Lopez, K. Cano, B. Demeler, B. Kim, S. C. Hardies,

F. Diaz-Griffero, and D. N. Ivanov. Nucleic acid binding by SAMHD1 contributes to the antiretroviral activity and is enhanced by the GpsN modification. *Nat Commun*, 12(1):731, 2021.

[80] J. Choi, J. Ryoo, C. Oh, S. Hwang, and K. Ahn. SAMHD1 specifically restricts retroviruses through its RNase activity. *Retrovirology*, 12:46, 2015.

[81] J. M. Antonucci, C. St Gelais, S. de Silva, J. S. Yount, C. Tang, X. Ji, C. Shepard, Y. Xiong, B. Kim, and L. Wu. SAMHD1-mediated HIV-1 restriction in cells does not involve ribonuclease activity. *Nat Med*, 22(10):1072–1074, 2016.

[82] Y. J. Crow, D. S. Chase, J. Lowenstein Schmidt, M. Szynkiewicz, G. M. Forte, H. L. Gornall, A. Oojageer, B. Anderson, A. Pizzino, G. Helman, M. S. Abdel-Hamid, G. M. Abdel-Salam, S. Ackroyd, A. Aeby, G. Agosta, C. Albin, S. Allon-Shalev, M. Arellano, G. Ariaudo, V. Aswani, R. Babul-Hirji, E. M. Baildam, N. Bahi-Buisson, K. M. Bailey, C. Barnerias, M. Barth, R. Battini, M. W. Beresford, G. Bernard, M. Bianchi, T. Billette de Villemeur, E. M. Blair, M. Bloom, A. B. Burlina, M. L. Carpanelli, D. R. Carvalho, M. Castro-Gago, A. Cavallini, C. Cereda, K. E. Chandler, D. A. Chitayat, A. E. Collins, C. Sierra Corcoles, N. J. Cordeiro, G. Crichiutti, L. Dabydeen, R. C. Dale, S. D'Arrigo, C. G. De Goede, C. De Laet, L. M. De Waele, I. Denzler, I. Desguerre, K. Devriendt, M. Di Rocco, M. C. Fahey, E. Fazzi, C. D. Ferrie, A. Figueiredo, B. Gener, C. Goizet, N. R. Gowrinathan, K. Gowrishankar, D. Hanrahan, B. Isidor, B. Kara, N. Khan, M. D. King, E. P. Kirk, R. Kumar, L. Lagae, P. Landrieu, H. Lauffer, V. Laugel, R. La Piana, M. J. Lim, J. P. Lin, T. Linnankivi, M. T. Mackay, D. R. Marom, C. Marques Lourenco, S. A. McKee, I. Moroni, J. E. Morton, M. L. Moutard, K. Murray, R. Nabbout, S. Nampoothiri, N. Nunez-Enamorado, P. J. Oades, I. Olivieri, J. R. Ostergaard, B. Perez-Dueñas, J. S. Prendiville, V. Ramesh, M. Rasmussen, L. Regal, F. Ricci, M. Rio, D. Rodriguez, A. Roubertie, E. Salvatici, K. A. Segers, G. P. Sinha, D. Soler, R. Spiegel, T. I. Stoedberg, R. Straussberg, K. J. Swoboda, M. Suri, U. Tacke, T. Y. Tan, J. te Water Naude, K. Wee Teik, M. M. Thomas, M. Till, D. Tonduti, E. M. Valente, R. N. Van Coster, M. S. van der Knaap, G. Vassallo, R. Vijzelaar, J. Vogt, G. B. Wallace, E. Wassmer, H. J. Webb, W. P. Whitehouse, R. N. Whitney, M. S. Zaki, S. M. Zuberi, J. H. Livingston, F. Rozenberg, P. Lebon, A. Vanderver, S. Orcesi, and G. I. Rice. Characterization of human disease phenotypes associated with mutations in TREX1, RNASEH2A, RNASEH2B, RNASEH2C, SAMHD1, ADAR, and IFIH1. *Am. J. Med. Genet. A*, 167A(2):296–312, 2015.

[83] T. E. White, A. Brandariz-Nuñez, A. Martinez-Lopez, C. Knowlton, G. Lenzi, B. Kim, D. Ivanov, and F. Diaz-Griffero. A SAMHD1 mutation associated with Aicardi-Goutieres syndrome uncouples the ability of SAMHD1 to restrict HIV-1 from its ability to downmodulate type I interferon in humans. *Hum. Mutat.*, 38 (6):658–668, 2017.

[84] J. H. Livingston and Y. J. Crow. Neurologic Phenotypes Associated with Mutations in TREX1, RNASEH2A, RNASEH2B, RNASEH2C, SAMHD1, ADAR1, and IFIH1: Aicardi-Goutières Syndrome and Beyond. *Neuropediatrics*, 47(6):355–360, 2016.

[85] G. I. Rice, J. Bond, A. Asipu, R. L. Brunette, I. W. Manfield, I. M. Carr, J. C. Fuller, R. M. Jackson, T. Lamb, T. A. Briggs, M. Ali, H. Gornall, L. R. Couthard, A. Aeby, S. P. Attard-Montalto, E. Bertini, C. Bodemer, K. Brockmann, L. A. Brueton, P. C. Corry, I. Desguerre, E. Fazzi, A. G. Cazorla, B. Gener, B. C. Hamel, A. Heiberg, M. Hunter, M. S. van der Knaap, R. Kumar, L. Lagae, P. G. Landrieu, C. M. Lourenco, D. Marom, M. F. McDermott, W. van der Merwe, S. Orcesi, J. S. Prendiville, M. Rasmussen, S. A. Shalev, D. M. Soler, M. Shinawi, R. Spiegel, T. Y. Tan, A. Vanderver, E. L. Wakeling, E. Wassmer, E. Whittaker, P. Lebon, D. B. Stetson, D. T. Bonthron, and Y. J. Crow. Mutations involved in Aicardi-Goutieres syndrome implicate SAMHD1 as regulator of the innate immune response. *Nat. Genet.*, 41(7):829–832, 2009.

[86] R. Behrendt, T. Schumann, A. Gerbaulet, L. A. Nguyen, N. Schubert, D. Alexopoulou, U. Berka, S. Lienenklaus, K. Peschke, K. Gibbert, S. Wittmann, D. Lindemann, S. Weiss, A. Dahl, R. Naumann, U. Dittmer, B. Kim, W. Mueller, T. Gramberg, and A. Roers. Mouse SAMHD1 has antiretroviral activity and suppresses a spontaneous cell-intrinsic antiviral response. *Cell Rep*, 4(4):689–696, 2013.

[87] J. Rehwinkel, J. Maelfait, A. Bridgeman, R. Rigby, B. Hayward, R. A. Liberatore, P. D. Bieniasz, G. J. Towers, L. F. Moita, Y. J. Crow, D. T. Bonthron, and C. Reis e Sousa. SAMHD1-dependent retroviral control and escape in mice. *EMBO J*, 32(18): 2454–2462, 2013.

[88] K. Schott, C. Majer, A. Bulashevska, L. Childs, M. H. H. Schmidt, K. Rajalingam, M. Munder, and R. König. SAMHD1 in cancer: curse or cure? *J Mol Med (Berl)*, 2021.

[89] J. L. Wang, F. Z. Lu, X. Y. Shen, Y. Wu, and L. T. Zhao. SAMHD1 is down regulated in lung cancer by methylation and inhibits tumor cell proliferation. *Biochem Biophys Res Commun*, 455(3-4):229–233, 2014.

[90] M. Rentoft, K. Lindell, P. Tran, A. L. Chabes, R. J. Buckland, D. L. Watt, L. Marjavaara, A. K. Nilsson, B. Melin, J. Trygg, E. Johansson, and A. Chabes. Heterozygous colon cancer-associated mutations of SAMHD1 have functional significance. *Proc. Natl. Acad. Sci. U.S.A.*, 113(17):4723–4728, 2016.

[91] R. Clifford, T. Louis, P. Robbe, S. Ackroyd, A. Burns, A. T. Timbs, G. Wright Colopy, H. Dreau, F. Sigaux, J. G. Judde, M. Rotger, A. Telenti, Y. L. Lin, P. Pasero, J. Maelfait, M. Titsias, D. R. Cohen, S. J. Henderson, M. T. Ross, D. Bentley, P. Hillmen, A. Pettitt, J. Rehwinkel, S. J. Knight, J. C. Taylor, Y. J. Crow, M. Benkirane, and A. Schuh. SAMHD1 is mutated recurrently in chronic

lymphocytic leukemia and is involved in response to DNA damage. *Blood*, 123(7): 1021–1031, 2014.

[92] P. Johansson, L. Klein-Hitpass, A. Choidas, P. Habenberger, B. Mahboubi, B. Kim, A. Bergmann, R. Scholtysik, M. Brauser, A. Lollies, R. Siebert, T. Zenz, U. Duehrsen, R. Kueppers, and J. Duerig. SAMHD1 is recurrently mutated in T-cell prolymphocytic leukemia. *Blood Cancer J*, 8(1):11, 2018.

[93] J. Liu, W. Lee, Z. Jiang, Z. Chen, S. Jhunjhunwala, P. M. Haverty, F. Gnad, Y. Guan, H. N. Gilbert, J. Stinson, C. Klijn, J. Guillory, D. Bhatt, S. Vartanian, K. Walter, J. Chan, T. Holcomb, P. Dijkgraaf, S. Johnson, J. Koeman, J. D. Minna, A. F. Gazdar, H. M. Stern, K. P. Hoeflich, T. D. Wu, J. Settleman, F. J. de Sauvage, R. C. Gentleman, R. M. Neve, D. Stokoe, Z. Modrusan, S. Seshagiri, D. S. Shames, and Z. Zhang. Genome and transcriptome sequencing of lung cancers reveal diverse mutational and splicing events. *Genome Res*, 22(12):2315–2327, 2012.

[94] V. Frattini, V. Trifonov, J. M. Chan, A. Castano, M. Lia, F. Abate, S. T. Keir, A. X. Ji, P. Zoppoli, F. Niola, C. Danussi, I. Dolgalev, P. Porrati, S. Pellegatta, A. Heguy, G. Gupta, D. J. Pisapia, P. Canoll, J. N. Bruce, R. E. McLendon, H. Yan, K. Aldape, G. Finocchiaro, T. Mikkelsen, G. G. Prive, D. D. Bigner, A. Lasorella, R. Rabadan, and A. Iavarone. The integrated landscape of driver genomic alterations in glioblastoma. *Nat Genet*, 45(10):1141–1149, 2013.

[95] S. Jones, X. Zhang, D. W. Parsons, J. C. Lin, R. J. Leary, P. Angenendt, P. Mankoo, H. Carter, H. Kamiyama, A. Jimeno, S. M. Hong, B. Fu, M. T. Lin, E. S. Calhoun, M. Kamiyama, K. Walter, T. Nikolskaya, Y. Nikolsky, J. Hartigan, D. R. Smith, M. Hidalgo, S. D. Leach, A. P. Klein, E. M. Jaffee, M. Goggins, A. Maitra, C. Iacobuzio-Donahue, J. R. Eshleman, S. E. Kern, R. H. Hruban, R. Karchin, N. Papadopoulos, G. Parmigiani, B. Vogelstein, V. E. Velculescu, and K. W. Kinzler. Core signaling pathways in human pancreatic cancers revealed by global genomic analyses. *Science*, 321(5897):1801–1806, 2008.

[96] B. A. Walker, C. P. Wardell, L. Melchor, S. Hulkki, N. E. Potter, D. C. Johnson, K. Fenwick, I. Kozarewa, D. Gonzalez, C. J. Lord, A. Ashworth, F. E. Davies, and G. J. Morgan. Intraclonal heterogeneity and distinct molecular mechanisms characterize the development of t(4;14) and t(11;14) myeloma. *Blood*, 120(5):1077–1086, 2012.

[97] D. W. Parsons, S. Jones, X. Zhang, J. C. Lin, R. J. Leary, P. Angenendt, P. Mankoo, H. Carter, I. M. Siu, G. L. Gallia, A. Olivi, R. McLendon, B. A. Rasheed, S. Keir, T. Nikolskaya, Y. Nikolsky, D. A. Busam, H. Tekleab, L. A. Diaz, J. Hartigan, D. R. Smith, R. L. Strausberg, S. K. Marie, S. M. Shinjo, H. Yan, G. J. Riggins, D. D. Bigner, R. Karchin, N. Papadopoulos, G. Parmigiani, B. Vogelstein, V. E. Velculescu, and K. W. Kinzler. An integrated genomic analysis of human glioblastoma multiforme. *Science*, 321(5897):1807–1812, 2008.

[98] M. Camici, M. Garcia-Gil, R. Pesi, S. Allegrini, and M. G. Tozzi. Purine-Metabolising Enzymes and Apoptosis in Cancer. *Cancers (Basel)*, 11(9), 2019.

[99] D. Hanahan and R. A. Weinberg. Hallmarks of cancer: the next generation. *Cell*, 144(5):646–674, 2011.

[100] C. M. Galmarini, J. R. Mackey, and C. Dumontet. Nucleoside analogues and nucleobases in cancer treatment. *Lancet Oncol*, 3(7):415–424, 2002.

[101] C. Schneider, T. Oellerich, H. M. Baldauf, S. M. Schwarz, D. Thomas, R. Flick, H. Bohnenberger, L. Kaderali, L. Stegmann, A. Cremer, M. Martin, J. Lohmeyer, M. Michaelis, V. Hornung, C. Schliemann, W. E. Berdel, W. Hartmann, E. Wardelmann, F. Comoglio, M. L. Hansmann, A. F. Yakunin, G. Geisslinger, P. Stroebel, N. Ferreiros, H. Serve, O. T. Keppler, and J. Cinatl. SAMHD1 is a biomarker for cytarabine response and a therapeutic target in acute myeloid leukemia. *Nat. Med.*, 23(2):250–255, 2017.

[102] K. V. Ho, D. A. Solimando, and J. A. Waddell. Clofarabine and Cytarabine Regimen for Acute Myeloid Leukemia. *Hosp Pharm*, 50(11):969–974, 2015.

[103] J. A. Hollenbaugh, J. Shelton, S. Tao, S. Amiralaei, P. Liu, X. Lu, R. W. Goetze, L. Zhou, J. H. Nettles, R. F. Schinazi, and B. Kim. Substrates and Inhibitors of SAMHD1. *PLoS One*, 12(1):e0169052, 2017.

[104] N. Herold, S. G. Rudd, K. Sanjiv, J. Kutzner, J. Bladh, C. B. J. Paulin, T. Helleday, J. I. Henter, and T. Schaller. SAMHD1 protects cancer cells from various nucleoside-based antimetabolites. *Cell Cycle*, 16(11):1029–1038, 2017.

[105] P. Malik and A. F. Cashen. Decitabine in the treatment of acute myeloid leukemia in elderly patients. *Cancer Manag Res*, 6:53–61, 2014.

[106] T. Oellerich, C. Schneider, D. Thomas, K. M. Knecht, O. Buzovetsky, L. Kaderali, C. Schliemann, H. Bohnenberger, L. Angenendt, W. Hartmann, E. Wardelmann, T. Rothenburger, S. Mohr, S. Scheich, F. Comoglio, A. Wilke, P. Stroebel, H. Serve, M. Michaelis, N. Ferreiros, G. Geisslinger, Y. Xiong, O. T. Keppler, and J. Cinatl. Selective inactivation of hypomethylating agents by SAMHD1 provides a rationale for therapeutic stratification in AML. *Nat Commun*, 10(1):3475, 2019.

[107] T. Rothenburger, K. M. McLaughlin, T. Herold, C. Schneider, T. Oellerich, F. Rothweiler, A. Feber, T. R. Fenton, M. N. Wass, O. T. Keppler, M. Michaelis, and J. Cinatl. SAMHD1 is a key regulator of the lineage-specific response of acute lymphoblastic leukaemias to nelarabine. *Commun Biol*, 3(1):324, 2020.

[108] N. Tsesmetzis, C. B. J. Paulin, S. G. Rudd, and N. Herold. Nucleobase and Nucleoside Analogues: Resistance and Re-Sensitisation at the Level of Pharmacokinetics, Pharmacodynamics and Metabolism. *Cancers (Basel)*, 10(7), 2018.

[109] J. K. Lamba. Genetic factors influencing cytarabine therapy. *Pharmacogenomics*, 10 (10):1657–1674, 2009.

[110] C. M. Galmarini, L. Jordheim, and C. Dumontet. Pyrimidine nucleoside analogs in cancer treatment. *Expert Rev Anticancer Ther*, 3(5):717–728, 2003.

[111] Y. T. Wang, B. Yuan, H. D. Chen, L. Xu, Y. N. Tian, A. Zhang, J. X. He, and Z. H. Miao. Acquired resistance of phosphatase and tensin homolog-deficient cells to poly(ADP-ribose) polymerase inhibitor and Ara-C mediated by 53BP1 loss and SAMHD1 overexpression. *Cancer Sci*, 109(3):821–831, 2018.

[112] S. Lapointe, A. Perry, and N. A. Butowski. Primary brain tumours in adults. *Lancet*, 392(10145):432–446, 2018.

[113] Q. T. Ostrom, H. Gittleman, P. Liao, T. Vecchione-Koval, Y. Wolinsky, C. Kruchko, and J. S. Barnholtz-Sloan. CBTRUS Statistical Report: Primary brain and other central nervous system tumors diagnosed in the United States in 2010-2014. *Neuro Oncol*, 19, 2017.

[114] D. N. Louis, H. Ohgaki, O. D. Wiestler, W. K. Cavenee, P. C. Burger, A. Jouvet, B. W. Scheithauer, and P. Kleihues. The 2007 WHO classification of tumours of the central nervous system. *Acta Neuropathol*, 114(2):97–109, Aug 2007.

[115] B. Oronsky, T. R. Reid, A. Oronsky, N. Sandhu, and S. J. Knox. A Review of Newly Diagnosed Glioblastoma. *Front Oncol*, 10:574012, 2020.

[116] M. Yao, S. Li, X. Wu, S. Diao, G. Zhang, H. He, L. Bian, and Y. Lu. Cellular origin of glioblastoma and its implication in precision therapy. *Cell Mol Immunol*, 15(8): 737–739, 2018.

[117] A. Sottoriva, I. Spiteri, S. G. Piccirillo, A. Touloumis, V. P. Collins, J. C. Marioni, C. Curtis, C. Watts, and S. Tavare. Intratumor heterogeneity in human glioblastoma reflects cancer evolutionary dynamics. *Proc Natl Acad Sci U S A*, 110(10):4009–4014, 2013.

[118] Y. Jiang, V. D. Marinescu, Y. Xie, M. Jarvius, N. P. Maturi, C. Haglund, S. Olofsson, N. Lindberg, T. Olofsson, C. Leijonmarck, G. Hesselager, I. Alafuzoff, M. Fryknaes, R. Larsson, S. Nelander, and L. Uhrbom. Glioblastoma Cell Malignancy and Drug Sensitivity Are Affected by the Cell of Origin. *Cell Rep*, 18(4):977–990, 2017.

[119] X. Zhang, K. Ding, J. Wang, X. Li, and P. Zhao. Chemoresistance caused by the microenvironment of glioblastoma and the corresponding solutions. *Biomed Pharmacother*, 109:39–46, 2019.

[120] M. Weller, E. Le Rhun, M. Preusser, J. C. Tonn, and P. Roth. How we treat glioblastoma. *ESMO Open*, 4(Suppl 2):e000520, 2019.

[121] C. Ling, C. Pouget, F. Rech, R. Pflaum, M. Treffel, F. Bielle, K. Mokhtari, J. M. Casse, J. M. Vignaud, M. Kalamarides, M. Peyre, and G. Gauchotte. J Neuropathol Exp NeurolEndothelial Cell Hypertrophy and Microvascular Proliferation in Meningiomas Are Correlated with Higher Histological Grade and Shorter Progression-Free Survival. *J Neuropathol Exp Neurol*, 75(12):1160–1170, 2016.

[122] T. Zeng, D. Cui, and L. Gao. Glioma: an overview of current classifications, characteristics, molecular biology and target therapies. *Front Biosci (Landmark Ed)*, 20: 1104–1115, 2015.

[123] M. Westphal and K. Lamszus. Circulating biomarkers for gliomas. *Nat Rev Neurol*, 11(10):556–566, 2015.

[124] K. Aoki and A. Natsume. Overview of DNA methylation in adult diffuse gliomas. *Brain Tumor Pathol*, 36(2):84–91, 2019.

[125] T. M. Malta, C. F. de Souza, T. S. Sabedot, T. C. Silva, M. S. Mosella, S. N. Kalkanis, J. Snyder, A. V. B. Castro, and H. Noushmehr. Glioma CpG island methylator phenotype (G-CIMP): biological and clinical implications. *Neuro Oncol*, 20(5):608–620, 2018.

[126] S. K. Singh, C. Hawkins, I. D. Clarke, J. A. Squire, J. Bayani, T. Hide, R. M. Henkelman, M. D. Cusimano, and P. B. Dirks. Identification of human brain tumour initiating cells. *Nature*, 432(7015):396–401, 2004.

[127] J. Wang, P. Ø. Sakariassen, O. Tsinkalovsky, H. Immervoll, S. O. Bøe, A. Svendsen, L. Prestegarden, G. Røsland, F. Thorsen, L. Stuhr, A. Molven, R. Bjerkvig, and P. Ø. Enger. CD133 negative glioma cells form tumors in nude rats and give rise to CD133 positive cells. *Int J Cancer*, 122(4):761–768, 2008.

[128] S. Donche, J. Verhoeven, B. Descamps, J. Bolcaen, K. Deblaere, T. Boterberg, C. Van den Broecke, C. Vanhove, and I. Goethals. The Path Toward PET-Guided Radiation Therapy for Glioblastoma in Laboratory Animals: A Mini Review. *Front Med (Lausanne)*, 6:5, 2019.

[129] C. Y. Lee. Strategies of temozolomide in future glioblastoma treatment. *Onco Targets Ther*, 10:265–270, 2017.

[130] M. Da Ros, V. De Gregorio, A. L. Iorio, L. Giunti, M. Guidi, M. de Martino, L. Genitori, and I. Sardi. Glioblastoma Chemoresistance: The Double Play by Microenvironment and Blood-Brain Barrier. *Int J Mol Sci*, 19(10), 2018.

[131] R. Stupp, S. Taillibert, A. Kanner, W. Read, D. Steinberg, B. Lhermitte, S. Toms, A. Idbaih, M. S. Ahluwalia, K. Fink, F. Di Meco, F. Lieberman, J. J. Zhu, G. Stragliotto, D. Tran, S. Brem, A. Hottinger, E. D. Kirson, G. Lavy-Shahaf, U. Weinberg, C. Y. Kim, S. H. Paek, G. Nicholas, J. Bruna, H. Hirte, M. Weller,

Y. Palti, M. E. Hegi, and Z. Ram. Effect of Tumor-Treating Fields Plus Maintenance Temozolomide vs Maintenance Temozolomide Alone on Survival in Patients With Glioblastoma: A Randomized Clinical Trial. *JAMA*, 318(23):2306–2316, 2017.

[132] X. Cui, Q. Wang, J. Zhou, Y. Wang, C. Xu, F. Tong, H. Wang, and C. Kang. Single-Cell Transcriptomics of Glioblastoma Reveals a Unique Tumor Microenvironment and Potential Immunotherapeutic Target Against Tumor-Associated Macrophage. *Front Oncol*, 11:710695, 2021.

[133] D. Hambardzumyan and G. Bergers. Glioblastoma: Defining Tumor Niches. *Trends Cancer*, 1(4):252–265, 2015.

[134] A. Goenka, D. Tiek, X. Song, T. Huang, B. Hu, and S. Y. Cheng. The Many Facets of Therapy Resistance and Tumor Recurrence in Glioblastoma. *Cells*, 10(3), 2021.

[135] K. D. Sutherland and J. E. Visvader. Cellular Mechanisms Underlying Intertumoral Heterogeneity. *Trends Cancer*, 1(1):15–23, 2015.

[136] V. Rajaratnam, M. M. Islam, M. Yang, R. Slaby, H. M. Ramirez, and S. P. Mirza. Glioblastoma: Pathogenesis and Current Status of Chemotherapy and Other Novel Treatments. *Cancers (Basel)*, 12(4), 2020.

[137] H. L. Kaufman, F. J. Kohlhapp, and A. Zloza. Oncolytic viruses: a new class of immunotherapy drugs. *Nat Rev Drug Discov*, 14(9):642–662, 2015.

[138] E. Le Rhun, M. Preusser, P. Roth, D. A. Reardon, M. van den Bent, P. Wen, G. Reifenberger, and M. Weller. Molecular targeted therapy of glioblastoma. *Cancer Treat Rev*, 80:101896, 2019.

[139] J. V. Gregory, P. Kadiyala, R. Doherty, M. Cadena, S. Habeel, E. Ruoslahti, P. R. Lowenstein, M. G. Castro, and J. Lahann. Systemic brain tumor delivery of synthetic protein nanoparticles for glioblastoma therapy. *Nat Commun*, 11(1):5687, 2020.

[140] R. M. Shallis, R. Wang, A. Davidoff, X. Ma, and A. M. Zeidan. Epidemiology of acute myeloid leukemia: Recent progress and enduring challenges. *Blood Rev*, 36: 70–87, 2019.

[141] T. Briot, E. Roger, S. Thepot, and F. Lagarce. Advances in treatment formulations for acute myeloid leukemia. *Drug Discov Today*, 23(12):1936–1949, 2018.

[142] R. L. Momparler. Optimization of cytarabine (ARA-C) therapy for acute myeloid leukemia. *Exp Hematol Oncol*, 2:20, 2013.

[143] B. Löwenberg, T. Pabst, E. Vellenga, W. van Putten, H. C. Schouten, C. Graux, A. Ferrant, P. Sonneveld, B. J. Biemond, A. Gratwohl, G. E. de Greef, L. F. Verdonck, M. R. Schaafsma, M. Gregor, M. Theobald, U. Schanz, J. Maertens, G. J.

Ossenkoppele, A. Ferrant, A. Delannoy, P. Mineur, J. Maertens, G. Verhoef, H. Demuynck, A. Bosly, C. Graux, D. A. Breems, P. Zachee, E. Jaeger, M. Theobald, J. Beck, T. Fischer, M. Bargetzi, M. Wernli, A. Gratwohl, D. Heim, M. F. Fey, T. Pabst, B. Chapuis, A. Herr, W. A. Wuillemin, M. Gregor, E. Jacky, U. Schans, S. Wittebol, J. Van Der Lelie, B. J. Biemond, B. De Valk, G. J. Ossenkoppele, P. C. Huijgens, P. W. Wijermans, M. R. Schaafsma, M. Legdeur, S. M. Daenen, E. Vellenga, P. J. Voogt, H. C. Schouten, D. H. Biesma, P. Sonneveld, J. Zijlmans, G. E. De Greef, B. Löwenberg, L. F. Verdonck, J. Kuball, and M. Van Marwijk Kooy. N Engl J MedCytarabine dose for acute myeloid leukemia. *N Engl J Med*, 364(11): 1027–1036, 2011.

[144] I. S. Tiong and A. H. Wei. New drugs creating new challenges in acute myeloid leukemia. *Genes Chromosomes Cancer*, 58(12):903–914, 2019.

[145] R. Nair, A. Salinas-Illarena, and H. M. Baldauf. New strategies to treat AML: novel insights into AML survival pathways and combination therapies. *Leukemia*, 35(2): 299–311, 2021.

[146] J. Zhang, Y. Gu, and B. Chen. Mechanisms of drug resistance in acute myeloid leukemia. *Onco Targets Ther*, 12:1937–1945, 2019.

[147] M. Frejno, C. Meng, B. Ruprecht, T. Oellerich, S. Scheich, K. Kleigrewe, E. Drecoll, P. Samaras, A. Hogrebe, D. Helm, J. Mergner, J. Zecha, S. Heinzlmeir, M. Wilhelm, J. Dorn, H. M. Kvasnicka, H. Serve, W. Weichert, and B. Kuster. Proteome activity landscapes of tumor cell lines determine drug responses. *Nat Commun*, 11(1):3639, 2020.

[148] T. T. Chen and J. Mealey. Effects of cytosine arabinoside and 1,3-bis(2-chloroethyl)-1-nitrosourea on human glial tumor cells. *Cancer Res*, 32(3):558–564, 1972.

[149] M. L. Slevin, E. M. Piall, G. W. Aherne, A. Johnston, and T. A. Lister. The pharmacokinetics of cytosine arabinoside in the plasma and cerebrospinal fluid during conventional and high-dose therapy. *Med Pediatr Oncol*, 10 Suppl 1:157–168, 1982.

[150] B. M. Frankel, D. Cachia, S. J. Patel, and A. Das. Targeting Subventricular Zone Progenitor Cells with Intraventricular Liposomal Encapsulated Cytarabine in Patients with Secondary Glioblastoma : A Report of Two Cases. *SN Compr Clin Med*, 2(6):836–843, 2020.

[151] T. Gramberg, N. Sunseri, and N. R. Landau. Evidence for an activation domain at the amino terminus of simian immunodeficiency virus Vpx. *J. Virol.*, 84(3):1387–1396, 2010.

[152] C. Bock, S. Reither, T. Mikeska, M. Paulsen, J. Walter, and T. Lengauer. BiQ Analyzer: visualization and quality control for DNA methylation data from bisulfite sequencing. *Bioinformatics*, 21(21):4067–4068, 2005.

[153] J. L. Schmid-Burgk, T. Schmidt, M. M. Gaidt, K. Pelka, E. Latz, T. S. Ebert, and V. Hornung. OutKnocker: a web tool for rapid and simple genotyping of designer nuclease edited cell lines. *Genome Res.*, 24(10):1719–1723, 2014.

[154] J. M. Posimo, A. S. Unnithan, A. M. Gleixner, H. J. Choi, Y. Jiang, S. H. Pulugulla, and R. K. Leak. Viability assays for cells in culture. *J Vis Exp*, (83):e50645, 2014.

[155] J. Lee, S. Kotliarova, Y. Kotliarov, A. Li, Q. Su, N. M. Donin, S. Pastorino, B. W. Purow, N. Christopher, W. Zhang, J. K. Park, and H. A. Fine. Tumor stem cells derived from glioblastomas cultured in bFGF and EGF more closely mirror the phenotype and genotype of primary tumors than do serum-cultured cell lines. *Cancer Cell*, 9(5):391–403, 2006.

[156] F. Cardamone, M. Falconi, and A. Desideri. Molecular dynamics characterization of the SAMHD1 Aicardi-Goutières Arg145Gln mutant: structural determinants for the impaired tetramerization. *J. Comput. Aided Mol. Des.*, 32(5):623–632, 2018.

[157] T. E. White, A. Brandariz-Nuñez, K. Han, S. L. Sawyer, B. Kim, and F. Diaz-Griffero. Modulation of LINE-1 Retrotransposition by a Human SAMHD1 Polymorphism. *Virol Rep*, 6:53–60, 2016.

[158] J. K. Lee, J. Wang, J. K. Sa, E. Ladewig, H. O. Lee, I. H. Lee, H. J. Kang, D. S. Rosenbloom, P. G. Camara, Z. Liu, P. van Nieuwenhuizen, S. W. Jung, S. W. Choi, J. Kim, A. Chen, K. T. Kim, S. Shin, Y. J. Seo, J. M. Oh, Y. J. Shin, C. K. Park, D. S. Kong, H. J. Seol, A. Blumberg, J. I. Lee, A. Iavarone, W. Y. Park, R. Rabadan, and D. H. Nam. Spatiotemporal genomic architecture informs precision oncology in glioblastoma. *Nat Genet*, 49(4):594–599, 2017.

[159] F. Wang, C. St Gelais, S. de Silva, H. Zhang, Y. Geng, C. Shepard, B. Kim, J. S. Yount, and L. Wu. Phosphorylation of mouse SAMHD1 regulates its restriction of human immunodeficiency virus type 1 infection, but not murine leukemia virus infection. *Virology*, 487:273–284, 2016.

[160] W. Chen, P. Cheng, J. Jiang, Y. Ren, D. Wu, and D. Xue. Epigenomic and genomic analysis of transcriptome modulation in skin cutaneous melanoma. *Aging (Albany NY)*, 12(13):12703–12725, 2020.

[161] Z. Chen, J. Hu, S. Ying, and A. Xu. Dual roles of SAMHD1 in tumor development and chemoresistance to anticancer drugs. *Oncol Lett*, 21(6):451, 2021.

[162] C. A. Yang, H. Y. Huang, Y. S. Chang, C. L. Lin, I. L. Lai, and J. G. Chang. DNA-Sensing and Nuclease Gene Expressions as Markers for Colorectal Cancer Progression. *Oncology*, 92(2):115–124, 2017.

[163] S. Kretschmer, C. Wolf, N. König, W. Staroske, J. Guck, M. Haeusler, H. Luksch, L. A. Nguyen, B. Kim, D. Alexopoulou, A. Dahl, A. Rapp, M. C. Cardoso,

A. Shevchenko, and M. A. Lee-Kirsch. SAMHD1 prevents autoimmunity by maintaining genome stability. *Ann Rheum Dis*, 74(3):e17, 2015.

[164] D. Bhojwani and C. H. Pui. Intrathecal liposomal cytarabine: more friend than foe? *Leuk Lymphoma*, 49(8):1427–1430, 2008.

[165] W. Wang, J. Sun, W. Zhang, and D. Zhou. Successful treatment of intracranial Rosai-Dorfman disease with cytarabine and dexamethasone: case report and review of literature. *Ann Hematol*, 99(5):1157–1159, 2020.

[166] J. Chng, T. Wang, R. Nian, A. Lau, K. M. Hoi, S. C. Ho, P. Gagnon, X. Bi, and Y. Yang. Cleavage efficient 2A peptides for high level monoclonal antibody expression in CHO cells. *MAbs*, 7(2):403–412, 2015.

[167] M. Pizzato, O. Erlwein, D. Bonsall, S. Kaye, D. Muir, and M. O. McClure. A one-step SYBR Green I-based product-enhanced reverse transcriptase assay for the quantitation of retroviruses in cell culture supernatants. *J Virol Methods*, 156(1-2): 1–7, 2009.

[168] M. Sena-Esteves and G. Gao. Titration of Lentivirus Vectors. *Cold Spring Harb Protoc*, 2018(4), 2018.

[169] N. E. Bowen, J. Temple, C. Shepard, A. Oo, F. Arizaga, P. Kapoor-Vazirani, M. Persaud, C. H. Yu, D. H. Kim, R. F. Schinazi, D. N. Ivanov, F. Diaz-Griffero, D. S. Yu, Y. Xiong, and B. Kim. Structural and functional characterization explains loss of dNTPase activity of the cancer-specific R366C/H mutant SAMHD1 proteins. *J Biol Chem*, page 101170, 2021.

[170] C. Goffinet, I. Allespach, S. Homann, H. M. Tervo, A. Habermann, D. Rupp, L. Oberbremer, C. Kern, N. Tibroni, S. Welsch, J. Krijnse-Locker, G. Banting, H. G. Krausslich, O. T. Fackler, and O. T. Keppler. HIV-1 antagonism of CD317 is species specific and involves Vpu-mediated proteasomal degradation of the restriction factor. *Cell Host Microbe*, 5(3):285–297, 2009.

[171] R. Jafari, H. Almqvist, H. Axelsson, M. Ignatushchenko, T. Lundbäck, P. Nordlund, and D. Martinez Molina. The cellular thermal shift assay for evaluating drug target interactions in cells. *Nat Protoc*, 9(9):2100–2122, 2014.

[172] R. S. Hegde and E. Zavodszky. Recognition and Degradation of Mislocalized Proteins in Health and Disease. *Cold Spring Harb Perspect Biol*, 11(11), 2019.

[173] P. Gao, X. Dong, Y. Wang, and G. H. Wei. Optimized CRISPR/Cas9-mediated single nucleotide mutation in adherent cancer cell lines. *STAR Protoc*, 2(2):100419, 2021.

Acknowledgements

This thesis was carried out at the Max von Pettenkofer Institute, Virology, at the Ludwig-Maximilians-University in Munich. I would like to express my deepest gratitude to my doctoral supervisor and head of virology Prof. Oliver T. Keppler. My way into the Ph.D. was a rather unconventional one, but he enforced me that I am capable of more and supported me as well as challenged me to grow.

In addition, I would also like to thank PD Dr. Barbara Adler and Dr. Niklas Thon for their time and input during my thesis advisory committee meetings as well as my defense committee members for their time and evaluation. Then, a big thank you and "¡Gracias!" to Dr. Ernesto Mejías Pérez for co-supervising and reviewing my thesis as well as openly sharing his wisdom.

It is important to me to send a big hug to my good friend and colleague Madeleine! During our Ph.D., we shared both joy and sorrow, held and uplifted each other when times were hard. I would have coped with things a lot worse if it wouldn't be for her. THANK YOU, my dear! I also wish to thank the whole Keppler lab, present and past members: Manuel, Qianhao, Marcel, Rebecca, Robin, Johanna, Niklas, Jelica, Kathi, Hong-Ru, Ina, Linda, Laura, Thimo, Simone, Max, Adrian and Burak. They created a working environment where I enjoyed to be. My thanks also goes to the surrounding working groups, including Baldauf, Schölz and Sewald lab. Here, I want to especially thank Patrícia for her friendship and Ramya for open brainstorming about our shared buddies SAMHD1 and Vpx. The other PIs gave me the feeling that I can always come to them when in need, thank you Christian, Xaver and Hanna-Mari!

I am grateful to all collaborators involved in this project: Prof. Jindrich Cinatl, Tamara Rothenburger, Prof. Lars Kaderali, Prof. Jörg-Christian Tonn, Dr. Rupert Egensperger, Michael Schmidt, Prof. Veit Hornung, Stefan Bauernfried, Saskia Schmidt, Prof. Gerd Geisslinger, Prof. Gerda Egger, Dr. Massimo Squatrito and Prof. Rainer Glaß.

Also, I am thanking my family and friends for their support during my Ph.D. This was an energy- and time-consuming period in my life and they always had my back. Many thanks to Mama & Bichi-Oma, Papa & Martina, Tante Corinna & Onkel Günther, Schneider Opa as well as Irene & Werner. And I also know that Bichi-Opa & Schneider-Oma will be so

proud of Dr. Stephanie. Thank you to my good friends Sarah and Nina for their friendship. And finally, thousand times thank you to Manuel! It is not always easy to be the partner of a Ph.D. student and I am very grateful that he was holding my hand all the way through. THANK YOU for everything, my love!

Last but not least, I am thanking my sister Lena-Maria for guiding and supporting me through every obstacle that I need to face. I miss you terribly every day! Full of love and thankfulness, I dedicate my Ph.D. thesis to you! <3

Munich, January 2022

Stephanie

Affidavit

LMU LUDWIG-MAXIMILIANS-UNIVERSITÄT MÜNCHEN | Promotionsbüro Medizinische Fakultät | MMRS

Affidavit

Stephanie Schneider

Feodor-Lynen-Straße 23

81377 Munich, Germany

I hereby declare, that the submitted thesis entitled:

The potential role of SAMHD1 in the chemotherapy of glioblastoma multiforme

is my own work. I have only used the sources indicated and have not made unauthorised use of services of a third party. Where the work of others has been quoted or reproduced, the source is always given.

I further declare that the submitted thesis or parts thereof have not been presented as part of an examination degree to any other university.

Munich, 18.11.2022 — Stephanie Schneider

Place, Date — Signature doctoral candidate

Confirmation of Congruency

LMU LUDWIG-MAXIMILIANS-UNIVERSITÄT MÜNCHEN

Promotionsbüro
Medizinische Fakultät

MMRS

Confirmation of congruency between printed and electronic version of the doctoral thesis

Stephanie Schneider

Feodor-Lynen-Straße 23

81377 Munich, Germany

I hereby declare, that the submitted thesis entitled:

The potential role of SAMHD1 in the chemotherapy of glioblastoma multiforme

is congruent with the printed version both in content and format.

Munich, 18.11.2022 — Stephanie Schneider

Place, Date — Signature doctoral candidate

List of Publications

A. Zutz, C. Schölz, **S. Schneider**, V. Pierini, M. Münchhoff, K. Sutter, G. Wittmann, U. Dittmer, R. Draenert, J. R. Bogner, O. T. Fackler, O. T. Keppler. SERINC5 is an unconventional HIV restriction factor that is upregulated during myeloid cell differentiation. *J Innate Immun*, 12(5):399-409, 2020.

R. Wang, **S. Schneider**, O. T. Keppler, B. Li, B. Rutz, A. Ciotkowska, C. G. Stief, M. Hennenberg. ADP ribosylation factor 6 promotes contraction and proliferation, suppresses apoptosis and is specifically inhibited by NAV2729 in prostate stromal cells. *J Mol Pharmacol*, 100(4):356-371, 2021.

M. Münchhoff, A. Graf, S. Krebs, C. Quartucci, S. Hasmann, J. C. Hellmuth, C. Scherer, A. Ostermann, S. Boehm, C. Mandel, A. S. Beker-Pennrich, M. Zoller, H. C. Stubbe, S. Munker, D. Munker, K. Milger, M. Gapp, **S. Schneider**, A. Ruhle, L. Jocham, L. Nicolai, K. Pekayvaz, T. Weinberger, H. Mairhofer, E. Khatamzas, K. Hofmann, P. M. Spaeth, S. Bender, S. Kääb, B. Zwissler, J. Mayerle, J. Behr, M. v. Bergwelt-Baildon, M. Reincke, B. Grabein, C. L. Hinske, H. Blum, O. T. Keppler. Genomic epidemiology reveals multiple introductions of SARS-CoV-2 followed by community and nosocomial spread, Germany, February to May 2020. *Euro Surveill.*, 26(43):2002066, 2021.

J. N. Mumm, S. Ledderose, A. Ostermann, M. Rudelius, J. C. Hellmuth, M. Münchhoff, D. Munker, C. Scherer, Y. Volz, B. Ebner, C. Giessen-Jung, C. Lampert, T. Vilsmaier, **S. Schneider**, M. Gapp, K. Milger-Kneidinger, J. Behr, M. v. Bergwelt-Baildon, O. T. Keppler, C. Stief, G. Magistro, M. Staehler, S. Rodler. Dynamics of urinary and respiratory shedding of Severe acute respiratory syndrome virus 2 (SARS-CoV-2) RNA excludes urine as a relevant source of viral transmission. *Infection*, 1-8, 2021.

M.A. Beck, H. Fischer, L. M. Grabner, T. Groffics, M. Winter, S. Tangermann, T. Meischel, B. Zaussinger-Haas, P. Wagner, C. Fischer, C. Folie, J. Arand, C. Schöfer, B. Ramsahoye, S. Lagger, G. Machat, G. Eisenwort, **S. Schneider**, A. Podhornik, M. Kothmayer, U. Reichart, M. Glösmann, I. Tamir, M. Mildner, R. Sheibani-Tezerji, L. Kenner, P. Petzelbauer, G. Egger, M. Sibilia, A. Ablasser, C. Seiser. DNA hypomethylation leads to cGAS-induced autoinflammation in the epidermis. *EMBO Journal*, 40(22):e108234, 2021.